

Evaluating the effects of fluid migration and microbial processes on the noble gas and
hydrocarbon geochemistry of shallow groundwater

Dissertation

Presented in Partial Fulfillment of the Requirements for the Degree Doctor of Philosophy in the
Graduate School of The Ohio State University

By

Colin James Stephen Whyte, B.S., M.S.,
Graduate Program in Earth Sciences

The Ohio State University

2020

Dissertation Committee

Dr. Thomas H. Darrah, Advisor

Dr. Franklin W. Schwartz

Dr. W. Berry Lyons

Dr. Michael Barton

Copyrighted by
Colin J. S. Whyte
2020

Abstract

The expansion of unconventional petroleum development enhanced production of natural gas and oil globally, but also raised concerns related to groundwater contamination resulting from drilling activities. Extensive research recently has focused on identifying contaminants (e.g., CH₄, brines) related to drilling or natural processes, as well as the processes that emplace these contaminants into shallow groundwater systems. The integrated utilization of inert (e.g., noble gas), hydrocarbon (e.g., C₁/C₂₊, compound-specific stable isotopes), and aqueous geochemical tracers has become a standard technique for identifying naturally-occurring hydrocarbon gas or brine from human-induced contamination. Still, it is often difficult to make determinations of groundwater contamination due to lack of understanding of the many processes that can alter the hydrocarbon and aqueous geochemistry following emplacement into groundwater (post-genetic modification) and a lack of baseline geochemical data.

Advection, diffusion, mixing with primary microbial gas, microbial oxidation, and secondary methanogenesis can all obfuscate the geochemical characterization of a groundwater system making it essential to understand the effects of these individual processes. Here, numerical models were developed using a hypothetical thermogenic natural gas to illustrate how traditional geochemical tracers are affected by post-genetic modification following gas emplacement.

The current work also examined the aqueous and gas geochemistry of groundwater samples collected from observation boreholes and residential drinking-water wells in the Saint-Édouard

region of southern Quebec, Canada, and from drinking-water wells that were previously interpreted to contain fugitive gas contamination in Parker County, TX. In the Saint-Édouard region, the widespread presence of hydrocarbons in shallow groundwater and the relative lack of petroleum development provides a rare opportunity to understand naturally-occurring hydrocarbons prior to drilling and in a nearly-pristine environment. In comparison, the drinking-water wells in Parker County, TX with prior evidence of fugitive gas provides an opportunity to broaden the geochemical framework used to identify fugitive gas contamination and develop a detailed understanding of the ongoing factors that alter groundwater geochemistry in regions influenced by fugitive gas contamination.

The Saint-Édouard dataset was combined with previously published stable isotopic and aqueous geochemical data, while the Parker County samples were analyzed for a suite of inorganic and stable isotopic tracers and major gas ratios in addition to more traditional geochemical tracers. Both datasets suggest microbial oxidation of thermogenic hydrocarbons is occurring in these regions, while positive trends in $\delta^{13}\text{C-DIC}$, $[\text{HCO}_3^-]$, and negative $\delta^{13}\text{C-CH}_4$ may indicate secondary methanogenesis. In the Saint-Édouard region, the absolute and relative abundances of noble gas isotopes suggest groundwater degassing, perhaps as the result of the addition of secondary microbial CH_4 . In Parker County, TX, the generation of H_2S following sulfate-paired oxidation of fugitive hydrocarbons enhances the potential environmental and health risks associated with fugitive gas contamination.

In combination, the numerical models for post-genetic modification and groundwater geochemical data from areas with natural and anthropogenic hydrocarbon contamination provide insight into the evolution of hydrocarbons in shallow groundwater.

Dedication

To my family who have provided me with unflinching support throughout my entire life.

Acknowledgments

The science contained within this document was funded by the Ohio State University's Noble Gas Laboratory and National Science Foundation (NSF EAR-1249255, NSF EAR-1441497). Additional travel grants were provided by the Ohio State University's School of Earth Sciences Friends of Orton Hall fund. I would like to acknowledge and thank Geneviève Bordeleau of Natural Resources Canada for providing access to the groundwater monitoring wells and her assistance during field work in Quebec. I would like to acknowledge the faculty members of my dissertation committee for their willingness to help guide and support me through the Ph.D. process. I would like to thank my advisor Dr. Thomas Darrah for being a tremendous mentor in the laboratory and as a scientific writer. I would also like to thank my family for their endless support and McKenzie for tolerating me during the writing of this document. Finally, I would like to thank my fellow lab group members: Myles, Brent, Erica, Billy, and Gus who have been good friends over the course of my graduate career. I'm particularly thankful for them picking up the slack I left in the laboratory as I took the time to write this thing.

Vita

- 2014.....B.S. Geological Sciences,
The Ohio State University,
Columbus, Ohio, USA
- 2014.....Research Associate,
School of Earth Sciences,
The Ohio State University,
Columbus, Ohio, USA
- 2015 to present.....Graduate Research Associate,
School of Earth Sciences,
The Ohio State University,
Columbus, Ohio, USA
- 2018.....M.S. Earth Sciences,
The Ohio State University,
Columbus, Ohio, USA

Publications

- Darrah, T.H., Jackson, R.B., Vengosh, A., Warner, N.R., Whyte, C.J., Walsh, T.B., Kondash, A.J., and Poreda, R.J., 2015. "The evolution of Devonian hydrocarbon gases in shallow aquifers of the northern Appalachian Basin: Insights from integrating noble gas and hydrocarbon geochemistry." *Geochimica et Cosmochimica Acta*, 170: 321-355. doi:10.1016/j.gca.2015.09.006.
- Hildenbrand, Z.L., Carlton Jr, D.D., Meik, J.M., Taylor, J.T., Fontenot, B.E., Walton, J.L., Henderson, D., Thacker, J.B., Korlie, S., Whyte, C.J., and Hudak, P.F., 2017. A reconnaissance analysis of groundwater quality in the Eagle Ford shale region reveals two distinct bromide/chloride populations. *Science of the Total Environment*, 575: 672-680. doi:10.1016/j.scitotenv.2016.09.070.
- Harkness, J.S., Darrah, T.H., Warner, N.R., Whyte, C.J., Moore, M.T., Millot, R., Kloppmann, W., Jackson, R.B., and Vengosh, A., 2017. The geochemistry of naturally occurring methane and saline groundwater in an area of unconventional shale gas development. *Geochimica et Cosmochimica Acta*, 208: 302-334. doi:10.1016/j.gca.2017.03.039.
- Harkness, J.S., Darrah, T.H., Moore, M.T., Whyte, C.J., Mathewson, P.D., Cook, T. and Vengosh, A., 2017. Naturally occurring versus anthropogenic sources of elevated molybdenum in groundwater: Evidence for Geogenic contamination from Southeast Wisconsin, United States. *Environmental Science & Technology*, 51(21): 12190-12199. doi:10.1021/acs.est.7b03716.
- Moore, M.T., Vinson, D.S., Whyte, C.J., Eymold, W.K., Walsh, T.B. and Darrah, T.H., 2018. Differentiating between biogenic and thermogenic sources of natural gas in coalbed methane reservoirs from the Illinois Basin using noble gas and hydrocarbon geochemistry. *Geological Society, London, Special Publications*, 468: SP468-8. doi:10.1144/SP468.8.
- Harkness, J.S., Swana, K., Eymold, W.K., Miller, J., Murray, R., Talma, S., Whyte, C.J., Moore, M.T., Maletic, E.L., Vengosh, A. and Darrah, T.H., 2018. Pre-drill Groundwater Geochemistry in the Karoo Basin, South Africa. *Groundwater*, 56(2): 187-203. doi:10.1111/gwat.12635.
- Eymold, W.K., Swana, K., Moore, M.T., Whyte, C.J., Harkness, J.S., Talma, S., Murray, R., Moortgat, J.B., Miller, J., Vengosh, A. and Darrah, T.H., 2018. Hydrocarbon-Rich Groundwater above Shale-Gas Formations: A Karoo Basin Case Study. *Groundwater*, 56(2): 204-224. doi:10.1111/gwat.12637.

Kreuzer, R.L., Darrah, T.H., Grove, B.S., Moore, M.T., Warner, N.R., Eymold, W.K., Whyte, C.J., Mitra, G., Jackson, R.B., Vengosh, A. and Poreda, R.J., 2018. Structural and Hydrogeological Controls on Hydrocarbon and Brine Migration into Drinking Water Aquifers in Southern New York. *Groundwater*, 56(2): 225-244. doi:10.1111/gwat.12638.

Fields of Study

Major Field: Earth Sciences

Table of Contents

Abstract	ii
Dedication	iv
Acknowledgements	v
Vita.....	vi
List of Tables	xii
List of Figures	xiii
Chapter 1. Introduction	1
Chapter 2. Numerical Modeling of Post-Genetic Modification Processes that Influence Thermogenic Gas Compositions in Shallow Groundwater	8
Abstract	8
2.1 Introduction	9
2.2 Geochemical Background	12
2.2.1 Hydrocarbons in Shallow Groundwater.....	12
2.2.2 Secondary Methanogenesis and Noble Gases.....	15
2.3 Numerical Modeling Methods.....	18
2.3.1 Advection.....	21
2.3.2 Diffusion	25
2.3.3 Microbial Oxidation.....	26
2.3.4 Secondary Methanogenesis.....	28
2.3.5 Mixing with Primary Microbial Gas.....	31
2.3.6 Applying Models to Published Datasets.....	32
2.4 Results	33
2.5 Discussion	43
2.6 Conclusions	49
Chapter 3. Noble gas insights into microbial hydrocarbon degradation processes in shallow groundwater of the Saint-Édouard region of southern Quebec, Canada	51
Abstract	51
3.1 Introduction	52
3.2 Background	54

3.2.1 Site Selection and Previous Work.....	54
3.2.2 Geologic Setting.....	57
3.2.3 Hydrogeology	60
3.2.4 Hydrocarbon Gas Geochemistry	61
3.2.5 Noble Gas Geochemistry	64
3.3 Methods	66
3.3.1 Sample Collection.....	66
3.3.2 Sample Analyses.....	68
3.3.3 Numerical Modeling	70
3.4 Results	73
3.4.1 Major Ion Geochemistry	73
3.4.2 Hydrocarbons and Stable Isotopes.....	74
3.4.3 Noble Gases	81
3.5 Discussion	88
3.5.1 Naturally-Occurring Hydrocarbons and Salinity in the Saint-Édouard region	88
3.5.2 Hydrocarbon Characterization Using Stable Isotopes and Noble Gas Geochemistry	90
3.5.3 Revisiting Secondary Methanogenesis	93
3.5.4 Noble Gas Constraints on the History of Hydrocarbon-Groundwater Interactions.....	96
3.6 Conclusions	102
Chapter 4. Geochemical evidence for fugitive gas contamination and associated water quality changes in drinking-water wells from Parker County, Texas	103
Abstract	103
4.1 Introduction	104
4.2 Geologic Background.....	107
4.2.1 Fort Worth Basin.....	107
4.2.2 Petroleum Systems in the Fort Worth Basin.....	112
4.2.3 Parker County, Texas and Study Area.....	112
4.3 Methods and Materials	114
4.3.1 Sample Selection.....	114
4.3.2 Sample Analyses.....	115
4.4 Results and Discussion.....	118

4.4.1 Baseline Groundwater Composition: Inorganic Constituents.....	118
4.4.2 Baseline Groundwater Composition: Dissolved Gas Geochemistry	125
4.4.3 Identifying Fugitive Gas Contamination	137
4.4.4 Secondary Processes and Challenges with Identifying the Source of Fugitive Gas Contamination	143
4.4.5 Comparison to Observations in Appalachian Basin	150
4.4.6 Implications of Fugitive Gas Contamination.....	151
4.5 Conclusions	152
Chapter 5. Concluding Remarks	154
References.....	156

List of Tables

Table 1.1. Definitions of various geochemical terms and parameters used throughout this dissertation	7
Table 2.1. Endmember Compositions.....	20
Table 2.2. Partition and Diffusion Coefficients (α)	26
Table 2.3. Fractionation Factors of Oxidation (α)	27
Table 2.4. Select Hydrocarbon Results from Numerical Models	34
Table 2.5. Select Noble Gas Isotopic Results from Numerical Models	35
Table 3.1. Dissolved Ion Geochemistry.....	74
Table 3.2. Hydrocarbon Geochemistry	75
Table 3.3. Major and Noble Gas Geochemistry	82
Table 4.1. Water Composition Data from Groundwater Samples	119
Table 4.2. Stable Isotopic Data from Groundwater Samples.....	123
Table 4.3. Major Gas Composition Data from Groundwater Samples.....	126
Table 4.4. Uranium (U) and Thorium (Th) Concentrations of Aquifer Lithologies	129
Table 4.5. Noble Gas Composition and Isotopic Data from Groundwater Samples	130
Table 4.6. Major and Hydrocarbon Gas Compositional and Stable Isotopic Data . from Produced Gases	132
Table 4.7. Noble Gas Compositional and Stable Isotopic Data from Produced Gases	136

List of Figures

Figure 1.1. Generalized diagram displaying various potential mechanisms of hydrocarbon gas contamination as a result of drilling and/or hydraulic fracturing, and sources of methane and microbial degradation in the subsurface	2
Figure 2.1. The C ₁ /C ₂₊ ratios vs. δ ¹³ C-CH ₄ of a Marcellus-like thermogenic gas (A) and published groundwater data (B).....	37
Figure 2.2. The δ ² H-CH ₄ vs. δ ¹³ C-CH ₄ of a Marcellus-like thermogenic gas (A) and published groundwater data (B)	38
Figure 2.3. Modeled ⁴ He/CH ₄ vs. ²⁰ Ne/ ³⁶ Ar of a Marcellus-like thermogenic gas (A) and published groundwater data (B).....	40
Figure 2.4. Modeled ⁸⁴ Kr/ ³⁶ Ar vs. ²⁰ Ne/ ³⁶ Ar of a Marcellus-like thermogenic gas (A) and published groundwater data (B)	41
Figure 2.5 Modeled ⁴ He/CH ₄ vs. δ ¹³ C-CH ₄ of a Marcellus-like thermogenic gas (A) and published groundwater data (B)	42
Figure 2.6. Modeled C ₁ /C ₂₊ vs. ²⁰ Ne/ ³⁶ Ar of a Marcellus-like thermogenic gas (A) and published groundwater data (B).....	46
Figure 2.7 Modeled δ ¹³ C-CH ₄ vs. ²⁰ Ne/ ³⁶ Ar of a Marcellus-like thermogenic gas (A) and published groundwater data (B).....	48
Figure 3.1. Map of Saint-Édouard region (A) and cross section (B).....	55
Figure 3.2. Generalized stratigraphic column of the Saint-Édouard study area	58
Figure 3.3. [HCO ₃], [C ₂ H ₆], δ ¹³ C-CH ₄ , and δ ¹³ C-DIC vs. [Cl] (left) and [CH ₄], [C ₂ H ₆], δ ¹³ C-CH ₄ , and δ ¹³ C-DIC vs. [HCO ₃] (right)	76
Figure 3.4. CH ₄ /C ₂ H ₆₊ vs. δ ¹³ C-CH ₄ (A) and δ ² H-CH ₄ vs. δ ¹³ C-CH ₄ (B).....	78
Figure 3.5. δ ¹³ C-DIC vs. [CH ₄] (A), δ ¹³ C-DIC vs. δ ¹³ C-CH ₄ (B)	80
Figure 3.6. [²⁰ Ne] (A), [CH ₄] (B), [N ₂] (C) and [⁴ He] (D) vs [³⁶ Ar]	83
Figure 3.7. ³ He/ ⁴ He (as R/R _A) vs. He/Ne (A), 1/[⁴ He] (B), and CH ₄ (C).....	85
Figure 3.8. ⁴ He/ ²⁰ Ne vs. CH ₄ / ³⁶ Ar (A) and ⁴ He/ ³⁶ Ar vs. CH ₄ / ³⁶ Ar (B).....	86
Figure 3.9. ⁸⁴ Kr/ ³⁶ Ar vs. ²⁰ Ne/ ³⁶ Ar (A) and ¹³² Xe/ ³⁶ Ar (C) (left), and ⁴ He/CH ₄ (B) and δ ¹³ C-DIC (D) vs. ²⁰ Ne/ ³⁶ Ar (right).....	87

Figure 3.10. Fractionation of ASW noble gases when compared to calculated ASW concentrations (A) and fractionation when each isotope, normalized to ^{36}Ar in the samples, are compared to that ratio in air (B)	98
Figure 3.11. $^{20}\text{Ne}/^{36}\text{Ar}$ vs. $^{84}\text{Kr}/^{36}\text{Ar}$ (A) and $^{20}\text{Ne}/^{36}\text{Ar}$ vs. $^{132}\text{Xe}/^{36}\text{Ar}$ (B)	100
Figure 4.1. Map of Fort Worth Basin and study area	108
Figure 4.2. Generalized west to east cross-section (A) and stratigraphic column (B) through southern Parker County, Texas	109
Figure 4.3. [Br] (A), [Sr] (B), [Na] (C), [Ca] (D), and $\delta^{18}\text{O}\text{-H}_2\text{O}$ (E) vs. [Cl] and B/Cl vs. Na/Cl (F) in domestic drinking-water wells in Parker County, TX.	121
Figure 4.4. Comparison of $\delta^{11}\text{B}$ (A) and $^{87}\text{Sr}/^{86}\text{Sr}$ (B) values measured in background drinking-water samples (blue) and drinking-water samples affected by fugitive gas contamination (red)	124
Figure 4.5. The ratios of $\text{CH}_4/^{36}\text{Ar}$ (A), $[\text{C}_2\text{H}_6]$ (B), [DIC] (as HCO_3) (C), and $\delta^{13}\text{C}\text{-DIC}$ (D) vs. [Cl]	128
Figure 4.6. $[\text{N}_2]$ (A) and $[\text{Ne}]$ (B) vs. $[\text{Ar}]$, $\delta^{13}\text{C}\text{-DIC}$ vs. $[\text{HCO}_3]$ (C), and $\delta^2\text{H}\text{-CH}_4$ (D), $\delta^{13}\text{C}\text{-DIC}$ (E), and $\delta^{13}\text{C}\text{-C}_2\text{H}_6$ (F) vs. $\delta^{13}\text{C}\text{-CH}_4$	134
Figure 4.7. CO_2/CH_4 (A) and $\delta^{15}\text{N}\text{-N}_2$ (B) vs. N_2/CH_4 , $\delta^{15}\text{N}\text{-N}_2$ vs. $\text{C}_2\text{H}_6+\text{CH}_4$ (C), and $\delta^{15}\text{N}\text{-N}_2$ vs. CO_2/CH_4 (D)	135
Figure 4.8. $[\text{SO}_4]$ vs. [Cl] (A), $\text{H}_2\text{S}/\text{SO}_4$ vs. $\text{C}_2\text{H}_6+\text{CH}_4$ (B), $[\text{SO}_4]$ vs. $[\text{HCO}_3]$ (C), and $[\text{H}_2\text{S}]$ vs. $\text{H}_2\text{S}\%$ of total [S] (D)	144

Chapter 1. Introduction

The development of unconventional drilling and hydraulic fracturing rejuvenated oil and natural gas production in the US Kerr (2010), however the increased drilling activity in the past ~15 years led to considerable environmental concern that these drilling practices may contaminate drinking-water aquifers near areas of unconventional development (Harkness et al., 2017b; Jackson et al., 2013; Osborn et al., 2011). In petroleum-rich sedimentary basins such as the Appalachian Basin and Fort Worth Basin in the USA, the natural migration of hydrocarbons and brines from deep formations to shallow groundwater are common (Darrah et al., 2015b; Harkness et al., 2017b; Kreuzer et al., 2018; Molofsky et al., 2013; Nicot et al., 2017c; Siegel et al., 2015; Warner et al., 2012), leading to significant debate as to the source of contamination (natural versus anthropogenic) when present in drinking-water aquifers (Darrah, 2018; Darrah et al., 2015b; Darrah et al., 2014; Harkness et al., 2017b; Jackson et al., 2013; Molofsky et al., 2013; Nicot et al., 2017a; Nicot et al., 2017b; Nicot et al., 2017c; Osborn et al., 2011; Siegel et al., 2015; Warner et al., 2012).

Recent attempts to distinguish between natural sources of hydrocarbons and other contaminants (e.g., brines) in shallow groundwater from anthropogenic contamination predominantly focused on developing a geochemical framework from which one could identify: 1) salinity sourced from water-rock interactions during the natural migration of hydrocarbons and brines compared to byproducts of hydraulic fracturing, 2) deeply-sourced thermogenic hydrocarbons compared to shallow microbial gas, and 3) the mechanisms of gas emplacement into shallow groundwater (e.g., natural hydrocarbon gas and brine migration versus leaking production

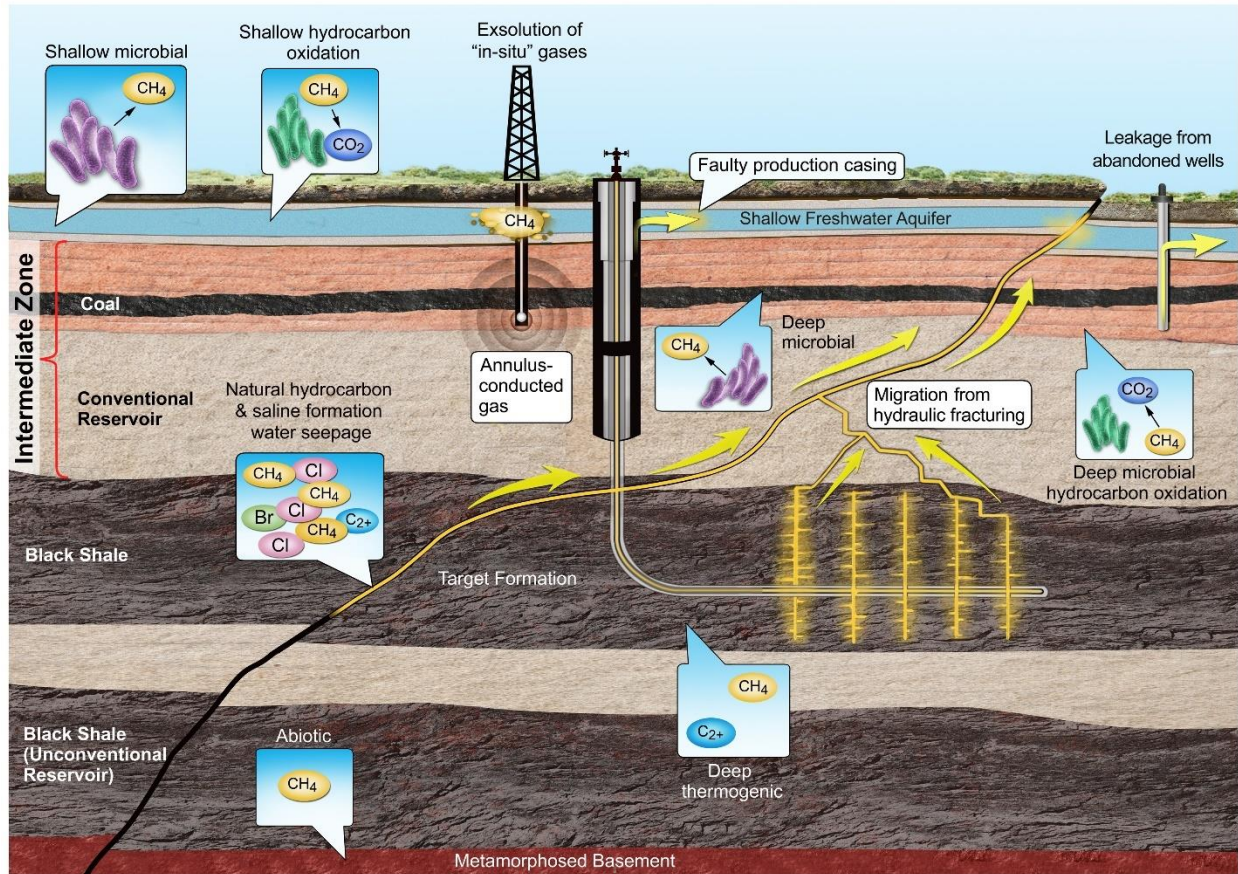


Figure 1.1: Generalized diagram displaying various potential mechanisms of hydrocarbon gas contamination as a result of drilling and/or hydraulic fracturing, and sources of methane and microbial degradation in the subsurface. Adapted from Darrah et al. (2014).

wells) (Darrah et al., 2015b; Darrah et al., 2014; Dusseault and Jackson, 2014; Fontenot et al., 2013; Harkness et al., 2017b; Harkness et al., 2015; Hildenbrand et al., 2015; Vengosh et al., 2014; Warner et al., 2012; Wen et al., 2016b; Wen et al., 2017; Wen et al., 2018) (Figure 1.1). However, lacking is a similar geochemical framework to identify processes that alter the geochemistry of hydrocarbon gas and brine once fluids have underwent migration (via either natural migration or fugitive gas contamination) into shallow groundwater systems (Wen et al., 2019; Woda et al., 2018). These alteration processes (commonly termed “post-genetic modification” processes) may include mixing with microbial gas, microbial oxidation, secondary methanogenesis, and additional stages of migration or groundwater degassing (see Table 1.1 for definitions of various geochemical terms to be used throughout this document).

The focus of this dissertation is to build a geochemical framework that identifies post-genetic modification of thermogenic hydrocarbon gases in groundwater systems. Through the integration of noble gas elemental (He-Xe) and isotopic (e.g., $^{20}\text{Ne}/^{36}\text{Ar}$, $^{84}\text{Kr}/^{36}\text{Ar}$, $^4\text{He}/\text{CH}_4$) geochemistry, major gas geochemistry (e.g., N_2/CH_4 , CO_2/CH_4), traditional hydrocarbon geochemical techniques commonly used to characterize natural gas (C_1/C_{2+} , $\delta^{13}\text{C}-\text{CH}_4$, $\delta^2\text{H}-\text{CH}_4$), and numerical modeling, I attempt to better the understanding of the evolution of hydrocarbons in groundwater. I have produced numerical models that explore various post-genetic modification processes that could influence a hypothetical thermogenic natural gas in groundwater and then I applied these models to previously published datasets to evaluate the influence of post-genetic modification on thermogenic natural gases in two case studies, as well as providing the work flow and numerical models necessary to evaluate these processes in future studies. I have analyzed and interpreted the dissolved gas and major ion geochemistry of suites of groundwater samples from

the Appalachian Basin and Fort Worth Basin in the USA in areas known to have naturally-occurring natural gas or fugitive hydrocarbon gas contamination to understand post-genetic modification in natural settings and secondary processes such as H₂S release following sulfate-paired oxidation of hydrocarbons. I anticipate that this work will build on the existing geochemical framework for understanding natural versus anthropogenically-migrated hydrocarbons and brine in shallow groundwater as well as the evolution of hydrocarbon gas that could influence drinking-water aquifers by a variety of mechanisms.

This dissertation is organized into five chapters. The first chapter, which is the current chapter, presents an overview of the current state of research related to understanding hydrocarbon contamination in shallow aquifers. This chapter also provides a summary of geochemical techniques to be used in the proceeding chapters.

The second chapter, “Numerical Modeling of Post-Genetic Modification Processes that Influence Thermogenic Gas Compositions in Shallow Groundwater,” describes numerical models that were produced using a hypothetical, dry, thermogenic hydrocarbon gas that is present in shallow groundwater to understand the effects of post-genetic modification on hydrocarbons. The models use hydrocarbon molecular (C₁/C₂₊) and stable isotopic compositions ($\delta^{13}\text{C-CH}_4$, $\delta^2\text{H-CH}_4$) and noble gas elemental (⁴He/CH₄) and isotopic compositions (²⁰Ne/³⁶Ar, ⁸⁴Kr/³⁶Ar). The post-genetic modification processes that are modeled include multi-phase (gas plus water) advection, diffusion, residual water phases following these processes, aerobic and anaerobic microbial oxidation, secondary methanogenesis, and mixing with primary microbial gas or older groundwater. These models were then applied to published groundwater data sets from the Appalachian Basin and Fort Worth Basin. The models indicate that while much of the groundwater

chemistry in these regions is influenced by multi-phase advection and mixing with primary microbial gas, subsets of samples have experienced oxidation or the addition of CH₄ as secondary microbial gas.

The third chapter, “Noble gas insights into microbial hydrocarbon degradation processes in shallow groundwater of the Saint-Édouard region of southern Quebec, Canada,” describes the dissolved gas and aqueous geochemistry of groundwater in an area of widespread, naturally-occurring hydrocarbons. The Saint-Édouard region has been targeted for unconventional natural gas development, but due to a *de facto* moratorium in the province only two natural gas wells that were drilled in the region and these well were not in production at the time of this study. The relative lack of petroleum production provides an opportunity to study naturally-occurring hydrocarbons in a relatively pristine hydrogeologic setting. The dissolved hydrocarbon gas geochemistry (C₁/C₂₊, $\delta^{13}\text{C-CH}_4$, $\delta^2\text{H-CH}_4$) in this region has previously suggested mixed microbial and thermogenic sources. When combined with major ion geochemistry (Cl, HCO₃), water geochemistry, noble gas geochemistry, and new hydrocarbon molecular data (e.g., C₁-C₆ hydrocarbons), the ubiquitous presence of thermogenic hydrocarbons and their correlation with [Cl] suggests the groundwater geochemistry in this region is dominated by two-component mixing between a thermogenic gas with brine and fresh groundwater with microbial methane. The high [HCO₃], positive $\delta^{13}\text{C-DIC}$, and more negative $\delta^{13}\text{C-CH}_4$ in samples with the most thermogenic hydrocarbons suggest partial microbial oxidation of thermogenic gases followed by secondary methanogenesis. The absolute and relative abundances of atmospherically-derived noble gas isotopes suggest significant stripping in the gas-rich samples. Solubility partitioning following oil-water interactions or groundwater degassing may explain the distinctively low $^{20}\text{Ne}/^{36}\text{Ar}$ and

enriched $^{84}\text{Kr}/^{36}\text{Ar}$ and $^{132}\text{Xe}/^{36}\text{Ar}$ found throughout the dataset, but the presence of only minute amounts of adsorbed oil compared to significant gas observed in the region suggests groundwater degassing, perhaps following the addition of secondary microbial, is the most likely explanation for the noble gas geochemistry.

The fourth chapter, “Geochemical evidence for fugitive gas contamination and associated water quality changes in drinking-water wells from Parker County, Texas,” describes a follow-up study to Darrah et al. (2014), which identified fugitive gas contamination in a subset of drinking-water wells in Parker County, Texas, using a combination of noble gas, hydrocarbon, and aqueous geochemistry. The goal of this work is to build upon the geochemical framework for identifying fugitive gas contamination, the source formation of contamination, and secondary environmental impacts by integrating additional geochemical tracers including stable isotopes of water, $\delta^{11}\text{B}$, $^{87}\text{Sr}/^{86}\text{Sr}$, $\delta^{13}\text{C}$ and $\delta^2\text{H}$ of CH_4 and C_2H_6 , $\delta^{13}\text{C}\text{-DIC}$, and $\delta^{15}\text{N}\text{-N}_2$, $[\text{H}_2\text{S}]$, and ratios of major gases (e.g., N_2/CH_4 , CO_2/CH_4) to the previously used techniques. The data presented here confirm the presence of a fugitive gas that is distinct from baseline, which represents mixing between a high salinity, high SO_4 endmember and recently recharged meteoric water. The utility of major gas ratios such as N_2/CH_4 and CO_2/CH_4 and $\delta^{15}\text{N}\text{-N}_2$ for identifying source formations of fugitive gas is dependent on the ability to constrain all additional sources of gas (e.g., N_2 from excess air, CO_2 from carbonate dissolution). The decrease in $[\text{SO}_4]$ coupled with increases in $[\text{H}_2\text{S}]$ and $[\text{HCO}_3]$ in the samples that contain fugitive gas suggest sulfate-paired microbial oxidation of hydrocarbons. Finally, the increase in $[\text{HCO}_3]$ and $\delta^{13}\text{C}\text{-DIC}$ and more negative $\delta^{13}\text{C}\text{-CH}_4$ also suggests the occurrence of secondary methanogenesis in groundwater that contains fugitive gas pollution.

The final chapter summarizes my dissertation and conclusions and proposes future work with respect to evaluating changes in drinking-water quality resulting from natural or anthropogenic contamination. My hope is that reading this dissertation will lead to an understanding of the potential impacts of hydrocarbons in groundwater on both drinking-water quality and the biogeochemical systems in shallow groundwater. Fugitive gas contamination is an ongoing concern related to increased unconventional petroleum development, and this work broadens the geochemical techniques used to identify contamination.

Table 1.1. Definitions of various geochemical terms and parameters used throughout this dissertation

Thermogenic Gas	Natural gas derived from the thermocatalytic cracking of kerogen (catagenesis) under sufficiently high temperatures
Primary Microbial Gas	Natural gas derived from methanogenic archaea utilizing a non-hydrocarbon carbon source (for example: acetate, CO ₂ produced during the dissolution of carbonate or through the microbial degradation of soil organic matter)
Acetoclastic Methanogenesis	Microbial methane produced during the fermentation of acetate (general formula: CH ₃ COOH → CH ₄ + CO ₂)
Hydrogenotrophic Methanogenesis	Microbial methane produced from the reduction of CO ₂ (general formula: CO ₂ + 8H ⁺ → CH ₄ + 2H ₂ O)
Post-Genetic Modification	Any process (for example: migration, microbial oxidation) acting upon a fluid after its generation that may alter its geophysical or geochemical state
Microbial Hydrocarbon Oxidation	The microbial degradation of hydrocarbons utilizing an electron acceptor such as O ₂ or SO ₄ , which results in the generation of CO ₂ and H ₂ O
Secondary Methanogenesis	The microbial generation of methane utilizing the CO ₂ produced during the microbial oxidation of heavy hydrocarbon gases (ethane or heavier aliphatic hydrocarbons) or oils through hydrogenotrophic methanogenesis
Isotopic (or Molecular) Fractionation	The result of preferential partitioning of gas species or isotopes between two coexisting phases in a natural system according to the relative physical parameters of that species (for example: mass, solubility)
Solubility Partitioning	Partitioning between any two gas constituents in between two or more fluid phases according to the differences in solubility between the two constituents
Bunsen Solubility Coefficient (β)	The ratio of dissolved gas volume per volume of solution when the partial pressure of gas is 1 atmosphere
Fractionation Factor (α)	The ratio of isotopes or gas species in one phase to the other coexisting phase in a Rayleigh Distillation process
δ	Lowercase delta, standard notation for describing stable isotopic compositions where δ represents the ratio of two isotopes of an element relative to a standard, expressed in parts per thousand (per mil, ‰)
C₁/C₂₊	The ratio of methane (C ₁) to heavier aliphatic hydrocarbon compounds (ethane (C ₂), propane (C ₃), butane (C ₄), etc.)
R/R_A	The ³ He/ ⁴ He ratio of a sample compared to the atmospheric ratio R _A (1.384 x 10 ⁻⁶)
Air Saturated Water (ASW)	The anticipated dissolved concentrations and ratios of atmospherically-derived gases in groundwater based on conditions of recharge (temperature, salinity, elevation)

Chapter 2. Numerical Modeling of Post-Genetic Modification Processes that Influence Thermogenic Gas Compositions in Shallow Groundwater

Abstract

The increased development of unconventional oil and natural gas in recent years has dramatically expanded energy production in North America. These energy development activities have also resulted in significant concerns regarding the risks of hydrocarbon contamination related to energy development in shallow aquifers. Improved characterization of background and baseline geochemistry has proven important to ongoing efforts to characterize and mitigate instances of human-induced contamination related to unconventional energy development. The utilization of gas and aqueous geochemical tracers (e.g., compound-specific stable isotopes, multiply substituted isotopologues, noble gases) are now commonly employed to identify the presence of contamination, discern naturally-occurring hydrocarbons from human-induced pollution, and develop targeted strategies for mitigating the most common factors that lead to contaminant releases (e.g., sufficiently deep cement casing, better balanced drilling practices). One of the major challenges that faces the utilization of many gas geochemical tracers for these purposes is the post-genetic modification of natural gas, and specifically these tracers, by oxidation, mixing, advection, and diffusion, especially for reactive tracers such as hydrocarbons and CO₂. While the integration of inert noble gases minimizes uncertainties associated with the use of relatively reactive tracers, the extent to which post-genetic processes influence noble gas composition has not been extensively modeled previously. Here, I modeled how various factors influence the composition

of hydrocarbons, noble gases, CO₂, and their isotopes in shallow aquifers, including: a) multi-phase advection (gas plus water/brine); b) diffusion; c) mixing; d) aerobic oxidation (either by respiration or as sulfate-paired oxidation); e) anaerobic oxidation; f) primary methanogenesis; and g) secondary methanogenesis. Modeling outcomes were then applied to available gas geochemical data sets.

By integrating modeling outcomes with published data from groundwater systems with elevated levels of natural gas, I determined that aerobic oxidation followed by secondary methanogenesis likely accounts for the previously unexplained, but commonly observed trend of elevated C₁/C₂₊ without significant changes in δ¹³C-CH₄ in natural gases unaffected by migration in shallow aquifers. By integrating modeling approaches with noble gas and hydrocarbon tracers, one can better differentiate the potential sources of natural gas and the processes that influence natural gas composition in shallow aquifers.

2.1 Introduction

The extraction of petroleum from unconventional hydrocarbon reservoirs during recent decades has placed renewed interest in understanding the presence, causes, and effects of naturally-occurring methane (CH₄) and other hydrocarbon gases in drinking-water aquifers. Developing suitable forensic techniques capable of determining the source and mechanisms that introduce and alter natural gases in shallow aquifers has become an important sub-discipline of environmental geochemistry (Darrah et al., 2015a; Darrah et al., 2015b; Darrah et al., 2014; Eymold et al., 2018; Harkness et al., 2017b; Jackson et al., 2013; Kreuzer et al., 2018; Molofsky et al., 2013; Nicot et al., 2017c; Siegel et al., 2015; Wen et al., 2016b; Wen et al., 2017).

Traditional geochemical techniques used to characterize natural gases (e.g., C_1/C_{2+} , $\delta^{13}C$ - CH_4 , δ^2H - CH_4 , $\delta^{13}C$ - CO_2) are commonly applied to identify the source of natural gas contamination in shallow aquifers. However, these highly labile tracers are heavily influenced by post-genetic processes, which limits their applicability and in some cases can lead to misinterpretations about the true source of natural gas. For example, these geochemical parameters can be obscured by microbial activity (oxidation and methanogenesis) or fluid transport phenomena (e.g., advection, diffusion), which are common in shallow groundwater (e.g., Darrah et al., 2015b; Darrah et al., 2014; Harkness et al., 2017b; Rowe and Muehlenbachs, 1999a; Rowe and Muehlenbachs, 1999b; Schout et al., 2018; Woda et al., 2018). Although certain post-genetic modification processes have been well-studied, (e.g., Darrah et al., 2014; Kinnaman et al., 2007; Martini et al., 2008; Moore et al., 2018; Schlegel et al., 2011; Vinson et al., 2017; Whiticar, 1999; Woda et al., 2018), it remains difficult to distinguish all of the factors that influence hydrocarbon geochemistry in the subsurface.

Rayleigh fractionation models are commonly used to evaluate how hydrocarbon tracers, including C_1/C_{2+} , $\delta^{13}C$ - CH_4 , or δ^2H - CH_4 , are influenced by various post-genetic processes. The degree of fractionation is process-dependent and proceeds according to the respective fractionation factors or α -values. These include closed-system anaerobic microbial oxidation of CH_4 (Whiticar, 1990; Whiticar et al., 1986), aerobic oxidation (Kinnaman et al., 2007), primary methanogenesis (e.g., Bordeleau et al., 2018a; Vinson et al., 2017), and open-system processes such as multi-phase (gas plus water) advection or diffusion followed by mixing (e.g., Bordeleau et al., 2018a; Darrah et al., 2015a; Harkness et al., 2018).

More recently, similar numerical models have been developed that include noble gas abundances ($^4\text{He}/\text{CH}_4$) and the ratios of atmospherically-derived isotopes ($^{20}\text{Ne}/^{36}\text{Ar}$, $^{84}\text{Kr}/^{36}\text{Ar}$). The numerical models have been critical for recent efforts to resolve the source of natural gases in shallow groundwater and better understand the fluid transport processes involved in gas emplacement (e.g., Battani et al., 2000; Darrah et al., 2015b; Darrah et al., 2014; Gilfillan et al., 2008; Gilfillan et al., 2009; Harkness et al., 2017b; Moore et al., 2018; Wen et al., 2016b; Wen et al., 2017). While these models may be useful for explaining the majority of geochemical data, they have not been modeled for many important tracers.

In an effort to better understand how post-genetic modification processes influence thermogenic hydrocarbons in groundwater, I developed a comprehensive set of numerical models for hydrocarbon molecular (C_1/C_{2+}) and stable isotopic ratios ($\delta^{13}\text{C}-\text{CH}_4$, $\delta^2\text{H}-\text{CH}_4$), and noble gas abundance ($^4\text{He}/\text{CH}_4$) and isotopic ratios ($^{20}\text{Ne}/^{36}\text{Ar}$, $^{84}\text{Kr}/^{36}\text{Ar}$). This work was done to illustrate how: a) multi-phase advection (gas plus water/brine); b) diffusion; c) mixing; d) aerobic oxidation (either by respiration or as sulfate-paired oxidation); e) anaerobic oxidation; f) primary methanogenesis; and g) secondary methanogenesis alter the composition of thermogenic natural gas in shallow aquifers.

Numerical models capable of predicting hydrocarbon behavior following the majority of these post-genetic processes have been developed and validated previously. Nonetheless, specific post-genetic modification processes (e.g., secondary methanogenesis) and combinations of processes (e.g., secondary methanogenesis followed by mixing) are unaddressed. Here, I focused on developing numerical models that predict the influence of previously unaddressed post-genetic modification mechanisms on hydrocarbon molecular and isotopic tracers (e.g., secondary

methanogenesis). Similarly, although numerical models have been developed to predict the behavior of noble gases following the majority of post-genetic processes (e.g., phase partitioning, diffusion), these prior efforts have seldom modeled either the relationship between noble gases and hydrocarbon tracers (e.g., $^4\text{He}/\text{CH}_4$) or the fractionation of heavy noble gases during the advection of a multi-phase fluid (e.g., Kr and Xe). Thus, a major focus on the current work examines the behavior of noble gases relative to hydrocarbons and the behavior of the heavy noble gases (i.e., Kr and Xe). The newly developed models demonstrate that multiple combinations of post-genetic modification processes can result in the geochemical signatures reported in previous groundwater studies and that these scenarios should be taken into account in future studies that investigate natural gas contamination in shallow groundwater settings.

2.2 Geochemical Background

2.2.1 Hydrocarbons in Shallow Groundwater

Excluding scenarios where mantle-derived or abiotic fluids are geologically relevant, hydrocarbon gases in shallow groundwater typically represent a mixture between microbial methane and natural gas derived from the thermocatalytic cracking of kerogen (catagenesis) (Darrah et al., 2015b; Eymold et al., 2018; Harkness et al., 2017b; Kreuzer et al., 2018). Thermogenic gases typically have C_1/C_{2+} that range from 0.1 to 100 and display a relatively enriched $\delta^{13}\text{C}-\text{CH}_4$ ($>-55\text{‰}$). Both C_1/C_{2+} and $\delta^{13}\text{C}-\text{CH}_4$ increase with increasingly higher temperatures (Faber and Stahl, 1984). In general, the relationship between thermal maturity and molecular and isotopic composition of natural gas is linear and predictable (Faber and Stahl, 1984; Whiticar, 1994).

By comparison, microbes predominantly produce CH₄ resulting in exceedingly high C₁/C₂₊ ratios (>2,000) and isotopically light δ¹³C-CH₄ (<-60‰) (Bernard, 1978; Schoell, 1980, 1983). Microbial CH₄ is also produced at relatively low temperatures (typically much less than 60°C) by either hydrogenotrophic (CO₂ reduction), acetoclastic (acetate fermentation), or methylotrophic methanogens (Whiticar, 1990). The stable isotopic compositions of hydrogen in CH₄ (δ²H-CH₄) are often useful for distinguishing between hydrogenotrophic (δ²H-CH₄ ranges from -250 and -170‰) and acetoclastic (δ²H-CH₄ ranges from -340 and -260‰) methanogenesis (Whiticar, 1990). Methane produced by methylotrophic methanogenesis is poorly characterized, but is thought to yield an intermediate composition (e.g., Vinson et al., 2017).

Following catagenesis, thermogenic hydrocarbons that migrate out of the source formations (primary migration) into overlying reservoirs or aquifers (secondary migration) experience fractionation of the molecular and isotopic components of natural gas. For example, during multi-phase fluid transport, the natural gas experiences kinetic fractionation according to solubility partitioning. In this scenario, [CH₄] is enriched in the gas phase relative to heavier aliphatic hydrocarbons. Similarly, the light stable isotopes of CH₄ (i.e., ¹²CH₄) are enriched in the gas phase relative to either ¹³CH₄, ¹²C¹DH₃, or heavier isotopologues. The degree of fractionation (α-value) is highly dependent upon the species, the physicochemical conditions (e.g., temperature, pressure, salinity), and the mechanisms of migration (Darrah et al., 2015b; Darrah et al., 2014).

The extent of fractionation by solubility partitioning is dependent on the ratio of gas volume to water volume (V_{gas}/V_{water}) (Aeschbach-Hertig et al., 2008; Aeschbach-Hertig et al., 1999; Ballentine et al., 2002; Holoher et al., 2003). Fluids with relatively low V_{gas}/V_{water} experience fractionation that approximates the relative differences in gas solubility, especially at

low temperatures. Conversely, although high $V_{\text{gas}}/V_{\text{water}}$ will preferentially transfer all gas species into the gas-phase, the degree of fractionation approaches zero at infinitely high $V_{\text{gas}}/V_{\text{water}}$.

Diffusion in water can also influence the composition of thermogenic natural gases. The degree of fractionation (α -value) by diffusion is dependent on the relative masses of species, where alpha values are equivalent to the ratio of the square root of the mass of each gas species. Diffusion is controlled by concentration-dependent gradients, which indicates that the influence of this mechanism is typically limited to relatively small distances and can be overwhelmed by the effects of groundwater advection (Darrah et al., 2015b; Norville and Muehlenbachs, 2018).

Following the introduction of a thermogenic gas into a shallow groundwater, its composition can be influenced by gas mixing. For example, mixing with microbial gas can increase the C_1/C_{2+} and lead to more negative $\delta^{13}\text{C-CH}_4$ (Whiticar, 1999; Whiticar et al., 1986). Conversely, mixing between multiple generations of different thermogenic gases, specifically of varying thermal maturity, can be more challenging to delineate (Jenden et al., 1993).

In addition to the introduction of primary microbial methane, microbes can also influence the composition of thermogenic gases by a combination of aerobic oxidation, anaerobic oxidation, and secondary methanogenesis. Aerobic oxidation of thermogenic hydrocarbons occurs when microbes preferentially consume heavier aliphatic hydrocarbons relative to CH_4 in the presence of oxygen or coupled to other processes such as sulfate reduction (Adams et al., 2013; Kniemeyer et al., 2007; Mastalerz et al., 2009). Aerobic oxidation leads to increasing C_1/C_{2+} ratios and more positive $\delta^{13}\text{C-CH}_4$ in the remaining, unoxidized natural gas (Kinnaman et al., 2007). In comparison, anaerobic oxidation typically occurs in anoxic conditions within sulfur-rich marine sediments and affects only CH_4 . Anaerobic oxidation results in an overall decrease in the C_1/C_{2+}

and more positive $\delta^{13}\text{C-CH}_4$ in the remaining, unoxidized natural gas (Kinnaman et al., 2007; Whiticar et al., 1986).

In relatively closed hydrogeologic systems, primary methanogenesis and microbial oxidation should result in coupled changes between $\delta^{13}\text{C-CH}_4$ and $\delta^{13}\text{C}$ of the substrate or $\delta^{13}\text{C-CO}_2$ (Whiticar, 1999; Whiticar et al., 1986). As discussed above, aerobic oxidation leads to an increase of the $\delta^{13}\text{C-CH}_4$ in the remaining, unoxidized natural gas. Importantly, because the oxidization of natural gas preferentially selects the light $\delta^{13}\text{C-CH}_4$, the CO_2 that is produced has a more negative $\delta^{13}\text{C-CO}_2$ than the bulk composition of heavier aliphatic hydrocarbons and is equivalent to the $\delta^{13}\text{C}$ of the oxidized compounds; these reactions also increase the [DIC] as the proportion of the newly formed CO_2 equilibrates with water. During methanogenesis, the extent of fractionation between $\delta^{13}\text{C-CH}_4$ and $\delta^{13}\text{C-substrate}$ is dependent on the metabolic pathway and the starting $\delta^{13}\text{C}$ of the carbon substrate (Whiticar et al., 1986). Because microbes preferentially utilize ^{12}C relative to ^{13}C during methanogenesis, microbial CH_4 will start isotopically light and will be progressively enriched as the amount of substrate remaining (which itself gets progressively isotopically heavier) decreases (Whiticar, 1999).

2.2.2 Secondary Methanogenesis and Noble Gases

Secondary methanogenesis refers to the sequential microbial oxidation of wet hydrocarbon gases or oil to form CO_2 , which is then utilized by hydrogenotrophic methanogens to form CH_4 (Scott et al., 1994; Sweeney and Taylor, 1999). While these paired processes of microbial degradation and methanogenesis have been used to explain isotopically heavy $\delta^{13}\text{C-CO}_2$ (>0‰) in some oil reservoirs and thermogenic gas seeps (Dessort et al., 2003; Etiope et al., 2009; Milkov

and Dzou, 2007; Pallasser, 2000), the importance of secondary methanogenesis in shallow groundwater systems has not been test thoroughly.

Aerobic or sulfate reduction-paired oxidation of wet hydrocarbons or oils will preferentially degrade heavier hydrocarbon compounds (C_2H_6+) and lighter isotopes (e.g., ^{12}C or 1H) relative to their heavier counterparts (e.g., ^{13}C or 2H) prior to their incorporation into CH_4 . As a result, the newly formed $\delta^{13}C-CO_2$ following oxidation will reflect mixing between the $\delta^{13}C$ of the oxidized compounds, which is itself a mixture of the amount of each compound that was consumed, and the original CO_2 in equilibrium with DIC. During oxidation, the C_1/C_{2+} will initially increase proportionally to the amount of C_2H_6+ that is consumed during oxidation. Once hydrogenotrophic methanogens convert CO_2 to CH_4 (secondary methanogenesis), the C_1/C_{2+} will further increase. It has been hypothesized that secondary microbial gas has intermediate C_1/C_{2+} ratios (between 1,000 and 10,000) and slightly enriched $\delta^{13}C-CH_4$ compared to primary microbial gas (between -60‰ and -40‰) (Milkov and Etiope, 2018). This chemical composition overlaps mixing between a migrated thermogenic hydrocarbon gas and primary microbial gas as well as mixing between thermogenic gas and “late-stage methanogenesis,” where extensive methanogenesis leads to enrichment in $\delta^{13}C-CH_4$ of the microbial CH_4 (Bordeleau et al., 2018a; Whiticar et al., 1986).

Due to the difficulty in identifying post-genetic modification and migration mechanisms using hydrocarbon molecular ratios and stable isotopes alone, recent studies in the Appalachian (Darrah et al., 2015b; Harkness et al., 2017b; Kreuzer et al., 2018), Illinois (Moore et al., 2018), Michigan (Wen et al., 2015; Wen et al., 2016a), and Fort Worth Basins (Darrah et al., 2014; Wen et al., 2016b; Wen et al., 2017) in the US, and the Karoo Basin in South Africa (Eymold et al.,

2018) have integrated noble gas elemental and isotopic ratios. Because they are chemically inert and their abundances and production in the atmosphere, hydrosphere, and crust are well understood, noble gases represent an ideal set of tracers for understanding the post-genetic evolution of hydrocarbon gases in groundwater. Particularly useful are the abundances of helium and the atmospherically-derived noble gases (e.g., ^{20}Ne , ^{36}Ar , ^{84}Kr).

Helium-4 is produced by the radioactive decay of uranium and thorium and can diffuse out of mineral grains and into pore fluids at geologically relevant temperatures ($>15^\circ\text{C}$ (Ballentine and Burnard, 2002; Hunt et al., 2012)). These characteristics make [^4He] a useful tool for estimating fluid (e.g., groundwater) residence times in the subsurface (Solomon et al., 1996). Additionally, because oxidation would only affect CH_4 and methanogenesis does not produce He, the $^4\text{He}/\text{CH}_4$ ratio has can be utilized to identify mixing with microbial gases and oxidation in shallow groundwater (Darrah et al., 2014; Moore et al., 2018).

Atmospherically-derived noble gas isotopes (e.g., ^{20}Ne , ^{36}Ar , ^{84}Kr) are incorporated into pore fluids at sediment burial and groundwater at recharge (termed air-saturated water or ASW). The concentrations of atmospherically-derived noble gases at solubility equilibrium can be predicted with reasonable certainty as a function of temperature, salinity, and pressure (i.e., elevation) (Smith and Kennedy, 1983; Weiss, 1970, 1971; Weiss and Kyser, 1978). In general, solubility of the individual noble gas species increases with increasing atomic mass ($^4\text{He} < ^{20}\text{Ne} < ^{36}\text{Ar} < ^{84}\text{Kr}$).

During the migration of a thermogenic gas, noble gas isotopes will fractionate in a similar manner to hydrocarbon molecules and stable isotopes. In the presence of free gas, the lighter isotopes (^4He , ^{20}Ne) will be enriched in the gas-phase, while heavier isotopes (^{36}Ar , ^{84}Kr) will

preferentially remain in the water phase (Darrah et al., 2015b; Darrah et al., 2014). These phenomena are commonly observed in scenarios in which multi-phase (gas plus water) migration occurs. If gas-water partitioning occurs during migration, the migrating gas phase will strip the dissolved noble gases out of the water phase and into the migrating gas phase. These scenarios were numerically modeled by Gilfillan et al. (2008) and Gilfillan et al. (2009) using an open-system Rayleigh Fractionation model for CO₂. This model was adapted to hydrocarbons by Darrah et al. (2014; 2015b). The assumptions and calculations involved in this model are explained in detail in Section 2.3.1.

Because of their chemically inert nature, noble gases retain evidence of prior instances of fractionation independent of oxidation or secondary methanogenesis. As a result, noble gases have the potential to be important tracers for these post-genetic modification processes in shallow groundwater.

2.3 Numerical Modeling Methods

I developed numerical models to predict, quantify, and illustrate how post-genetic modification influences the hydrocarbon molecular (C₁/C₂+), stable isotope ($\delta^{13}\text{C-CH}_4$, $\delta^2\text{H-CH}_4$), and noble gas composition ($^{20}\text{Ne}/^{36}\text{Ar}$, $^{84}\text{Kr}/^{36}\text{Ar}$, $^4\text{He}/\text{CH}_4$) of natural gas during transport to and residence within a shallow aquifer. Specifically, I evaluated these factors using several representative initial natural gas compositions and models for how multi-phase (gas plus brine) mixing, advection, diffusion, aerobic oxidation, anaerobic CH₄ oxidation, and secondary methanogenesis processes affect the resulting gas composition.

Because of the extensive interest in natural gas contamination in groundwater aquifers overlying the Marcellus Shale (e.g., Darrah et al., 2015b; Darrah et al., 2014; Harkness et al.,

2017b; Jackson et al., 2013; Molofsky et al., 2013; Osborn et al., 2011; Warner et al., 2012) and the presence of ample data sets from this region (Darrah et al., 2014; Hunt et al., 2012; Jenden et al., 1993), I first modelled how a theoretical natural gas with a composition analogous to Marcellus Shale production gas from northeastern Pennsylvania would be altered by the aforementioned post-genetic modification processes. Marcellus-like production gases are consistent with a dry hydrocarbon gas that is typical of natural gas produced from a marine (Type II kerogen) black shale (see Table 2.1).

In geologic settings where thermogenic hydrocarbons have naturally migrated to shallow aquifers such as in the Northern Appalachian Basin, the distance between source rock and drinking-water aquifer can be more than 2000m. These distances make it difficult to envision a scenario where the migrating gas volume has not been fractionated in anyway (see Darrah et al. (2015b) or Harkness et al. (2017b)) unless large volumes of gas were released along well annuli or leaking well casings without interaction with the water-saturated crust. Therefore, the models produced here are more similar to scenarios of fugitive gas contamination where thermogenic gas leaks directly into shallow aquifers and is assumed to experience little fractionation due to migration processes as described in Darrah et al. (2014).

In addition to the Marcellus-like thermogenic endmember, two microbial endmembers are considered. These include microbial methane produced during hydrogenotrophic (CO₂ reduction) and acetoclastic (acetate fermentation) methanogenesis (Whiticar, 1994). The hydrocarbon molecular and stable isotopic ($\delta^{13}\text{C-CH}_4$, $\delta^2\text{H-CH}_4$) ratios used in the mixing models for hydrogenotrophic and acetoclastic methanogenesis in Figure 2.2 are based from Schoell (1983)

Table 2.1. Endmember Compositions

Gas	[CH ₄]	[C ₂ H ₆]	[C ₃ H ₈]	[C ₄ H ₁₀]	$\frac{\text{CH}_4}{\text{C}_2\text{H}_6}$	$\frac{\text{CH}_4}{\text{C}_3\text{H}_8}$	$\delta^{13}\text{C}-\text{CH}_4$	$\delta^{13}\text{C}-\text{C}_2\text{H}_6$	$\delta^{13}\text{C}-\text{C}_3\text{H}_8$	$\delta^{13}\text{C}-\text{C}_4\text{H}_{10}$	$\delta^2\text{H}-\text{CH}_4$	$\delta^2\text{H}-\text{C}_2\text{H}_6$	$\delta^2\text{H}-\text{C}_3\text{H}_8$	$\frac{^4\text{He}}{\text{CH}_4}$	$\frac{^{20}\text{Ne}}{^{36}\text{Ar}}$	$\frac{^{84}\text{Kr}}{^{36}\text{Ar}}$
	(%)	(%)	(%)	(%)	(%)	(%)	(‰)	(‰)	(‰)	(‰)	(‰)	(‰)	(‰)	x10 ⁻⁶		
Thermogenic	96.8	1.49	0.039	0.014	62.7	-35.8	-41	-39	-30	-160	-130	-120	250	0.14	0.039	
Microbial (Hydrogenotrophic)	99.99	0.01			10,000	-75				-190				0.14	0.039	
Microbial (Acetoclastic)	99.95	0.05			2,000	-60				-325				0.14	0.039	

and Whiticar (1994) and are as follows: $C_1/C_{2+} = 10,000$; $\delta^{13}\text{C-CH}_4 = -75\text{‰}$ and $\delta^2\text{H-CH}_4 = -190\text{‰}$, and $C_1/C_{2+} = 2,000$; $\delta^{13}\text{C-CH}_4 = -60\text{‰}$ and $\delta^2\text{H-CH}_4 = -325\text{‰}$, respectively (Table 2.1).

All initial groundwater conditions for the atmospherically-derived noble gases (^{20}Ne , ^{36}Ar , ^{84}Kr) are assumed to be consistent with ASW based on the conditions of local aquifers. Using conditions consistent with northeastern Pennsylvania overlying the Marcellus Fairway, air-saturated water equilibration is assumed to have occurred at temperatures of 10°C , a salinity of 0.1‰ , and at an average elevation of 600m. The complete geochemical composition of the endmembers used can be found in Table 2.1.

2.3.1 Advection

In all modeling scenarios, I assume that multi-phase (gas plus water/brine) advection (light blue dashed lines in all figures) occurs according to a gas stripping and re-dissolution model (GSS-R). The GSS-R model was originally developed for CO_2 (Gilfillan et al., 2008; Gilfillan et al., 2009) and adapted for hydrocarbons (Darrah et al., 2015b; Darrah et al., 2014). This modelling approach has been utilized in many previous studies that examine post-genetic modification of natural gases by multi-phase fluid advection (Eymold et al., 2018; Harkness et al., 2017b; Kreuzer et al., 2018; Moore et al., 2018; Wen et al., 2016b; Wen et al., 2017; Woda et al., 2018). The models I developed assume that gas transport is initiated when natural gas pressures exceed local depth- and salinity-dependent saturation levels (also termed “bubble point”) of the water (Darrah et al., 2015b). Natural gas pressures can exceed the bubble point in water when catagenesis produces thermogenic natural gas, microbes produce sufficient volumes of methane, or when exogenous sources of higher-pressure gas are introduced to shallow aquifers (e.g., the release of

fugitive gas). In any of these scenarios, the free gas phase will buoyantly migrate upwards through the water-saturated crust into shallow formations.

The formation of a gas phase will allow individual gas species to partition between the gas phase and water according to the Bunsen solubility coefficients (β_x) of each gas species and the *in situ* ratio of gas volume to water volume ($V_{\text{gas}}/V_{\text{water}}$) (Aeschbach-Hertig et al., 2008; Aeschbach-Hertig et al., 1999; Ballentine et al., 2002; Holocher et al., 2003). The Bunsen solubility coefficient is defined as the ratio of dissolved gas volume per volume of solution when the partial pressure of gas is 1 atmosphere, following Equation 2.1:

$$\beta_x = [X_{\text{atm}}]/[X_{\text{water}}] \quad (2.1)$$

The partition coefficient between two gas constituents, termed alpha (α), is calculated as the ratio of the respective Bunsen coefficients (β_x/β_y) for each individual gas where x and y are two different gas species.

In general, the solubility of each gas species increases with increasing atomic and molecular mass (${}^4\text{He} < {}^{20}\text{Ne} < {}^{36}\text{Ar} = \text{CH}_4 < {}^{84}\text{Kr}$, ${}^{12}\text{CH}_4 < {}^{13}\text{CH}_4 < \text{C}_2\text{H}_6$) (Ballentine et al., 2002; Fuex, 1980; Kipfer et al., 2002; Smith and Kennedy, 1983; Weiss, 1970, 1971; Weiss and Kyser, 1978). The less soluble and typically lighter constituents (e.g., ${}^4\text{He}$, ${}^{20}\text{Ne}$, ${}^{12}\text{CH}_4$) will be preferentially enriched in the gas phase, while the larger masses (e.g., ${}^{36}\text{Ar}$, ${}^{84}\text{Kr}$, ${}^{13}\text{CH}_4$, C_2H_6) remain in the liquid phase. When gas migrates as a free gas phase in the water-saturated crust, especially within groundwater that is not already saturated with natural gas, the composition of the natural gas is fractionated by phase partitioning.

The extent of fractionation between two gas constituents is largely dependent on the $V_{\text{gas}}/V_{\text{water}}$, where the maximum fractionation (α) occurs as $V_{\text{gas}}/V_{\text{water}}$ approaches zero. In

comparison, the relative compositions of gas constituents in the gas phase will get progressively closer to the original groundwater or brine composition when $V_{\text{gas}}/V_{\text{water}}$ approaches infinity as all of the gases will partition into the gas phase without quantifiable fractionation. This type of fractionation is described using the equation for closed-system Rayleigh fractionation (Equation 2.2):

$$(A/B)_{\text{groundwater}} = (A/B)_0 * f^{(\alpha-1)} \quad (2.2)$$

Where $(A/B)_{\text{groundwater}}$ is the resulting isotopic or molecular ratio, $(A/B)_0$ is the original ratio between dissolved gases A and B in the groundwater, f is the fraction (from 1 to 0) of B remaining in the water phase, and α is the alpha value that defined the degree of fractionation that occurs between the two constituents during gas-water partitioning (Zhou et al., 2012).

In a one-stage model where gas is “stripped” from the water phase into the gas phase, the maximum fractionation possible between two gas constituents would not exceed the α value. However, because the ratios of atmospheric noble gases in many crustal fluids have been observed to exceed the maximum degree of fractionation predicted for one-stage (closed-system) of gas partitioning according to Rayleigh fractionation (e.g., Darrah et al., 2015b; Harkness et al., 2017b; Moore et al., 2018; Zhou et al., 2012) an open-system Rayleigh fractionation model is thought to better describe the process of gas-water partitioning during multiple-stage advective fluid transport (Darrah et al., 2015b; Zhou et al., 2012). The open-system Rayleigh fractionation model suggests that a buoyantly migrating gas would experience fractionation of noble gases, hydrocarbon molecular ratios, and hydrocarbon stable isotopic ratios.

In scenarios in which the volume of natural gas reached overlying formations where the *in situ* dissolved gas concentrations were below the saturation point, gases may re-dissolve into the

groundwater according to open-system Rayleigh fractionation. This process results in a dissolved gas composition that is fractionated relative to air-equilibrated water (e.g., $^{20}\text{Ne}/^{36}\text{Ar} > \text{ASW}$). If this processes occurred in multiple stages of dissolution and exsolution during gas transport, the migrating gas phase would be significantly more fractionated ($^{20}\text{Ne}/^{36}\text{Ar} \gg \text{ASW}$) with respect to ASW values than those observed in a one-stage process.

The solubilities used in the GSS-R model to quantify the degree of fractionation for noble gases were calculated using Weiss (1970), Weiss (1971), and Weiss and Kyser (1978), while the partition coefficients were calculated from Smith and Kennedy (1983) and are shown in Table 2.2. Partition coefficients between hydrocarbon molecules ($\text{C}_1\text{-C}_4$) and stable isotopes ($^{12}\text{CH}_4$ and $^{13}\text{CH}_4$, $\text{C}^2\text{H}^1\text{H}_3$ and C^1H_4) were calculated using Fuex (1980) (Table 2.2). Because the partition coefficients between CH_4 and each heavier hydrocarbon molecule are different, the Rayleigh Fractionation equation is applied to C_1/C_2 , C_1/C_3 , and C_1/C_4 separately and the final result is taken as the inverse sum and expressed in Equation 2.3:

$$(A/B) = 1/[1/(A/B)_1 + 1/(A/B)_2 + 1/(A/B)_3 \dots 1/(A/B)_x] \quad (2.3)$$

where $(A/B)_{1-x}$ are the Rayleigh Fractionation results for C_1/C_2 , C_1/C_3 , C_1/C_4 , etc., respectively.

Rayleigh Fractionation calculations for all numerical models of stable isotope fractionation first requires conversion of the delta notation to a decimal value in which 1.0 is 0‰. After modelling was completed, I then converted decimal values back to the familiar delta notation using Equation 2.4:

$$\delta^{13}\text{C} (\text{‰}) = (I - 1) * 1000 \quad (2.4)$$

where I is the residual isotopic value following fractionation in decimal notation.

Because the exact timing and thermal history of natural gas migration in the subsurface is often difficult to constrain, especially for naturally-occurring gas contamination, I modeled partition coefficients across a range of temperatures for the modeling of a variety of tracers (e.g., $^4\text{He}/\text{CH}_4$, $^{20}\text{Ne}/^{36}\text{Ar}$). All other advection models use α -values at an equilibration temperature of 25°C because there is a lack of temperature-dependent calibration of partition coefficients for stable isotopes and hydrocarbon gas species heavier than propane. With all advection models, the composition of residual groundwater phases were also modeled to illustrate the effects of groundwater that remains following degassing. The residual groundwater phases were modeled using the inverse of the partitioning coefficient for multi-phase advection.

2.3.2 Diffusion

Diffusion (red dashed line in all figures) was modeled using the same initial starting composition described above and assumes that a hydrocarbon-rich gas diffused into groundwater consistent with previously developed models Darrah et al. (2015b). Similar to multi-phase advection, all diffusion models were produced using Equation 2. The relative fractionation factors (α) between any two constituents were calculated using ratios of the square roots of their masses ($\alpha = D_x/D_y$, where $D_x = \text{sqrt}(M_x)$ and $D_y = \text{sqrt}(M_y)$), following methods described previously (Darrah et al., 2015b). Diffusional fractionation α -values for stable isotopes were modelled assuming the addition of either ^{13}C or one ^2H . While temperature will influence the rate of bulk diffusion, the relative fractionation between any two constituents is anticipated to be constant across all temperatures. As a result, I did not model diffusion fractionation across a range of temperatures (Table 2.2).

Table 2.2. Partition and Diffusion Coefficients (α)

Gas Constituent	Advection Equilibration Temperature (°C)	Multi-Phase Advection	Multi-Phase Advection Residual	Diffusion	Diffusion Residual
CH ₄ /C ₂ H ₆	25	0.3964	2.5227	0.7303	1.3693
CH ₄ /C ₃ H ₈	25	0.5667	1.7646	0.603	1.6584
CH ₄ /C ₄ H ₁₀	25	0.6667	1.4999	0.5252	1.904
¹² CH ₄ / ¹³ CH ₄	25	1.0005	0.9995	1.03	0.9709
C ¹ H ₄ /CDH ₃	25	1.0005	0.9995	1.03	0.9709
⁴ He/CH ₄	25	0.2797	3.5753	0.5	2
	75	0.4966	2.0137		
	100	0.595	1.6807		
	150	0.7551	1.3243		
	200	0.8655	1.1554		
²⁰ Ne/ ³⁶ Ar	25	0.3237	3.0893	0.7487	1.3356
	75	0.4879	2.0496		
	100	0.5478	1.8255		
	150	0.6226	1.6062		
	200	0.6509	1.5363		
⁸⁴ Kr/ ³⁶ Ar	25	1.8046	0.5541	1.5257	0.6554
	100	1.4671	0.6816		
	150	1.3159	0.7599		
	200	1.1773	0.8494		

2.3.3 Microbial Oxidation

Microbially-induced aerobic oxidation (gray dashed line in all figures) and anaerobic CH₄ oxidation (yellow dashed line in all figures) were modeled assuming a Marcellus-like natural gas endmember consistent with that described above. All oxidation models assume a closed hydrogeologic system that can be described by Rayleigh distillation (Equation 2). The fractionation factors (α) resulting from the differential rates of degradation between CH₄ and higher order aliphatic hydrocarbons during aerobic oxidation are taken from Kinnaman et al.

(2007). During aerobic oxidation, ethane (C₂H₆), propane (C₃H₈), butane (C₄H₁₀), etc. are preferentially consumed before CH₄ in a hydrocarbon mixture (Table 2.3). Similar to solubility partitioning during multi-phase advection, the efficiency at which microbes consume ethane, propane, and heavier aliphatic hydrocarbons, differ for each compound. As a result, I calculate the Rayleigh Fractionation of various hydrocarbons separately for C₁/C₂, C₁/C₃, and C₁/C₄. The results are then summed using Equation 3 to produce the C₁/C₂₊ ratio. In anaerobic CH₄ oxidation, only CH₄ is consumed (Whiticar et al., 1986), so simply using *f* to represent the fraction of the total [CH₄] consumed is adequate for calculating the residual C₁/C₂₊ (Table 2.3).

Table 2.3. Fractionation Factors of Oxidation (α)

Gas Constituent	Aerobic Oxidation	Anaerobic Oxidation
CH₄/C₂H₆	0.0541	
CH₄/C₃H₈	0.0057	
CH₄/C₄H₁₀	0.008	
$\delta^{13}\text{C-CH}_4$	0.9735	0.9921
$\delta^{13}\text{C-C}_2\text{H}_6$	0.992	
$\delta^{13}\text{C-C}_3\text{H}_8$	0.9952	
$\delta^{13}\text{C-C}_4\text{H}_{10}$	0.9971	
$\delta^2\text{H-CH}_4$	0.7619	0.7619
$\delta^2\text{H-C}_2\text{H}_6$	0.938	
$\delta^2\text{H-C}_3\text{H}_8$	0.9849	
⁴He/CH₄	1.00E-06	1.00E-06

The stable isotopic compositions are calculated using α values between $\delta^{13}\text{C-CH}_4$ and $\delta^{13}\text{C-CO}_2$ for both aerobic and anaerobic oxidation, which both result in an increase in the $\delta^{13}\text{C-CH}_4$ of the residual CH₄. The α -values for aerobic oxidation were taken from Kinnaman et al. (2007) and

include $\delta^{13}\text{C}$ and $\delta^2\text{H}$ while the α -values for anaerobic oxidation were taken from Whiticar et al. (1986) and only includes $\delta^{13}\text{C}$. These α -values are reported in Table 2.3.

To model microbial oxidation while integrating noble gas chemistry (e.g., $^4\text{He}/\text{CH}_4$), it is assumed that only the $[\text{CH}_4]$ will change because noble gases are chemically inert (Darrah et al., 2014). Therefore, the fractionation factor between ^4He and CH_4 is infinitely large. For the purpose of the model, an enrichment factor of 1×10^6 is used (i.e., $\alpha = 1/1,000,000$), which would generally be in the range of lowest detectable CH_4 concentrations following nearly complete oxidation.

2.3.4 Secondary Methanogenesis

Secondary methanogenesis is suggested to occur when a wet hydrocarbon gas or oil is oxidized by microbes to form CO_2 , which is subsequently converted to CH_4 via hydrogenotrophic methanogenesis (CO_2 reduction). For these models, it is assumed that the CO_2 pool utilized during methanogenesis is only that which resulted from the aerobic microbial oxidation of the thermogenic hydrocarbon gas compounds and that the local groundwater systems contain sufficiently high levels of oxidizers (e.g., O_2 , SO_4) to allow aerobic oxidation to run to completion.

In this model, the composition of CH_4 formed by secondary methanogenesis is directly dependent on the initial composition of hydrocarbon compounds available to be oxidized. The volume of CH_4 that can be produced during secondary methanogenesis can be calculated from the original composition of the thermogenic gas (Table 2.1). For example, the carbon from 1 mole of thermogenic CH_4 , C_2H_6 , C_3H_8 , and C_4H_{10} can be converted into 1, 2, 3, and 4 moles of microbial CH_4 , respectively, if all carbon is converted to methane without dissolution into pore waters. The proportions of hydrocarbon compounds that are converted to CO_2 during aerobic oxidation compared to the amount of gas still available (f), and thus the carbon available to generate

secondary microbial CH₄, can be calculated using the Rayleigh Fractionation reactions of the individual hydrocarbon compounds (Kinnaman et al., 2007). Although studies have shown that C₃H₈ is preferentially oxidized first during aerobic oxidation and is followed by other C₂H₆+ hydrocarbons before CH₄ (e.g., Boreham et al., 2001; Kinnaman et al., 2007), the absolute rates of oxidation in natural settings is difficult to quantify. Therefore, I assume oxidation occurs at rates proportional to the α -values for C₁-C₄ hydrocarbons. As aerobic oxidation proceeds (f), the [C₂H₆+] decreases while the [CH₄] increases proportionally due to the addition of secondary microbial CH₄. This process is used to model the C₁/C₂+ ratio and to calculate the amount of CH₄ that would be added to the ⁴He/CH₄ ratio during secondary methanogenesis, which like oxidation only affects the [CH₄].

In comparison, the $\delta^{13}\text{C-CH}_4$ that results from secondary methanogenesis represents a complex mixture of: 1) the original $\delta^{13}\text{C}$ of the carbon pool; 2) the $\delta^{13}\text{C}$ of the oxidized hydrocarbon compounds, which vary due to different α -values between $\delta^{13}\text{C-C}_x$ and $\delta^{13}\text{C-CO}_2$; 3) the weighted proportion of each compound that is oxidized, which also varies as a result of the different efficiencies for which microbes degrade specific hydrocarbons; 4) the fraction of the total thermogenic gas volume that is oxidized (f); and 5) the efficiency that microbes utilize the newly produced CO₂ to generate new CH₄ (Kinnaman et al., 2007; Vinson et al., 2017).

Because the $\delta^{13}\text{C-C}_x$ of the C₂H₆+ components of thermogenic gases are typically more positive than the $\delta^{13}\text{C-CH}_4$ (at least in gases that do not experience isotopic reversals, e.g., Burruss and Laughrey (2010), Tilley and Muehlenbachs (2013), Zumberge et al. (2012)), the oxidization of C₂H₆+ hydrocarbons to CO₂ followed by methanogenesis will lead to more positive $\delta^{13}\text{C-CH}_4$ in the resulting mixture. However, because microbes preferentially utilize isotopically light carbon

(¹²C) during oxidation and methanogenesis, partial oxidation or partial utilization of the CO₂ during methanogenesis will shift the δ¹³C-CH₄ of newly formed methane in a more negative direction than the original isotopic mixture (δ¹³C-C_x) of the C₂H₆+ components.

The model produced herein assumes closed-system conditions and complete aerobic oxidation of C₁-C₄ hydrocarbons followed immediately by secondary methanogenesis. More specifically, it is assumed that the CO₂ that results from the aerobic oxidation of hydrocarbons is immediately and completely converted back to secondary microbial CH₄ with each change in *f*. The α-values for δ¹³C-C₁₋₄ were taken from Kinnaman et al. (2007) for a hydrocarbon mixture. At each stage of aerobic oxidation, the stable isotopic composition in decimal notation (I_{C_x}) of the oxidized portion of hydrocarbon compound C_x is calculated using Equation 2.5:

$$I_{C_x} = [I_0 - (I_{ox} * f)] / (1-f) \quad (2.5)$$

Where I_{ox} is the residual stable isotopic composition of hydrocarbon C_x following aerobic oxidation (Equation 2), and I₀ is the original stable isotopic composition of the hydrocarbon C_x. The stable isotopic composition for newly formed CH₄ generated by secondary methanogenesis (I_{secondary}) can then be calculated by multiplying I_{C_x} by the respective proportions of carbon produced during oxidation of C₁₋₄ hydrocarbon compounds and taking the sum according to Equation 2.6:

$$I_{secondary} = \sum(Pmol_{C_x} * I_{C_x}) \quad (2.6)$$

Where Pmol_{C_x} is the fraction of moles of carbon in the mixture derived from a given hydrocarbon species C_x, and I_{C_x} is the stable isotopic value calculated for that hydrocarbon species in Equation 2.5.

The final result for the $\delta^{13}\text{C}\text{-CH}_4$ generated during secondary methanogenesis is described using a mixing equation between the original CH_4 and the newly formed CH_4 following the additional of secondary microbial gas according to Equation 2.7:

$$I_M = [\text{CH}_4]_{\text{original}}/[\text{CH}_4]_{\text{secondary}} * I_0 + (1 - [\text{CH}_4]_{\text{original}}/[\text{CH}_4]_{\text{secondary}}) * I_{\text{secondary}} \quad (2.7)$$

Where I_M is the resulting stable isotopic composition following mixing between secondary CH_4 and the original thermogenic CH_4 in decimal notation, I_0 is the original measured stable isotopic composition of CH_4 , $I_{\text{secondary}}$ is the stable isotopic composition calculated in Equation 2.6, $[\text{CH}_4]_{\text{original}}$ is the original abundance of CH_4 , and $[\text{CH}_4]_{\text{secondary}}$ is the new total CH_4 following the addition of secondary microbial gas.

This method is replicated to calculate the $\delta^2\text{H}\text{-CH}_4$ formed by secondary methanogenesis. The moles of CH_4 that can be produced based on the moles of H liberated by aerobic oxidation of one mole of CH_4 , C_2H_6 , and C_3H_8 , respectively, are 1, 1, and 2, respectively. For example, without other sources of hydrogen available for microbes to utilize in the generation of CH_4 , the oxidation of C_2H_6 would result in an excess of two hydrogen atoms and one carbon atom. However, the utilization of excess C and H are not investigated as part of this work. Therefore, the imperfect conversion of thermogenic H to microbial CH_4 should be treated qualitatively.

2.3.5 Mixing with Primary Microbial Gas

Two-component mixing models (blue dashed lines in all figures) have been calculated between the thermogenic endmember and microbial gases produced from hydrogenotrophic (CO_2 reduction) and acetoclastic (acetate fermentation) methanogenesis using simple two-component mixing for hydrocarbon molecular and noble isotopic ratios following Equation 2.8. Equation 2.8 can also be used to calculate mixing between any two gas components (mixing of CH_4 formed by

hydrogenotrophic (CO₂ reduction) and acetoclastic (acetate fermentation) processes or mixing between two thermogenic natural gases. Equation 2.8 is described as:

$$[M] = [A] * (f) + [B] * (f-1) \quad (2.8)$$

where A and B are the composition of the two gas constituents, M is the resulting mixture, and *f* is the fraction of each component. The molecular (C₁/C₂₊) and stable isotopic (δ¹³C-CH₄, δ²H-CH₄) ratios used in the mixing models for hydrogenotrophic and acetoclastic methanogenesis in Figure 2.2 are based from Schoell (1983) and Whiticar (1994) and are reported in Table 2.1.

In all models it is assumed that the microbial endmembers have noble gases concentrations and ratios that are equal to solubility equilibrium with the atmosphere (Weiss, 1970, 1971; Weiss and Kyser, 1978). Where mixing is modeled between the thermogenic endmember that has already experienced solubility partitioning due to multi-phase advection and a microbial endmember (Figures 2.3, 2.6-2.8). The ²⁰Ne/³⁶Ar value was chosen arbitrarily along the fractionation trend for illustrative purposes.

2.3.6 Applying Models to Published Datasets

The models produced in this study were then applied to a compilation of published groundwater studies (Darrah et al., 2015b; Darrah et al., 2014; Harkness et al., 2017b; Nicot et al., 2017c; Wen et al., 2016b; Wen et al., 2017) that examined the geochemistry of groundwater in aquifers overlying shales targeted for unconventional energy development in the Appalachian and Fort Worth basins. In all figures where these data are included, samples from the Appalachian Basin are represented by diamonds (Darrah et al., 2014), squares (Darrah et al., 2015b), and circles (Harkness et al., 2017b). Data published from the Fort Worth Basin are represented by upward triangles (Darrah et al., 2014), downward triangles (Nicot et al., 2017c), hexagons (Wen et al.,

2016b), and stars (Wen et al., 2017). The symbol color in figures with published data represent the measured degree of fractionation (α) between ^{20}Ne and ^{36}Ar from near ASW (blue) to significantly fractionated (red).

2.4 Results

The numerical modeling outputs that evaluate the influence of post-genetic modification processes on hydrocarbon molecular and stable isotopic compositions (C_1/C_2+ , $\delta^{13}\text{C}-\text{CH}_4$, $\delta^2\text{H}-\text{CH}_4$) and noble gas elemental and isotopic compositions ($^4\text{He}/\text{CH}_4$, $^{20}\text{Ne}/^{36}\text{Ar}$, $^{84}\text{Kr}/^{36}\text{Ar}$) of a Marcellus-like natural gas in shallow groundwater are presented in Figures 2.1-2.7. Figures are designed such that modelling outputs are first illustrated by quantifying the possible influences of post-genetic modification for a theoretical gas from the Marcellus region (A, top) and then applied to published data (B, bottom).

Select values of each numerical model using the hypothetical thermogenic, hydrogenotrophic microbial, and acetoclastic microbial gases (starting compositions outlined in Table 2.1) endmembers are reported in Tables 2.4-5 by proportion of reaction (f). These fractions include 0.80, 0.50, 0.20, and 0.01 of the extent by which Rayleigh Fractionation (i.e., 20%, 50%, 80%, and 99% of the reaction, respectively) alters the original composition (Tables 2.4-5). In all figures, multi-phase (free gas migrating through water and/or the migration of gas plus water) advection, diffusion, and residual water phases from these processes are represented by dashed light blue, dashed red, dotted light blue, and dotted red lines, respectively. Aerobic and anaerobic oxidation are represented by dashed gray and yellow lines, respectively, while mixing with microbial gases or old groundwater are shown as dashed blue lines. Secondary methanogenesis is

Table 2.4. Select Hydrocarbon Results from Numerical Models

Model	<i>f</i>	$\frac{\text{CH}_4}{\text{C}_2\text{H}_6+}$	$\delta^{13}\text{C}-\text{CH}_4$	$\delta^2\text{H}-\text{CH}_4$
			(‰)	(‰)
Advection Equilibration Temperature (°C)		25.0	25	25
Multi-Phase Advection	0.80	71.1	-35.9	-171.1
	0.50	93.7	-36.1	-195.0
	0.20	159	-36.6	-239.0
	0.01	908	-38.0	-368.5
Multi-Phase Advection Residual Phase	0.80	46.0	-34.8	-149.4
	0.50	23.0	-32.6	-125.7
	0.20	6.0	-28.3	-78.3
	0.01	0.1	-13.9	98.5
Diffusion	0.80	66.5	-41.9	-165.3
	0.50	75.5	-55.1	-176.8
	0.20	96.2	-79.9	-198.4
	0.01	215	-157.8	-266.3
Diffusion Residual Phase	0.80	57.6	-29.7	-154.8
	0.50	48.1	-16.1	-143.4
	0.20	33.7	10.4	-120.9
	0.01	9.8	103.9	-42.1
Mixing with Acetoclastic Methanogenesis	0.80	79.2	-40.7	-193.4
	0.50	124	-48.0	-243.1
	0.20	285	-55.2	-292.4
	0.01	1.54E+03	-59.8	-323.4
Mixing with Hydrogenotrophic Methanogenesis	0.80	79.7	-43.7	-166.1
	0.50	128	-55.6	-175.1
	0.20	314	-67.3	-184.1
	0.01	3.94E+03	-74.6	-189.7
Aerobic Oxidation	0.80	76.6	-30.4	-149.0
	0.50	119	-18.4	-124.2
	0.20	275	4.9	-74.7
	0.01	4.50E+03	86.6	111.0
Anaerobic Oxidation	0.80	50.2	-34.2	
	0.50	31.4	-30.6	
	0.20	12.5	-23.8	
	0.01	0.6	-0.7	
Secondary Methanogenesis	0.80	77.5	-35.9	-160.5
	0.50	122	-36.1	-161.1
	0.20	289	-36.1	-161.2
	0.01	3.46E+03	-35.8	-160.2

Table 2.5. Select Noble Gas Isotopic Results from Numerical Models

Model	<i>f</i>	$\frac{^4\text{He}}{\text{CH}_4}$ $\times 10^{-6}$				$\frac{^{20}\text{Ne}}{^{36}\text{Ar}}$				$\frac{^{84}\text{Kr}}{^{36}\text{Ar}}$					
		25	75	100	150	200	25	75	100	150	200	25	100	150	200
Advection Equilibration Temperature (°C)	0.80	2.91E+02	2.78E+02	2.72E+02	2.63E+02	2.57E+02	0.161	0.156	0.154	0.152	0.151	0.0338	0.0363	0.0374	0.0385
	0.50	4.06E+02	3.51E+02	3.28E+02	2.95E+02	2.74E+02	0.221	0.198	0.190	0.181	0.177	0.0233	0.0292	0.0323	0.0355
	0.20	7.69E+02	5.48E+02	4.70E+02	3.66E+02	3.08E+02	0.402	0.311	0.284	0.252	0.241	0.0114	0.0193	0.0244	0.0303
	0.01	6.44E+03	2.42E+03	1.55E+03	7.54E+02	4.59E+02	2.956	1.409	1.076	0.768	0.676	1.06E-03	4.87E-03	9.62E-03	0.0180
Multi-Phase Advection Residual Phase	0.80	1.45E+02	2.02E+02	2.17E+02	2.33E+02	2.42E+02	9.01E-02	0.112	0.118	0.123	0.125	0.0439	0.0428	0.0421	0.0413
	0.50	4.41E+01	1.26E+02	1.58E+02	2.01E+02	2.25E+02	3.43E-02	6.91E-02	8.03E-02	9.31E-02	9.76E-02	0.0540	0.0496	0.0470	0.0443
	0.20	4.49E+00	5.14E+01	8.64E+01	1.51E+02	1.96E+02	5.37E-03	2.72E-02	3.86E-02	5.44E-02	6.06E-02	0.0802	0.0657	0.0582	0.0506
	0.01	2.26E-03	2.58E+00	1.16E+01	5.79E+01	1.24E+02	1.13E-05	1.23E-03	3.38E-03	9.09E-03	1.25E-02	0.2988	0.1681	0.1181	0.0789
Diffusion	0.80	2.78E+02					0.148					0.0358			
	0.50	3.50E+02					0.166					0.0281			
	0.20	5.46E+02					0.207					0.0176			
	0.01	2.38E+03					0.435					3.74E-03			
Diffusion Residual Phase	0.80	2.03E+02					0.130					0.0430			
	0.50	1.28E+02					0.112					0.0504			
	0.20	5.25E+01					0.083					0.0685			
	0.01	2.75E+00					0.031					0.1892			
Aerobic Oxidation	0.80	3.09E+02													
	0.50	4.90E+02													
	0.20	1.19E+03													
	0.01	2.27E+04													
Anaerobic Oxidation	0.80	3.09E+02													
	0.50	4.90E+02													
	0.20	1.19E+03													
	0.01	2.27E+04													
Secondary Methanogenesis	0.80	2.49E+02													
	0.50	2.46E+02													
	0.20	2.42E+02													
	0.01	2.37E+02													

represented by dashed pink lines. In all figures, arrows represent hypothetical or general trends as opposed to trends derived quantitatively by numerical modelling.

The overall trends of C_1/C_{2+} , stable isotopes of CH_4 ($\delta^{13}C-CH_4$, δ^2H-CH_4), and noble gas ratios ($^4He/CH_4$, $^{20}Ne/^{36}Ar$, $^{84}Kr/^{36}Ar$) following multi-phase advection, mixing, methanogenesis and oxidation are consistent with what has been observed in previous marine and groundwater studies (e.g., Darrah et al., 2015b; Darrah et al., 2014; Harkness et al., 2017b; Wen et al., 2016b; Wen et al., 2017; Whiticar, 1990; Whiticar et al., 1986), coalbed methane studies (e.g., Moore et al., 2018) and incubation experiments (e.g., Kinnaman et al., 2007).

The numerical models show that C_1/C_{2+} increase as a result of multi-phase advection, diffusion, aerobic oxidation, secondary methanogenesis, and mixing with primary microbial gas (Figures 2.1, 2.6). Conversely, C_1/C_{2+} will decrease as a result of anaerobic oxidation and is lower in the residual groundwater that remains following multi-phase advection or diffusion (Figure 2.1, 2.6). Both $\delta^{13}C-CH_4$ and δ^2H-CH_4 become more negative during multi-phase advection, diffusion, and mixing with primary microbial gas, but become more positive during both aerobic and anaerobic microbial oxidation processes or in the residual groundwater that remains following multi-phase advection or diffusion (Figures 2.1-2.2, 2.5, 2.7).

The models display significant variations in the sensitivity of the C_1/C_{2+} ratios compared to stable isotopic compositions. Solubility partitioning due to multi-phase advection significantly increases the C_1/C_{2+} ratio (700% increase at $f = 0.01$), while both the $\delta^{13}C-CH_4$ and δ^2H-CH_4 are offset by only $\sim -2\%$ when the GSS-R model is nearly complete (i.e., f approaches 0) (Figure 2.1-2.2, 2.5-2.7). In contrast, diffusion more significantly affects stable isotopic compositions compared to C_1/C_{2+} (Figure 2.1). Interestingly, the $\delta^{13}C-CH_4$ and δ^2H-CH_4 models for multi-phase

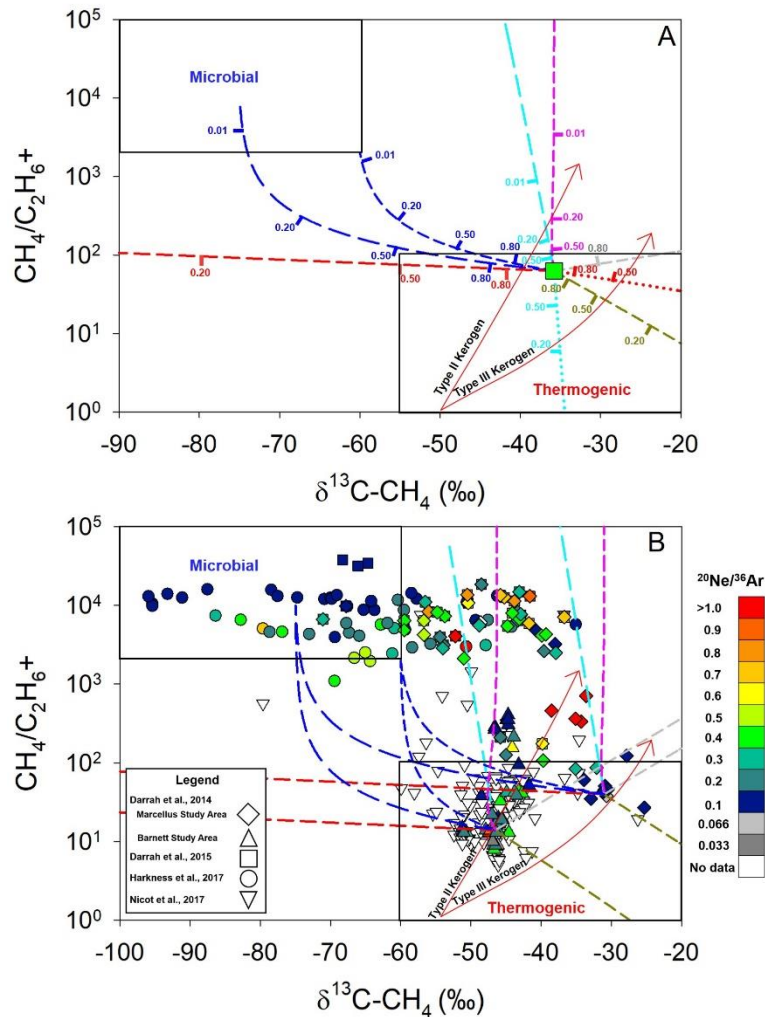


Figure 2.1: The C_1/C_{2+} ratios vs. $\delta^{13}C-CH_4$ of a Marcellus-like thermogenic gas (A) and published groundwater data (B). The microbial and thermogenic zones and thermal maturation lines for Type II and Type III kerogen-derived thermogenic gases were interpreted from Whiticar (1994). The light blue dashed and dotted lines are modeled trends from multi-phase advection and the residual water phase, respectively. The red dashed and dotted lines represent diffusion into above formation waters and a residual phase after diffusion, respectively. The gray and yellow lines are modeled trends of aerobic and anaerobic microbial oxidation, respectively. The dark blue dashed lines represent simple two-component mixing between the thermogenic endmember and primary microbial gas via hydrogenotrophic or acetoclastic methanogenesis. The pink lines represent secondary hydrogenotrophic methanogenesis following the aerobic microbial oxidation of thermogenic hydrocarbons. These models show that theoretically a combination of aerobic microbial oxidation followed by secondary methanogenesis, diffusion, or mixing may also achieve similar chemical compositions as multi-phase advection followed by mixing. Subsets of data from the Appalachian Basin and Fort Worth Basin (dark blue symbols with elevated C_1/C_{2+} and $\delta^{13}C-CH_4 > \sim 50\text{‰}$) that were originally suggested to result from migration show evidence of *in situ* oxidation followed by secondary methanogenesis.

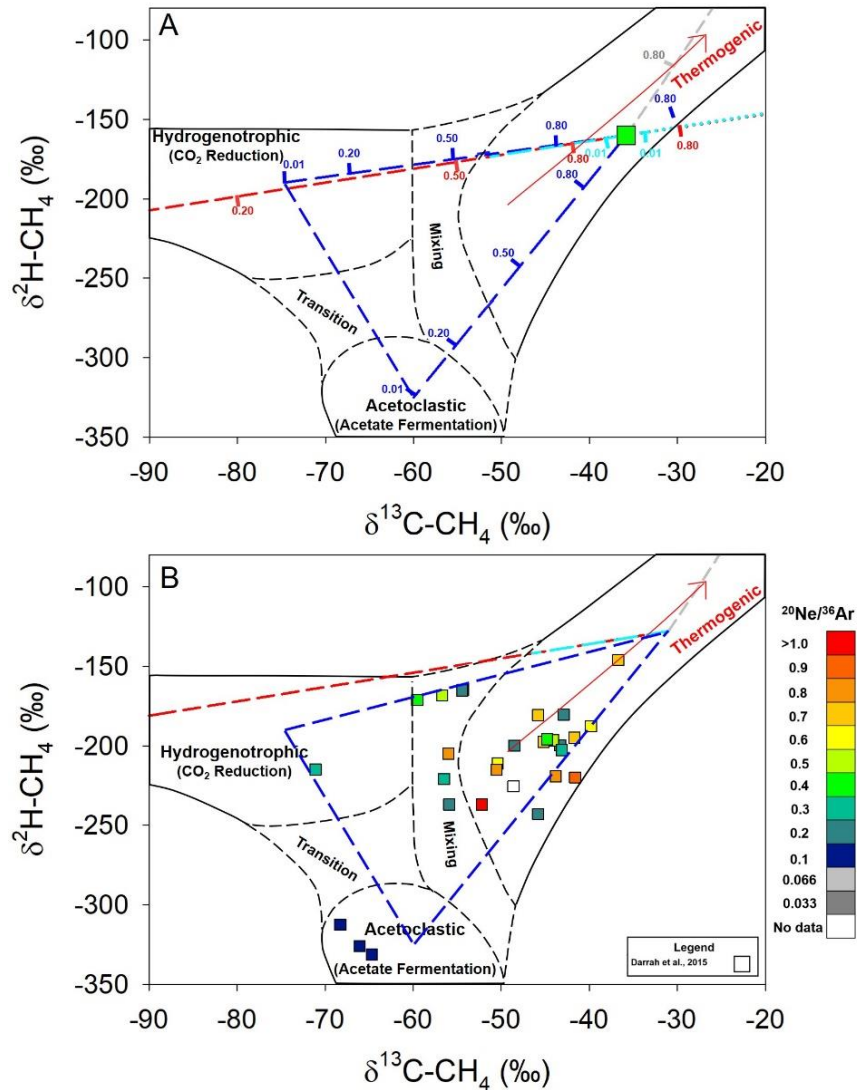


Figure 2.2: The $\delta^2\text{H-CH}_4$ vs. $\delta^{13}\text{C-CH}_4$ of a Marcellus-like thermogenic gas (A) and published groundwater data (B). The hydrogenotrophic and acetoclastic microbial methane, mixing, transition, and thermogenic zones are derived from Schoell (1983) and Whiticar (1990). The green square is the theoretical thermogenic gas endmember. The light blue dashed and dotted lines are modeled trends from multi-phase advection and the residual water phase, respectively. The red dashed and dotted lines represent diffusion into above formation waters and a residual phase after diffusion, respectively. The gray line is a modeled microbial oxidation trend. The blue dashed lines represent simple two-component mixing between the thermogenic and microbial methane endmembers. Multi-phase advection follows a similar trend as diffusion, and both of these processes can obfuscate mixing between thermogenic and microbial gas.

advection and diffusion follow nearly identical trends (Figure 2.2), although diffusion produces much greater degrees of fractionation at a given fraction.

The ultimate change in $\delta^{13}\text{C-CH}_4$ and $\delta^2\text{H-CH}_4$ following aerobic and anaerobic oxidation are dependent on the relative concentrations of thermogenic CH_4 and C_2H_6+ , the original $\delta^{13}\text{C-C}_x$ of the components that have been oxidized, and the extent of oxidation. Overall, $\delta^2\text{H-CH}_4$ is fractionated to a much greater extent than $\delta^{13}\text{C-CH}_4$ following oxidation (Figure 2.2; Table 2.4).

Due to the inert chemical nature of noble gases, physical processes including advection, diffusion, the residual water phases from these processes, and mixing were modeled for noble gas ratios ($^{20}\text{Ne}/^{36}\text{Ar}$, $^{84}\text{Kr}/^{36}\text{Ar}$) and the ratios of He to CH_4 ($^4\text{He}/\text{CH}_4$) (Figure 2.3-2.7). Oxidation and secondary methanogenesis have also been modeled for $^4\text{He}/\text{CH}_4$ (Figure 2.5; Table 2.5). Overall, fractionation from solubility partitioning increases as equilibration temperatures decrease. The maximum fractionation achievable by diffusion is higher than multi-phase advection at all temperatures $>100^\circ\text{C}$ (Figure 2.3A, 2.4A). At temperatures relevant to shallow groundwater studies ($<30^\circ\text{C}$) multi-phase advection will typically have smaller α -values than diffusion (Figures 2.3A, 2.4A; Table 2.5). Hydrocarbon oxidation and secondary methanogenesis only affect CH_4 resulting in increases and decreases in the $^4\text{He}/\text{CH}_4$ ratio, respectively (Table 2.5). However, the $^4\text{He}/\text{CH}_4$ is not particularly sensitive to secondary methanogenesis as the ultimate change following 100% conversion of the C_2H_6+ hydrocarbons to secondary microbial CH_4 in the Marcellus-like endmember is a decrease from $^4\text{He}/\text{CH}_4 = 250 \times 10^{-6}$ to $\sim 237 \times 10^{-6}$. It should be noted that thermogenic gases with higher concentrations of C_2H_6+ hydrocarbons, such as those observed overlying the Barnett Fm. in the Fort Worth Basin, may result in larger decreases in $^4\text{He}/\text{CH}_4$ following secondary methanogenesis. Because migration and mixing (depending on the

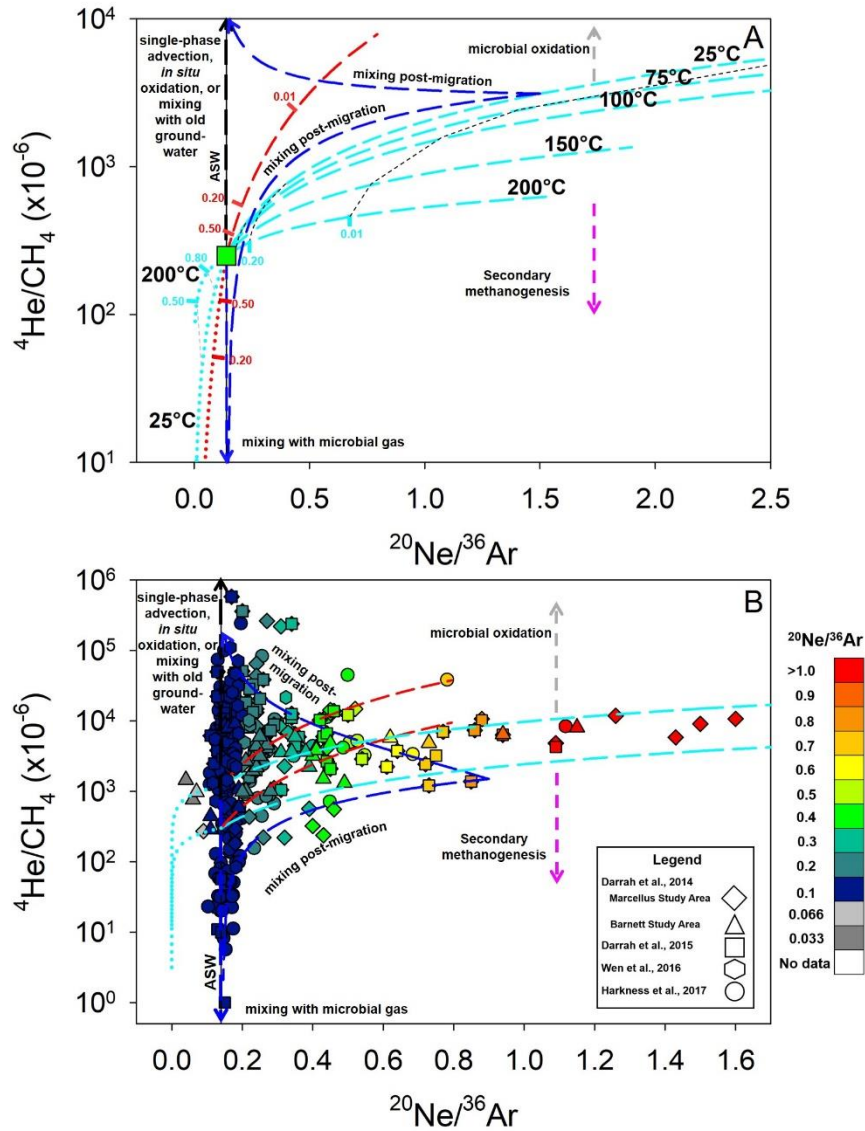


Figure 2.3: Modeled $^4\text{He}/\text{CH}_4$ vs. $^{20}\text{Ne}/^{36}\text{Ar}$ of a Marcellus-like thermogenic gas (A) and published groundwater data (B). Note that in (B) the x-axis range was shortened for visualization. The light blue dashed and dotted lines are modeled trends from multi-phase advection and the residual water phase, respectively, at an equilibration temperature of 25°C. The red dashed and dotted lines represent diffusion into above formation waters and a residual phase after diffusion, respectively. In multi-phase advection, the most significant fractionation occurs at the lower temperatures. When applied to published data, the models suggest it may be difficult to discern between mixing and advection or diffusional processes when the $^{20}\text{Ne}/^{36}\text{Ar}$ is relatively low (<0.6). Additionally, the $^4\text{He}/\text{CH}_4$ ratios for microbial gas will be significantly influenced by the residence time of the groundwater in which microbial gas is generated.

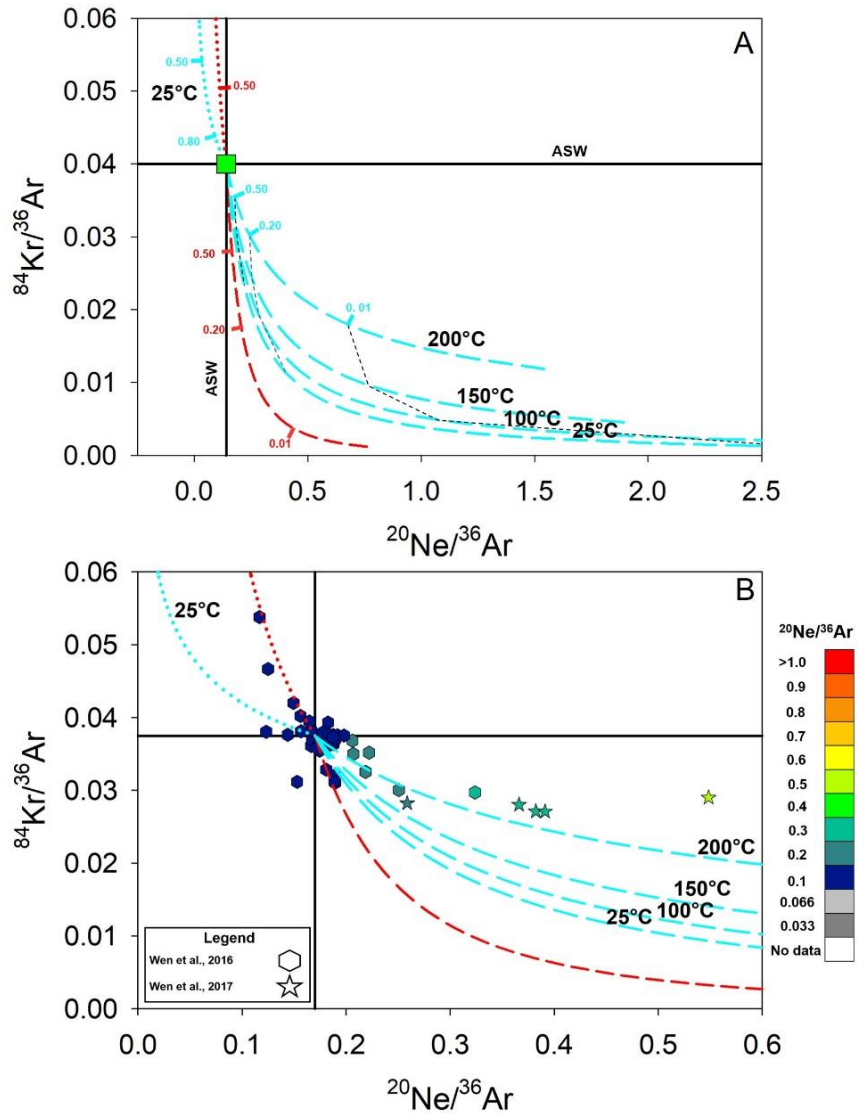


Figure 2.4: Modeled $^{84}\text{Kr}/^{36}\text{Ar}$ vs. $^{20}\text{Ne}/^{36}\text{Ar}$ of a Marcellus-like thermogenic gas (A) and published groundwater data (B). Note that in (B) the x-axis range was shortened for visualization. The light blue dashed and dotted lines are modeled trends from multi-phase advection and the residual water phase, respectively, at varying equilibration temperatures. The red dashed and dotted lines represent diffusion into above formation waters and a residual phase after diffusion, respectively. In multi-phase advection, the most significant fractionation occurs at the lower temperatures.

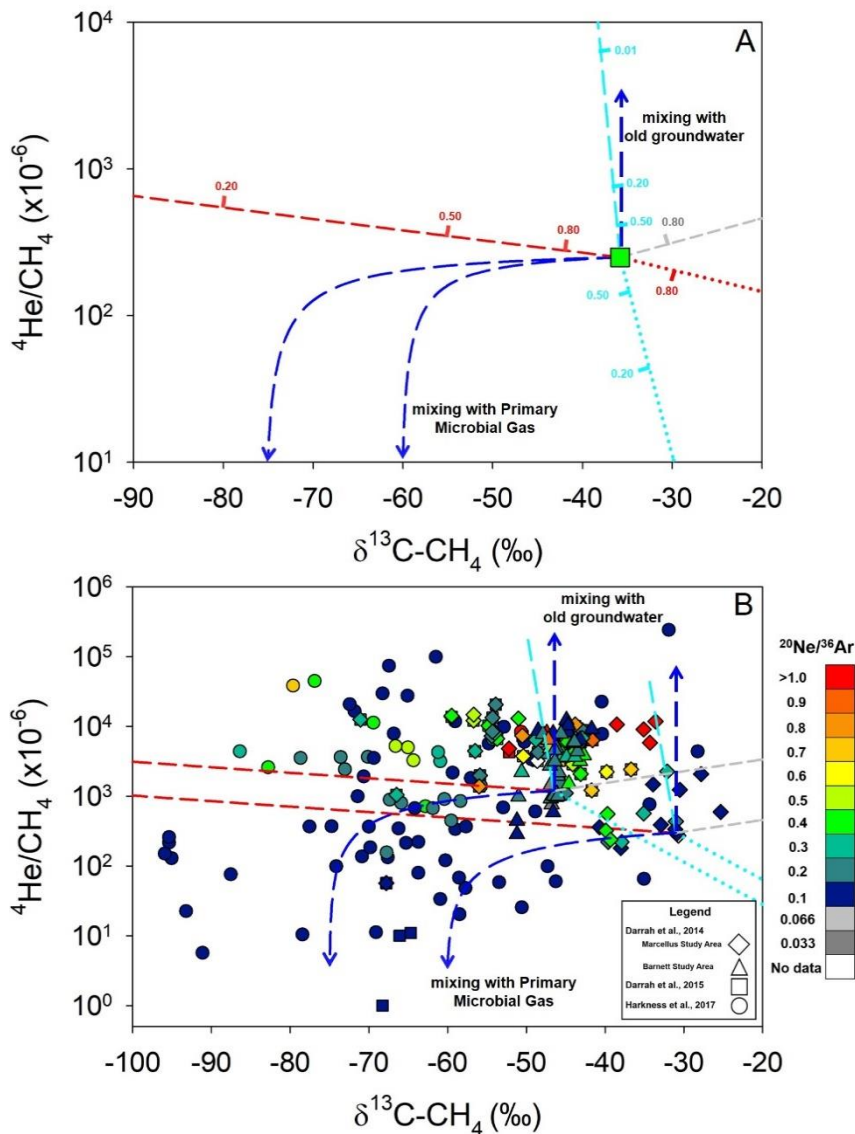


Figure 2.5: Modeled $^4\text{He}/\text{CH}_4$ vs. $\delta^{13}\text{C}-\text{CH}_4$ of a Marcellus-like thermogenic gas (A) and published groundwater data (B). The light blue dashed and dotted lines are modeled trends from multi-phase advection and the residual water phase, respectively. The red dashed and dotted lines represent diffusion into above formation waters and a residual phase after diffusion, respectively. The gray lines are modeled trends of microbial oxidation. Because helium is chemically inert, oxidation and methanogenesis would only affect $[\text{CH}_4]$, thus resulting in upward and downward trends, respectively. Overall, groundwater residence time and migration appear to have significant influence on the $^4\text{He}/\text{CH}_4$ ratios. The $[\text{He}]$ of a microbial endmember is unknown and more dependent on the age of the groundwater.

overall initial [^4He] in each) can change the $^4\text{He}/\text{CH}_4$ ratio by orders of magnitude (e.g., see Darrah et al., 2015b; Darrah et al., 2014; Harkness et al., 2017b), these processes are likely more important.

To my knowledge, this is the first attempt to quantitatively model the C_1/C_{2+} , $\delta^{13}\text{C}-\text{CH}_4$, and $\delta^2\text{H}-\text{CH}_4$ trends associated with secondary methanogenesis (e.g., pink line in Figure 2.1). The small degree of changes in $\delta^{13}\text{C}-\text{CH}_4$ and $\delta^2\text{H}-\text{CH}_4$ following secondary methanogenesis (<1‰) prohibit the identification of this process when these tracers are compared to each other. However, when $\delta^{13}\text{C}-\text{CH}_4$ is compared to C_1/C_{2+} , a distinct sub-vertical trend is produced. While C_1/C_{2+} increases with each increasing fraction, the $\delta^{13}\text{C}-\text{CH}_4$ models yield a more complicated progression. The mixed $\delta^{13}\text{C}-\text{CH}_4$ initially becomes more negative reflecting the conversion of lighter $\delta^{13}\text{C}-\text{CO}_2$ to CH_4 until $f = \sim 0.63$. Beyond $f = \sim 0.63$, the trend becomes progressively more positive reflecting the corresponding shift in newly oxidized $\delta^{13}\text{C}-\text{C}_x$ hydrocarbons and resulting $\delta^{13}\text{C}-\text{CO}_2$ that is converted to CH_4 . In theory, this inflection would be consistent with the preferential utilization of isotopically light carbon (^{12}C) during oxidation and methanogenesis, which should eventually result in $\delta^{13}\text{C}-\text{CH}_4$ that is more positive than the original composition as f approaches 0 and the residual, enriched $\delta^{13}\text{C}$ is utilized.

2.5 Discussion

Characterizing the source and post-genetic processes that influence natural gas in shallow groundwater is essential to ongoing efforts to understand the occurrence of naturally-occurring CH_4 and to identify groundwater pollution related to fugitive gas releases. The source of natural gas is commonly determined by comparing C_1/C_{2+} versus $\delta^{13}\text{C}-\text{CH}_4$ (“Bernard Plot”) or $\delta^{13}\text{C}-\text{CH}_4$ versus $\delta^2\text{H}-\text{CH}_4$ (“Schoell” or “Whiticar” plots) (Figure 2.1-2.2). These approaches typically

provide good first-order classifications of thermogenic and microbial gases and can readily identify some processes of post-genetic modification such as microbial oxidation.

However, the “source” of elevated C_1/C_{2+} (e.g., between 100 and 2,000) and relatively enriched $\delta^{13}C-CH_4$ (e.g., between -50 and -35‰) compared to known thermogenic and microbial gas endmembers, respectively, remains unresolved despite their common occurrence in many groundwater systems (Darrah et al., 2015b; Eymold et al., 2018; Harkness et al., 2017b; Milkov and Etiope, 2018; Moore et al., 2018; Prinzhofer and Pernaton, 1997), specifically with aquifers overlying petroleum-rich sedimentary basins. To demonstrate the value of the recently developed numerical models, I investigated the potential sources and post-genetic processes that may account for this previously unidentified source of natural gas in shallow aquifers.

The source of natural gas with highly elevated C_1/C_{2+} and relatively enriched $\delta^{13}C-CH_4$ compared to primary microbial gas cannot be explained by a single-stage of oxidation or two-component mixing with any known microbial or thermogenic endmembers. Some prior work suggests that these trends may relate to fluid transport phenomena (i.e., diffusion or solubility partitioning) (Darrah et al., 2015b; Darrah et al., 2014; Harkness et al., 2017b; Kreuzer et al., 2018; Lorant et al., 1998; Prinzhofer and Huc, 1995) and others suggest more complicated scenarios involving multiple stages of oxidation and mixing may play a role (Harkness et al., 2017b; Martini et al., 2003; Martini et al., 2008; Milkov and Etiope, 2018; Moore et al., 2018).

By applying the newly developed numerical models to previously published datasets from the Appalachian Basin (Darrah et al., 2015b; Darrah et al., 2014; Harkness et al., 2017b) and Fort Worth Basin (Darrah et al., 2014; Nicot et al., 2017c; Wen et al., 2016b; Wen et al., 2017), I conclude that a large portion of samples that display evidence for highly elevated C_1/C_{2+} must

have experienced some degree of fractionation during fluid transport. This interpretation is largely based on the presence of highly elevated $^{20}\text{Ne}/^{36}\text{Ar}$ (warm symbol colors) in these samples, which can only be accounted for by physical processes that occur during fluid migration since oxidation or methanogenesis would not influence noble gas composition.

The mechanism of fluid transport that delivers natural gas to shallow aquifers can be evaluated using a comparison of $^4\text{He}/\text{CH}_4$ and $^{20}\text{Ne}/^{36}\text{Ar}$ (Figure 2.3B). Initial $^4\text{He}/\text{CH}_4$ endmembers for the Appalachian and Fort Worth Basin were assumed to be 300 and 1,200, respectively. For each study area, I modeled multi-phase advection and diffusion. When considering both $^4\text{He}/\text{CH}_4$ and $^{20}\text{Ne}/^{36}\text{Ar}$, it becomes apparent that samples with elevated $^{20}\text{Ne}/^{36}\text{Ar}$ (above ~ 0.3) require advection as a multi-phase fluid. Based on this conclusion, I assume that hydrocarbon species would be influenced by the same processes. Nonetheless, the fraction (f) to which hydrocarbon tracers must undergo multi-phase advection to account for the highest observed C_1/C_{2+} (i.e., $f = \gg 99\%$) dramatically exceeds the fractions calculated based on noble gas data (Figures 2.6-2.7). Moreover, since the elevated C_1/C_{2+} and relatively enriched $\delta^{13}\text{C}-\text{CH}_4$ compared to primary microbial gas are observed in the gas-rich endmember in groundwater samples, such a high fraction for solubility partitioning is exceedingly unlikely.

Additionally, there is a second subset of samples with elevated C_1/C_{2+} and relatively enriched $\delta^{13}\text{C}-\text{CH}_4$ without elevated $^{20}\text{Ne}/^{36}\text{Ar}$ ratios (< 0.2 , dark blue symbols) (Figure 2.1B). These observations suggest that additional mechanisms may be responsible for elevated C_1/C_{2+} in this additional subset of samples. As a result, I explore the influences of oxidation and secondary methanogenesis to a greater extent.

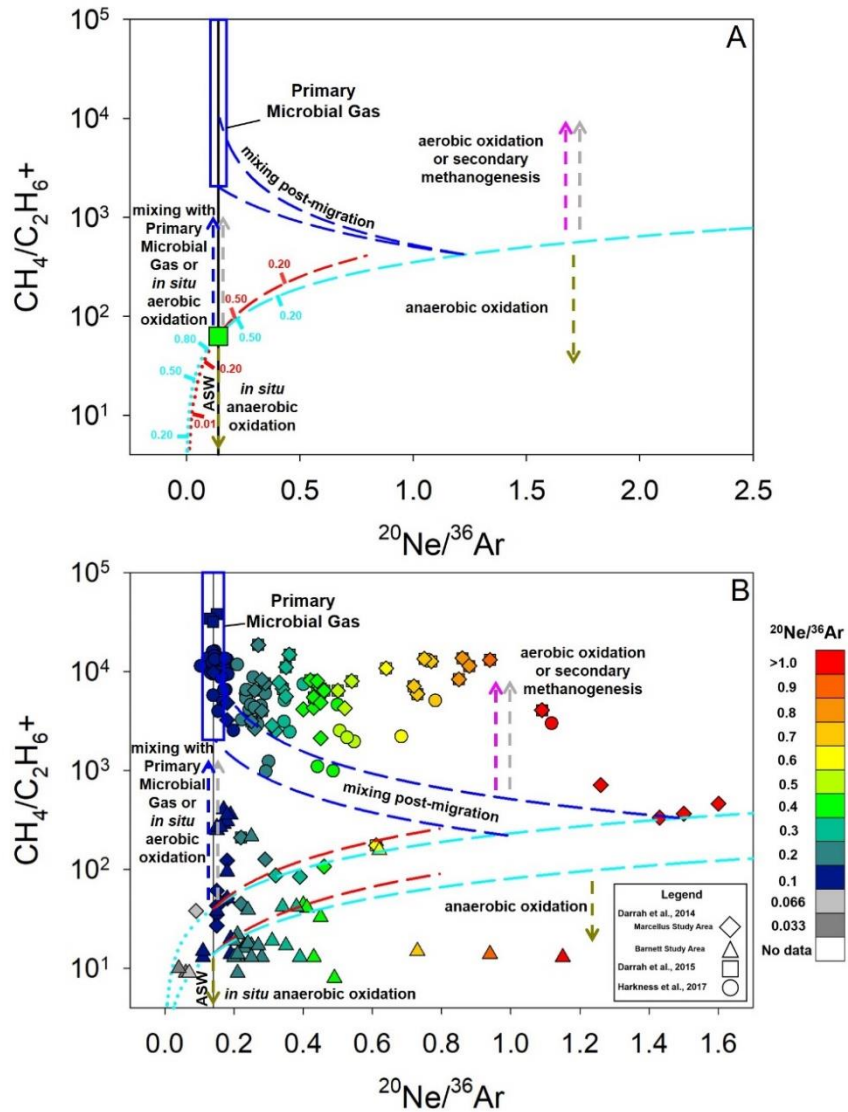


Figure 2.6: Modeled C_1/C_{2+} vs. $^{20}Ne/^{36}Ar$ of a Marcellus-like thermogenic gas (A) and published groundwater data (B). Note that in (B) the x-axis range was shortened for visualization. The light blue dashed and dotted lines are modeled trends from multi-phase advection and the residual water phase, respectively. The red dashed and dotted lines represent diffusion into above formation waters and a residual phase after diffusion, respectively. Elevated or decreased C_1/C_{2+} ratios with no fractionation between ^{20}Ne and ^{36}Ar is indicative of *in situ* microbial oxidation, whereas vertical deviations in C_1/C_{2+} with fractionated $^{20}Ne/^{36}Ar$ may suggest oxidation following multi-phase advection of a thermogenic gas or secondary methanogenesis. A subset of samples from the Appalachian Basin with elevated $^{20}Ne/^{36}Ar$ ratios also do not follow a mixing trajectory with primary microbial gas, suggesting oxidation. However, because there is evidence of extensive migration and mixing with primary microbial gas in these datasets, it is difficult to discern if secondary methanogenesis has occurred in addition to aerobic oxidation.

The modeled trends associated with aerobic oxidation followed by secondary methanogenesis can account for the trends observed in the majority of samples independent of evidence for fractionation during fluid migration (i.e., elevated $^{20}\text{Ne}/^{36}\text{Ar}$). It is important to note that the models suggest that neither phase partitioning during multi-phase advection nor aerobic oxidation alone or in combination can account for the highly elevated C_1/C_{2+} ratios. Moreover, oxidation would significantly increase the $\delta^{13}\text{C}\text{-CH}_4$ (gray lines in Figure 2.1B).

In comparison, oxidation of thermogenic hydrocarbons followed by secondary methanogenesis would greatly increase the C_1/C_{2+} ratios while the $\delta^{13}\text{C}\text{-CH}_4$ would reflect a mixture between the $\delta^{13}\text{C}$ of the original CH_4 and the weighted mean average of the oxidized hydrocarbon compounds, the extent of oxidation, and the efficiency that the produced CO_2 was utilized during methanogenesis. If the thermogenic gas was only partially oxidized, the resulting $\delta^{13}\text{C}\text{-CH}_4$ from secondary methanogenesis would be slightly more negative because microbes will preferentially select isotopically light carbon (^{12}C). Conversely, complete oxidation followed by complete utilization of the CO_2 to generate secondary methane should result in slightly more positive $\delta^{13}\text{C}\text{-CH}_4$ reflecting the $\delta^{13}\text{C}$ of the C_2H_6+ compounds that were oxidized.

The utilization of predictive numerical models suggests that multiple-stage processes are required to account for the previously unresolved “source” of elevated C_1/C_{2+} (e.g., between 100 and 2,000) and relatively enriched $\delta^{13}\text{C}\text{-CH}_4$ (e.g., between -50 and -35‰) compared to known thermogenic and microbial gas endmembers. First, the hydrocarbon and noble gas composition was partially fractionated during multi-phase fluid transport from source rocks to shallow aquifers; these processes would have increased the C_1/C_{2+} , maintained relatively enriched $\delta^{13}\text{C}\text{-CH}_4$ compared to primary microbial gas, and yielded a highly elevated $^{20}\text{Ne}/^{36}\text{Ar}$. Next, aerobic

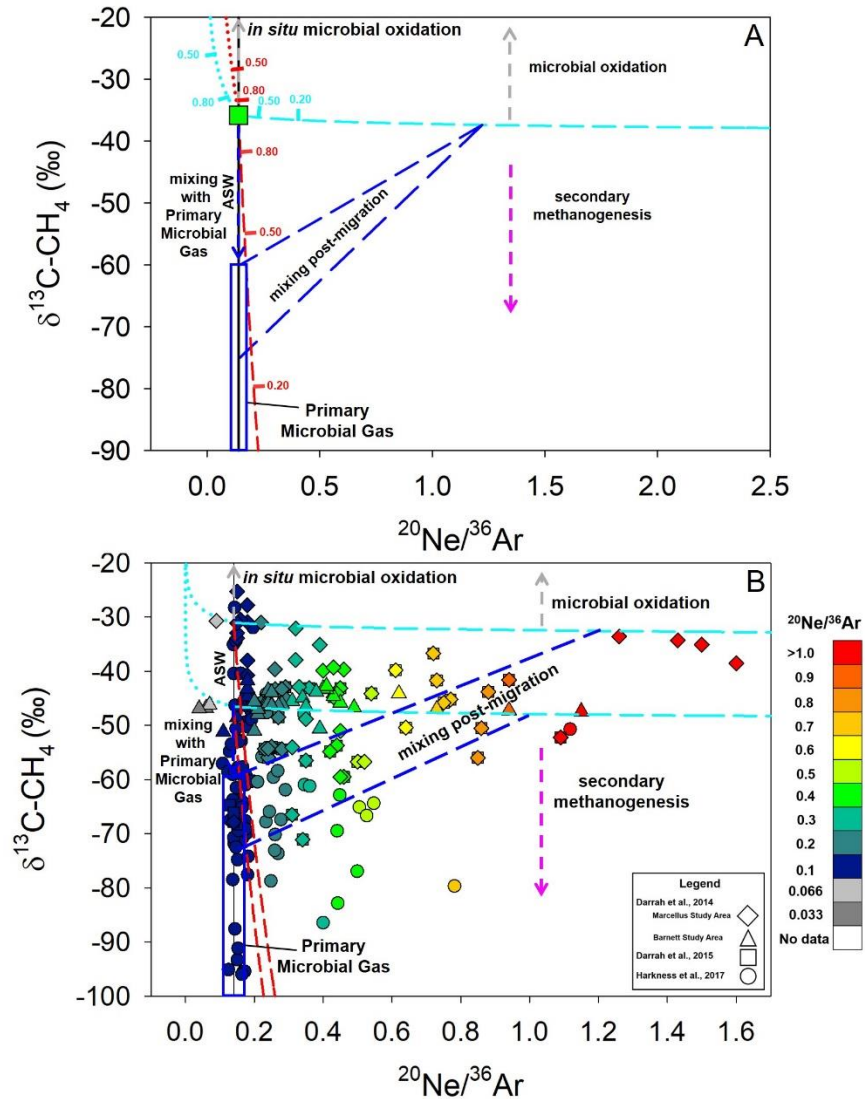


Figure 2.7. Modeled $\delta^{13}\text{C-CH}_4$ vs. $^{20}\text{Ne}/^{36}\text{Ar}$ of a Marcellus-like thermogenic gas (A) and published groundwater data (B). Note that in (B) the x-axis range was shortened for visualization. The light blue dashed and dotted lines are modeled trends from multi-phase advection and the residual water phase, respectively. The red dashed and dotted lines represent diffusion into above formation waters and a residual phase after diffusion, respectively. Enriched $\delta^{13}\text{C-CH}_4$ ratios with no fractionation between ^{20}Ne and ^{36}Ar is indicative of *in situ* oxidation, whereas enriched $\delta^{13}\text{C-CH}_4$ with fractionated $^{20}\text{Ne}/^{36}\text{Ar}$ may suggest oxidation following multi-phase advection of a thermogenic gas. In comparison, more negative $\delta^{13}\text{C-CH}_4$ with fractionated $^{20}\text{Ne}/^{36}\text{Ar}$ may suggest secondary methanogenesis. However, it may be difficult to discern between mixing post-migration and secondary methanogenesis using $\delta^{13}\text{C-CH}_4$ alone based on the large range in $\delta^{13}\text{C-CH}_4$ for primary microbial gas.

oxidation would have preferentially degraded the C₂H₆+ hydrocarbons further increasing the C₁/C₂+ and leading to a small positive shift in the δ¹³C-CH₄ (and a corresponding negative shift in the δ¹³C-CO₂) without any further changes in ²⁰Ne/³⁶Ar. Finally, the newly formed pool of CO₂ from aerobic oxidation would be converted to secondary microbial methane via hydrogenotrophic methanogenesis. This final stage would further increase the C₁/C₂+ and lead to small changes in the δ¹³C-CH₄ depending on the volume and isotopic composition of the oxidized components of C₂H₆+ hydrocarbons, also without any further changes in ²⁰Ne/³⁶Ar. Although not discussed herein, each of the figures show consistent evidence for multi-stage post-genetic modification of natural gas during transport to and residence within groundwater that can be resolved through the use of new numerical modelling methods.

The second subset of samples with elevated C₁/C₂+ and relatively enriched δ¹³C-CH₄ compared to known thermogenic and microbial gas endmembers, but without elevated ²⁰Ne/³⁶Ar requires a different interpretation. The data can be accounted for by aerobic oxidation, presumably of an *in situ* thermogenic natural gas based on the lack of quantifiable fractionation in ²⁰Ne/³⁶Ar, followed by secondary methanogenesis. Alternatively, these data may suggest that the three-stage process described above occurred in conditions of sufficiently high ratio of gas to water volumes such that there was not observable fractionation of ²⁰Ne/³⁶Ar.

2.6. Conclusion

Numerical models were developed to identify post-genetic modification of thermogenic gases that are present in shallow groundwater. These models utilize hydrocarbon molecular ratios (C₁/C₂+), δ¹³C-CH₄ and δ²H-CH₄, and noble gas elemental and isotopic compositions, and include multi-phase advection, diffusion, aerobic and anaerobic microbial oxidation, mixing with primary

microbial gas, and secondary methanogenesis. The results suggest noble gases (e.g., $^4\text{He}/\text{CH}_4$ and $^{20}\text{Ne}/^{36}\text{Ar}$) are an important geochemical tracer when trying to understand migration of a thermogenic gas into shallow groundwater followed by microbial degradation. The ratios of atmospheric noble gas isotopes can unambiguously differentiate fractionation related to transport phenomena relative to hydrocarbon oxidation and/or mixing with methane derived from secondary methanogenesis. For example, thermogenic hydrocarbons in groundwater that do not have fractionated $^{20}\text{Ne}/^{36}\text{Ar}$ but show changes in the C_1/C_{2+} ratios, increased $^4\text{He}/\text{CH}_4$ ratios, and more positive $\delta^{13}\text{C}-\text{CH}_4$ indicate *in situ* microbial oxidation and possible secondary methanogenesis, while these changes relative to modeled advection trends may indicate degradation of a migrated thermogenic gas. Finally, intermediate hydrocarbon compositions (e.g., C_1/C_{2+} between 100 and 1,000, $\delta^{13}\text{C}-\text{CH}_4$ between -60 and -40‰) that were previously explained by multi-phase advection followed by mixing with primary microbial gas may instead be a result of the microbial oxidation of thermogenic hydrocarbons followed by secondary methanogenesis if the noble gas ratios do not indicate the groundwater has experienced significant multi-phase migration. In summation, by integrating numerical modelling with gas geochemical data, I was able to resolve the history of previously unresolved source of natural gas.

Chapter 3. Noble gas insights into microbial hydrocarbon degradation processes in shallow groundwater of the Saint-Édouard region of southern Quebec, Canada

Abstract

The expansion of unconventional energy development in the past decade has placed a renewed focus on the need to understand how petroleum development affects shallow aquifers. Significant volumes of work have focused on identifying contaminants (e.g., brine, hydrocarbon gases, organics) related to unconventional drilling. Still, the lack of adequate baseline data in areas targeted for drilling and an incomplete understanding of the complex suite of processes that influence groundwater geochemistry have complicated these investigations. Because elevated levels of naturally-occurring methane were previously observed in groundwater from the Saint-Édouard region of southern Quebec, Canada, it represents an opportune location to examine the factors that control hydrocarbon composition in groundwater. Here, I characterize the naturally-occurring gas- and salt-rich groundwater from the Saint-Édouard region by integrating published dissolved ion and hydrocarbon gas geochemistry with noble gas (He-Xe) and new hydrocarbon molecular (C₁-C₆₊) data. My focus was to gain an understanding of the post-genetic modification processes that influence natural gas composition in shallow aquifers. The study included 22 groundwater samples collected from drinking-water and observation wells. Methane was ubiquitous across the region, while ethane was present in the majority of samples suggesting the omnipresence of a thermogenic gas component throughout the study area. Atmospheric noble gases (²⁰Ne, ³⁶Ar, ⁸⁴Kr, ¹³²Xe) were significantly lower than anticipated air-equilibrated water concentrations throughout the dataset, and specifically in natural gas-rich samples, suggesting gas-

water partitioning likely during degassing. Interestingly, the extent of fractionation, which appears to be related to either the presence of a residual fluid following oil-water interaction or following extensive degassing of natural gas, correlates positively to $\delta^{13}\text{C-DIC}$ and $[\text{HCO}_3]$, suggesting thermogenic hydrocarbons derived from oil are the likely carbon substrate being oxidized and later metabolized to form secondary microbial methane in the region.

3.1 Introduction

In recent decades, the extraction of natural gas from unconventional petroleum targets has dramatically increased hydrocarbon production throughout North America. The expansion of unconventional drilling has also catalyzed significant debate regarding whether methane (CH_4) found in aquifers near drilling is natural contamination or was introduced by drilling processes (Darrah, 2018; Harkness et al., 2017a; Jackson et al., 2014; Molofsky et al., 2013; Nicot et al., 2017c; Osborn et al., 2011; Siegel et al., 2015; Vengosh et al., 2014; Woda et al., 2018). The controversies surrounding suspected incidents of pollution associated with unconventional drilling has placed renewed attention on understanding the geological, hydrogeological, geochemical, and microbiological mechanisms that influence naturally-occurring contamination in groundwater (Jackson et al., 2014; Vengosh et al., 2014).

As a result, there has been a focus in recent work to document the occurrence of CH_4 in shallow groundwater systems and describe the characteristics of naturally-occurring CH_4 in these settings (Baldassare et al., 2014; Bordeleau et al., 2018a; Bordeleau et al., 2018b; Darrah et al., 2015b; Eymold et al., 2018; Harkness et al., 2018; Humez et al., 2016; Kreuzer et al., 2018; Molofsky et al., 2013; Rivard et al., 2018b). For example, naturally-occurring CH_4 and brines have been associated with valley bottoms, proximity to faults, and cross-cutting structural lineaments

(Darrah et al., 2015b; Kreuzer et al., 2018; Osborn et al., 2012; Warner et al., 2012; Weaver et al., 1995).

Despite all of this recent work, the question of whether elevated CH₄ levels are related to naturally-occurring contamination or anthropogenic pollution remains highly contentious. Much of this confusion relates to the fact the compendium of published data suggests that CH₄ is commonly (nearly ubiquitously) observed in aquifers within or overlying hydrocarbon-bearing sedimentary basins. These considerations often make it difficult to apportion contamination related to anthropogenic activities (e.g., Darrah et al., 2015b; Darrah et al., 2014; Harkness et al., 2017b; Jackson et al., 2014; Jackson et al., 2013; Molofsky et al., 2013; Nicot et al., 2017a; Nicot et al., 2017b; Osborn et al., 2011; Siegel et al., 2015; Warner et al., 2012). For example, natural processes including mixing, methanogenesis, methanotrophy, diffusion, and multi-phase advection all influence the composition of natural gas in shallow aquifers and often obfuscate simple interpretations of the source of contaminants if not considered in a comprehensive manner.

Ongoing work that develops and validates a suite of geochemical tracers capable of deciphering between natural and anthropogenic CH₄ contamination has emerged as an important branch of environmental geochemistry. Here, I examine the factors that influence the presence of naturally-occurring hydrocarbon contamination in the Saint-Édouard region of Quebec, Canada by deploying a comprehensive suite of gas geochemical tracers.

Prior work in the Saint-Édouard region has evaluated the role of the aforementioned processes in determining the geochemistry of gas and inorganic constituents in shallow aquifers (Bordeleau et al., 2018a; Bordeleau et al., 2018b; Moritz et al., 2015; Rivard et al., 2018b). Specifically, these works integrated a suite of water, inorganic, and hydrocarbon tracers to better

describe the occurrence of natural CH₄ from this region. Here, I integrate noble gases (He, Ne, Ar, Kr, and Xe) and additional hydrocarbon tracers with previously published datasets (Bordeleau et al., 2018a; Bordeleau et al., 2018b; Rivard et al., 2018b) in an attempt to better characterize the source, emplacement history, microbial processes, and water-hydrocarbon interactions that occur in the Saint-Édouard region of Quebec, Canada.

3.2 Background

3.2.1 Site Selection and Previous Work

The Saint-Édouard region (Figure 3.1) is a ~500 km² area in the St. Lawrence Lowlands of southern Quebec, Canada, which remains nearly undisturbed by oil and gas activity, but has received growing attention as a potential location for unconventional production in the near future. The primary target formation for hydrocarbon extraction is the Upper Ordovician Utica Shale, which is already widely targeted for hydrocarbon extraction throughout the US portion of the Appalachian Basin. In the US, recoverable natural gas reserves from the Utica Shale are estimated at over 38 trillion cubic feet (TcF) (Kirschbaum et al., 2012) and estimates of recoverable natural gas from the Utica Shale in Quebec, specifically, range between 22 and 47 TcF (Duchaine et al., 2012).

In southern Quebec, preliminary exploration of the Utica Shale took place between 2006 and 2010 at which time a *de facto* moratorium on hydraulic fracturing was enacted in the province. Prior to the moratorium, twenty-eight exploration natural-gas wells were drilled throughout the St. Lawrence Lowlands, including two in the Saint-Édouard region (Talisman A267 and A275-horizontal). Eighteen of the 28 wells were hydraulically stimulated (Lavoie et al., 2014), but none were put into production. Nonetheless, indications based on the preliminary results of this drilling

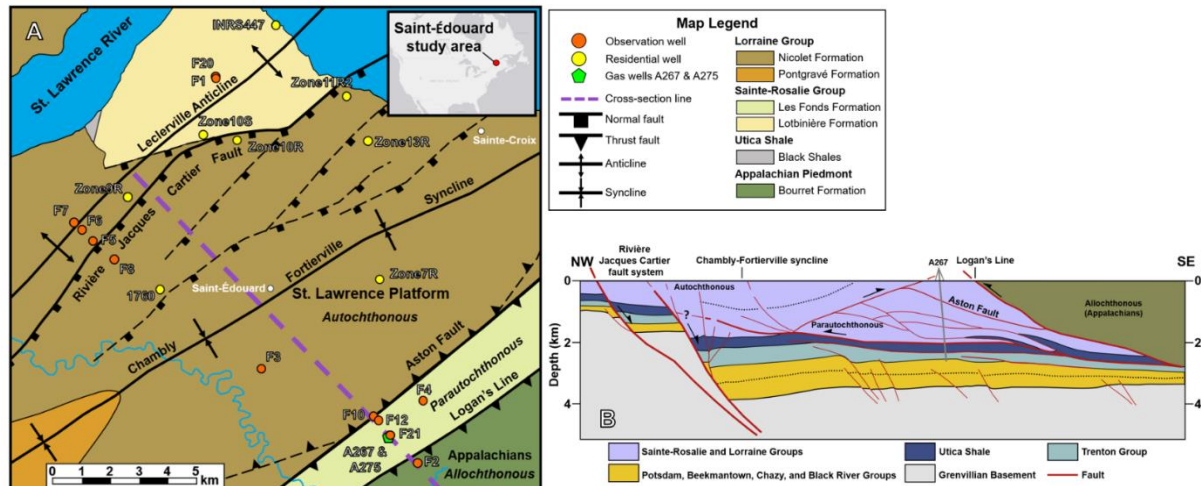


Figure 3.1: Map of Saint-Édouard region (A) and cross section (B). Adapted from Bordeleau et al. (2018a) and Lavoie et al. (2016).

program suggest that the Utica Shale in this region will produce dominantly natural gas. Still, today this area is considered relatively pristine with respect to petroleum production as the subsurface resources in the Utica Shale and overlying Lorraine Group (which are considered less economic for oil and gas potential) remain untapped and hence largely unaffected by hydraulic fracturing (Bordeleau et al., 2018a; Bordeleau et al., 2018b; Lavoie et al., 2016), making this a prime location for studying the natural occurrence of hydrocarbons in groundwater.

In 2012, the Geological Survey of Canada initiated a newly focused research project in the Saint-Édouard region designed to assess the potential impact of oil and gas production on the regional groundwater system. To facilitate this project, 21 groundwater observation wells were drilled to access groundwater and rock cores/cuttings. Extensive petrologic characterization was conducted on samples from 12 of the 21 observation wells to assess a wide array of geological factors including tectonostratigraphy, mineralogy, fracture networks, the presence/type of petroleum, porosity, and permeability (e.g., Ladevèze et al., 2019; Ladevèze et al., 2016; Lavoie

et al., 2016; Rivard et al., 2018b). Aqueous and hydrocarbon geochemistry of groundwater samples were characterized in all of the observation wells along with 30 residential wells in the Saint-Édouard region (Bordeleau et al., 2018a; Bordeleau et al., 2018b; Rivard et al., 2018b). Previous work by Moritz et al. (2015), Bordeleau et al. (2018a), Bordeleau et al. (2018b), and Rivard et al. (2018b) examined specific aspects of the groundwater geochemistry of the Saint-Édouard region. This work identified high concentrations of dissolved CH₄ and heavier aliphatic hydrocarbons (e.g., ethane (C₂H₆), propane (C₃H₈)). The preliminary geochemical assessment suggests that naturally-occurring natural gas is nearly ubiquitous across the region prior to oil and gas development. These works suggested that the natural gas is derived from a mixture of microbial and thermogenic genetic sources of natural gas. This detailed subsurface characterization and groundwater geochemical investigation provides an opportunity to integrate noble gas tracers to interrogate the origin and post-genetic processes that influence hydrocarbons in the region.

The Utica Shale and shales of the Lorraine Group are considered potential sources of the thermogenic natural gas observed in these groundwater studies. Lavoie et al. (2016) found that shallower bedrock units also contain significant, oil-window hydrocarbons that could be a result of: a) lower thermal maturity source rocks or b) mixing between hydrocarbons derived from the Lorraine Group and Utica Shale, combined with additional sources of microbial CH₄.

To date, the potential migration pathways that would facilitate transport of hydrocarbons from the Utica Shale and deeper units in the Lorraine Group are yet to be determined (Bordeleau et al., 2018a; Lavoie et al., 2016). Zones of fracturing and faulting may act as pathways for thermogenic fluid migration, as was shown in regions southwest of the study area near the Yamaska Fault (of which the Rivière Jacques-Cartier Fault is the northeastern extension). In this

region, there is a significant correlation between proximity to the fault and [CH₄] (Moritz et al., 2015), similar to observations from upstate New York and Pennsylvania (Darrah et al., 2015b; Kreuzer et al., 2018; Warner et al., 2012). Nonetheless, the potential for fault-controlled hydrocarbon transport has not been directly tested in the Saint-Édouard region (Bordeleau et al., 2018a).

3.2.2 Geologic Setting

In the Saint-Édouard region Upper Cambrian to Upper Ordovician sedimentary packages are termed the St. Lawrence Platform (Figure 3.2). This package lies unconformably above the Precambrian basement and is covered by relatively thin and variable Quaternary glacial deposits (Globensky, 1987; Ladevèze et al., 2016). The Grenville-age metamorphic basement is overlain by the Upper Cambrian Potsdam Group that is dominantly sandstone (Lavoie, 2008). The Lower Ordovician Beekmantown Group sits unconformably atop the Potsdam Group and consists of intertidal limestones and dolostones (Salad Hersi, 2012). An unconformity separates the Beekmantown Group from the overlying series that includes the Middle to Upper Ordovician Chazy, Black River, and Trenton Groups that are defined by a deepening-upward transition from limestone to mudstone (Globensky, 1987; Lavoie et al., 2016). The Utica Shale lies directly above the Trenton Group and is composed of organic-rich, marine micrites and calcareous siltstones. The Utica shale has a thickness of ~100-250 m with a general increase in thickness from north to south (Castonguay et al., 2010; Séjourné et al., 2013), and in this area is conformably overlain by two flysch turbidite deposits from the Sainte-Rosalie and Lorraine Groups (Globensky, 1993).

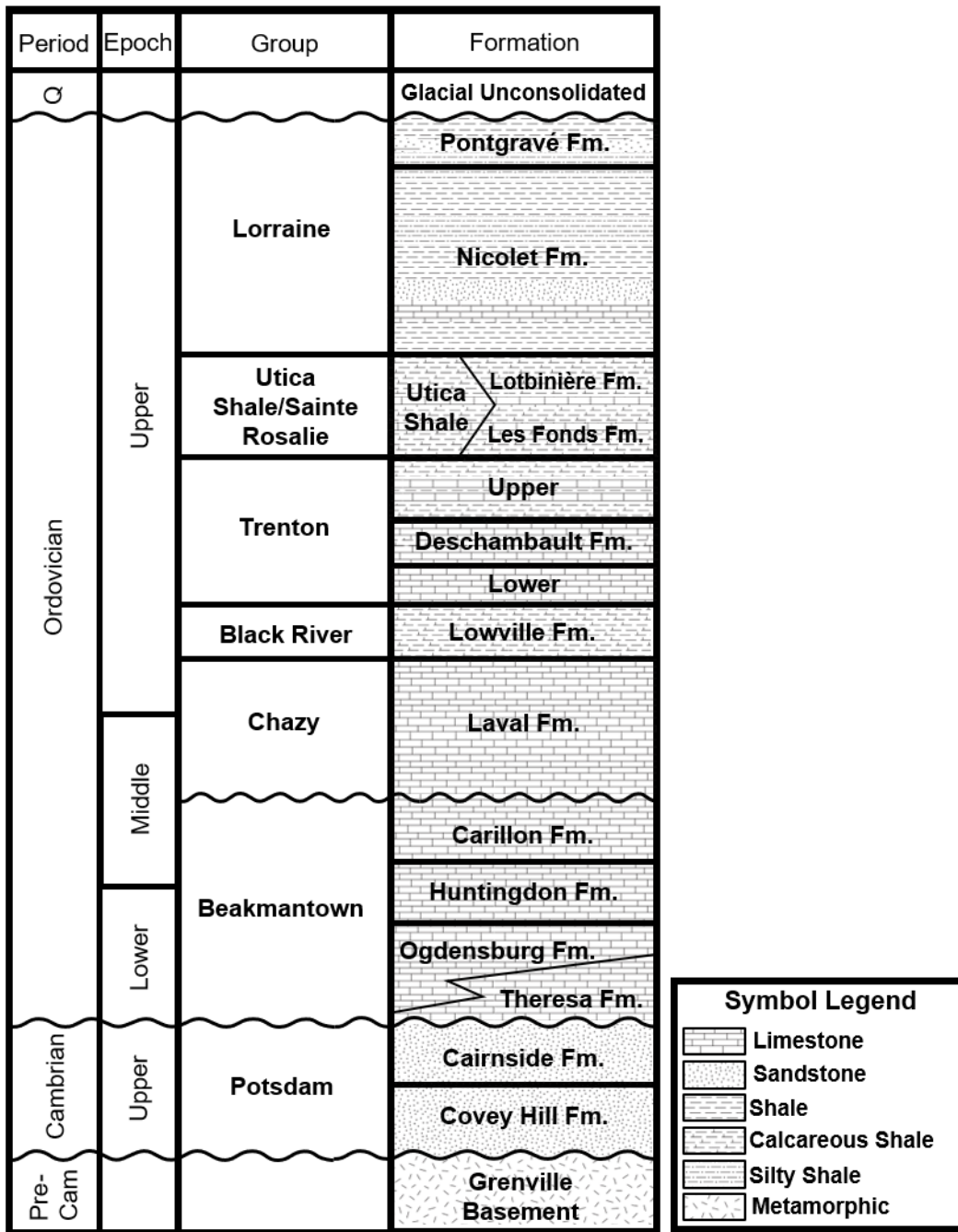


Figure 3.2: Generalized stratigraphic column of the study area. Adapted from Lavoie et al. (2016).

The Sainte-Rosalie Group is a succession of siltstone, mudstone, silty shale, and minor dolomite (Globensky, 1993). The Sainte-Rosalie Group has two members: the Les Fonds and Lotbinière Formations (Fm.) (Globensky, 1993), though the Lotbinière Fm. is only found in the northernmost portion of the Saint-Édouard region (Globensky, 1993). The Lorraine Group overlies the Sainte-Rosalie Group and is the thickest stratigraphic unit of the St. Lawrence Platform with a maximum estimated thickness of 3,800 m (Globensky, 1993); it also represents the uppermost stratigraphic unit of the St. Lawrence Platform preserved in the region. The Lorraine Group is dominantly composed of interbedded fine-grained sandstones and siltstones with thin layers of limestone or calcareous sandstone (Comeau et al., 2004). The Lorraine Group is mostly comprised of the Nicolet Fm., although the Pontgravé Fm. is present in the far southwest portion of the study area (Figure 3.1).

The bedrock has commonly been divided into three structural domains that transition from the northwest to southeast. These three zones are termed autochthonous, parautochthonous, and allochthonous (Castonguay et al., 2010; St.-Julien et al., 1983). The autochthonous domain is the least deformed and contains high-angle normal faults in the northwestern portion of the study area (Rivière Jacques-Cartier Fault system; Figure 3.1) that dip southeast and extend to the Grenville Basement (Lavoie et al., 2016). The regional Chambly-Fortierville syncline occurs in the central portion of the autochthonous domain, but only includes the Upper Ordovician sedimentary units (Castonguay et al., 2010; Séjourné et al., 2013). The parautochthonous domain is largely made up of the Les Fonds Fm., and deformation increases to the southeast towards the Appalachians, where compression resulted in multiple *en echelon* imbricate thrust faults (Clark and Globensky, 1973). In the Saint-Édouard region, the parautochthonous domain is bounded in the southeast by the east

dipping thrust fault known as Logan's Line, in the northwest by a back-thrust fault represented at the surface by the Aston Fault, and a basal thrust fault at ~2 km depth (Lavoie et al., 2016) (Figure 3.1). The allochthonous domain, which makes up only a small portion in the southeast of the study area, represents the western edges of the Appalachian Piedmont. This area is composed of severely deformed thrust sheets of Cambrian to Upper Ordovician mudstones and carbonates that exhibit faulting, folding, and layer-parallel shortening (Clark and Globensky, 1973).

3.2.3. Hydrogeology

The Saint-Édouard region is a relatively flat, low-lying (elevation ranges from ~0 m near the St. Lawrence River to ~160 m in the Appalachian Piedmont), agricultural region. Quaternary deposits, primarily derived from the last major glaciation, are heterogeneous both in thickness (e.g., 0.9 to 40.8 m at the locations of the observation wells) and lithology (Ladevèze et al., 2016). Additionally, Quaternary deposits consists dominantly of tightly-packed, fine-grained sediments and hence have low hydraulic conductivities (e.g., at F1 and F2, 10^{-8} to 10^{-7} m/s) (Ladevèze et al., 2016).

Groundwater dominantly flows through fractured bedrock that often behaves as confined or semi-confined aquifers (Ladevèze et al., 2016). Borehole geophysics studies suggest that for all bedrock units, groundwater flow is dominantly restricted to the top 30 m (Ladevèze, 2017), and regional groundwater flow in these aquifers occurs generally from southeast in the area of the Appalachian Piedmont to northwest near the St. Lawrence River (Ladevèze et al., 2016). Hydraulic conductivities through the fractured top-of-rock aquifers are still low to moderate. The highest hydraulic conductivities in the study area are within the Nicolet Fm. (10^{-7} to 10^{-5} m/s). By comparison, the underlying Sainte-Rosalie Group displays extremely low hydraulic conductivities

that range from 10^{-9} to 10^{-7} m/s (Ladevèze et al., 2016). Within these formations, hydraulic conductivity is highest within ~1 km of the Rivière Jacques-Cartier Fault in the northwest portion of the study area (Bordeleau et al., 2018b).

3.2.4 Hydrocarbon Gas Geochemistry

In order to differentiate between natural or anthropogenic sources of hydrocarbon gases and evaluate the relevant hydrogeological factors that control natural gas occurrence and composition in groundwater, it is essential to constrain the source and processes that may alter natural gases in groundwater (commonly termed “post-genetic modification”). The ratio of CH₄ to heavier aliphatic hydrocarbons (C₁/C₂₊) and stable isotopic compositions ($\delta^{13}\text{C}$, $\delta^2\text{H}$) are commonly used to constrain the sources of natural gas.

The molecular and stable isotopic composition of hydrocarbons are determined by the temperatures of thermocatalytic cracking of kerogen, termed catagenesis. The window of catagenesis (i.e., oil and gas window) ranges between 60 to 250°C. The earliest generation of oil-associated gas have diagnostically low C₁/C₂₊ (e.g., <10) and relatively light hydrocarbon stable isotopic compositions (e.g., $\delta^{13}\text{C}\text{-CH}_4 = -55\text{‰}$; $\delta^2\text{H}\text{-CH}_4 = -260\text{‰}$) in comparison to hydrocarbons produced at higher temperatures and higher gas-to-oil ratios. For example, as temperatures increase from 60 to 250°C, the $\delta^{13}\text{C}\text{-CH}_4$ and $\delta^2\text{H}\text{-CH}_4$ increase along a trend from approximately -55‰ to -25‰ and -260‰ to -130‰, respectively (Bernard et al., 1976; Schoell, 1980; Whiticar et al., 1985; Whiticar, 1994) (trend depicted in Figure 3.4A).

In contrast, microbial production of CH₄ (methanogenesis) occurs at lower temperatures (<80°C) via microbial degradation of organic compounds or the reduction of CO₂ (Schoell, 1980; Whiticar et al., 1986). Microbial processes produce almost exclusively CH₄ with diagnostically

high C₁/C₂₊ ratios (>2,000) and more negative stable carbon isotopic composition of CH₄ ($\delta^{13}\text{C}-\text{CH}_4 < -60\text{‰}$) because microbes preferentially utilize the lighter carbon isotope (¹²C) during methanogenesis (Schoell, 1983; Whiticar et al., 1985).

The sources of microbial CH₄ can be distinguished by the $\delta^2\text{H}-\text{CH}_4$. Hydrogenotrophic CH₄ have $\delta^2\text{H}-\text{CH}_4$ between -250‰ and -170‰. Methane formed by acetate fermentation has $\delta^2\text{H}-\text{CH}_4$ between -340‰ and -260‰. By comparison, methylotrophic methanogenesis is poorly characterized in the subsurface but is thought to produce an intermediate $\delta^2\text{H}-\text{CH}_4$ (e.g., Vinson et al., 2017).

The molecular and isotopic fingerprints of hydrocarbon gases following their formation can also be altered in a variety of ways. Each of these factors creates complexity in identifying the source of natural gas in the subsurface, specifically within relatively oxidizing and microbially-rich groundwater. Importantly, recent work demonstrates that careful consideration of multiple geochemical proxies can be used to interpret and distinguish between these processes. The original natural gas composition can be altered by mixing of natural gas from different sources (e.g., mixing between thermogenic and microbial natural gas), fractionation related to preferential selection imparted during various fluid transport mechanisms (e.g., diffusion, single-phase advection, multi-phase advection), thermal or bacterially-driven oxidation (methanotrophy), or a combination thereof (Darrah et al., 2015b; Harkness et al., 2017b; Moore et al., 2018).

During either fluid migration (multi-phase advection) or diffusion, lighter compounds (e.g., CH₄ relative to C₂H₆ or He relative to Ar) and isotopes (¹²C relative to ¹³C or methane with ¹²CH₄ relative to either ¹³CH₄ or ¹²CH₃D) are preferentially enriched in the migrating fluids, while residual fluids are preferentially enriched in heavier compounds and isotopes (Darrah et al., 2015b;

Eymold et al., 2018; Fuex, 1980; Harkness et al., 2017b; Moore et al., 2018; Pernaton et al., 1996; Pinti and Marty, 1995; Prinzhofer and Pernaton, 1997; Prinzhofer and Huc, 1995). Importantly, the degree of fractionation between any two components varies according to the mechanism of fluid transport. As a result, gas measurements can be used to distinguish the mechanisms of fluid transport and better define the source of natural gas in shallow aquifers.

Microbial oxidation alters the C_1/C_{2+} ratio and yields more positive $\delta^{13}C-CH_4$ signatures in the residual natural gas. In scenarios where natural gases undergo oxidation, the mechanism of oxidation imparts diagnostic signatures that can be used to track oxidation processes in the subsurface. Aerobic oxidation (by either aerobic respiration or via sulfate-paired oxidation) preferentially consumes higher order hydrocarbons (C_{2+} , and C_3H_8 preferably) compared to CH_4 resulting in an increase of the C_1/C_{2+} and yields more positive $\delta^{13}C-CH_4$ signatures in the residual natural gas. By comparison, microbially-mediated anaerobic oxidation consumes CH_4 almost exclusively resulting in lower C_1/C_{2+} ratios, but yields more positive $\delta^{13}C-CH_4$ signatures in the residual natural gas (Kessler et al., 2006; Knemeyer et al., 2007; Mastalerz et al., 2009; Pape et al., 2010).

In some cases, post-genetic processes can even catalyze the formation of new generations of microbial CH_4 . For example, microbial CH_4 can also be produced when microbes first oxidize oil or natural gas to form CO_2 and later symbiotic microbes form CH_4 by hydrogenotrophic processes (i.e., commonly termed secondary methanogenesis) (Scott et al., 1994; Sweeney and Taylor, 1999). It is important to note that regardless of the mechanism in which secondary methanogenesis occurs, the natural gas mixture would have increased C_1/C_{2+} . In contrast, the relationship between secondary methanogenesis and $\delta^{13}C-CH_4$ is complex and depends upon: a)

the hydrocarbon species that are oxidized; b) the efficiency of hydrocarbon oxidation; and c) the efficiency by which methanogens utilize the CO₂ and DIC pools.

The $\delta^{13}\text{C}$ -DIC is also affected by the summation of oxidation processes. Originally, the DIC pool is similar to air-saturated water ($\delta^{13}\text{C}$ -DIC = $\sim 0\text{‰}$), but quickly shifts to more negative values following the oxidation of organic matter ($\delta^{13}\text{C}$ -DIC = $< -20\text{‰}$). If oxidation occurs in the absence of secondary methanogenesis, CO₂ will preferentially dissolve into water leading to a negative shift in $\delta^{13}\text{C}$ -DIC. By comparison, because microbes utilize CO₂ for hydrogenotrophic methanogenesis and preferentially utilize the isotopically lighter $\delta^{13}\text{C}$ -CO₂, the residual DIC becomes isotopically heavier in waters associated with the formation of microbial CH₄ (Schoell, 1983; Vinson et al., 2017; Whiticar et al., 1985).

3.2.5 Noble Gas Geochemistry

Noble gases are chemically inert and unaffected by microbial activity or changes in oxygen fugacity. The elemental and isotopic abundances of noble gases are also well constrained in the atmosphere, crust, hydrosphere, and mantle. These characteristics make noble gases useful for understanding the sources of subsurface fluids, migration processes, as well as reconstructing the history of post-genetic processes that influence hydrocarbon compositions observed in groundwater (Ballentine and Burnard, 2002; Darrah et al., 2015b; Eymold et al., 2018; Harkness et al., 2017b; Moore et al., 2018).

Atmospheric noble gases (e.g., ²⁰Ne, ³⁶Ar, ⁸⁴Kr, ¹³²Xe) are incorporated into waters in accordance with Henry's Law of solubility. The composition of atmospheric gases incorporated into meteoric waters (e.g., groundwater, surface water, or pore water) are termed air-saturated water (ASW). Importantly, the ASW composition is well-constrained globally with minor

variations associated with temperature (dissolved gas contents increase as temperatures decrease), salinity (gas contents decrease as salt content increases), and pressure, which is a proxy for elevation (gas contents decrease with increasing elevation). The solubility of noble gases increases with atomic mass: He<Ne<Ar<Kr<Xe (Smith and Kennedy, 1983; Weiss, 1970, 1971; Weiss and Kyser, 1978).

Crustal noble gases can be produced directly from the radioactive decay of U, Th (^4He) and K ($^{40}\text{Ar}^*$), which are termed radiogenic, or indirectly (e.g., when an alpha particle collides with ^{18}O to yield $^{21}\text{Ne}^*$) which are termed nucleogenic (Ballentine and Burnard, 2002). Crustal noble gas isotopes diffuse out of mineral grains and into the pore fluids as a function of temperature and a given noble gas constituent's mineral-specific diffusional constant. For example, in quartz grains, the closure temperatures (i.e., the maximum temperature of retention within the mineral) for ^4He , $^{21}\text{Ne}^*$, and $^{40}\text{Ar}^*$ are approximately 12°C, 80°C, and 200°C, respectively (Ballentine et al., 1994; Hunt et al., 2012), which makes these isotopes useful in identifying thermogenic hydrocarbon gases.

Since the source of ASW noble gas isotopes is fixed and their concentrations are predictable based on recharge conditions, these tracers are useful in groundwater studies that try to understand mixing and to identify post-genetic alterations of gases such as fractionation due to solubility partitioning or oxidation in the subsurface. The $^{20}\text{Ne}/^{36}\text{Ar}$ and $^{84}\text{Kr}/^{36}\text{Ar}$ ratios can be particularly useful in identifying fractionation as a result of multi-phase (gas plus water or oil plus water) partitioning (e.g., of a migrating thermogenic gas and brine) (Gilfillan et al., 2008; Gilfillan et al., 2009). For example, these ratios have been used in previous Appalachian Basin groundwater studies to model the effects of different migration mechanisms at varying temperatures on gas-rich

brines, which include single or multiple-phase advection of gas and brine or diffusion (Darrah et al., 2015b; Darrah et al., 2014; Harkness et al., 2017b).

Similar to the partitioning between water and gas in groundwater, noble gases also partition between oil and water. Although the solubility of noble gases in oil also increase with mass, the heavier noble gases (Kr and Xe) are significantly more enriched in the oil phase (by up to 3 orders of magnitude) compared to water (Battani et al., 2000; Kharaka and Specht, 1988; Pinti and Marty, 1995; Torgersen and Kennedy, 1999). As a result, groundwater that interacted with oil may be preferentially enriched in Kr and Xe (e.g., ^{84}Kr , ^{132}Xe) as compared to groundwater that equilibrated with natural gas.

In some geologic settings, the mantle can also contribute to the noble gas budget of fluids in shallow aquifers (e.g., Darrah et al., 2015b; Siegel et al., 2004; Torgersen et al., 1994). Mantle contributions can most easily be identified by measuring the primordial components of helium in groundwater samples. Helium isotope systematics are denoted by the R/R_A value, where R is the $^3\text{He}/^4\text{He}$ of a given sample compared to the $^3\text{He}/^4\text{He}$ of air or R_A , which is equal to 1.384×10^{-6} . In typical crustal settings, the helium isotopic compositions reflect a mixture between air-saturated water ($R/R_A = 0.985$ with a He/Ne of ~ 0.230) and the crust (i.e., crustal production values typically display $R/R_A = \sim 0.02$ and elevated He/Ne) (Oxburgh et al., 1986). By comparison, the earth's mantle retains primordial ^3He components that can easily be resolved in most crustal settings.

3.3 Methods

3.3.1 Sample Collection

A total of twenty-two groundwater samples ($n=22$) were collected. Each of the samples were collected from fractured top-of-rock units that serve as aquifers in the Nicolet Fm., the Les

Fonds Fm., or Lotbinière Fm. Of the 22 groundwater samples, 14 were collected from observation wells at depths ranging between 7 and 146 m and collected using either a Grundfos (Bjerringbro, Denmark) Redi-Flo2 submersible pump (n=13) or a peristaltic pump (n=1). In previous studies, groundwater collected from these sampling devices and analyzed for both inorganic tracers and hydrocarbon gases were shown to yield statistically indistinguishable results (Bordeleau et al., 2018a; Bordeleau et al., 2018b; Rivard et al., 2018a).

For groundwater observations wells, the pumps were lowered to the desired depth. Groundwater was first purged to ensure that samples were representative of the ambient groundwater. Specifically, purging continued until physicochemical parameters such as temperature, pH, dissolved oxygen, redox potential, and electrical conductivity were stable. Prior studies (Bordeleau et al., 2018a; Bordeleau et al., 2018b) observed rapidly decreasing salinity of observation wells F3 and F7 during purging due to freshwater inflow, so these groundwater wells were only purged during sample collection. Observation well F21 was the only well sampled using a peristaltic pump, which was necessary because the sampling depth (~146m) exceeded the operating conditions of the available submersible pumps. In addition, eight groundwater samples (n=8) were collected from residential drinking-water wells at depths between 12 and 46m and prior to any water treatment systems or pressure tanks. Similar to the methods used for collecting samples from the observation wells, the residential drinking-water wells were purged until physicochemical parameters were stable prior to sample collection.

Samples for gas geochemical analyses were collected using 9.52 mm (3/8-inch) outside diameter, refrigeration-grade copper tubes that were connected in-line with the flowing water. More than 50 copper tube volumes of groundwater were flowed through before the copper tube

was sealed off using brass refrigeration clamps following methods described in detail in previous studies (e.g., Darrah et al., 2015b; Darrah et al., 2014; Harkness et al., 2017a; Harkness et al., 2017b). Two wells (observation well F7 and residential well Zone9R) were sampled twice and analyzed in replicate to evaluate data reproducibility. Further detail on sampling methods can be found elsewhere (e.g., Eymold et al., 2018; Moore et al., 2018; Rivard et al., 2018a).

3.3.2 Sample Analyses

Field parameters and physicochemical data (pH, temperature, conductivity, dissolved oxygen, redox potential) were collected in the field using a HI Multiparameter meter (Hanna Instruments, Woonsocket, RI, USA). Major ions (HCO_3^- , Cl^-), tritium (^3H), stable isotopes of carbon ($\delta^{13}\text{C}$) in DIC and CH_4 , and stable isotopes of hydrogen in CH_4 were reproduced from Bordeleau et al. (2018a) and Bordeleau et al. (2018b).

Analyses of dissolved major gas (e.g., N_2 , O_2), noble gas (He, Ne, Ar, Kr, Xe), and hydrocarbon molecular (e.g., C_1 to C_{6+}) concentrations, and noble gas isotopic (e.g., $^3\text{He}/^4\text{He}$, $^4\text{He}/^{20}\text{Ne}$, $^{20}\text{Ne}/^{36}\text{Ar}$, $^{84}\text{Kr}/^{36}\text{Ar}$, $^{132}\text{Xe}/^{84}\text{Kr}$) compositions were conducted at the Ohio State University Noble Gas Laboratory. Gas extraction and preparation prior to analysis follows standard methods reported previously (Darrah et al., 2013; Eymold et al., 2018; Harkness et al., 2017a). The copper tubes were attached to a stainless-steel, ultra-high vacuum line evacuated to $1\text{-}3 \times 10^{-9}$ torr and continuously monitored using a four-digit 0-20 torr MKS capacitance manometer and Granville-Phillips Micro-Ion ion gauge.

Each groundwater sample was released into a borosilicate bulb, which was placed in a sonic bath for approximately 30 minutes to allow complete exsolution of gases into the sample inlet line (Darrah et al., 2014; Harkness et al., 2017b). The exsolved volume of gas was expanded

into the vacuum line to measure major gases and was screened for noble gas levels using a Stanford Research Systems Residual Gas Analyzer 200 quadrupole mass spectrometer (Moore et al., 2018) before preparation for noble gas analyses. Samples were purified for noble gas analyses by first removing reactive gases through consecutive exposure to a Zr-Al getter (SAES ST-707) held at 450°C and a SAES SORB-AC cartridge held at 250°C that was then cooled to room temperature (Darrah and Poreda, 2012; Darrah et al., 2013). He and Ne were separated from Ar, Kr, and Xe using an activated charcoal finger held at liquid nitrogen temperatures, and an aliquot was inlet into the mass spectrometer for sequential analysis of He and Ne (Darrah et al., 2013). The activated charcoal finger was then reheated to room temperature to release the trapped heavy noble gases for analysis.

Noble gas abundances and isotopic composition were measured using a Thermo Fisher Helix Split Flight Tube (SFT) noble gas mass spectrometer. Samples were compared to replicate analyses of a cross-validated atmospheric air standard (Lake Erie Air). The average external precision for noble gas measurements was less than 3.56% with values reported in parentheses (^4He (1.06%), ^{22}Ne (1.53%), and ^{40}Ar (0.76%), ^{84}Kr (3.41%), and ^{132}Xe (3.56%)). Standard errors for noble gas isotope ratios were approximately 0.00867 times the ratio of air (or 1.20×10^{-8}) for the $^3\text{He}/^4\text{He}$ ratio, less than 0.431% and 0.673% for $^{20}\text{Ne}/^{22}\text{Ne}$ and $^{21}\text{Ne}/^{22}\text{Ne}$, respectively, and 0.534% and 0.459% for $^{38}\text{Ar}/^{36}\text{Ar}$ and $^{40}\text{Ar}/^{36}\text{Ar}$, respectively.

The major and hydrocarbon gases were analyzed for gas composition using a Thermo Fisher Trace 1310 Gas Chromatograph equipped with a Thermal Conductivity Detector (TCD) and Flame Ionization Detector (FID). The methods used in major gas and hydrocarbon gas analyses follow previously described methods (Darrah et al., 2013; Heilweil et al., 2015; Hunt et

al., 2012; Kang et al., 2016). Briefly, samples are compared to a series of gas standards including a cross-validated atmospheric air standard (Lake Erie Air) and a series of synthetic natural gas standards from Praxair (Moore et al., 2018). The precision is estimated using the measurement of “known-unknown” internal standards. Standard errors for the current measurements were less than $\pm 3.71\%$ for major gases above the detection limit and the average external precision analyses are: CH₄ (1.79%), C₂H₆ (1.96%), C₃H₈ (3.71%), N₂ (1.46%), CO₂ (2.04%), and O₂ (1.17%).

3.3.3 Numerical Modeling

We evaluate the conditions and mechanisms of hydrocarbon emplacement and the potential for oil-water and gas-water interactions in aquifers by modeling mixing between theoretical *in situ* microbial CH₄ endmembers and thermogenic gases found in the study area, as well as evaluating fractionation of noble gases through various multi-phase (gas plus water and separately oil plus water) interactions (Battani et al., 2000; Bosch and Mazon, 1988; Darrah et al., 2015b; Darrah et al., 2014; Jackson et al., 2013; Pinti and Marty, 1995).

To model the potential effects of mixing of various hydrocarbon gas components, the theoretical thermogenic gas end-member ($C_1/C_{2+} = 1$, $\delta^{13}C\text{-CH}_4 = -45.4\text{‰}$, $\delta^2H\text{-CH}_4 = -223\text{‰}$) was modeled based on data presented in Lavoie et al. (2016), which included $\delta^{13}C\text{-C}_{1-3}$ and $\delta^2H\text{-CH}_4$ data from the Upper Ordovician sedimentary units. Potential microbial mixing components include one relatively low C_1/C_{2+} (2,000) and enriched $\delta^{13}C\text{-CH}_4$ (-60‰) microbial CH₄ endmember and one higher C_1/C_{2+} (10,000) and more depleted $\delta^{13}C\text{-CH}_4$ (-75‰) microbial CH₄ endmember for comparison. I also examine the potential for interaction between water and oil. As part of these calculations, we assume noble gas compositions consistent with the solubility of noble gas in oil following Kharaka and Specht (1988), recognizing the uncertainty related to these

assumptions. Modeled concentrations of ASW noble gases in light oil at 25°C for ^4He , ^{20}Ne , ^{36}Ar , ^{84}Kr , and ^{132}Xe are $1.31 \times 10^2 \mu\text{ccSTP/kg}$, $3.20 \times 10^2 \mu\text{ccSTP/kg}$, $6.64 \times 10^3 \mu\text{ccSTP/kg}$, $4.20 \times 10^2 \mu\text{ccSTP/kg}$, and $5.45 \times 10^1 \mu\text{ccSTP/kg}$, respectively.

In all models, the expected ASW conditions for noble gas and nitrogen abundances are assumed using the local average elevation, measured salinity of groundwater, and the temperature of recharge. For this study, an average elevation of 80 m and salinity of 0.1‰ were used in ASW calculations. The mean monthly temperatures in this area range from -10°C (January) to 20.5°C (July) (NOAA; <https://www.noaa.gov>) with a mean annual temperature of ~6°C. However, because recharge into shallow aquifers is minimal in temperature conditions below freezing temperatures, I assumed average temperature of recharge exclude winter months where average low and high temperatures are <0°C (December to February). As a result, the assumed average temperature of recharge is calculated to be ~9°C, which falls within the range of present-day temperatures for groundwater recharge used in other noble gas studies in the St. Lawrence Lowlands (Pinti et al., 2011; Vautour et al., 2015). Using these parameters, the calculated dissolved concentrations of air-saturated water for ^4He , ^{20}Ne , ^{36}Ar , ^{84}Kr , and ^{132}Xe are $4.63 \times 10^1 \mu\text{ccSTP/kg}$, $1.83 \times 10^2 \mu\text{ccSTP/kg}$, $1.32 \times 10^3 \mu\text{ccSTP/kg}$, $53.2 \mu\text{ccSTP/kg}$, and $3.69 \mu\text{ccSTP/kg}$, respectively. The saturation of groundwater with respect to increasing CH_4 would occur at ~44 ccSTP/kg. For the hydrocarbon gases, I assume an original composition of $\text{C}_1/\text{C}_{2+} = 1$, $\delta^{13}\text{C}-\text{CH}_4 = -45.4\text{‰}$ for thermogenic hydrocarbons. In the absence of noble gas data from produced oils and natural gases, I model noble gas fractionation for oils assuming an original air-saturated water composition and varying oil-water and oil-gas mixtures in the original component.

Using these hypothetical starting values, I examine the potential for kinetic fractionation of noble gases and hydrocarbon gases during partitioning between multiple phases (gas plus water; oil plus water). Kinetic fractionation was modeled by integrating a groundwater gas stripping and re-dissolution model (GGS-R) that was originally developed for CO₂ (Gilfillan et al., 2008; Gilfillan et al., 2009) and adapted for hydrocarbons (Darrah et al., 2015b; Darrah et al., 2014; Harkness et al., 2017b). These models assume that a multi-phase fluid migrates buoyantly through the water-saturated crust to overlying formations. During this fluid migration process, gases partition between the phases according to their respective Bunsen solubility coefficients (β_x , which is the ratio at equilibrium of the volume of gas dissolved per volume of solution when the partial pressure of gas is 1 atmosphere (atm)) and the *in situ* (i.e., in formation) ratio of gas volume to water volume ($V_{\text{gas}}/V_{\text{water}}$) or $V_{\text{oil}}/V_{\text{water}}$ (Aeschbach-Hertig et al., 2008; Aeschbach-Hertig et al., 1999; Ballentine et al., 2002; Barry et al., 2018; Bosch and Mazor, 1988; Holocher et al., 2003; Kharaka and Specht, 1988). As a result, lower solubility constituents (e.g., CH₄, ¹²CH₄) will be enriched in the gas phase compared to those that are more soluble (e.g., ⁴He < ²⁰Ne < ³⁶Ar = CH₄ = ¹²CH₄ < ¹³CH₄ < C₂H₆) (C₂H₆+, ¹³CH₄), which will preferentially remain in the liquid phase. Our models assume low gas or oil to water conditions (i.e., $V_{\text{gas}}/V_{\text{water}}$ and $V_{\text{oil}}/V_{\text{water}}$ approach 0), which results in the maximum fractionation between the two constituents. The maximum fractionation value is equivalent to ratio of their respective Bunsen coefficients (β_x/β_x), termed alpha (α). Multi-stage re-dissolution, such as when CH₄ bubbles migrate into overlying pore fluids that had below-saturation levels of CH₄ and dissolve into the aqueous phase over geologic timescales, and are then subsequently exsolved into the gas-phase, may fractionate constituents above α (Darrah et al., 2015b).

3.4. Results

3.4.1 Major Ion Geochemistry

Major ion geochemistry (e.g., Cl, HCO₃) is a critical parameter for evaluating the types of water, mixing, and other processes that occur in groundwater systems. Dissolved ion geochemical data from groundwater have been reported in more detail elsewhere (Bordeleau et al., 2018a; Bordeleau et al., 2018b; Rivard et al., 2018b). Here, I will focus on comparing key dissolved inorganic constituents to hydrocarbon and noble gas components, which have shown significant potential in previous studies that identified the presence of diluted brines, microbial processes (e.g., oxidation, methanogenesis), and the mechanism of thermogenic hydrocarbon migration (Darrah et al., 2015b; Harkness et al., 2017b; Moore et al., 2018; Warner et al., 2012).

Chloride and bicarbonate (HCO₃ or DIC) are the dominant anions in groundwater from this region (Table 3.1). Groundwater [Cl] and [HCO₃] range from 0.6 to 9.8 x10³ mg/L and 2.2 x 10² to 1.2 x 10³ mg/L, respectively (Table 3.1; Figure 3.3). Note that there are significant positive correlations between [HCO₃] and [Cl] (r²=0.706, p=0.002), and between these constituents and [C₂H₆] (r²=0.520 and p=0.032, r²=0.676 and p=0.006, respectively), stable isotopes of carbon in methane (δ¹³C-CH₄) (r²=0.548 and p=0.015, r²=0.532 and p=0.041, respectively) and DIC (δ¹³C-DIC) (r²=0.622, p=0.003, r²=0.473 and p=0.064, respectively) (Figure 3.3). Chloride is also positively correlated with He (r²=0.661, p=0.014). The relationships found between chloride, thermogenic gases, and groundwater in this study area are consistent with results found in other sedimentary basins where paired thermogenic hydrocarbons and brine have been observed (Darrah et al., 2015b; Eymold et al., 2018; Harkness et al., 2017b; Harkness et al., 2018; Warner et al.,

2012). These data suggest a singular source of thermogenic gas and brine in the Saint-Édouard region and suggest that the DIC (as HCO₃) and δ¹³C-DIC in the region are likely influenced by the presence of thermogenic fluids and/or oxidized components of thermogenic fluids.

Table 3.1. Dissolved Ion Geochemistry.

Sample ID	Well Type	Sample Depth (m)	[Cl] ^b (mg/L)	[HCO ₃] ^b (mg/L)
F1	Observation	7.4	3	433
F2	Observation	21.5	180	513
F3	Observation	22.7	7	280
F4	Observation	58.0	190	704
F5	Observation	14.4	93	683
F6	Observation	10.0	55	603
F7deep	Observation	48.0	9800	572
F7deep_dup*	Observation	48.0	9800	572
F8	Observation	20.2	1	222
F10	Observation	23.8	34	363
F12	Observation	20.4	350	332
F20deep	Observation	48.5	5100	863
F21	Observation	146.7	1700	1166
Zone7R	Residential	85.6	78	477
Zone9R	Residential	45.7	76	458
Zone9R_dup*	Residential	45.7	76	458
Zone10R	Residential	56.4	1400	910
Zone10S	Residential	4.7	13	354
Zone11R2	Residential	97.6	475	1217
Zone13R	Residential	50.0	250	622
INRS447	Residential	12.8	290	875
1760	Residential	50.3	33	597
*duplicate				
^b replicated from Bordeleau et al. (2018b)				

3.4.2 Hydrocarbons and Stable Isotopes

The dissolved gas concentrations of hydrocarbon gases (C₁-C₅), major gases (e.g., N₂), and stable isotopic compositions from the Saint-Édouard region can be found in Table 3.2. All 22 samples contained quantifiable levels of CH₄, with [CH₄] ranging from 0.25 to 101 ccSTP/kg

Table 3.2. Hydrocarbon Geochemistry. Dissolved abundances are in ccSTP/kg.

Sample ID	[CH ₄]	[C ₂ H ₆]	[C ₃ H ₈]	[i-C ₄ H ₁₀]	[n-C ₄ H ₁₀]	[i-C ₅ H ₁₂]	[n-C ₅ H ₁₂]	[C ₆ +]	[N ₂]	[O ₂]	[Ar]	$\frac{N_2}{Ar}$	$\frac{CH_4}{C_3H_8+}$	$\delta^{13}C-DIC^a$ (‰)	$\delta^{13}C-CH_4^b$ (‰)	$\delta^2H-CH_4^b$ (‰)
F1	16.5	3.83E-01	6.37E-03	bdl	bdl	bdl	bdl	bdl	3.42	0.01	6.11E-02	56.1	43	1.5	-59.6	-253
F2	33.3	3.78E-02	4.22E-03	2.18E-03	2.26E-03	9.48E-04	7.51E-04	bdl	3.13	0.02	6.75E-02	46.4	692	10.1	-56.9	-244
F3	2.51E-01	bdl	bdl	bdl	bdl	bdl	bdl	bdl	12.8	0.01	0.290	44.0	12,340	-9.4	-81.3	-322
F4	35.0	2.06E-02	2.37E-03	2.28E-03	7.31E-04	4.91E-04	7.84E-04	bdl	5.58	0.01	9.08E-02	61.5	1,284	10.2	-61.1	-251
F5	31.5	1.94E-03	bdl	bdl	bdl	bdl	bdl	bdl	11.7	0.01	0.245	47.8	16,200	-2.0	-81.5	-258
F6	27.5	3.47E-03	1.19E-03	bdl	bdl	bdl	bdl	bdl	12.8	0.01	0.274	46.8	5,902	-0.4	-72.0	-250
F7deep	101	1.04E-02	bdl	bdl	bdl	bdl	bdl	bdl	4.22	0.04	1.87E-02	223.0	9,665	32.5	-52.2	-232
F7deep_dup*	107	1.11E-02	bdl	bdl	bdl	bdl	bdl	bdl	4.22	0.04	2.00E-02	209.0	9,608	32.5	-52.2	-232
F8	5.37E-01	bdl	bdl	bdl	bdl	bdl	bdl	bdl	13.2	0.01	0.316	41.9	1,811	-14.0	-89.6	-329
F10	18.9	2.72E-02	2.95E-03	1.60E-03	1.24E-03	3.30E-04	4.86E-04	bdl	14.1	0.00	0.276	51.0	558	0.8	-56.2	-236
F12	18.7	2.66E-02	1.78E-03	9.61E-04	3.05E-04	1.81E-04	bdl	bdl	15.7	0.00	0.306	51.2	627	-6.8	-67.1	-255
F20deep	24.5	4.36	1.08	3.21E-02	8.30E-02	3.30E-03	1.81E-03	bdl	5.52	0.01	0.114	48.4	4	23.3	-53.6	-246
F21	43.9	1.61	1.12	3.44E-01	3.33E-01	1.53E-01	1.52E-01	bdl	10.4	0.01	0.025	433.4	12	26.2	-52.0	-236
Zone7R	11.4	1.10E-02	3.56E-03	1.39E-03	2.28E-03	8.41E-04	1.16E-03	bdl	19.4	0.00	0.263	73.7	563	-14.2	-60.4	-234
Zone9R	2.03	1.34E-04	bdl	bdl	bdl	bdl	bdl	bdl	12.7	0.02	0.281	54.0	15,210	-12.3	-65.5	-243
Zone9R_dup*	4.96E-01	bdl	bdl	bdl	bdl	bdl	bdl	bdl	13.5	0.01	0.268	50.4	14,690	-12.3	-65.5	-243
Zone10R	14.9	8.78E-03	2.60E-03	1.18E-03	1.23E-03	5.56E-04	8.51E-04	bdl	14.4	0.01	0.341	42.3	982	15.5	-58.2	-258
Zone10S	5.58E-02	5.52E-03	4.38E-03	2.12E-03	3.76E-03	2.20E-03	2.86E-03	2.30E-04	11.2	0.01	0.358	31.2	3	-16.7	11.5	-53.2
Zone11R2	21.5	4.75E-02	1.80E-02	4.35E-03	5.53E-03	1.47E-03	1.67E-03	1.55E-04	16.9	0.00	0.253	67.0	274	11.5	-53.2	-248
Zone13R	2.93E-01	9.33E-03	6.40E-03	3.59E-03	5.99E-03	4.60E-03	5.79E-03	4.49E-04	15.9	0.00	0.395	40.3	8	-13.3	-54.5	-248
INRS447	21.0	7.39E-02	4.48E-02	bdl	bdl	bdl	bdl	bdl	12.1	0.00	0.224	53.9	177	-0.2	-59.2	-243
1760	1.42	2.15E-02	2.14E-02	1.64E-02	2.34E-02	1.79E-02	1.94E-02	1.08E-03	13.9	0.00	0.373	37.2	12	-14.6	-72.6	-227
ASW at 9°C 1 atm									14.7	8.04	0.393	37.5				

*duplicate

^areplicated from Borteleau et al., (2018a)

^breplicated from Borteleau et al., (2018b)

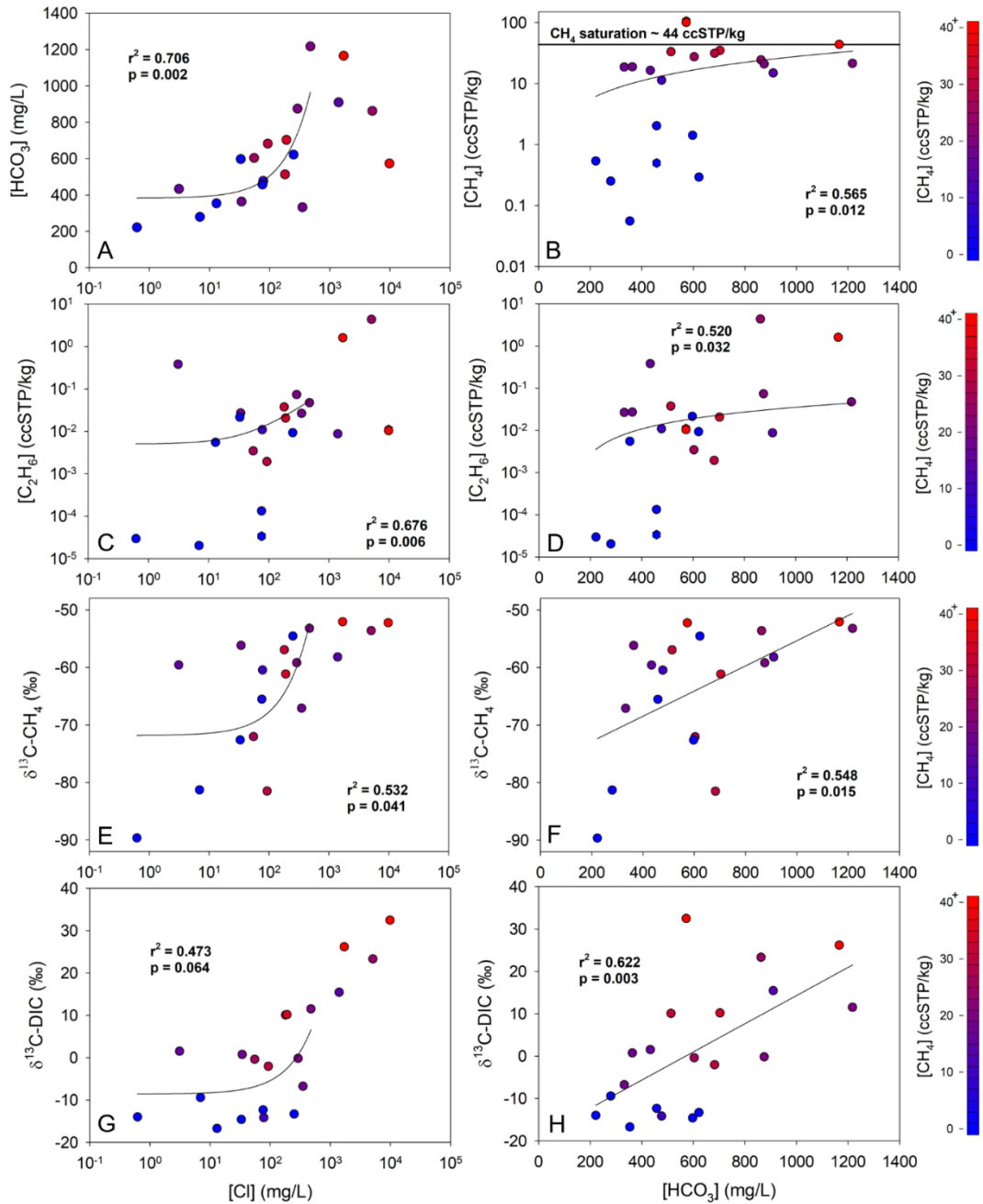


Figure 3.3: [HCO₃], [C₂H₆], δ¹³C-CH₄, and δ¹³C-DIC vs. [Cl] (left) and [CH₄], [C₂H₆], δ¹³C-CH₄, and δ¹³C-DIC vs. [HCO₃] (right). Symbol color corresponds to [CH₄] and hexagons are duplicate samples. The strong statistical correlations suggest coherent mixing between a thermogenic gas-rich diluted brine and fresh groundwater in the Saint-Édouard region. The presence of thermogenic gases appears to be related to [HCO₃] and enriched δ¹³C-DIC, where positive values are generally associated with methanogenesis. This suggests thermogenic gases may be the dominant carbon source for microbial methane.

(Figure 3.3B). Ethane concentrations ranged from below detection limits (5×10^{-5} ccSTP/kg) to 4.36 ccSTP/kg with an average of 0.33 ccSTP/kg (Figure 3.3C-D). Propane concentrations ranged from below detection limits (2×10^{-5} ccSTP/kg in the current study) to 1.12 ccSTP/kg with an average of 0.155 ccSTP/kg (Table 3.2).

The ratio of CH₄ to heavier aliphatic hydrocarbons (C₁/C₂₊) quantifies natural gas dryness and provides an important indicator for the genetic source of natural gas in the subsurface. The C₁/C₂₊ from the current data set ranged from very low (2.7) to 1.8×10^4 with an average of 4.1×10^3 (Figure 3.4). Interestingly, the sample with the highest [CH₄] observed in the current work (F7deep) has a relatively high C₁/C₂₊ (9.6×10^3). The lower limit (e.g., measured in residential well Zone 10S and observation wells F20 and F21) of this range consists of very “wet” gases. Because microbes dominantly produce CH₄, these observations confirm the unambiguous presence of thermogenic gases. Gases with this low degree of dryness are consistent with oil-associated natural gas (Whiticar, 1994). In comparison, the upper limit (e.g., measured in residential drinking-water well Zone 9R and observation well F3) of this range is almost exclusively CH₄ (C₁/C₂₊ >12,000), which is commonly described as a “dry” natural gas. Gas samples with this degree of dryness are typical of CH₄ derived from a microbial source.

Like the molecular composition of hydrocarbons (C₁/C₂₊), the stable isotopic composition of carbon ($\delta^{13}\text{C-CH}_4$) and hydrogen ($\delta^2\text{H-CH}_4$) in methane provide important insights into the source of natural gases in groundwater. For example, a comparison of the C₁/C₂₊ and $\delta^{13}\text{C-CH}_4$ (often called a “Bernard Plot”) is particularly useful for identifying the source of natural gas (Figure 3.4A). Similarly, a comparison of $\delta^2\text{H-CH}_4$ and $\delta^{13}\text{C-CH}_4$ isotopes in methane (often called a “Schoell or Whiticar plot”) can further identify the source of microbial CH₄ and potential

mixtures of natural gas (Figure 3.4B). The majority of samples in this dataset plot as an ambiguous mixture of microbial and thermogenic natural gas (e.g., C_1/C_{2+} between 100 and 1,000, $\delta^{13}C-CH_4$ between -60 and -50‰). All of the data from our study plot outside the ranges of production gases from the Utica Shale or from shallower shales of the Lorraine Group in the Saint-Édouard region as reported by Chatellier et al. (2013). With the exception of three samples that may be explained by simple two-component mixing between the anticipated local thermogenic endmember based on the work of Lavoie et al. (2016) and microbial CH_4 , the majority of the hydrocarbon data have C_1/C_{2+} above typical thermogenic hydrocarbon gases and slightly more negative $\delta^{13}C-CH_4$ (Figure 3.4A).

The majority of the δ^2H-CH_4 and $\delta^{13}C-CH_4$ data fall into the intermediate zone of mixed gas between hydrogenotrophic methanogenesis (CO_2 reduction) and low thermal maturity thermogenic gas without clearly identifying the proportions of contributions from each source (Figure 3.4B). As this mixture overlaps the “transition zone”, I cannot exclude the potential for mixing with acetoclastic CH_4 in the majority of samples or the potential for multiple thermogenic gas sources.

A comparison of $[CH_4]$ and $\delta^{13}C-CH_4$ to the $\delta^{13}C-DIC$ of water provides additional insight on the genetic history of this apparently complex mixture. Methane concentrations have a significant positive correlation with $\delta^{13}C-DIC$ ($r^2 = 0.794$, $p < 0.001$), with the highest measured $[CH_4]$ occurring in samples with the most enriched $\delta^{13}C-DIC$ values (up to +32.5‰) (Figure 3.5A). Despite the occurrence of exceptionally enriched $\delta^{13}C-DIC$ values in a subset of samples from this study, which is consistent with methanogenesis, these samples display the most thermogenic-like natural gas compositions in the current dataset. In fact, the subset of samples with enriched $\delta^{13}C-$

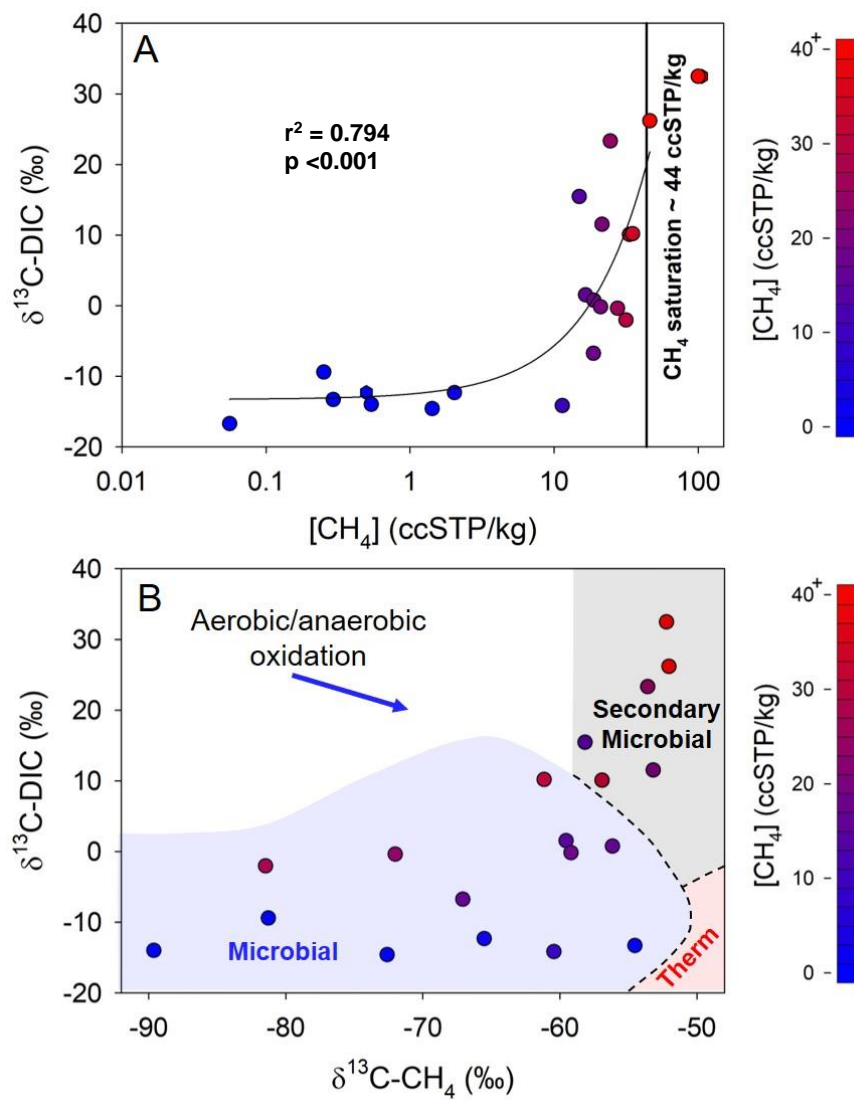


Figure 3.5: $\delta^{13}\text{C-DIC}$ vs. $[\text{CH}_4]$ (A) and $\delta^{13}\text{C-DIC}$ vs. $\delta^{13}\text{C-CH}_4$ (B). Symbol color corresponds to $[\text{CH}_4]$ and hexagons are duplicate samples. Figure 3.5B was replicated from Bordeleau et al. (2018a) with new $[\text{CH}_4]$ data and the shaded regions representing microbial, secondary microbial, and thermogenic gases were adapted from Milkov and Etiope (2018).

DIC display the lowest C_1/C_{2+} , highest $[CH_4]$, $[C_2H_6]$, and $[C_3H_8]$, and most enriched $\delta^{13}C-CH_4$ in the current study. This subset also exhibits the highest $[HCO_3]$ and $[Cl]$ (Table 3.2; Figures 3.3G-H, 3.5). In Figure 3.4A, the subset of samples with enriched $\delta^{13}C-DIC$ follow a subvertical trend and have C_1/C_{2+} below 2,000 and $\delta^{13}C-CH_4$ above $\sim -62\%$. These data predominantly plot between a thermogenic endmember consistent with source rock formations in the Lorraine and Saint Rosalie Groups (Lavoie et al., 2016) and primary microbial CH_4 .

Like the compound-specific data, this sub-vertical trend in Figure 3.4A of increasing C_1/C_{2+} with only a minor decrease in the $\delta^{13}C-CH_4$ is consistent with either kinetic fractionation during multi-phase (gas plus water) migration (Darrah et al., 2015b) or the formation of CH_4 by secondary methanogenesis following the oxidation of thermogenic hydrocarbons. In the latter process, hydrocarbons are first oxidized to CO_2 , which when equilibrated with water, produce elevated $[HCO_3]$ in the water. In fact, the relative abundance of HCO_3 provides a crude indicator of the relative extent of hydrocarbon oxidation assuming it is not all utilized by hydrogenotrophic microbial consortia. As these microbes utilize the CO_2 , they select isotopically lighter CO_2 preferentially leaving a residual pool of highly enriched $\delta^{13}C-DIC$ and increasing proportions of CH_4 (Vinson et al., 2017).

3.4.3. Noble Gases

Noble gas (He, Ne, Ar, Kr, and Xe) concentrations and isotopic compositions from the Saint-Édouard region can be found in Table 3.3. Concentrations of 4He ranged from near ASW levels (48.0 $\mu ccSTP/kg$) to $7.12 \times 10^3 \mu ccSTP/kg$ with an average of $6.75 \times 10^2 \mu ccSTP/kg$. Interestingly, the samples with the highest $[^4He]$ (Zone 7R, 1760, and F10), correspond to relatively low $[CH_4]$ ($<20 \text{ ccSTP/kg}$), indicative of relatively old groundwater (Table 3.3).

Table 3.3 Major and Noble Gas Geochemistry. Dissolved abundances are in ccSTP/kg.

Sample ID	[⁴ He] (x10 ⁻⁶)	[²⁰ Ne] (x10 ⁻⁶)	[³⁶ Ar] (x10 ⁻⁶)	[⁸⁴ Kr] (x10 ⁻⁶)	[¹³⁵ Xe] (x10 ⁻⁶)	³ He/ ⁴ He (R/R _a)	²⁰ Ne/ ²² Ne	²¹ Ne/ ²² Ne	³⁸ Ar/ ³⁶ Ar	⁴⁰ Ar/ ³⁶ Ar	⁴ He/ ²⁰ Ne	²⁰ Ne/ ³⁶ Ar	⁸⁴ Kr/ ³⁶ Ar	¹³⁵ Xe/ ³⁶ Ar	¹³⁵ Xe/ ⁸⁴ Kr	CH ₄ / ³⁶ Ar	⁴ He/CH ₄ (x10 ⁶)	³ H ⁺ (T.U.)
F1	112	14.8	205	10.3	8.45E-01	0.129	9.790	0.0289	0.1880	297.27	7.565	0.072	0.0504	0.0041	0.0819	8.06E+04	6.79	6.8
F2	56.0	8.25	227	11.0	9.00E-01	0.098	9.914	0.0290	0.1912	295.52	6.782	0.036	0.0574	0.0040	0.0818	1.47E+05	1.68	3.8
F3	52.8	135	979	36.0	1.86	2.585	9.800	0.0289	0.1869	295.52	3.903E-01	0.138	0.0367	0.0019	0.0517	2.57E+02	2.10E+02	1.3
F4	404	11.6	304	21.3	2.14	0.035	9.781	0.0294	0.1862	297.22	34.87	0.038	0.0765	0.0070	0.1005	1.15E+05	11.6	1.3
F5	139	82.5	823	38.3	2.96	0.185	9.832	0.0289	0.1879	296.62	1.681	0.100	0.0466	0.0036	0.0773	3.83E+04	4.40	
F6	219	95.4	923	42.4	3.35	0.148	9.811	0.0289	0.1935	295.97	2.297	0.103	0.0460	0.0036	0.0790	2.98E+04	7.96	
F7/deep	197	5.16	62.4	2.55	1.57E-01	0.042	9.786	0.0289	0.1895	299.03	38.18	0.083	0.0409	0.0025	0.0615	1.61E+06	1.96	
F7/deep_dup*	227	5.43	67.0	3.12	2.11E-01	0.042	9.830	0.0289	0.1887	298.09	41.84	0.081	0.0466	0.0031	0.0675	1.59E+06	2.13	
F8	63.9	165	1,060	44.2	2.15	1.876	9.761	0.0289	0.1904	295.60	3.875E-01	0.155	0.0415	0.0020	0.0486	5.05E+02	1.19E+02	12.4
F10	1,180	76.0	932	41.9	2.96	0.028	9.781	0.0293	0.1885	295.05	15.52	0.082	0.0456	0.0032	0.0705	2.02E+04	62.6	
F12	143	79.3	1,030	43.0	2.91	0.162	9.978	0.0295	0.1887	295.51	1.804	0.077	0.0469	0.0028	0.0676	1.82E+04	7.64	
F20/deep	54.3	40.3	383	11.6	9.03E-01	0.331	9.926	0.0293	0.1869	296.65	1.350	0.105	0.0463	0.0024	0.0775	6.41E+04	2.22	3.6
F21	50.8	5.23	84.2	5.19	5.80E-01	0.084	9.847	0.0289	0.1902	297.06	9.723	0.062	0.0617	0.0069	0.1117	5.22E+05	1.16	4.7
Zone7R	7,120	147	880	36.2	3.11	0.021	9.987	0.0302	0.1872	297.75	48.45	0.167	0.0388	0.0035	0.0860	1.29E+04	6.25E+02	4.2
Zone9R	48.0	106	945	37.2	2.00	0.733	9.800	0.0289	0.1989	296.05	4.504E-01	0.113	0.0394	0.0021	0.0537	2.15E+03	23.6	8.2
Zone9R_dup*	45.8	102	902	40.0	2.95	0.733	9.804	0.0289	0.1853	295.88	4.504E-01	0.113	0.0444	0.0033	0.0738	5.50E+02	92.3	8.2
Zone10R	144	170	1,150	43.3	3.22	0.380	9.944	0.0290	0.1881	296.05	8.442E-01	0.149	0.0428	0.0028	0.0743	1.30E+04	9.64	5.3
Zone10S	59.7	214	1,200	49.3	3.69	0.986	9.975	0.0290	0.1889	296.28	2.788E-01	0.178	0.0414	0.0031	0.0750	4.64E+01	1.07E+03	15.8
Zone11R2	1,110	142	850	35.7	2.48	0.117	9.750	0.0291	0.1872	296.01	7.822	0.167	0.0416	0.0029	0.0693	2.53E+04	51.6	1.5
Zone13R	175	219	132	42.4	2.92	0.635	9.962	0.0290	0.1862	296.60	8.009E-01	0.165	0.0388	0.0022	0.0689	2.21E+02	5.98E+02	11.7
INRS447	49.4	117	753	29.8	2.37	1.184	9.822	0.0289	0.1896	296.36	4.215E-01	0.156	0.0395	0.0031	0.0796	2.79E+04	2.35	5.7
1760	2,130	137	1,250	32.3	2.32	0.035	9.939	0.0305	0.1893	297.61	15.48	0.110	0.0364	0.0019	0.0713	1.14E+03	1.49E+03	9.9
ASW at 9°C 1 atm	46.3	183	1,320	53.2	3.69	0.985	9.780	0.0289	0.1880	295.50	9.780	0.138	0.0402	0.0028	0.0696			

*duplicate

Concentrations for ^{20}Ne , ^{36}Ar , ^{84}Kr , and ^{132}Xe ranged from 5.2 to 2.2×10^2 $\mu\text{ccSTP/kg}$, 6.2×10^1 to 1.3×10^3 $\mu\text{ccSTP/kg}$, 2.55 to 49.2 $\mu\text{ccSTP/kg}$, and 0.16 to 3.69 $\mu\text{ccSTP/kg}$, respectively, which are all below the calculated solubility values for air-equilibrated groundwater in the region (Table 3). The concentrations of ASW noble gases are generally lower in the subset of samples with elevated $[\text{CH}_4]$ (Figure 3.6).

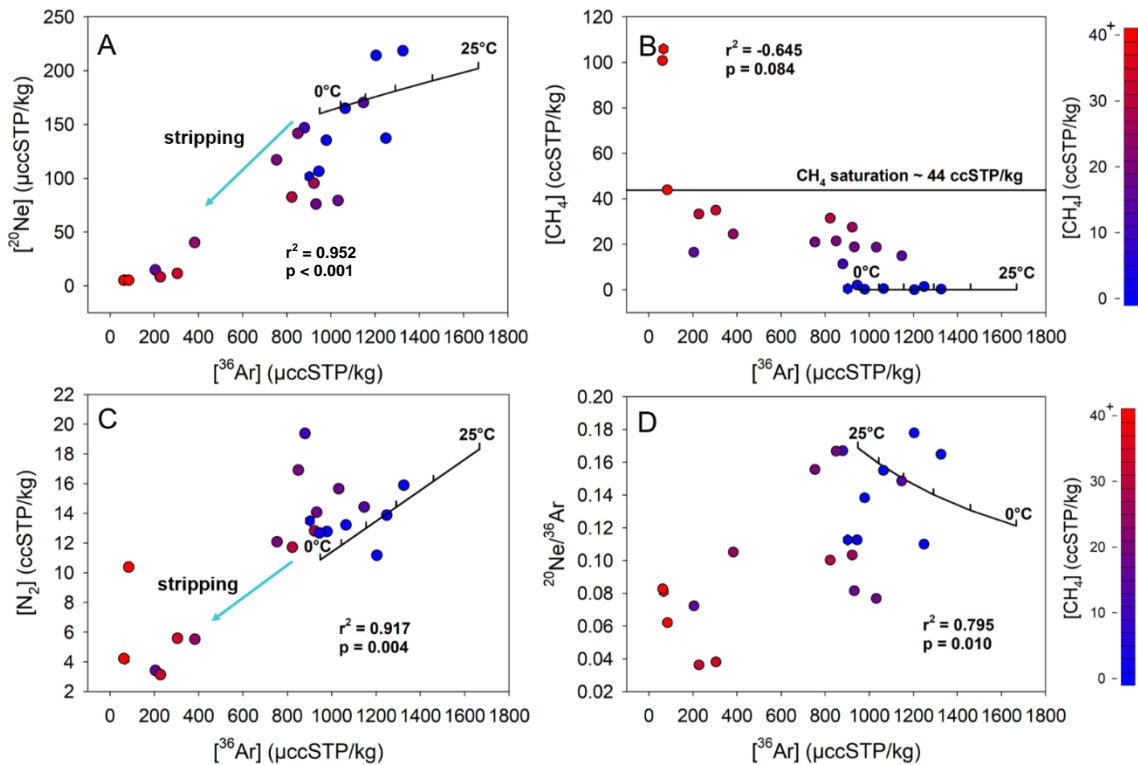


Figure 3.6: ^{20}Ne (A), $[\text{CH}_4]$ (B), $[\text{N}_2]$ (C) and $[\text{He}]$ (D) vs. ^{36}Ar . Symbol color corresponds to $[\text{CH}_4]$ and hexagons are duplicate samples. The decrease in atmospheric gas concentrations below the calculated air-equilibrated values suggest stripping of gases in the hydrocarbon rich samples. Significant fractionations of ASW noble gas ratios are also present in the samples that experienced stripping (Figure 3.6D).

Noble gas isotopic ratios are reported in Table 3.3. The helium isotopic compositions ($^3\text{He}/^4\text{He}$) ranged from crustal values of 0.021 R_A with high He/Ne to significantly above ASW values of 2.585 R_A (ASW $^3\text{He}/^4\text{He} = 0.985R_A$) with low He/Ne (Figure 3.7). The former helium isotope values are consistent with older groundwater and helium associated with thermogenic natural gas. By comparison, the $^3\text{He}/^4\text{He}$ of 2.585 R_A with low He/Ne is consistent with significant contributions of tritiogenic ^3He (i.e., ^3He produced from the radioactive decay of ^3H). A subset of three (n=3) samples display quantifiable amounts of mantle-derived ^3He (up to ~2%) demonstrated by higher $^3\text{He}/^4\text{He}$ than anticipated based on the modeled mixing lines between either ASW or tritiated water with a crustal endmember (Figure 3.7A). The presence of small amounts (<3%) of mantle-derived ^3He is consistent with previous studies from the region (Pinti et al., 2011; Vautour et al., 2015).

The $^{20}\text{Ne}/^{22}\text{Ne}$ and $^{21}\text{Ne}/^{22}\text{Ne}$ in all samples ranged from 9.750 to 9.987 and 0.0289 to 0.0305, respectively. Each of these values are at or within 2.1 and 5.5% of ASW values for $^{20}\text{Ne}/^{22}\text{Ne}$ (9.78) and $^{21}\text{Ne}/^{22}\text{Ne}$ (0.0289), respectively, with quantifiable contributions of nucleogenic ^{21}Ne and ^{22}Ne . Similarly, the $^{38}\text{Ar}/^{36}\text{Ar}$ and $^{40}\text{Ar}/^{36}\text{Ar}$ are all within 5% of near ASW values ($^{38}\text{Ar}/^{36}\text{Ar}=0.188$ and $^{40}\text{Ar}/^{36}\text{Ar}=295.5$), with small amounts of radiogenic $^{40}\text{Ar}^*$ (maximum $^{40}\text{Ar}/^{36}\text{Ar} = 299.0$, average $^{40}\text{Ar}/^{36}\text{Ar} = 296.5$) specifically in samples that contain elevated CH_4 and quantifiable concentrations of C_2H_6 , C_3H_8 , and elevated levels of other radiogenic noble gases (e.g., ^4He) (Table 3.3).

Ratios of crustal noble gases (i.e., ^4He) to ASW noble gases can be used to identify mixing between thermogenic and microbial gas and young groundwater (Figure 3.8). The $^4\text{He}/^{20}\text{Ne}$ and $^4\text{He}/^{36}\text{Ar}$ ratios both show positive trends with $\text{CH}_4/^{36}\text{Ar}$, suggesting that the majority of samples

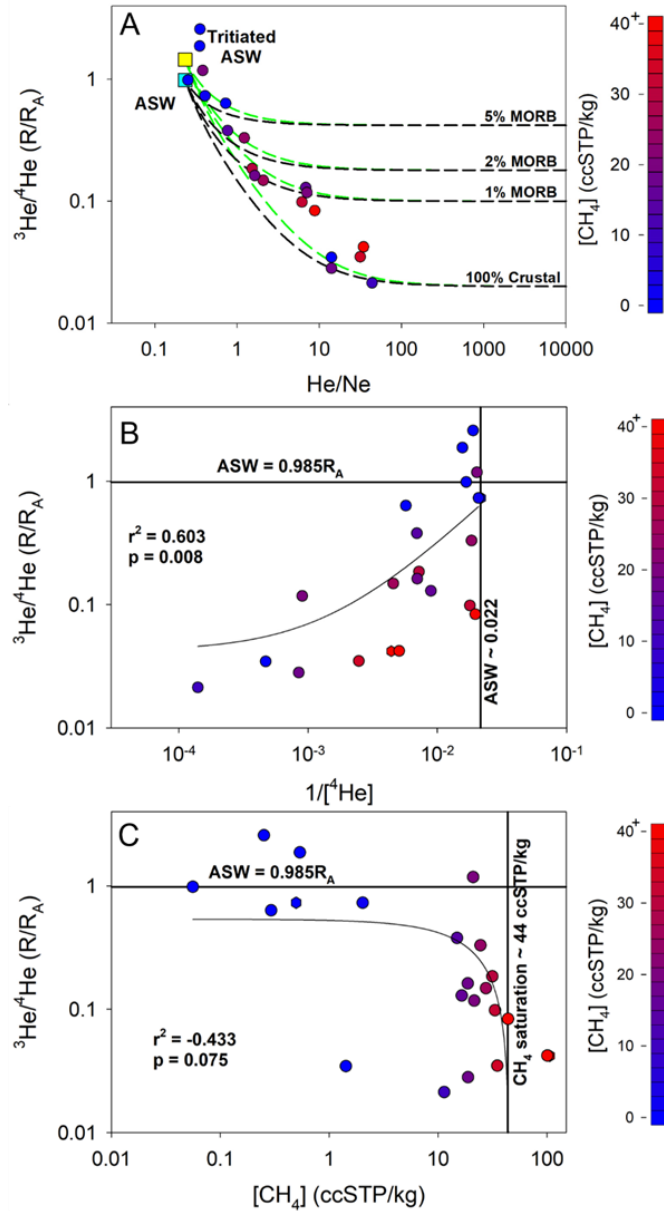


Figure 3.7: Helium isotopic ratios ($^3\text{He}/^4\text{He}$, shown as R/R_A) vs. He/Ne (A), $1/[^4\text{He}]$ (B), and CH_4 (C). Symbol color corresponds to $[\text{CH}_4]$ and hexagons are duplicate samples. In Figure 3.7A, the dashed black and green lines represent mixing between ASW and a hypothetical tritium-active ASW, respectively, with crust and increasing proportions of MORB-mantle ($\sim 8R_A$) fluids. The helium isotopic composition suggests mixing between young, tritiated groundwater with crustal-derived fluids (e.g., thermogenic natural gas) that also contain up to $\sim 2\%$ mantle-derived helium.

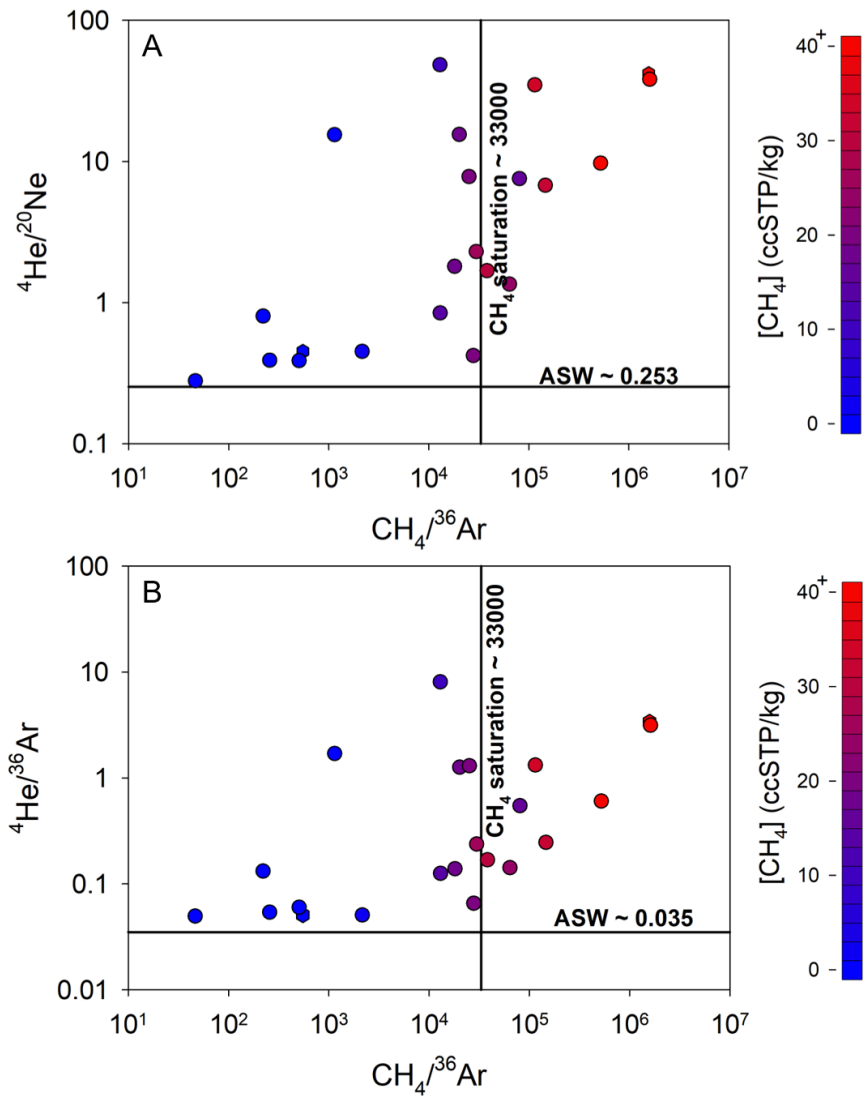


Figure 3.8: $^4\text{He}/^{20}\text{Ne}$ vs. $\text{CH}_4/^{36}\text{Ar}$ (A) and $^4\text{He}/^{36}\text{Ar}$ vs. $\text{CH}_4/^{36}\text{Ar}$ (B). Symbol color corresponds to $[\text{CH}_4]$ and hexagons are duplicate samples. The vertical line represents the $\text{CH}_4/^{36}\text{Ar}$ ratio when groundwater is saturated with CH_4 . The positive trend in both figures suggest groundwater in the Saint-Édouard region is largely a two-component mixture between older, gas-rich fluids (elevated ^4He , CH_4) and a young meteoric water (low ^4He compared to other ASW noble gases, little CH_4). Young groundwater mixing with microbial gas will follow a horizontal trend of increasing CH_4 with little addition of terrigenous ^4He .

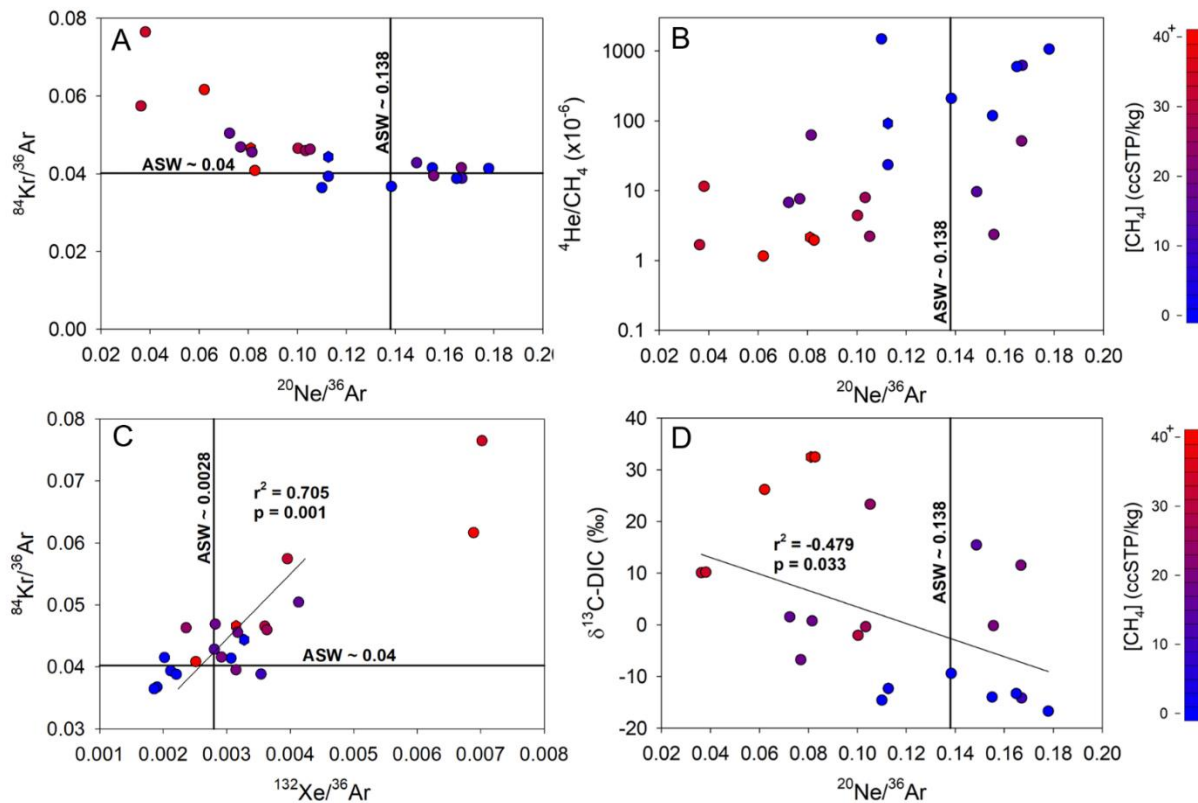


Figure 3.9: $^{84}\text{Kr}/^{36}\text{Ar}$ vs. $^{20}\text{Ne}/^{36}\text{Ar}$ (A) and $^{132}\text{Xe}/^{36}\text{Ar}$ (C) (left), and $^4\text{He}/\text{CH}_4$ (B) and $\delta^{13}\text{C-DIC}$ vs. $^{20}\text{Ne}/^{36}\text{Ar}$ (D) (right). Symbol color corresponds to $[\text{CH}_4]$ and hexagons are duplicate samples. A groundwater that has experienced solubility partitioning from a migrating gas phase displays elevated levels of the lighter isotopes (^4He , ^{20}Ne) in the migrated gas phase, while the heavier gases remain in the groundwater. As seen in Figures 3.9A-C, the data display the opposite trend, which can occur if the groundwater represents the residual water phase following gas-phase partitioning (either of air-equilibrated water or water previously equilibrated with oil).

from the current dataset likely fall along a mixing line between thermogenic gas and young (i.e., low ^4He) groundwater. It is important to note that even though samples from the current study area display relatively low [^4He] compared to other areas in the Appalachian Basin, the samples with the highest hydrocarbon gas concentrations actually display the highest ratios of thermogenic gas to water (i.e., $^4\text{He}/^{20}\text{Ne}$ or $^4\text{He}/^{36}\text{Ar}$).

The composition of ASW noble gases can illustrate fractionation processes associated with differences in solubility between various fluids in the subsurface (e.g., oil and groundwater, gas and groundwater). Most samples in this study display significant fractionation of ASW noble gas ratios with respect to the anticipated ASW values (~ 0.138 , ~ 0.0402 , and ~ 0.0028 for $^{20}\text{Ne}/^{36}\text{Ar}$, $^{84}\text{Kr}/^{36}\text{Ar}$, $^{132}\text{Xe}/^{36}\text{Ar}$ ratios, respectively) (Table 3.3). The majority of samples display $^{20}\text{Ne}/^{36}\text{Ar}$ ratios significantly below the ASW value (as low as 0.036), suggesting significant depletion of the light noble gases. Consistent with these trends, both the $^{84}\text{Kr}/^{36}\text{Ar}$ (up to 0.0765) and $^{132}\text{Xe}/^{36}\text{Ar}$ (up to 0.0070) display an enrichment of up to ~ 2 times the ASW value for $^{84}\text{Kr}/^{36}\text{Ar}$ and ~ 2.5 times the ASW value for $^{132}\text{Xe}/^{36}\text{Ar}$ (Figures 3.9A, 3.9C). In general, the degree of fractionation with respect to anticipated ASW values corresponds to increasing [CH_4]. It is important to note that in all cases, the absolute abundance of the ASW noble gas isotopes in the current dataset are all significantly below the anticipated values (i.e., the noble gases appear partially stripped).

3.5. Discussion

3.5.1 Naturally-Occurring Hydrocarbons and Salinity

Prior work suggests that salinity in the Saint-Édouard region is a combination of regional groundwater flow from the Appalachian Piedmont, residual water from the Champlain Sea that existed from $\sim 13,000$ to 11,000 years ago, and migrated deep brine (Bordeleau et al., 2018a;

Bordeleau et al., 2018b). While the current study does not investigate the source of dissolved ions in detail and therefore cannot rule out the importance of brine contributions from trapped Champlain Sea brines, the significant correlations between chloride and thermogenic gases (e.g., C_2H_6 , 4He) and $\delta^{13}C-CH_4$ (Figure 3.3) suggest the groundwater in the Saint-Édouard region is dominated by 2-component mixing between a thermogenic hydrocarbon-rich brine and fresh groundwater that is relatively rich in microbial CH_4 , consistent with previous groundwater studies in the Appalachian Basin (Darrah et al., 2015b; Harkness et al., 2017b; Molofsky et al., 2013; Warner et al., 2012).

Previously, the elevated levels of DIC in groundwater from the Saint-Édouard region have been attributed to a combination of marine carbonate dissolution during water-rock interactions ($\delta^{13}C-DIC \sim 0\%$) mixing with the oxidation of organic carbon ($\delta^{13}C-DIC \sim -25\%$) (Bordeleau et al., 2018b). Here, I demonstrate a positive correlation between $[HCO_3^-]$, $[Cl^-]$, thermogenic hydrocarbon molecular and isotopic fingerprints, and highly elevated $\delta^{13}C-DIC$ (Figure 3.3). I envision two possibilities for the correlation between $[HCO_3^-]$, $[Cl^-]$, and thermogenic gases: 1) the emplacement of a DIC-rich thermogenic hydrocarbon brine or 2) the emplacement of a thermogenic hydrocarbon brine that underwent either oil biodegradation or aerobic oxidation of thermogenic hydrocarbon compounds following gas emplacement.

The first possibility is supported by Bordeleau et al. (2018a), which modeled Rayleigh fractionation between $\delta^{13}C-CH_4$ and $\delta^{13}C-DIC$ to explain the very positive $\delta^{13}C-DIC$ values (up to $+32.5\%$) in some samples using a mixed marine carbonate and soil source of DIC. The second possibility is supported by Lavoie et al. (2016), who suggested oxidation of higher-chain hydrocarbons followed by hydrogenotrophic secondary methanogenesis in the deepest observation

wells in the Saint-Édouard region. Here, noble gases will be integrated with existing data in an attempt to determine the source of hydrocarbons, HCO₃, and refine the understanding of the microbial processes that alter hydrocarbon and water geochemistry in the Saint-Édouard region.

3.5.2 Hydrocarbon Characterization Using Stable Isotopes and Noble Gas Geochemistry

The dissolved gas geochemistry of groundwater in the Saint-Édouard region represents a combination of primary microbial, thermogenic, and intermediate gas compositions (Figures 3.4-5), consistent with previous studies (Bordeleau et al., 2018a; Lavoie et al., 2016). Though discussed in further detail in Bordeleau et al. (2018a), the comparison of C₁/C₂₊, δ²H-CH₄ with δ¹³C-CH₄ (Figure 3.4B) shows that most samples display a significant contribution of microbial CH₄ with an affinity toward CH₄ generation by hydrogenotrophic CO₂ reduction. Nonetheless, the most gas-rich groundwater samples have the highest proportions of thermogenic contributions.

Samples that exhibit geochemical signatures consistent with primary methanogenesis typically have negative δ¹³C-DIC, which is representative of the local DIC source, and near air-equilibrated water concentrations and ratios of atmospheric noble gases (e.g., ²⁰Ne/³⁶Ar, ⁸⁴Kr/³⁶Ar, ¹³²Xe/³⁶Ar). Additionally, these samples have characteristically negative δ¹³C-CH₄ (<-60‰) and δ²H-CH₄ (<-170‰), and high C₁/C₂₊ ratios (>2,000) (Darrah et al., 2015b; Darrah et al., 2014; Harkness et al., 2017b; Vinson et al., 2017). Although all samples in this study have atmospheric noble gas concentrations below predicted ASW values (Figures 3.5, 3.10), I can conclude that four samples (wells F3, F5, F8, and Zone 9R) most likely have CH₄ that is primarily microbial in origin. Though three samples (F20deep, F21, Zone 13R) have a strong thermogenic gas signature (δ¹³C-CH₄ >-55‰ and C₁/C₂₊ <15), the rest of the samples in this study have intermediate hydrocarbon compositions (δ¹³C-CH₄ between -73 and -52‰ and C₁/C₂₊ <10,000) that could be a result of

mixing or post-genetic modification of thermogenic natural gas by kinetic fractionation during fluid transport or microbial oxidation, which requires further investigation.

To evaluate simple two-component mixing between microbial and thermogenic gas, I modeled mixing between a thermogenic endmember determined from the bulk rock analyses in the Saint-Édouard region reported in Lavoie et al. (2016) and generalized microbial gases (black dashed lines in Figure 3.4A). The thermogenic endmember was chosen as the data point that lies closest to a typical thermal maturation trend line for Type II (marine) kerogen (Whiticar, 1994), which should be the least affected by microbial activity. Based on the modeled trends, mixing between microbial and thermogenic endmembers cannot account for the majority of data in the present dataset. In fact, only data from observation wells F6 and F12, and drinking-water well 1760 are consistent with trends anticipated by mixing.

The migration of thermogenic hydrocarbons as a multi-phase (gas plus brine) fluid by geological processes can explain elevated C_1/C_{2+} and more negative $\delta^{13}C-CH_4$. This interpretation is consistent with observations from other areas of the Appalachian (Darrah et al., 2015b; Harkness et al., 2017b; Kreuzer et al., 2018), Illinois (Moore et al., 2018), Michigan (Wen et al., 2015; Wen et al., 2016a), and Fort Worth Basins (Darrah et al., 2014; Wen et al., 2016b; Wen et al., 2017) in the US, and the Karoo Basin in South Africa (Eymold et al., 2018). In an attempt to understand the potential for hydrocarbon transport through the water-saturated crust to influence the gas composition in the study area, I also modeled multi-phase solubility partitioning assuming the same thermogenic endmember used to model mixing (shown as the sub-vertical blue line in Figure 3.4A). Multi-phase migration of hydrocarbon gas through water (gas plus brine) will enrich the migrated gas phase in lighter gas molecules and isotopes (e.g., CH_4 versus C_2H_6 ; ^{12}C versus ^{13}C).

The modeled fractionation trend associated with two-phase migration followed by mixing with microbial gas could account for the intermediate C_1/C_{2+} values and the relatively enriched $\delta^{13}C$ - CH_4 compared to primary microbial CH_4 . However, multi-phase migration of thermogenic hydrocarbons should also be enriched in the lighter noble gases (e.g., 4He , ^{20}Ne) compared to the heavier isotopes (^{36}Ar , ^{84}Kr , ^{132}Xe) (Darrah et al., 2015b; Darrah et al., 2014; Harkness et al., 2017b; Moore et al., 2018). Many samples in this study with intermediate C_1/C_{2+} and $\delta^{13}C$ - CH_4 values instead have significantly *lower* $^{20}Ne/^{36}Ar$ (<0.10) than anticipated ASW values (~0.138) (e.g., observation wells: F2, F4, F10). Potential causes of the ASW noble gas fractionation are explained in more detail in Section 5.4, but the depleted trend for light isotopes precludes multi-phase migration as the primary mechanism.

Due to the distinct lack of evidence for multi-phase migration, other post-genetic processes that may increase the C_1/C_{2+} require evaluation. The aerobic microbial oxidation of heavier aliphatic hydrocarbons compared to CH_4 (Kinnaman et al., 2007) or anaerobic microbial oxidation coupled to sulfate-reduction (i.e., sulfate-paired oxidation) would result in increased C_1/C_{2+} (Adams et al., 2013; Kniemeyer et al., 2007; Mastalerz et al., 2009). Although Lavoie et al. (2016) suggested anaerobic hydrocarbon oxidation as the mechanism of microbial hydrocarbon degradation in the deepest bulk rock gases, the ubiquitous presence of tritium throughout the study area and low but quantifiable amounts of oxygen in many samples (Tables 3.2 and 3.3), suggests that either aerobic oxidation or sulfate-paired oxidation is possible in the Saint-Édouard region.

Either mechanism of microbial oxidation would convert hydrocarbons to CO_2 (which dissociates to HCO_3 in groundwater) and theoretically cause the $\delta^{13}C$ -DIC to decrease towards the carbon source (Whiticar, 1999). Instead, the highest $[HCO_3]$ in the Saint-Édouard region

corresponds to the most positive $\delta^{13}\text{C-DIC}$ samples, the latter of which is indicative of extensive methanogenesis (Scott et al., 1994; Vinson et al., 2017). Surprisingly, the subset of samples with high $[\text{HCO}_3^-]$ and more positive $\delta^{13}\text{C-DIC}$ are the same samples that also have the highest amounts of CH_4 and Cl , and the highest proportions of thermogenic gas observed in the study (e.g., samples F20deep and F21 have C_1/C_{2+} and $\delta^{13}\text{C-DIC}$ of 4 and 12, and +23.3‰ and +26.2‰, respectively) (Figures 3.3D, 3.3F, 3.3G, 3.5A). These findings suggest that both microbial oxidation (high $[\text{HCO}_3^-]$) and some form of methanogenesis (enriched $\delta^{13}\text{C-DIC}$) are most prevalent in the areas with high amounts of thermogenic hydrocarbons, suggesting that the presence of thermogenic natural gas may have a role in the formation of microbial CH_4 .

3.5.3 Revisiting Secondary Methanogenesis

In previous work, the extent of microbial oxidation was inferred, but could not be quantified due to the lack of C_2H_6 and C_3H_8 data in many samples (Bordeleau et al., 2018a). With the exception of the deepest samples (e.g., F21), Bordeleau et al. (2018a) proposed that the enriched $\delta^{13}\text{C-DIC}$ in shallow groundwater in the Saint-Édouard region resulted from closed-system kinetic equilibrium reactions between $\delta^{13}\text{C-DIC}$ and $\delta^{13}\text{C-CH}_4$ during microbial methanogenesis, which utilized DIC from a combination of carbonate dissolution and soil. More generally, they suggested ongoing methanogenesis would eventually result in enriched $\delta^{13}\text{C-DIC}$ (>+30‰) and $\delta^{13}\text{C-CH}_4$ (>-50‰, which overlaps the range observed for thermogenic gas) as the available DIC pool decreases (referred to by Bordeleau et al. (2018a) as “late-stage methanogenesis”). In a closed system, it would also be expected that thermogenic hydrocarbons that have undergone microbial oxidation would result in negative $\delta^{13}\text{C-DIC}$ in the groundwater.

Based on the concurrently high $[\text{HCO}_3^-]$ (reflecting oxidation), enriched $\delta^{13}\text{C-DIC}$ (reflecting methanogenesis), and occurrence of thermogenic gases in the Saint-Édouard region, there is potential to achieve the same hydrocarbon observations following closed-system microbial oxidation of thermogenic hydrocarbons paired with secondary methanogenesis. A comparison of $\delta^{13}\text{C-DIC}$ and $\delta^{13}\text{C-CH}_4$ (Figure 3.5B) shows that most of our data fall into either primary microbial or secondary microbial CH_4 (particularly in the samples with the two highest $[\text{CH}_4]$ observed in the study). These results are not unexpected as secondary microbial CH_4 often follows microbial oxidation of wet hydrocarbon gases and/or oils (Scott et al., 1994; Sweeney and Taylor, 1999).

Aerobic respiration or sulfate-paired oxidation of hydrocarbons will produce increasing volumes of CO_2 (and DIC), which leads to larger volume of labile carbon pool that is then used by other microbes during hydrogenotrophic (CO_2 reduction) methanogenesis (Whiticar, 1994; Whiticar et al., 1986). Importantly, if the newly generated CO_2 is completely converted to secondary CH_4 , the C_1/C_{2+} of the natural gas will increase greatly. In comparison, because the vast majority of C_{2+} hydrocarbons have $\delta^{13}\text{C-C}_x$ values more positive than that of CH_4 , the complete oxidation of oil or heavier hydrocarbons followed by the complete conversion of CO_2 to CH_4 would lead to more positive $\delta^{13}\text{C-CH}_4$ (Figure 3.4A). During microbial oxidation, microbes preferentially select the light $\delta^{13}\text{C-C}_x$ components of each species, which will lead to a small negative offset between the original $\delta^{13}\text{C-CH}_4$ and the newly formed methanogenic component (pink trend in Figure 3.4A). The degree of negative shift is determined by the $\delta^{13}\text{C-C}_x$ of the oxidized component, the fractionation factor (α) associated with oxidation of the specific hydrocarbon species, and the fraction of the thermogenic gas volume that undergoes oxidation

(Anderson et al., 2017; Kinnaman et al., 2007; Valentine et al., 2010). If the fraction of hydrocarbons that undergo oxidation approaches 1.0 and an equivalent volume of CH₄ is generated by secondary methanogenesis, the $\delta^{13}\text{C-CH}_4$ of the new bulk CH₄ would reflect a mixture between the weighted $\delta^{13}\text{C}$ composition of heavier hydrocarbons that were degraded and original $\delta^{13}\text{C-CH}_4$ (Figure 3.4A). Additionally, the [DIC] and $\delta^{13}\text{C-DIC}$ would ultimately be unchanged in this scenario.

However, if there is only partial oxidation of hydrocarbons or partial conversion of the oxidized CO₂ to secondary CH₄, the isotopic composition of both CH₄ and CO₂ will be fractionated according to the relevant α values and the fraction of hydrocarbons that undergo methanogenesis or dissolution, respectively. As a result, while the C₁/C₂₊ increases, there may be a negative shift in the resulting $\delta^{13}\text{C-CH}_4$ if microbes utilize a fraction of the isotopically lighter carbon (i.e., up and to the left in Figure 3.4A). Further, if the CO₂ dissolves into formation water there will be an increase in [HCO₃] and a slight positive shift in $\delta^{13}\text{C-DIC}$ that may become significantly enriched with later utilization of the labile carbon pool via secondary methanogenesis (Vinson et al., 2017). Finally, while the labile carbon pool would decrease following methanogenesis, if the volume of thermogenic gas was sufficiently large, partial oxidation followed by secondary methanogenesis may still result in relatively high [HCO₃]. In this scenario, the $\delta^{13}\text{C-CH}_4$ would predominantly resemble a mixture between the original $\delta^{13}\text{C-CH}_4$ and the $\delta^{13}\text{C}$ of the thermogenic hydrocarbons with a small but quantifiable negative shift equivalent to the fraction of CO₂ lost to dissolution. Therefore, I suggest the simplest explanation for the summation of hydrocarbon data in this study is partial oxidation of thermogenic natural gas followed by secondary methanogenesis, where the

relatively high $[\text{HCO}_3^-]$ measured in samples with high thermogenic gas contents and enriched $\delta^{13}\text{C-DIC}$ may in fact represent the remaining DIC pool following secondary methanogenesis.

Secondary methanogenesis was previously proposed by Lavoie et al. (2016) to explain the trend of decreasing $[\text{C}_2\text{H}_6]$ and $[\text{C}_3\text{H}_8]$ in samples with higher $[\text{CH}_4]$ in bulk rocks from the Saint-Édouard region (well F21), which was supported by elevated $[\text{DIC}]$, $\delta^{13}\text{C-DIC}$, and $\delta^{13}\text{C-CH}_4$ in groundwater from the region (Bordeleau et al., 2018a). Additionally, Lavoie et al. (2016) noted that most of the shallow bedrock in the Saint-Édouard region was hydrocarbon-rich and within the oil window of thermal maturity. Stable isotope studies of oil reservoirs that have been degraded by microbial oxidation show $\delta^{13}\text{C-DIC}$ can be significantly enriched ($>0\%$) in the formation waters (Carothers and Kharaka, 1980; Pallasser, 2000), which could help explain very positive $\delta^{13}\text{C-DIC}$ ($>+20\%$) in some of the samples with wet hydrocarbons ($\text{C}_1/\text{C}_{2+} < 15$). Although minor oil is observed in rock cores retrieved from Sainte-Rosalie Group in this region (Lavoie et al., 2016), natural gas is abundant. As a result, the oxidation of higher aliphatic hydrocarbons is more likely the dominant mechanism that influences hydrocarbon and water chemistry in this region.

3.5.4 Noble Gas Constraints on the History of Hydrocarbon-Groundwater Interactions

The depletion of noble gas concentrations (^{20}Ne , ^{36}Ar , ^{84}Kr , ^{132}Xe) relative to the anticipated air-equilibrated water levels in the hydrocarbon-rich samples suggests stripping has influenced the composition of gas-rich groundwater in the region (Figures 3.6, 3.10A). Further, the relative proportions of the ASW noble gases show fractionation between the lighter noble gases (^{20}Ne) compared to heavier (^{36}Ar , ^{84}Kr , ^{132}Xe) in these samples, where lighter gases are more depleted (i.e., preferentially lost) with respect to ASW values (Figures 3.6D, 3.9, 3.10A).

The migration of thermogenic hydrocarbon gases through groundwater preferentially enriches the migrated gas in the light noble gases (i.e., ^4He , ^{20}Ne). In the present study, the opposite trend is observed. As a result, one might hypothesize that the groundwater composition in gas-rich samples from the Saint-Édouard region is the remnant of prior stages of gas-water partitioning (i.e., a residual fluid); this could account for the preferential depletion of the less soluble noble gases (i.e., ^{20}Ne , ^{36}Ar). Alternatively, water that previously equilibrated with oil can display similar trends (Bosch and Mazor, 1988; Pinti and Marty, 1995; Wen et al., 2017). Because the bedrock formations in the Saint-Édouard region are hydrocarbon-rich and lie within the oil maturity window (Lavoie et al., 2016), I explore the potential for oil-groundwater interactions in this region.

In an attempt to understand the role that oil may have on the groundwater system in the study area, I have integrated two numerical models developed by Bosch and Mazor (1988) and refined by subsequent works (Battani et al., 2000; Pinti and Marty, 1995; Torgersen and Kennedy, 1999; Wen et al., 2016b; Wen et al., 2017). The first model normalizes the measured value in each sample for each noble gas to the measured [^{36}Ar], and then that ratio is normalized to the atmospheric ratio (Figure 3.10B). In this model, enriched ^{20}Ne and depleted ^{84}Kr and ^{132}Xe relative to ASW (light blue line) suggests gas-water equilibration, whereas depleted ^{20}Ne and enriched ^{84}Kr and ^{132}Xe relative to ASW suggests oil-water equilibration (Bosch and Mazor, 1988).

The second model is a theoretical Rayleigh distillation trend calculated using increasing oil/water ratios (Bosch and Mazor, 1988; Pinti and Marty, 1995). This model assumes an ASW starting groundwater composition that is then fractionated based on the differences in solubility between water and oil, which is assumed to be devoid of dissolved noble gases originally. For simplicity, this model uses alpha values for phase partitioning between pure water and light oil at

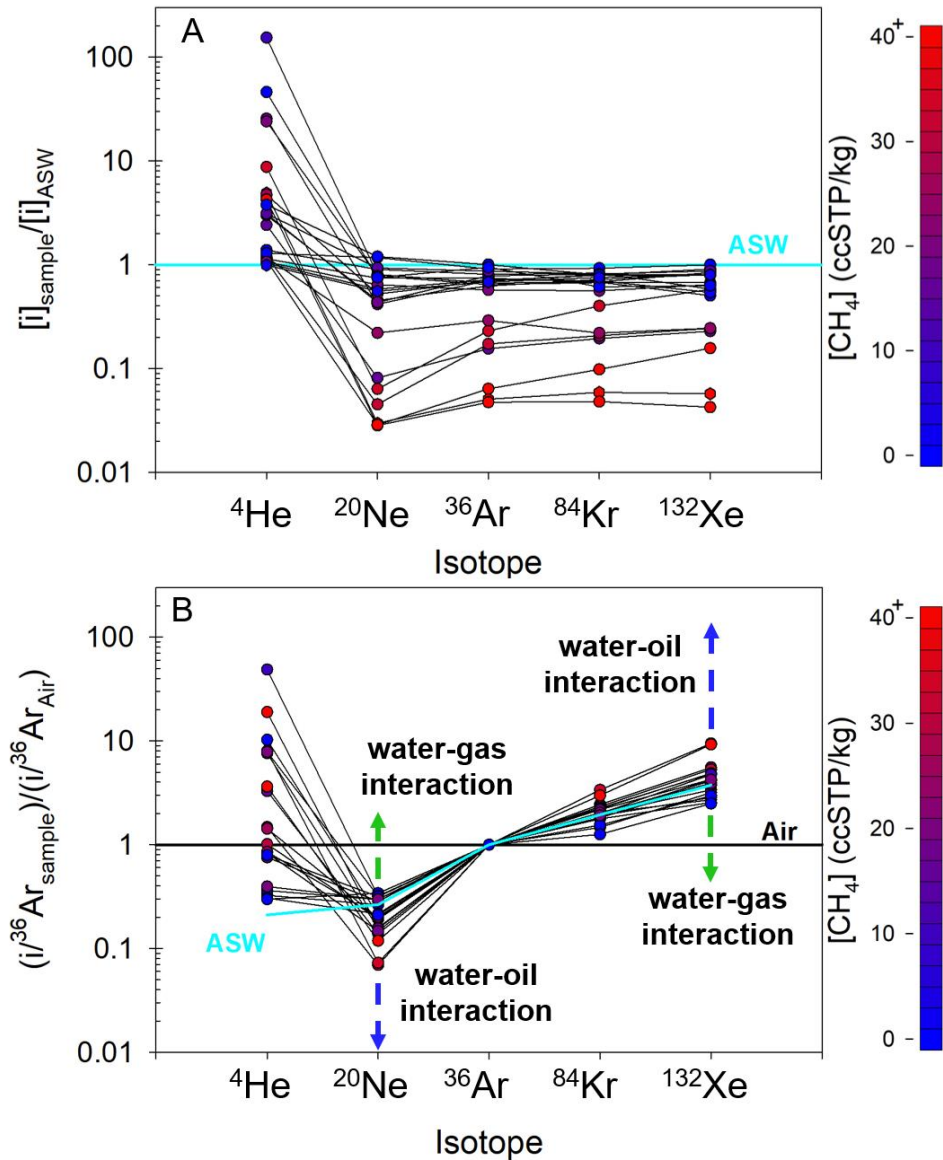


Figure 3.10: Fractionation of ASW noble gases when compared to calculated ASW concentrations (A) and fractionation when each isotope, normalized to ^{36}Ar in the samples, are compared to that ratio in air (B). Symbol color corresponds to $[CH_4]$ and hexagons are duplicate samples. In both figures, ^4He shows evidence of terrigenous inputs. In Figure 10A, the heavier noble gases in the methane-rich samples show a trend of increasing depletion from ASW with decreasing atomic mass (i.e., Ne is the most depleted). In Figure 10B, the trend of depleted Ne with Kr and Xe enrichment compared to ASW is consistent water-oil interaction as opposed to water-gas interaction (Bosch and Mazor, 1988).

25°C as reported in Kharaka and Specht (1988). An initial temperature of 25°C is assumed, which is consistent with previous studies (e.g., Wen et al., 2017) and provides a suitable fit for the data. In this study area, the Utica Shale (the most volumetrically significant hydrocarbon reservoir) has a present thermal maturity that lies in the dry gas window (Chatellier et al., 2013), while some oil has been observed in the shallower Sainte-Rosalie Group in the Saint-Édouard region (Lavoie et al., 2016). Therefore, I also model oil-water partitioning using an initial temperature of 25°C for illustrative purposes.

I incorporate the Rayleigh fractionation model using alpha values for each fractionation process and compare the measured and modeled $^{20}\text{Ne}/^{36}\text{Ar}$ versus $^{84}\text{Kr}/^{36}\text{Ar}$ and $^{132}\text{Xe}/^{36}\text{Ar}$ (Figure 3.11) to explore two hypotheses to explain this data: 1) residual water after equilibrium with oil and 2) residual groundwater following partial degassing and stripping. Overall, the data show good first-order agreement to both trends of degassing and oil-water equilibration.

To a first order, oil-water equilibration could explain the relative depletion of atmospheric noble gases relative to the anticipated ASW equilibrium and the relative trends for noble gas fractionation ($^{84}\text{Kr}/^{36}\text{Ar}$, $^{132}\text{Xe}/^{36}\text{Ar}$) (Figures 3.9-11). However, groundwater that previously equilibrated with oil should display elevated $^{20}\text{Ne}/^{36}\text{Ar}$ compared to ASW (Wen et al., 2017). Instead, data from the current study area displays systematic depletion of Ne relative to Ar, Kr, and Xe (Figure 3.10), which are highly soluble in liquid hydrocarbons. The relative depletion of neon with respect to the heavier noble gases suggests that the fractionation is likely affected by degassing of groundwater. For these reasons, I conclude that groundwater degassing is the most likely scenario to account for all of the noble gas data.

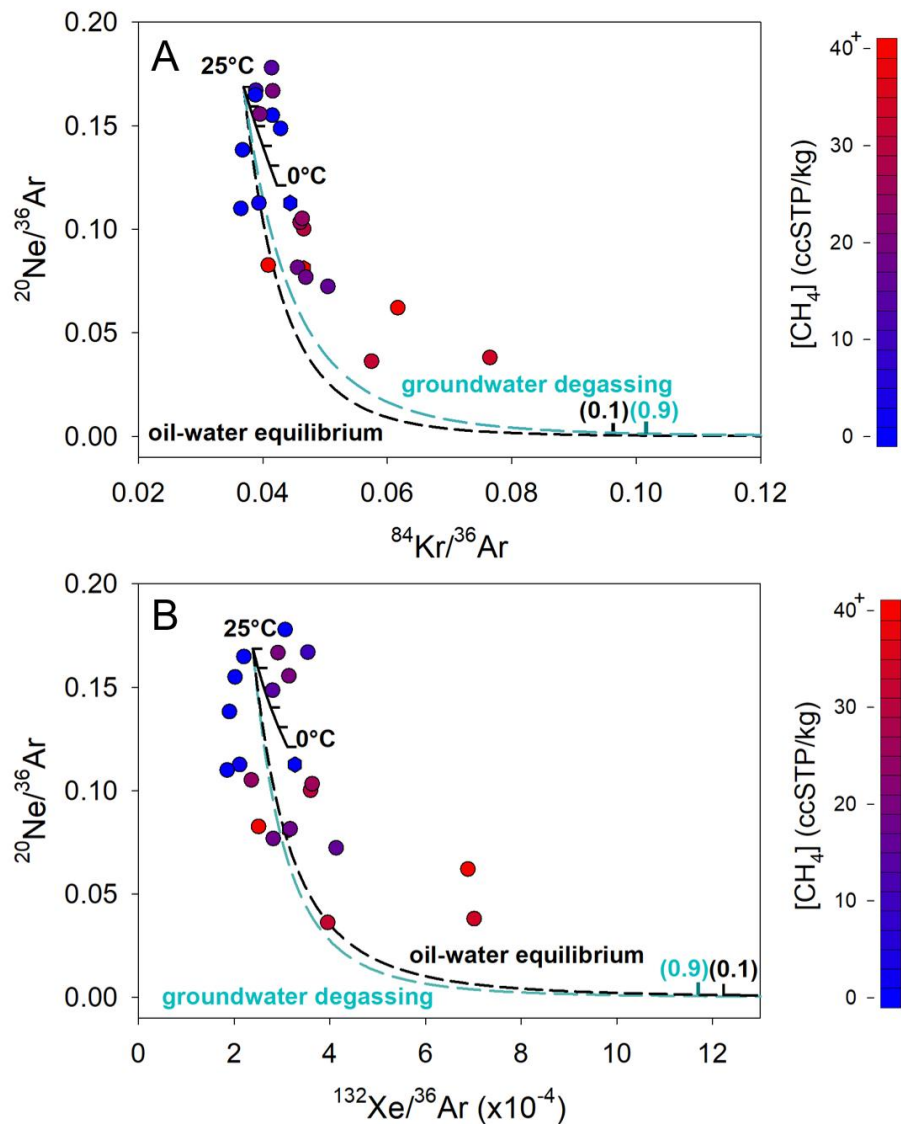


Figure 3.11: $^{20}Ne/^{36}Ar$ vs. $^{84}Kr/^{36}Ar$ (A) and $^{20}Ne/^{36}Ar$ vs. $^{132}Xe/^{36}Ar$ (B). Symbol color corresponds to $[CH_4]$ and hexagons are duplicate samples. The black dashed line is a modeled water-oil equilibration trend at 25°C with increasing oil/water ratios adapted from Bosch and Mazor (1988). The noble gas composition of oil was assumed using Kharaka and Specht (1988) solubility values for light oil. The teal dashed line is a theoretical groundwater degassing model representing progressively more degassed water at 25°C. This model was adapted from a groundwater gas stripping and re-dissolution model (GGS-R) (Gilfillan et al., 2008; Gilfillan et al., 2009) and results in the residual water being enriched in heavier noble gas isotopes. These trends show both scenarios may result in similar ASW noble gas isotopic compositions if the true noble gas composition of the oil is unknown, therefore degassing must be ruled out before oil can be attributed to groundwater that has similar isotopic compositions as what is seen in the Saint-Édouard region.

I recognize that the groundwater composition could also be influenced by multiple stage process (e.g., prior history of oil-water equilibration followed by groundwater degassing). Although this two-stage model is not required to account for the observed data, based on the observations of oil shows in cores retrieved from the Sainte-Rosalie Group, I examine if a multistage process could account for the observed data. A similar model was first proposed by Battani et al. (2000) and was applied to groundwater overlying the oil- and gas-rich Barnett Shale in Texas in Wen et al. (2017). This model postulated that water equilibrated with oil, which preferentially reduced noble gases in the residual water phase and that the residual water was later degassed. However, as discussed above, low $^{20}\text{Ne}/^{36}\text{Ar}$ and quantitative stripping of heavier noble gases (i.e., lower concentrations of heavier noble gases than anticipated for ASW) differ from the results obtained in Battani et al. (2000) and Wen et al. (2017), which were all significantly above ASW. As a result, I conclude that hydrocarbon-groundwater interactions in the region are dominated by the degassing of groundwater.

For stripping/degassing to occur, the gas concentrations must exceed the saturation level of dissolved gases in the groundwater (i.e., exceed the bubble point), which is dependent on salinity, temperature, and pressure (i.e., groundwater depth). Theoretically, degassing could occur if the gas saturation level of groundwater is surpassed such as via the influx of exogenous fluids (e.g., thermogenic natural gas, mantle-derived CO_2) or the addition of *in situ* microbial gas (Dowling et al., 2002; Kreuzer et al., 2018). Because microbial gas is widespread in the Saint-Édouard region and the most fractionated ASW noble gas ratios correspond to the highest Cl and DIC abundances and the most enriched $\delta^{13}\text{C}\text{-CH}_4$ and $\delta^{13}\text{C}\text{-DIC}$ (Figure 3.8D), I suggest that degassing is most likely related to primary or secondary methanogenesis. In combination with the

lack of abundant liquid oil, I conclude that degassing/stripping of air-saturated noble gases, perhaps by the formation of secondary methanogenesis, is the most likely cause of extensive degassing.

3.6 Conclusions

The combination of aqueous and gas geochemical tracers suggest that the composition of groundwater in the Saint-Édouard region likely evolved in response to a series of complex, multi-stage processes. I envision that first thermogenic natural gas and brine were emplaced in modern aquifers following/during primary and secondary hydrocarbon migration. Next, as thermogenic hydrocarbons interacted with either methanotrophic microbes in relatively oxidizing aquifers, thermogenic hydrocarbons were oxidized to CO₂. Finally, following oxidation of hydrocarbons to CO₂, hydrogenotrophic methanogens converted a portion of the oxidation byproduct (i.e., CO₂) to CH₄ (secondary methanogenesis). In combination, these processes can account for concomitant presence of highly elevated C₁/C₂⁺, progressively more negative δ¹³C-CH₄, higher [DIC], and more positive δ¹³C-DIC.

In general, the observed data and subsequent interpretations highlight the importance of adequately characterizing baseline water and gas geochemistry in areas targeted for shale gas development. Further, these data suggest that the observed aqueous and gas geochemical techniques can be influenced by a series of complex processes that obfuscate the true genetic source of natural gas in groundwater. However, here I show that through careful integration of hydrocarbon and noble gas data, one can identify the sequence of post-genetic modification processes that influence the composition of natural gas in groundwater and determine the original source of natural gas.

Chapter 4. Geochemical evidence for fugitive gas contamination and associated water quality changes in drinking-water wells from Parker County, Texas

Abstract

Extensive development of horizontal drilling and hydraulic fracturing have enhanced energy production but have also raised some concerns about drinking-water quality in areas of shale-gas development. One particularly controversial case that has received significant public and scientific attention involves possible contamination of groundwater in the Trinity aquifer in Parker County, Texas. Despite extensive prior work, controversy about the origin of natural gas and the mechanism of its emplacement in the Trinity aquifer within this study area remains. Here, I present a detailed geochemical dataset collected across three sampling campaigns along with the summation of other published data from the area. Data include major and trace dissolved ions, trace metals, molecular gas compositions (e.g., C₁/C₂₊, N₂/CH₄, CO₂/CH₄, H₂S), compound-specific stable isotopes of hydrocarbons ($\delta^{13}\text{C}$ and $\delta^2\text{H}$), dissolved inorganic carbon ($\delta^{13}\text{C}$ -DIC), CO₂ ($\delta^{13}\text{C}$), nitrogen ($\delta^{15}\text{N}$ -N₂), water ($\delta^{18}\text{O}$, $\delta^2\text{H}$, ^3H), noble gases (He, Ne, Ar, Kr, and Xe), boron ($\delta^{11}\text{B}$), and strontium ($^{87}\text{Sr}/^{86}\text{Sr}$) of 20 drinking-water wells sourced from the Trinity aquifer. The compendium of data confirms the occurrence of mixing between a natural salt- (Cl >400 mg/L) and hydrocarbon-rich source of water with a low-salinity, shallow, and younger groundwater. The naturally occurring salt- and gas-rich groundwater originated from the dissolution of evaporites and reverse base-exchange reactions, while hydrocarbon gases display strong evidence for sulfate-paired oxidation, in some cases followed by secondary methanogenesis (i.e., utilization of newly

oxidized CO₂ to form CH₄). As compared to this well-characterized baseline of water quality, the data confirm the presence of fugitive gas contamination that originated from intermediate-depth strata (i.e., the Strawn Group) in a subset of five drinking-water samples. Similar to recent observations in the Marcellus region, the data suggest that following fugitive gas contamination there is direct evidence for post-genetic secondary water quality changes that occur following sulfate-paired hydrocarbon oxidation and secondary methanogenesis. Importantly, no evidence for upward brine migration or contamination by chemicals used in hydraulic fracturing was identified.

4.1 Introduction

The significant expansion of horizontal drilling and hydraulic fracturing of unconventional hydrocarbon reservoirs has rejuvenated American energy output throughout the last decade (Kerr, 2010). However, public and political support for unconventional energy extraction has been frequently tempered by environmental concerns, including the potential for compromised drinking-water quality from hydrocarbon gas contamination, hydraulic fracturing fluids, salinization, or naturally occurring radioactive materials (NORMs) near shale gas development (Darrah et al., 2014; Drollette et al., 2015; Fontenot et al., 2013; Harkness et al., 2017b; Heilweil et al., 2015; Hildenbrand et al., 2015; Jackson et al., 2013; Llewellyn et al., 2015; Nicot et al., 2017c; Osborn et al., 2011; Vengosh et al., 2014; Wen et al., 2019; Woda et al., 2018).

The most commonly reported groundwater water-quality concern relates to elevated levels of methane (CH₄) in groundwater, commonly termed fugitive gas contamination. Several studies have suggested that shale gas drilling can lead to fugitive gas contamination in a subset of drinking-water wells near shale-gas drilling sites (Darrah et al., 2014; Heilweil et al., 2015; Jackson et al., 2013; Osborn et al., 2011; Woda et al., 2018). Conversely, other studies suggest that CH₄ is

naturally occurring and unrelated to shale gas development (Baldassare et al., 2014; Darrah et al., 2015b; Eymold et al., 2018; Harkness et al., 2017b; Kreuzer et al., 2018; Molofsky et al., 2013; Nicot et al., 2017c; Siegel et al., 2015; Wen et al., 2016b). Therefore, the relationship between elevated CH₄ and other aliphatic hydrocarbon gases (ethane, propane, etc.) in groundwater and shale gas exploration remains controversial, as do the mechanisms by which fugitive gas contamination reaches shallow aquifers in instances where releases occur.

To date, the debate on possible fugitive gas contamination has focused on determining the source(s) and mechanism(s) (both natural and anthropogenic) from which hydrocarbon gases originate and migrate to shallow aquifers (Darrah et al., 2014; Dusseault and Jackson, 2014; Jackson et al., 2013; Osborn et al., 2011), the frequency of fugitive gas releases (Baldassare et al., 2014; Molofsky et al., 2013; Siegel et al., 2015), and more recently an assessment of how fugitive gas contamination events influence groundwater geochemistry and quality (Woda et al., 2018). Combined, these efforts have led to a better understanding of the frequency of fugitive gas contamination events, improved interpretation of the factors that cause them, and a characterization of the potential suite of associated environmental risks.

Previous studies in shallow aquifers overlying the Barnett Shale (Barnett) in Parker County, TX examined molecular hydrocarbon ratios (e.g., C₂H₆+ / CH₄), carbon and hydrogen isotopes of CH₄ (i.e., δ²H-CH₄ and δ¹³C-CH₄), compound-specific carbon isotopes of higher order aliphatic hydrocarbons (δ¹³C-C₂H₆), stable isotopes of nitrogen (δ¹⁵N-N₂), noble gases (He-Xe), BTEX compounds, dissolved ions (e.g., Cl, Br, NO₃, SO₄), and trace metals (e.g., As) (Darrah et al., 2014; Fontenot et al., 2013; Hildenbrand et al., 2015; Larson et al., 2018; Nicot et al., 2017c; Wen et al., 2016b; Wen et al., 2017). Data included in these studies provided a method to

distinguish a subset of drinking-water wells with fugitive gas contamination from the majority of drinking-water wells that contained naturally-occurring hydrocarbon gases. Although the mechanism and pathway have remained controversial, prior work implicates that the leakage of natural gas was sourced from an intermediate-depth formation (i.e., the Strawn Groups) into the overlying Trinity aquifer and influenced a subset of five drinking-water wells (Darrah et al., 2014; Wen et al., 2016b). Uncertainty remains as to whether gas sourced from the Strawn Groups (referred here throughout as “Strawn” gas) was released as a result of shale-gas drilling activities, changes in local water use (aquifer drawdown), or by pathways created when drinking-water wells were drilled near the study area (Darrah et al., 2014; Larson et al., 2018; Nicot et al., 2017c; Wen et al., 2016b). Here, additional geochemical data were incorporated in order to conduct a more comprehensive geochemical evaluation of 20 drinking-water wells associated with this controversial case overlying the Barnett Shale in Parker County, TX (Figure 4.1).

The detailed dataset includes major ions (e.g., Na, Ca, Mg, dissolved inorganic carbon (DIC as HCO_3), Cl, Br, SO_4), the isotopic composition of DIC ($\delta^{13}\text{C}$ -DIC), water ($\delta^{18}\text{O}$ and $\delta^2\text{H}$), boron ($\delta^{11}\text{B}$), and strontium ($^{87}\text{Sr}/^{86}\text{Sr}$), the molecular composition of major gases (C_1 to C_{6+} , N_2 , H_2S , CO_2), the isotopic composition of major and hydrocarbon gases ($\delta^{13}\text{C}$ - C_1 , $\delta^2\text{H}$ - C_1 , $\delta^{13}\text{C}$ - C_2 , and $\delta^{15}\text{N}$ - N_2), and noble gases (e.g., $^3\text{He}/^4\text{He}$, $^4\text{He}/^{20}\text{Ne}$, $^{20}\text{Ne}/^{36}\text{Ar}$, $^{40}\text{Ar}/^{36}\text{Ar}$) from samples collected at three points in time over a one year period.

The comprehensive set of information presented herein is critical for creating a general framework to distinguish anthropogenic contamination from natural processes of gas-rich brine migration. This work was designed to address four critical questions related to the potential for fugitive gas contamination: 1) do comprehensive geochemical analyses support previous

conclusions of fugitive gas contamination in Parker County, TX?; 2) does the complete dataset confirm that intermediate Strawn-sourced natural gas is responsible for fugitive gas contamination?; 3) does fugitive gas contamination lead to secondary changes in water quality, such as sulfate reduction, the generation of toxic H₂S (Van Stempvoort et al., 2005; Van Stempvoort et al., 2007; Woda et al., 2018), or the redox/base exchange controlled release of salts, oxyanions, or metals (e.g., As, Fe, Mn) from the aquifer rocks (Bennett and Dudas, 2003; Wen et al., 2019; Woda et al., 2018) via secondary reactions?; and finally 4) is there evidence for upward brine (or hydraulic fracturing fluid) migration associated with fugitive gas contamination?

The combination of geochemical and hydrological data allows us to: 1) determine the source of naturally-occurring saline groundwater and hydrocarbon gases in the area; 2) identify the source of fugitive gas contamination; and 3) resolve the extent to which secondary gas-water interactions (e.g., CH₄ oxidation, sulfate reduction, base-exchange reactions) occur in shallow aquifers. This integrated approach will provide an improved template for future fugitive gas investigations in other study areas in the USA and abroad.

4.2 Geologic Background

4.2.1 Fort Worth Basin

The current study area is located near the southern border of Parker County, Texas within the Fort Worth Basin. The Fort Worth Basin is a northeastward deepening sedimentary trough that covers approximately 38,000 km² throughout north-central Texas in the southern United States (Figure 4.1). The stratigraphy is dominantly composed of Paleozoic sedimentary packages that reach a maximum thickness of ~3,700 m near the western margin of the Muenster Arch, which is a subsurface structural high in the northeast corner of the basin (Flippin, 1982; Pollastro et al.,

2007; Walper, 1982). The basin formed as a foreland depression in response to the advancing Ouachita fold belt onto the North American continental margin during the late Mississippian (~359

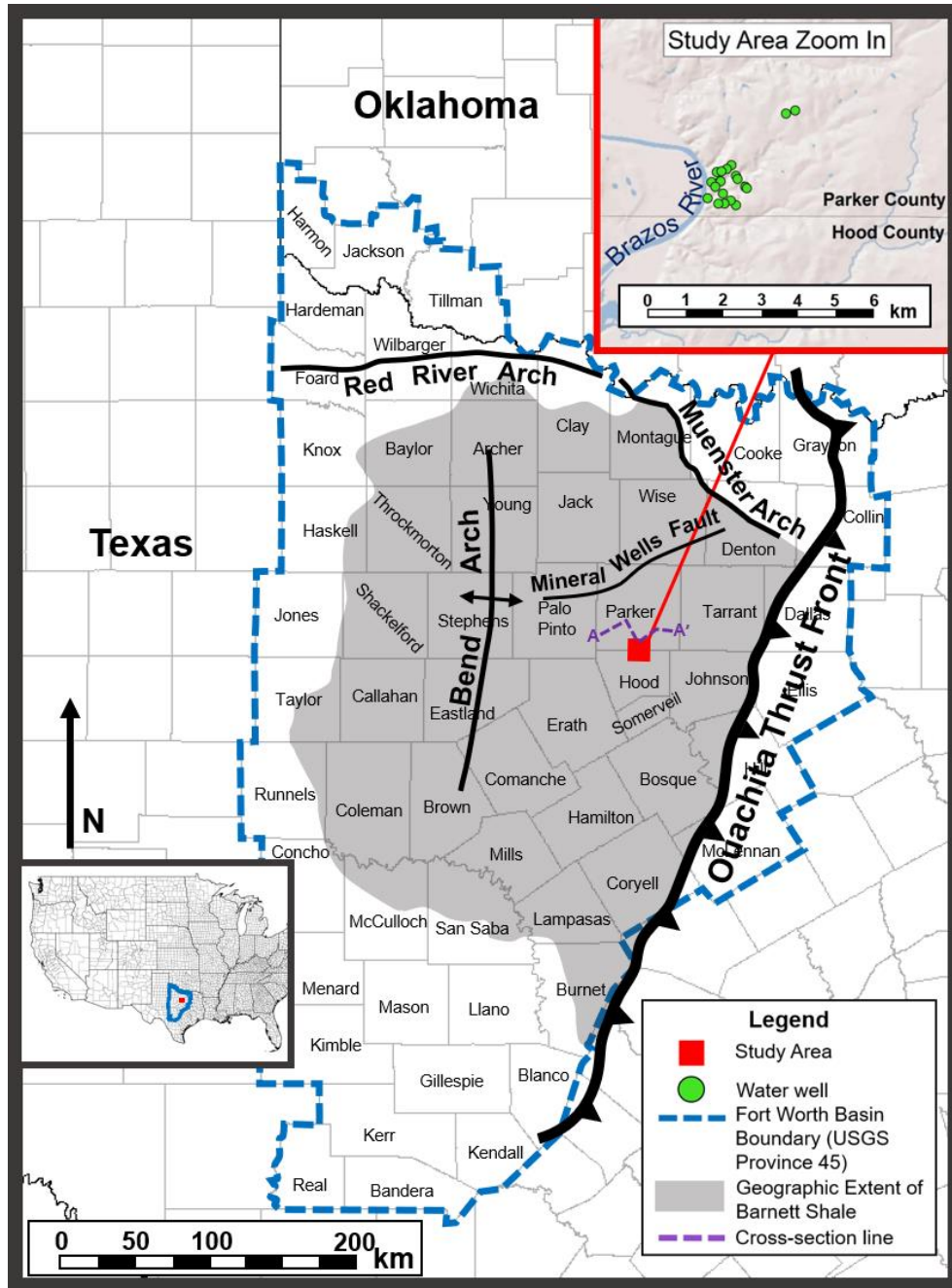


Figure 4.1: Map of Fort Worth Basin and study area. The geographic extent of the Barnett Shale is shaded in gray. Structural features and boundaries have been adapted from Pollastro et al. (2003).

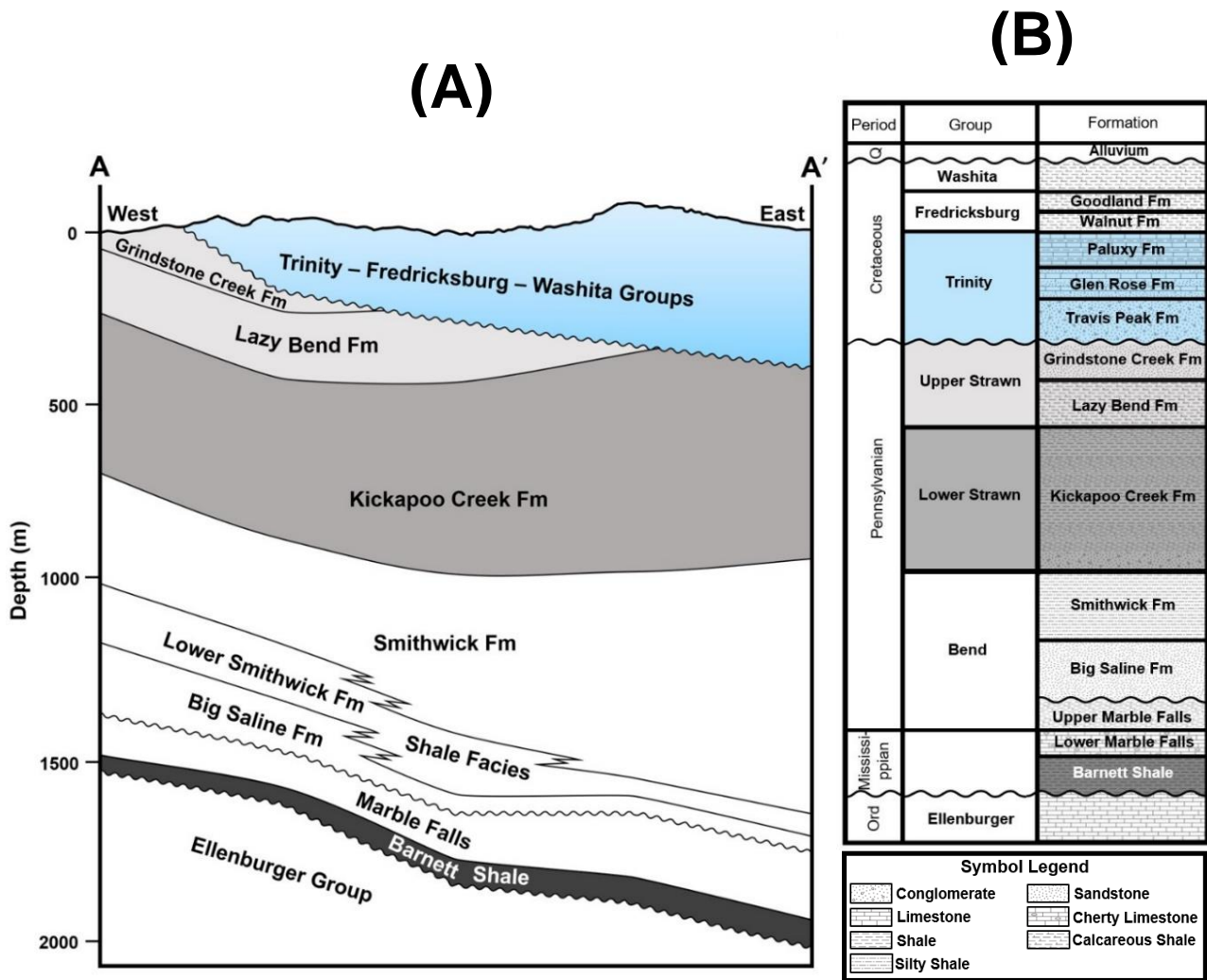


Figure 4.2: Generalized west to east cross-section (A) and stratigraphic column (B) through southern Parker County, Texas. Adapted from Herkommer and Denke (1982). Cretaceous units include the major aquifers in the study area and are shaded in blue. The light and dark gray shaded units are members of the Upper and Lower Strawn Groups, respectively, which are suggested to be the source of natural gas into shallow aquifers in the study area.

to 323 Ma) through the early Pennsylvanian (~323 to 299 Ma). Basin subsidence continued until crust from the North American plate began subducting under a marginal volcanic arc, which eventually led to the thrusting of marginal marine strata towards the continental interior (Walper, 1982). The northwestward migrating hinge of the fold belt resulted in the deposition of transgressive sequences that included the organic-rich Barnett Shale over a once-stable carbonate shelf deposited nearly continuously from the Cambrian through the Ordovician (Figure 4.2). Deformation of the shelf margin reactivated fault systems in the Fort Worth Basin, producing structural features that include the Llano Uplift to the south, the Red River and Muenster Arches to the north and northeast, and the Bend Arch to the west (Hill et al., 2007; Walper, 1982) (Figure 4.1). Within this geographic area, there is also the prominent northeast-southwest trending Mineral Wells Fault System that has been mapped in the subsurface in the Palo Pinto, Parker, Wise, and Denton county areas (Pollastro et al., 2003) (Figure 4.1). Because it does not correlate with the other structural features in the Fort Worth Basin, the origin of the Mineral Wells Fault System remains controversial and poorly understood; the leading hypothesis suggests that it was either activated or reactivated during the Paleozoic (Montgomery et al., 2005; Pollastro et al., 2007).

Total sedimentary deposition includes an ~3,700 m thick stratigraphic sequence in the Fort Worth Basin. The Cambrian-Mississippian carbonate platform, which contains occasional interbedded shales, is ~1,200 to 1,500 m thick. Cambrian to Ordovician carbonates (e.g., Ellenburger Group) were deposited directly over Precambrian granite and diorite basement following major erosional events that removed Silurian and Devonian strata, leaving an unconformity above the Ellenburger Group (Henry, 1982; Turner, 1957). Transgressive sequences of carbonates, calcareous shales, and gray shales lie above the unconformity (Bend, Lower and

Upper Strawn, and Canyon Groups) and comprise the remaining Paleozoic strata (Herkommer and Denke, 1982; Walper, 1982). Additionally, a sea level drop following the deposition of the Ellenburger Group sequence resulted in prolonged exposure and karsting in the upper members (Kerans, 1988). The organic-rich shale of the Barnett was unconformably deposited over the Ellenburger Group during the late-Mississippian (~354-323 Ma) and has a maximum thickness of 305 m near the western margin of the Muenster Arch (Henry, 1982; Hill et al., 2007; Pollastro et al., 2007). Gray calcareous shales and limestones of the Marble Falls Fm. were deposited directly above the Barnett, which are separated from the overlying Pennsylvanian strata by another disconformity (Flippin, 1982; Henry, 1982).

Pennsylvanian clastic sediments and carbonates overlie the Cambrian-Mississippian carbonate platform; these formations are ~1,800 to 2,100 m thick. Erosion of Permian and Upper Pennsylvanian strata preceded Cretaceous sediment deposition (Walper, 1982), which resulted from westward progression of the Western Interior Seaway (Flippin, 1982). Relatively thin sequences of Cretaceous rocks overlie the Pennsylvanian sequences in the eastern portion of the Fort Worth Basin (Pollastro et al., 2007). Cretaceous units in the Fort Worth Basin include those from the Comanche Series, which represent the stratigraphically youngest units, excluding thin lenses of alluvium (Herkommer and Denke, 1982). The Comanche Series, including the Trinity, Fredricksburg, and Washita Groups, constitute the principal drinking-water aquifers in Parker County. These formations are primarily sandstone and limestone with minor amounts of calcareous mudstone (Herkommer and Denke, 1982).

4.2.2 Petroleum Systems in the Fort Worth Basin

Commercial oil and gas activities in the Fort Worth Basin over the last 15 years have primarily focused on the Barnett (Bowker, 2007; Hill et al., 2007; Montgomery et al., 2005), with peak production occurring between 2012-2014 (Texas, 2019b). In general, the Fort Worth Basin contains multiple producing oil and gas reservoirs, including the unconventional Barnett and conventional Ellenburger, Bend, Strawn, and Canyon Groups (Pollastro et al., 2007). Geochemical studies suggest most of the hydrocarbon reservoirs are largely of Barnett origin that were released and migrated episodically as a result of primary and secondary migration or hydrodynamic flow (Jarvie et al., 2001; Jarvie et al., 2003). The Barnett has produced hydrocarbons of varying thermal maturity (i.e., oil, oil-associated-gas, dry gas) across the Fort Worth Basin. Oil has been produced in the northern portion of the basin and west of the Bend Arch where the basin shallows. By comparison, oil-associated-gas and dry gas are produced progressively eastward towards the Muenster Arch, where the Barnett is buried most deeply and at its highest thermal maturity (Pollastro et al., 2007). Anomalously high thermal maturities in the Barnett have been identified near the Mineral Wells Fault System and are thought to be related to hydrothermal fluid interactions (e.g., Pollastro et al., 2003).

4.2.3 Parker County, Texas and Study Area

Locally, the thermal maturity of the Barnett is within the oil-associated-gas window (Rodriguez and Philp, 2010). To date, seven horizontal unconventional gas wells and one vertical well have been drilled in or under the study area, with two unconventional wells currently in production in the southern portion of the study area (Texas, 2019a). Previous studies suggest that the Barnett has had substantial fluid loss (dominantly as oil) to the overlying Bend and Strawn

Groups in the Fort Worth Basin (Hill et al., 2007; Kornacki and McCaffrey, 2011; Montgomery et al., 2005; Pollastro et al., 2007). In Parker County, rocks from the Strawn Groups have a maximum thickness of over 750 m. The lower Strawn Group is known to contain shales with interbedded hydrocarbon-charged intervals (Nicot et al., 2017c). The Mineral Wells Fault System has been mapped in the northwest portion of the county, but there is no evidence that this fault or secondary faults extend southward into the study area (Pollastro et al., 2007). Overall, the Paleozoic units in Parker County dip northeastward toward the depocenter of the basin near the Muenster Arch (Herkommer and Denke, 1982) (Figure 4.2), and the overlying Cretaceous units, which are separated by an angular unconformity, dip to the east (Nicot et al., 2017c).

The primary aquifers in the study area include formations in the Trinity Group, which consist of multiple shallow marine Cretaceous formations that increase in thickness from west (~0 m) to east (~600 m) and lie directly over the Upper Strawn Group (Herkommer and Denke, 1982; Nicot et al., 2017c). The Trinity Group has three members. The Travis Peak Fm. (Lower Trinity, also known as Twin Mountains Formation) composed of sandstones and conglomerates. The Glen Rose Fm. (Middle Trinity) is sandstone with interbedded limestone. The Paluxy Fm. (Upper Trinity) is shale with interbedded sandstone (Henry, 1982; Herkommer and Denke, 1982). Within the study area, the Glen Rose Fm. behaves as an aquitard (Nicot et al., 2017c), while the Paluxy Fm. is not present. As a result, the Travis Peak Fm. (Lower Trinity) is the primary groundwater source.

The study area is bounded to the west by the Brazos River that acts as a local zone of groundwater discharge (Figure 4.1). Regional groundwater flow is predominantly west to east (Nicot et al., 2013). In addition to lateral groundwater flow, Nicot et al. (2013) suggest

hydrogeologic connectivity between adjacent sandstones of the Strawn Groups and overlying Trinity Groups, which may facilitate localized fluid migration of deeper brine and hydrocarbons within the Trinity Aquifer system.

4.3 Materials and Methods

4.3.1 Sample Selection

This study examined groundwater above and produced gas samples from the Barnett and overlying formations (Strawn) in Parker County, TX. Elevated levels of CH₄ in a subset of domestic drinking-water wells at this site have been the source of substantial controversy. As a result, we collected groundwater samples from twenty (n=20) domestic drinking-water wells multiple times over a one-year period near the city of Weatherford (Figure 4.1; Tables 4.1-3).

The study area is within the Fort Worth Basin underlain by the Barnett Shale (~1,500-2,000 m depth) (Figure 4.2A). The typical depth of drinking-water wells in the study area was 60 to 75 m. In all figures, the groundwater samples are plotted as circles (December, 2012), inverted triangles (August, 2013), and squares (November, 2013) according to collection time. Similarly, the abundance of CH₄ from all plots is preserved using a gray-scale intensity where white corresponds to CH₄ concentrations of 0 ccSTP/L and ranges up to black for >60 ccSTP/L. All drinking-water wells that were previously identified as having fugitive gas contamination are denoted by light green rims around data symbols.

Production gases from the Strawn and Barnett in Parker County were collected from producing conventional (i.e., vertical) natural-gas-wells drilled to each target formation according to methods described previously (Hunt et al., 2012) (Table 4.4). Producing natural-gas wells from the Barnett and Strawn near the study area were also sampled as part of a recent groundwater study

by Nicot et al. (2017c) who reported hydrocarbon molecular abundances (C₁-C₃ %) and stable isotopes of carbon for C₁-C₃ hydrocarbons and stable isotopes of hydrogen for C₁-C₂ hydrocarbons (Figures 4.6-7).

4.3.2 Sample Analysis

Prior to sampling, drinking-water wells were purged and simultaneously monitored for pH, electrical conductivity, and temperature until stable values were obtained. Water samples were collected before any treatment systems and were filtered and preserved following USGS protocols (USGS, 2011). Water samples and produced gas samples were collected in-line with either copper tubes or evacuated borosilicate flasks and flushed with at least 50 volumes of sample prior to sealing (Darrah et al., 2015b).

Groundwater samples were analyzed for major ions (e.g., Na⁺, Ca²⁺, Mg²⁺, HCO₃⁻ (as DIC)), Cl⁻, Br⁻, SO₄²⁻), isotopic compositions of DIC ($\delta^{13}\text{C-DIC}$), water ($\delta^{18}\text{O-H}_2\text{O}$, $\delta^2\text{H-H}_2\text{O}$, ^3H), boron ($\delta^{11}\text{B}$), and strontium ($^{87}\text{Sr}/^{86}\text{Sr}$), molecular composition of major gases (C₁ to C₆₊, N₂, H₂S, CO₂), isotopic compositions of hydrocarbon gases and N₂ ($\delta^{13}\text{C-CH}_4$, $\delta^2\text{H-CH}_4$, $\delta^{13}\text{C-C}_2\text{H}_6$, and $\delta^{15}\text{N-N}_2$), and noble gas elemental ([He], [Ne], [Ar]) and isotopic ($^3\text{He}/^4\text{He}$, $^{20}\text{Ne}/^{22}\text{Ne}$, $^{21}\text{Ne}/^{22}\text{Ne}$, $^{38}\text{Ar}/^{36}\text{Ar}$, $^{40}\text{Ar}/^{36}\text{Ar}$, $^{20}\text{Ne}/^{36}\text{Ar}$) compositions according to standard methods reported previously.

The methods for the analyses of inorganic constituents (e.g., Na⁺, Ca²⁺, Mg²⁺, Cl⁻, Br⁻, SO₄²⁻) were identical to those reported previously (Osborn et al., 2011; Warner et al., 2012). Major anions, major cations, and trace metals were measured by ion chromatography (IC), direct current plasma optical emission spectrometry (DCP-OES), and VG PlasmaQuad-3 inductively coupled plasma mass spectrometry (ICP-MS), respectively. The detection limit for each analyte was determined by multiplying the standard deviation of repeated blank measurements as determined

by the slope of the external standard by three. Alkalinity was measured by titrating the sample with HCl to pH 4.5. Boron ($^{11}\text{B}/^{10}\text{B}$) and strontium isotope ($^{87}\text{Sr}/^{86}\text{Sr}$) ratios were analyzed at Duke University by a Thermo Fisher Triton thermal ionization mass spectrometer (TIMS) following methods reported previously (Harkness et al., 2017a; Harkness et al., 2018; Warner et al., 2014). Stable oxygen and hydrogen isotopes of water ($\delta^{18}\text{O}\text{-H}_2\text{O}$ and $\delta^2\text{H}\text{-H}_2\text{O}$) and $\delta^{13}\text{C}\text{-DIC}$ were measured at Duke University by continuous flow isotope ratio mass spectrometry using a Thermo Finnigan TCEA and Delta+ XL mass spectrometer by methods reported previously (Harkness et al., 2017b; Harkness et al., 2018).

Dissolved gas samples for hydrocarbon composition and stable isotopes were collected in the field using procedures detailed by Isotech Laboratories (Isotech, 2011), stored on ice until delivery to their facilities, and analyzed for the concentrations of $\text{C}_1\text{-C}_5$ and the carbon and hydrogen isotopic compositions of CH_4 ($\delta^{13}\text{C}\text{-CH}_4$ and $\delta^2\text{H}\text{-CH}_4$) and ethane ($\delta^{13}\text{C}\text{-C}_2\text{H}_6$ and $\delta^2\text{H}\text{-C}_2\text{H}_6$). Procedures for stable isotope analyses of gas are summarized in Osborn et al. (2011). The stable carbon isotopic compositions of CH_4 ($\delta^{13}\text{C}\text{-CH}_4$) were determined for all samples with $[\text{CH}_4]$ exceeding 0.5 ccSTP/L, while the stable carbon isotopic composition of ethane ($\delta^{13}\text{C}\text{-C}_2\text{H}_6$) is available for a subset of samples with $[\text{C}_2\text{H}_6]$ exceeding ~0.1 ccSTP/L. Isotech Laboratories uses chromatographic separation followed by combustion and dual-inlet isotope ratio mass spectrometry to measure dissolved gas concentrations and stable isotopic composition (detection limits for CH_4 , ethane (C_2H_6), and propane (C_3H_8) were 0.001, 0.0005, and 0.0001 mol %, respectively). The isotopic composition of N_2 was determined on headspace gases by coupling a GC (Thermo Fisher Trace Ultra) with a Finnigan Delta S MS. The GC was equipped with a 30 m x 0.53 micron molecular sieve column (MS5A capillary), using TCD detected timing protocols

following methods reported previously (with helium as a carrier gas) (Darrah et al., 2013). To determine the abundance of H₂S gas, the headspace gas of groundwater samples was collected in pre-evacuated 25mL borosilicate flasks with a Teflon stopcock. Gas samples were then equilibrated with H₂O₂ for four hours and measured as SO₄²⁻ using ion chromatography (Darrah et al., 2013; Montegrossi et al., 2001). Based on the comparison of these measurements to field colorimetric methods (lead acetate test strips obtained from Indigo Instruments, Ontario, CN), the analytical error is estimated to be ~20%. Importantly, because H₂S is highly soluble, measured concentrations should be considered minimum values.

Noble gas samples were collected in refrigeration-grade copper tubes that were flushed in-line with at least 50 volumes of sample water prior to sealing with stainless steel clamps by methods reported previously (Darrah et al., 2015b; Eymold et al., 2018; Kreuzer et al., 2018). Major gas components (e.g., N₂, O₂, Ar, CH₄, C₂H₆) were measured using an SRS quadrupole mass spectrometer (MS) and an SRI gas chromatograph (GC) (Eymold et al., 2018; Moore et al., 2018). The isotopic analyses of noble gases were performed using a VG 5400 MS at the University of Rochester following methods reported previously (Darrah and Poreda, 2012; Darrah et al., 2013; Hunt et al., 2012). Standard analytical errors were ± 3% for noble gas concentrations ([⁴He], [²²Ne], [⁴⁰Ar]). Isotopic errors were approximately ±0.01 times the ratio of air for ³He/⁴He (or 1.384 x 10⁻⁶), <±0.5% and <±1% for ²⁰Ne/²²Ne and ²¹Ne/²²Ne, respectively, and <±1% for ³⁸Ar/³⁶Ar and ⁴⁰Ar/³⁶Ar, respectively.

Tritium analyses were performed to evaluate the contributions from modern meteoric water. Tritium concentrations were measured by the in-growth of ³He using a Thermo Fisher Helix SFT noble gas MS at The Ohio State University by methods reported previously (Darrah et al.,

2015b; Solomon et al., 1995; Solomon et al., 1992). The [U] and [Th] in Trinity aquifer outcrop samples collected in Parker County, TX were analyzed to evaluate the potential for *in situ* radiogenic production and/or release of ^4He . Analyses were conducted by standard methods using ICP-MS at Ohio State (Cuoco et al., 2013; Darrah et al., 2009).

4.4 Results and Discussion

4.4.1 Baseline Groundwater Composition: Inorganic Constituents

Ideally, baseline groundwater quality and geochemical composition should be established prior to the onset of shale-gas drilling activities. Unfortunately, the absence of baseline water quality data is a common challenge in studies that attempt to evaluate fugitive gas and other forms of contamination (Darrah, 2018; Darrah et al., 2015a). Recognizing the limitations of not having pre-drill data, baseline groundwater compositions were determined by assessing the geochemistry of drinking-water wells from which homeowners reported no changes in water quality over time. Though it is obviously an imperfect experimental design, geochemical observations suggest that the drinking-water wells included as baseline: a) display statistically insignificant changes over time; b) display statistically significant linear trends in cross-plots of conservative ionic tracers; and c) are statistically indistinguishable from other published data across the region (Darrah et al., 2014; Larson et al., 2018; Wen et al., 2017). For these reasons, I conclude that the selection of samples for the baseline cohort are a reasonable approximation of baseline water quality in the region.

The water chemistry data from the present study area reveal a wide range of solute concentrations from dilute groundwater with Cl \sim 25 mg/L to highly saline water with Cl of \sim 430

Table 4.1: Water composition data from groundwater samples. Concentrations are in mg/L unless specified.

Sample	pH	Temperature (°C)	TDS	[Cl]	[Br]	[NO ₃]	[H ₂ S]	[SO ₄]	[HCO ₃]	[Na]	[Ca]	[Mg]	[Sr]	[Fe]	[Ba]	[Mn]	[Si]	[B] (ppb)	Aquifer
December 2012																			
BSA-1	9.41	16.3	n/a	24.58	0.09	DNR	DNR	2.22	636.00	DNR	1.06	0.44	0.11	DNR	DNR	DNR	DNR	652.94	Trinity
BSA-2	10.43	14.9	n/a	96.08	0.38	DNR	DNR	29.84	589.00	DNR	1.47	0.63	0.15	DNR	DNR	DNR	DNR	758.40	Trinity
BSA-3	9.24	16.2	n/a	57.93	0.19	DNR	DNR	52.49	484.00	DNR	1.09	0.42	0.10	DNR	DNR	DNR	DNR	448.83	Trinity
BSA-4	9.18	16.1	n/a	61.56	0.17	DNR	DNR	22.27	504.00	DNR	1.29	0.56	0.13	DNR	DNR	DNR	DNR	473.09	Trinity
BSA-5	8.73	15.8	n/a	235.73	0.67	DNR	DNR	109.56	492.00	DNR	2.32	1.15	0.25	DNR	DNR	DNR	DNR	423.87	Trinity
BSA-6	9.26	13.2	n/a	78.98	0.25	DNR	DNR	49.57	481.00	DNR	1.17	0.53	0.12	DNR	DNR	DNR	DNR	460.45	Trinity
BSA-7	8.82	16.0	n/a	91.73	0.37	DNR	DNR	66.07	498.00	DNR	1.32	0.55	0.13	DNR	DNR	DNR	DNR	417.41	Trinity
BSA-8	8.18	17.4	n/a	90.44	bdl	DNR	DNR	74.01	500.00	DNR	8.30	2.53	0.25	DNR	DNR	DNR	DNR	399.61	Trinity
BSA-9	9.04	16.3	n/a	347.73	bdl	DNR	DNR	142.37	447.00	DNR	3.47	1.60	0.35	DNR	DNR	DNR	DNR	434.50	Trinity
BSA-10	8.57	18.6	n/a	396.72	1.03	DNR	DNR	121.28	419.00	DNR	29.67	8.88	0.94	DNR	DNR	DNR	DNR	485.61	Trinity
BSA-11	9.42	19.5	n/a	247.08	0.87	DNR	DNR	112.16	464.00	DNR	3.20	1.45	0.31	DNR	DNR	DNR	DNR	481.46	Trinity
BSA-12	8.67	13.8	n/a	152.44	bdl	DNR	DNR	96.64	483.00	DNR	2.13	0.86	0.20	DNR	DNR	DNR	DNR	462.71	Trinity
August 2013																			
BSA-1-2	9.43	16.80	339	22.52	0.04	0.16	DNR	bdl	637.91	263.29	3.42	0.86	0.09	0.12	0.01	0.004	4.99	618.96	Trinity
BSA-2-2	10.27	16.10	541	238.17	0.39	0.17	DNR	12.06	604.64	370.94	4.47	1.41	0.23	0.10	0.05	0.019	4.79	685.70	Trinity
BSA-3-2	9.15	16.70	306	70.37	0.11	0.14	DNR	59.10	472.20	202.41	3.38	0.79	0.09	0.12	0.01	0.003	4.33	283.58	Trinity
BSA-5-2	8.91	17.20	478	243.96	0.25	0.18	DNR	99.41	465.09	359.70	4.82	1.56	0.25	0.11	0.06	0.017	4.46	330.70	Trinity
BSA-6-2	9.31	15.90	327	71.74	0.07	0.14	DNR	40.31	511.97	194.73	3.26	0.80	0.08	0.07	0.02	0.024	3.69	464.77	Trinity
BSA-7-2	8.64	14.87	343	91.09	0.10	0.24	DNR	62.96	505.09	275.73	3.49	0.93	0.11	0.10	0.02	0.006	4.66	392.09	Trinity
BSA-8-2	8.24	17.24	348	87.43	0.13	0.17	DNR	62.86	513.58	248.62	6.81	2.07	0.17	0.11	0.02	0.019	4.67	383.17	Trinity
BSA-10-2	8.61	18.60	562	327.32	0.25	0.24	DNR	101.02	448.43	429.54	10.82	3.67	0.46	0.10	0.06	0.007	5.26	400.14	Trinity
BSA-11-2	9.36	18.14	498	260.05	0.23	0.24	DNR	113.92	472.59	316.66	4.41	1.47	0.22	0.09	0.04	0.009	3.75	364.19	Trinity
BSA-12-2	8.51	16.58	390	135.36	0.13	0.16	DNR	78.88	508.76	310.58	4.01	1.14	0.16	0.11	0.04	0.014	4.68	636.01	Trinity
BSA-13	8.71	17.70	513	292.17	0.20	0.05	DNR	97.64	438.36	350.13	4.45	1.46	0.23	0.09	0.07	0.020	4.20	324.09	Trinity
BSA-14	8.35	19.65	321	79.61	0.11	0.12	DNR	59.48	482.14	258.79	4.46	1.00	0.12	0.12	0.03	0.041	5.06	274.83	Trinity
BSA-15	8.14	16.47	300	57.25	0.18	bdl	DNR	46.41	488.52	237.26	2.38	0.77	0.14	0.04	0.05	0.005	5.68	299.09	Trinity
BSA-16	9.01	15.99	605	375.43	0.27	bdl	DNR	120.74	454.64	418.64	5.00	1.79	0.29	0.10	0.09	0.000	4.20	269.33	Trinity
November 2013																			
BSA-1-3	9.37	15.97	556	21.09	0.08	bdl	1.71	3.49	618.61	224.70	2.58	0.52	0.06	bdl	0.02	0.032	4.61	644.26	Trinity
BSA-2-3	10.19	14.87	753	163.23	0.27	0.07	4.92	18.23	583.77	280.95	3.19	0.87	0.11	bdl	0.03	0.012	4.81	845.27	Trinity
BSA-3-3	9.22	16.24	602	78.40	0.14	0.17	0.24	63.72	467.84	227.94	2.42	0.45	0.05	bdl	0.02	0.011	4.66	433.40	Trinity
BSA-6-3	9.21	14.99	702	96.09	0.13	0.04	2.65	65.02	502.07	288.84	4.60	0.80	0.09	0.01	0.05	0.028	5.31	450.22	Trinity
BSA-7-3	8.67	15.97	n/a	DNR	DNR	DNR	DNR	DNR	DNR	DNR	DNR	DNR	DNR	DNR	DNR	DNR	DNR	DNR	Trinity
BSA-8-3	8.61	16.24	683	99.66	0.11	0.03	2.50	76.73	511.24	246.71	7.07	2.12	0.13	0.01	0.03	0.012	4.83	412.85	Trinity
BSA-10-3	8.53	17.65	1055	322.66	0.31	0.05	2.82	99.95	450.67	394.62	12.65	3.91	0.27	bdl	0.05	0.013	5.16	488.89	Trinity
BSA-11-3	9.44	15.41	906	266.42	0.22	0.05	2.22	114.45	467.11	290.74	4.13	1.47	0.17	0.01	0.05	0.026	4.40	466.89	Trinity
BSA-12-3	8.56	16.48	828	155.90	0.25	0.10	4.05	85.32	487.31	341.66	4.97	1.04	0.12	bdl	0.05	0.008	5.19	493.23	Trinity
BSA-17	8.34	18.25	888	265.61	0.23	0.07	3.60	93.80	423.80	315.06	4.08	1.49	0.17	bdl	0.06	bdl	5.21	390.99	Trinity
BSA-18	8.26	16.26	542	26.28	0.11	bdl	0.69	66.94	496.15	202.39	2.52	0.51	0.06	bdl	0.02	bdl	4.42	573.75	Trinity
BSA-19	8.26	15.50	559	26.23	0.11	bdl	4.35	44.74	482.16	246.33	4.34	0.61	0.07	bdl	0.04	bdl	5.41	486.65	Trinity
BSA-20	8.34	16.14	689	99.10	0.16	0.08	3.20	65.21	481.36	282.78	4.70	0.81	0.09	bdl	0.04	0.034	5.22	428.12	Trinity
Background Avg.	8.76	16.78	583	177.33	0.28	0.13	2.65	83.50	473.77	300.07	5.19	1.59	0.21	0.09	0.04	0.01	4.79	424.32	
Impacted Avg.	9.39	15.81	525	103.63	0.18	0.12	2.94	41.79	554.57	275.39	3.66	1.05	0.13	0.08	0.03	0.02	4.68	558.97	

mg/L. The analyses indicate that mixing between naturally occurring low- and high-salinity endmembers controls the primary dissolved ion water chemistry of samples collected as part of this study. The relatively high-salinity ($[\text{Cl}] > 400$ mg/L) endmember is characterized by a predominance of relatively elevated levels of dissolved inorganic carbon (DIC, as HCO_3), Na, Cl, Sr, and SO_4 , but relatively low Ca and Mg contents (Table 4.1). This endmember typically has low molar ratios of Br/Cl (3×10^{-4}) and Na/Cl (1.8), and $\delta^{13}\text{C-DIC}$ ($< -12\text{‰}$), but heavy ^{18}O and ^2H ($\delta^{18}\text{O} > -3.5\text{‰}$, $\delta^2\text{H} > -22\text{‰}$) relative to the lower salinity water (Figures 4.3-4; Tables 4.1-2). The distinctively low molar ratios of Br/Cl and relatively high SO_4 (~ 150 mg/L) in the saline endmember indicate that the saline groundwater likely originated from evaporite (e.g., halite, gypsum) dissolution. Conversely, the Na/Cl is higher than the values anticipated from the dissolution of NaCl salts alone (~ 1) (Table 4.1), which suggests that base-exchange reactions led to further Na enrichment and Ca depletion following subsequent water-rock interactions (Figure 4.3F).

Importantly, the chemical composition of the higher salinity endmember is distinctly different from the composition of the underlying Barnett brine (e.g., Br/Cl $> 1.5 \times 10^{-3}$, Ca enrichment) and rules out the possibility that the elevated salinity in shallow groundwater is derived from natural mixing with source-rock formational brines from the Barnett. These results are in contrast to shallow aquifers overlying the Marcellus Shale in PA, which display indications of a past history of upward migration of brine (Warner et al., 2012). However, these observations do not preclude the migration of hydrocarbon or saline-rich waters from other source formations overlying the Barnett (e.g., Strawn, Bend, or Marble Falls).

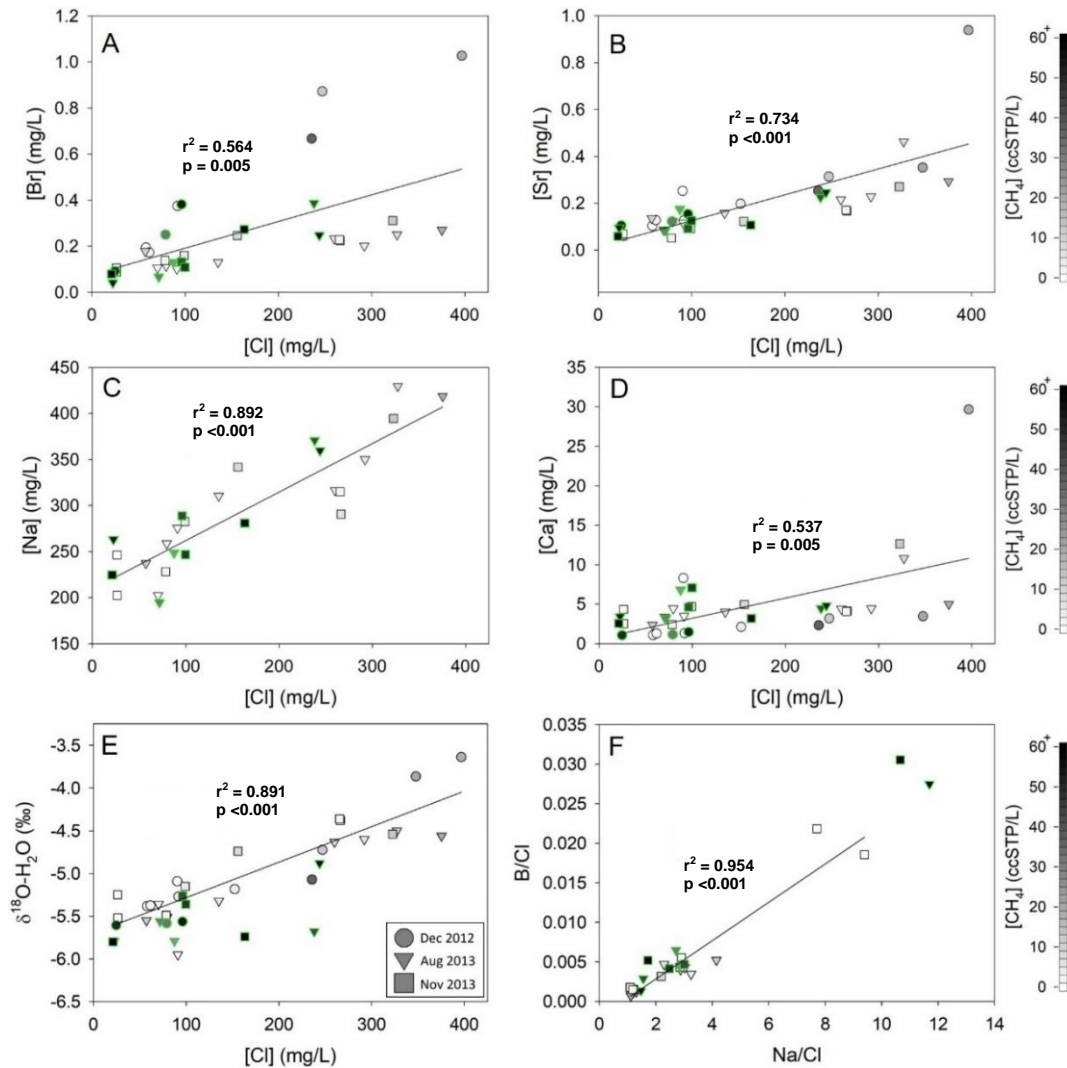


Figure 4.3: [Br] (A), [Sr] (B), [Na] (C), [Ca] (D), and $\delta^{18}\text{O-H}_2\text{O}$ (E) vs. [Cl] and B/Cl vs. Na/Cl (F) in domestic drinking-water wells in Parker County, TX. Methane concentrations [CH₄] are shown using gray-scale intensity (0 to 60+ ccSTP/L). Without pre-drill geochemical data, measured baseline geochemical compositions of groundwater are assumed to represent background conditions based on linear correlations of various ions; it should be noted that drinking-water well owners also did not report changes in water quality over time. These background samples are shown in grey symbols, while samples with evidence of fugitive gas contamination are shown in green-rimmed symbols. The strong linear correlations between dissolved solids and stable water isotopes ($\delta^2\text{H}$ and $\delta^{18}\text{O}$) and chloride indicate a conservative 2-component mixing relationship between two naturally occurring end-members; a highly saline end-member derived from base-exchange reactions with an evaporite and a low-salinity groundwater controlled by carbonate dissolution. With the exception of HCO₃ and SO₄, these relationships are preserved for all inorganic components even following fugitive gas contamination indicating that brine components do not migrate to these shallow aquifers, at least on the time scales of this study.

Based upon prior regional hydrological assessments (Nicot et al., 2013; Nicot et al., 2017c), the saline component could be sourced from the Strawn that migrate into the overlying Trinity Group. The reported groundwater geochemistry from Strawn formations differed little from Trinity Group aquifers, with similar ranges in [Na], [Cl], [Ca], and [HCO₃] (Nicot et al., 2017c). However, on average the Strawn Group waters were slightly higher in [Na] (238 mg/L compared to 161 mg/L), [Cl] (99 mg/L compared to 67 mg/L), and [SO₄] (84mg/L compared to 61mg/L), and lower in [Ca] (27 mg/L compared to 43 mg/L) compared to water from the Trinity Group formations (Nicot et al., 2017c). These data indicate the challenges associated with distinguishing water sourced from the Strawn or Trinity aquifers using dissolved ion chemistry. Therefore, the extent of mixing with Strawn groundwater remains unresolved in this dataset.

The $\delta^{11}\text{B}$, $\delta^{13}\text{C-DIC}$, and $^{87}\text{Sr}/^{86}\text{Sr}$ also support the hypothesis that drinking-water in this area is not influenced by the Barnett (Table 4.2). Low $\delta^{11}\text{B}$ (10-12‰) reflects either B desorption from clay minerals or dissolution of gypsum and carbonate rocks and is clearly distinct from typical oil-field brine compositions (>30‰) (Vengosh et al., 2005; Warner et al., 2014) (Figure 4.4A). The $^{87}\text{Sr}/^{86}\text{Sr}$ ratios of the saline water (0.70846) are similar to values reported from the lower end of the Middle Trinity aquifer (Wong et al., 2014), which are located ~270 km south of the current study area (Wong et al., 2014) (Figure 4.4B). These $^{87}\text{Sr}/^{86}\text{Sr}$ data are the closest proximity to the current study that have been reported for Trinity Group groundwater and are consistent with Paleozoic marine carbonates and reflect minimal contributions of radiogenic Sr to the $^{87}\text{Sr}/^{86}\text{Sr}$ values anticipated for Paleozoic seawater (Figure 4.4B). Finally, the low $\delta^{13}\text{C-DIC}$ (<-12‰) values observed in the saline endmember is common to groundwater systems with elevated levels of natural hydrocarbons and reflects an equilibrium with CO₂ that originated from

Table 4.2. Stable Isotopic Data from Groundwater Samples.

Sample	$\delta^2\text{H-H}_2\text{O}$ (‰)	$\delta^{18}\text{O-H}_2\text{O}$ (‰)	$\delta^{13}\text{C-CH}_4$ (‰)	$\delta^3\text{H-CH}_4$ (‰)	$\delta^{13}\text{C-C}_2\text{H}_6$ (‰)	$\delta^3\text{H-C}_2\text{H}_6$ (‰)	$\delta^{13}\text{C-DIC}$ (‰)	$\delta^{15}\text{N-N}_2$ (‰)	$\delta^{34}\text{S-Sr}$	^3H (T.U.)	Aquifer
December 2012											
BSA-1	-33.86	-5.61	-46.65	DNR	-33.55	DNR	-7.5	DNR	DNR	d.n.r.	Trinity
BSA-2	-33.74	-5.56	-50.64	DNR	-33.15	DNR	-1.5	DNR	DNR	d.n.r.	Trinity
BSA-3	-32.12	-5.38	-44.85	DNR	bdl	DNR	-9.0	DNR	5.84	DNR	Trinity
BSA-4	-30.84	-5.37	-47.90	DNR	bdl	DNR	-10.0	DNR	11.18	DNR	Trinity
BSA-5	-30.34	-5.07	-45.80	DNR	-34.10	DNR	-9.2	DNR	8.01	DNR	Trinity
BSA-6	-33.06	-5.58	-44.60	DNR	-32.80	DNR	-8.7	DNR	bdl	DNR	Trinity
BSA-7	-31.58	-5.27	-46.60	DNR	bdl	DNR	-9.4	DNR	5.37	DNR	Trinity
BSA-8	-30.00	-5.09	-48.50	DNR	-33.90	DNR	-10.1	DNR	5.81	DNR	Trinity
BSA-9	-23.34	-3.86	-42.70	DNR	bdl	DNR	-11.4	DNR	bdl	DNR	Trinity
BSA-10	-22.41	-3.64	-45.48	DNR	-30.70	DNR	-11.8	DNR	bdl	DNR	Trinity
BSA-11	-28.69	-4.72	-44.90	DNR	bdl	DNR	-10.2	DNR	bdl	DNR	Trinity
BSA-12	-30.59	-5.18	-46.45	DNR	-33.30	DNR	-9.5	DNR	bdl	DNR	Trinity
August 2013											
BSA-1-2	-34.43	-5.79	-46.75	-190.8	-34.15	-160.1	-7.6	DNR	8.21	0.70852	Trinity
BSA-2-2	-36.47	-5.68	-51.19	-198.6	-33.10	-158.4	-1.1	DNR	11.43	0.70852	Trinity
BSA-3-2	-33.87	-5.36	-44.70	-124.4	bdl	bdl	-8.9	DNR	bdl	bdl	Trinity
BSA-5-2	-30.42	-4.88	-46.89	-190.1	-34.06	-161.8	-6.5	DNR	bdl	bdl	Trinity
BSA-6-2	-33.64	-5.56	-46.86	-186.0	-34.19	-158.1	-7.7	DNR	4.86	0.70849	Trinity
BSA-7-2	-33.98	-5.95	bdl	bdl	bdl	bdl	-9.3	DNR	bdl	bdl	Trinity
BSA-8-2	-32.70	-5.79	-47.44	-190.8	-34.18	-161.9	-9.1	DNR	5.81	0.70843	Trinity
BSA-10-2	-26.52	-4.50	-46.02	-180.3	-31.31	bdl	-10.6	DNR	7.83	0.70846	Trinity
BSA-11-2	-30.76	-4.63	-43.30	-151.1	-17.50	bdl	-10.0	DNR	7.98	0.70847	Trinity
BSA-12-2	-31.51	-5.32	-46.18	-155.9	-32.90	bdl	-9.6	DNR	5.83	0.70848	Trinity
BSA-13	-29.67	-4.60	-43.47	-157.7	-19.30	bdl	-10.5	DNR	7.68	0.70850	Trinity
BSA-14	-33.70	-5.51	-44.12	-128.9	-12.70	bdl	-9.2	DNR	bdl	bdl	Trinity
BSA-15	-33.01	-5.55	-46.98	-164.8	-30.04	bdl	-9.2	DNR	bdl	bdl	Trinity
BSA-16	-29.90	-4.56	-46.36	-172.9	-33.84	-159.4	-11.5	DNR	9.40	0.70849	Trinity
November 2013											
BSA-1-3	-36.60	-5.80	-46.22	-187.3	-34.0	-163.7	-7.4	-4.910	bdl	bdl	Trinity
BSA-2-3	-37.44	-5.74	-51.17	-198.0	-33.18	-158.0	-2.0	-5.624	bdl	bdl	Trinity
BSA-3-3	-33.63	-5.49	-44.68	-127.7	bdl	bdl	-9.2	0.030	bdl	bdl	Trinity
BSA-6-3	-33.03	-5.26	-46.60	-185.3	-34.2	-162.5	-7.4	-3.620	bdl	bdl	Trinity
BSA-7-3	DNR	DNR	DNR	DNR	DNR	DNR	DNR	0.150	DNR	DNR	Trinity
BSA-8-3	-33.21	-5.36	-47.00	-186.4	-33.8	-159.3	-8.9	-3.161	bdl	bdl	Trinity
BSA-10-3	-28.40	-4.54	-46.08	-179.3	-31.69	bdl	-10.4	-0.316	7.75	0.70846	Trinity
BSA-11-3	-27.98	-4.38	-43.18	-151.20	-17.80	bdl	-9.6	-0.570	7.13	0.70846	Trinity
BSA-12-3	-32.16	-4.74	-46.48	-168.70	-33.50	bdl	-9.5	-1.060	bdl	bdl	Trinity
BSA-17	-30.05	-4.36	-43.22	-131.00	-28.00	bdl	-10.5	0.011	7.21	0.70847	Trinity
BSA-18	-36.74	-5.52	-45.60	-175.00	-33.40	bdl	-6.9	0.076	6.81	0.70848	Trinity
BSA-19	-35.14	-5.25	-41.70	bdl	bdl	bdl	-8.3	0.082	bdl	bdl	Trinity
BSA-20	-32.38	-5.15	-43.94	-126.60	-19.90	bdl	-9.5	-0.847	bdl	bdl	Trinity
Background Avg.	-30.74	-4.96	-45.17	-153.03	-27.88	-159.40	-9.74	-0.32	7.42	0.70847	5.13
Impacted Avg.	-34.05	-5.55	-47.67	-190.37	-33.70	-160.42	-6.28	-3.43	7.58	0.70849	4.29

a combination of the degradation of organic matter (e.g., -12 to -60‰) and dissolution of marine carbonate (e.g., ~0‰), similar to what has been reported in other groundwater systems with elevated levels of natural hydrocarbons (Figure 4.5) (Aharon et al., 1992).

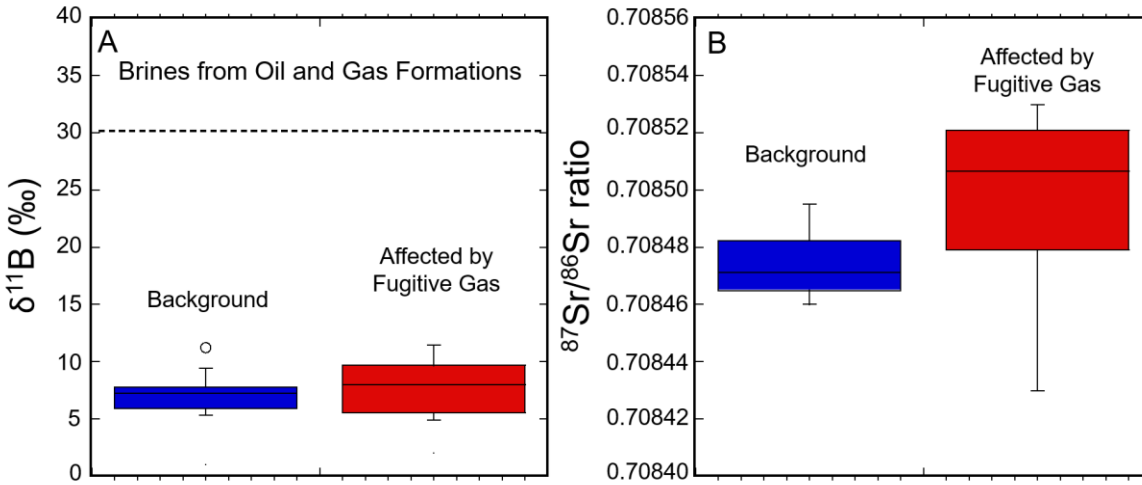


Figure 4.4: Comparison of $\delta^{11}\text{B}$ (A) and $^{87}\text{Sr}/^{86}\text{Sr}$ (B) values measured in background drinking-water samples (blue) and drinking-water samples affected by fugitive gas contamination (red). The data show no isotopic difference in the boron or strontium isotopic composition and the $\delta^{11}\text{B}$ values are much lower than the expected oil and gas brines with (>30‰).

In contrast, the low salinity ($[\text{Cl}] = \sim 25 \text{ mg/L}$) shallow groundwater endmember displays relatively low concentrations of major dissolved elements (e.g., Cl, Ca, Na) (Table 4.1). This endmember is characterized by high ratios of Na/Cl (15), Br/Cl (1.8×10^{-3}), and B/Cl (0.06), lower $\delta^{18}\text{O}$ (-5.6‰) and $\delta^2\text{H}$ (-33.9‰) of water, relatively high [DIC] (>500 mg/L), and more positive $\delta^{13}\text{C}$ -DIC (~-8‰) than the saline endmember, and relatively low $\delta^{11}\text{B}$ (5-6‰), while the $^{87}\text{Sr}/^{86}\text{Sr}$ ratio (0.70848) is quantifiably more radiogenic than the high salinity endmember (Figures 4.3-5; Tables 4.1-2). In combination, these data suggest that the chemistry of the low-salinity endmember is controlled by CaCO_3 dissolution followed by reverse base-exchange reactions that remove Ca

from solution and displace Na and B from clay mineral surfaces with relatively low $\delta^{11}\text{B}$ values, increasing the Na and B in the residual groundwater (Figures 4.3-5).

Thus, the inorganic geochemistry of baseline groundwater samples in the Trinity aquifer can be described as a conservative two-component mixing relationship between the highly saline and low-salinity groundwater endmembers (Figures 4.3-5). Importantly, this relationship is consistent for various geochemical species, including dissolved ions and their isotopes (e.g., Cl, Br, SO_4 , Ca, Na, $\delta^{11}\text{B}$, $^{87}\text{Sr}/^{86}\text{Sr}$) and stable isotopes of water (i.e., ^{18}O and ^2H). These observations support the interpretation that baseline groundwater reflects the dilution of a single saline water source with minor modification by base-exchange reactions.

4.4.2 Baseline Groundwater Composition: Dissolved Gas Chemistry

The presence of natural gas in shallow aquifers can correspond to a variety of natural and anthropogenic sources and processes (Baldassare et al., 2014; Darrah et al., 2014; Kornacki and McCaffrey, 2011; Kornacki and McCaffrey, 2014; Siegel et al., 2015). Natural processes include: (1) *in situ* microbial CH_4 production in aquifers containing elevated levels of organic matter and (2) exogenous thermogenic natural gas sourced from underlying gas-bearing formations (e.g., Strawn formations) (Baldassare et al., 2014; Darrah et al., 2014; Kornacki and McCaffrey, 2011; Kornacki and McCaffrey, 2014; Wen et al., 2016b).

Natural gas released by human activities can also introduce elevated levels of hydrocarbons into shallow aquifers. Common mechanisms for human-induced CH_4 release include leakage: (1) through a poorly or uncemented petroleum-well annulus from either target formations or overlying gas-charged formations; (2) along petroleum-wells with faulty well casings (Darrah et al., 2014; Dusseault and Jackson, 2014; Jackson et al., 2013); (3) initiated by changes in aquifer pressure

Table 4.3: Major Gas Composition Data from Groundwater Samples. Concentrations are in ccSTP/L.

Sample	[CH ₄]	[C ₂ H ₆]	[C ₃ H ₈]	[i-C ₄ H ₁₀]	[n-C ₄ H ₁₀]	[i-C ₅ H ₁₂]	[n-C ₅ H ₁₂]	[C ₆ +]	[CO ₂]	[N ₂]	[O ₂]	[Ar]	CH ₄ C ₃ H ₈ + C ₂ H ₆	C ₃ H ₈ + CH ₄	N ₂ Ar	CH ₄ Ar	N ₂ CH ₄	CO ₂ CH ₄	Aquifer
December 2012																			
BSA-1	51.20	3.97	2.07	DNR	DNR	DNR	DNR	DNR	DNR	2.14	0.01	0.05	8.48	0.118	41.2	2.91E+05	0.04	DNR	Trinity
BSA-2	54.70	4.31	4.50E-02	DNR	DNR	DNR	DNR	DNR	DNR	4.43	bdl	0.09	12.57	0.080	48.6	1.78E+05	0.08	DNR	Trinity
BSA-3	1.49	4.17E-03	bdl	DNR	DNR	DNR	DNR	DNR	DNR	16.57	0.02	0.32	357.31	0.003	51.1	1.36E+03	11.12	DNR	Trinity
BSA-4	2.49	0.18	bdl	DNR	DNR	DNR	DNR	DNR	DNR	16.14	0.01	0.38	13.90	0.072	42.6	1.95E+03	6.48	DNR	Trinity
BSA-5	37.76	1.14	1.68E-02	DNR	DNR	DNR	DNR	DNR	DNR	18.24	0.02	0.45	32.53	0.031	40.4	2.48E+04	0.48	DNR	Trinity
BSA-6	32.78	2.44	0.17	DNR	DNR	DNR	DNR	DNR	DNR	7.46	bdl	0.11	12.54	0.080	70.0	9.11E+04	0.23	DNR	Trinity
BSA-7	1.60	0.01	bdl	DNR	DNR	DNR	DNR	DNR	DNR	13.97	0.01	0.34	288.37	0.003	41.6	1.41E+03	8.74	DNR	Trinity
BSA-8	1.12	0.03	bdl	DNR	DNR	DNR	DNR	DNR	DNR	24.69	0.01	0.44	38.22	0.026	55.9	7.51E+02	22.04	DNR	Trinity
BSA-9	21.40	0.51	8.11E-03	DNR	DNR	DNR	DNR	DNR	DNR	21.31	0.08	0.47	41.05	0.024	45.2	1.34E+04	1.00	DNR	Trinity
BSA-10	18.74	0.99	1.44E-03	DNR	DNR	DNR	DNR	DNR	DNR	14.30	0.02	0.39	18.99	0.053	36.3	1.41E+04	0.76	DNR	Trinity
BSA-11	12.47	0.30	1.31E-03	DNR	DNR	DNR	DNR	DNR	DNR	15.75	0.01	0.36	42.06	0.024	44.2	1.04E+04	1.26	DNR	Trinity
BSA-12	5.14	0.30	2.18E-03	DNR	DNR	DNR	DNR	DNR	DNR	13.40	bdl	0.35	16.9	0.059	38.6	4.39E+03	2.61	DNR	Trinity
August 2013																			
BSA-1-2	71.48	7.87	2.04	0.19	0.38	0.06	0.06	0.07	0.07	2.40	0.04	0.05	6.7	0.148	43.8	3.85E+05	0.03	9.46E-04	Trinity
BSA-2-2	45.44	3.59	0.04	0.01	bdl	bdl	bdl	bdl	bdl	3.84	0.09	0.09	12.5	0.080	43.6	1.53E+05	0.08	1.46E-03	Trinity
BSA-3-2	1.76	0.01	bdl	bdl	bdl	bdl	bdl	bdl	bdl	16.60	0.02	0.32	306.7	0.003	51.9	1.63E+03	9.43	1.74E-02	Trinity
BSA-5-2	71.14	7.02	2.00	0.23	0.41	0.08	0.07	0.07	0.03	1.23	0.06	0.03	7.3	0.138	42.3	7.23E+05	0.02	3.99E-04	Trinity
BSA-6-2	33.92	2.55	0.55	0.05	0.08	0.01	0.01	0.01	0.05	7.09	0.06	0.17	10.4	0.096	40.7	5.76E+04	0.21	1.52E-03	Trinity
BSA-7-2	1.60	0.01	bdl	bdl	bdl	bdl	bdl	bdl	bdl	13.97	0.01	0.34	230.1	0.004	41.6	1.41E+03	8.74	1.96E-02	Trinity
BSA-8-2	27.50	2.11	0.54	0.07	0.11	0.02	0.02	0.02	0.02	4.07	0.08	0.10	9.6	0.105	40.6	8.12E+04	0.15	8.53E-04	Trinity
BSA-10-2	8.60	0.51	bdl	bdl	0.00	bdl	bdl	bdl	0.10	20.89	0.05	0.48	16.9	0.059	43.2	5.26E+03	2.43	1.11E-02	Trinity
BSA-11-2	5.29	0.13	bdl	bdl	bdl	bdl	bdl	bdl	0.07	18.25	0.04	0.44	40.8	0.024	41.8	3.58E+03	3.45	1.27E-02	Trinity
BSA-12-2	5.30	0.31	0.02	bdl	bdl	bdl	bdl	bdl	0.02	14.24	0.02	0.30	15.8	0.063	47.1	5.18E+03	2.69	8.85E-03	Trinity
BSA-13	4.68	0.12	bdl	bdl	bdl	bdl	bdl	bdl	0.04	12.00	0.04	0.28	39.0	0.026	42.8	4.94E+03	2.56	8.72E-03	Trinity
BSA-14	3.24	0.02	bdl	bdl	bdl	bdl	bdl	bdl	0.04	14.26	0.06	0.32	155.5	0.006	44.8	3.02E+03	4.39	1.12E-02	Trinity
BSA-15	10.06	0.45	bdl	bdl	bdl	bdl	bdl	bdl	0.03	15.67	0.05	0.36	22.3	0.045	43.4	8.23E+03	1.56	3.09E-03	Trinity
BSA-16	18.22	1.41	0.49	0.08	0.11	0.03	0.02	0.02	0.07	18.96	0.02	0.43	8.6	0.117	44.2	1.25E+04	1.04	3.75E-03	Trinity
November 2013																			
BSA-1-3	64.87	7.26	2.11	0.19	0.35	0.06	0.04	0.06	0.02	2.10	0.04	0.06	6.5	0.154	39.0	3.57E+05	0.03	3.02E-04	Trinity
BSA-2-3	69.02	4.74	0.09	0.01	0.01	bdl	bdl	bdl	bdl	3.88	0.05	0.09	14.2	0.070	46.0	2.42E+05	0.06	4.49E-04	Trinity
BSA-3-3	2.44	0.01	bdl	bdl	bdl	bdl	bdl	bdl	0.03	17.29	0.01	0.34	406.3	0.002	50.7	2.11E+03	7.10	1.06E-02	Trinity
BSA-6-3	45.01	3.17	0.76	0.07	0.11	0.02	0.01	0.01	0.02	6.76	0.04	0.14	10.9	0.092	49.0	1.01E+05	0.15	3.49E-04	Trinity
BSA-7-3	1.72	0.01	bdl	bdl	bdl	bdl	bdl	bdl	0.02	15.64	0.04	0.35	267.9	0.004	44.2	1.43E+03	9.09	1.34E-02	Trinity
BSA-8-3	49.33	3.30	0.96	0.12	0.17	0.03	0.02	0.02	0.01	2.92	0.02	0.09	10.7	0.093	32.8	1.86E+05	0.06	2.69E-04	Trinity
BSA-10-3	12.74	0.64	bdl	bdl	bdl	bdl	bdl	bdl	0.10	21.39	bdl	0.46	19.9	0.050	46.8	8.58E+03	1.68	7.66E-03	Trinity
BSA-11-3	8.28	0.17	bdl	bdl	bdl	bdl	bdl	bdl	0.05	18.33	0.03	0.42	44.0	0.023	43.9	5.47E+03	2.46	7.35E-03	Trinity
BSA-12-3	8.28	0.53	0.05	bdl	bdl	bdl	bdl	bdl	0.04	12.71	0.01	0.29	14.3	0.070	44.3	8.78E+03	1.54	4.32E-03	Trinity
BSA-17	2.95	0.03	bdl	bdl	bdl	bdl	bdl	bdl	0.02	19.28	0.02	0.42	94.5	0.011	46.4	2.10E+03	6.53	1.43E-02	Trinity
BSA-18	1.79	0.04	bdl	bdl	bdl	bdl	bdl	bdl	0.03	20.54	0.03	0.40	42.3	0.024	51.7	5.87E+02	11.48	1.78E-02	Trinity
BSA-19	1.09	0.00	bdl	bdl	bdl	bdl	bdl	bdl	0.02	18.66	0.07	0.41	603.1	0.002	45.6	7.87E+02	17.12	2.23E-02	Trinity
BSA-20	5.10	0.02	bdl	bdl	bdl	bdl	bdl	bdl	0.03	17.76	0.03	0.38	215.0	0.005	46.3	3.97E+03	3.48	5.15E-03	Trinity
Background Avg.	7.57	0.29	0.07	0.08	0.05	0.03	0.02	0.02	0.04	17.07	0.03	0.38	126.39	0.03	45.06	5.63E+03	5.60	0.01	
Impacted Avg.	51.37	4.36	0.95	0.10	0.20	0.04	0.03	0.04	0.04	4.03	0.05	0.09	10.20	0.10	44.81	2.37E+05	0.10	0.00	

gradients during drilling; (4) via abandoned petroleum-wells; or (5) along existing or incipient faults and fractures (e.g., blowout at depth; (Brantley et al., 2014; Darrah et al., 2014)). The contributions from various sources can be resolved by a combination of hydrological, geological, and geochemical interpretations (e.g., Baldassare et al., 2014; Darrah et al., 2014; Jackson et al., 2013; Kornacki and McCaffrey, 2011; Kornacki and McCaffrey, 2014; Siegel et al., 2015).

The majority of samples in the present study exhibit CH₄ and higher aliphatic hydrocarbon concentrations that are significantly and positively correlated with [Cl] ($r^2=0.611$ and $p= <0.001$, $r^2=0.644$ and $p= <0.001$, respectively) and other dissolved inorganic components (e.g., Br, Na, Sr) (Figures 4.3, 4.5). These variations suggest that CH₄ in this subset of samples is naturally occurring and likely controlled by the same migration processes as the saline groundwater described above. In the samples with hydrocarbon concentrations that correlate to dissolved inorganic components, the concentrations of CH₄ range up to 21.4 ccSTP/L (Table 4.3). These levels are well below the CH₄ saturation point of shallow groundwater ([CH₄]= ~40ccSTP/L at the water table), but are above Department of Interior recommended action levels ([CH₄] = 10ccSTP/L) (Eltschlager et al., 2001).

Noble gases, including ⁴He, serve as a valuable set of tracers capable of identifying the source, mechanism of migration, and relative contribution of exogenous fluids (e.g., brine or thermogenic hydrocarbon gases) in shallow aquifers (Darrah et al., 2014; Drollette et al., 2015; Heilweil et al., 2015; Jackson et al., 2013). In groundwater, ⁴He concentrations reflect a combination of: 1) atmospheric inputs, 2) *in situ* production from U-Th-decay, 3) release of ⁴He that previously accumulated in detrital grains, and 4) flux from exogenous sources (Darrah et al., 2015b). Based on the measured [U]=0.435 ppm and [Th]=0.172 ppm in Trinity aquifer rocks

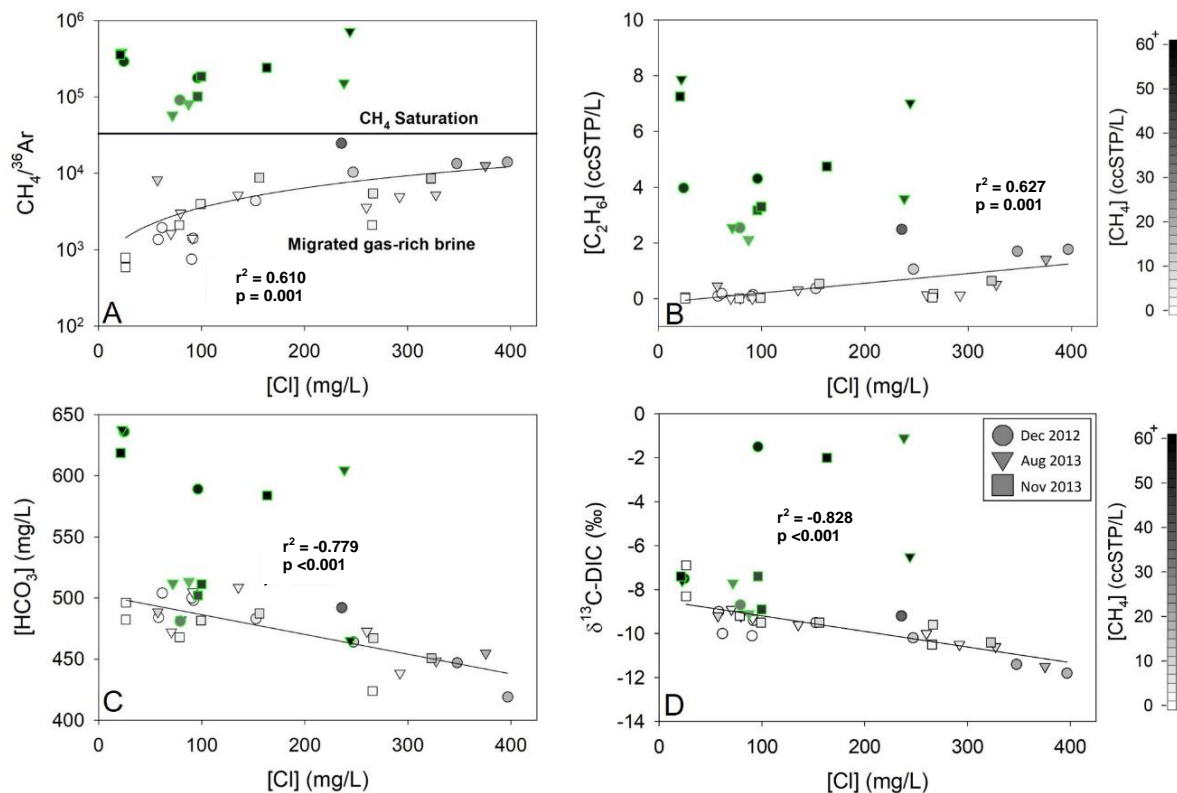


Figure 4.5: The ratios of $\text{CH}_4/^{36}\text{Ar}$ (A), $[\text{C}_2\text{H}_6]$ (B), $[\text{DIC}]$ (as HCO_3^-) (C), and $\delta^{13}\text{C-DIC}$ (D) vs. $[\text{Cl}]$. In background samples, hydrocarbon gases, $[\text{DIC}]$, and $\delta^{13}\text{C-DIC}$ show a strong 2-component mixing relationship with Cl (and other inorganic components), which serves as a proxy for the naturally-occurring salt-rich end-member. These observations indicate that naturally-occurring hydrocarbon gases coexist with the salt-rich end-member. Five samples suspected of fugitive gas contamination show substantially higher levels of thermogenic natural gases (i.e., $\text{CH}_4/^{36}\text{Ar}$ above the saturation point for methane in shallow aquifers and elevated $[\text{C}_2\text{H}_6]$), increased $[\text{DIC}]$, and enriched $\delta^{13}\text{C-DIC}$.

(Table 4.4), the range of *in situ* production and accumulation for ^4He is <0.45 to 2.5×10^{-9} ccSTP/kg of water/yr assuming a porosity of 25%. Diffusion coefficients were measured on aquifer lithology (dominantly carbonates) and used to model ^4He release rates, which yield an average initial $[\text{}^4\text{He}]$ of 7.4 to 9.2×10^{-6} ccSTP/g of rock (Table 4.4) following previously reported methods (Darrah et al., 2015b). While these crustal mineral diffusional release rates exceed steady-state production by orders of magnitude, the maximum release rates only range up to $\sim 0.683 \times 10^{-7}$ ccSTP/L/yr.

Table 4.4. Uranium (U) and Thorium (Th) concentrations of aquifer lithologies.

Sample	Uranium mg/kg	Thorium mg/kg
Trinity-1	0.461	0.212
Trinity-2	0.416	0.164
Trinity-3	0.429	0.139
Average	0.435	0.172
UCC	2.8	10.7
Model Value	0.435	0.172

Because the measured $[\text{}^4\text{He}]$ in drinking-water wells from this study ($\sim 9,742 \times 10^{-6}$ ccSTP/L up to 0.08 ccSTP/L [$\sim 82,535 \times 10^{-6}$ ccSTP/L]), specifically in the methane- and salt-rich endmember (Table 4.5), exceed the combined maximum possible contributions from ASW ($[\text{}^4\text{He}]_{\text{ASW}} = 45 \times 10^{-6}$ ccSTP/L), *in situ* production ($[\text{}^4\text{He}]_{\text{in situ}} = 9.2 \times 10^{-6}$ ccSTP/g), and release from detrital grains ($[\text{}^4\text{He}]_{\text{release}} = 2.5 \times 10^{-9}$ ccSTP/L of water/yr) by orders of magnitude, these hydrocarbon- and salt-rich fluids are likely derived from an exogenous source that has migrated into the shallow aquifer over time.

Table 4.5: Noble Gas Composition and Isotopic Data from Groundwater Samples. Concentrations are in ccSTP/L.

Sample	[¹ He] (x10 ⁻⁶)	[²⁰ Ne] (x10 ⁻⁶)	[³⁶ Ar] (x10 ⁻⁶)	³ He/ ⁴ He (R/R _A)	²⁰ Ne/ ²² Ne	²¹ Ne/ ²² Ne	³⁸ Ar/ ³⁶ Ar	⁴⁰ Ar/ ³⁶ Ar	⁴ He/ ²⁰ Ne	²⁰ Ne/ ³⁶ Ar	⁴ He/ ⁴⁰ Ar*	⁴ He/CH ₄ x 10 ⁶	Aquifer
December 2012													
BSA-1	6.76E+04	19.60	175.68	0.0384	9.94	0.0287	0.1930	327.1	3448.3	0.495	12.2	1.32E+03	Trinity
BSA-2	1.22E+05	120.06	307.43	0.035	9.890	0.0275	0.1900	315.6	1015.2	0.391	19.7	2.23E+03	Trinity
BSA-3	1.84E+04	210.69	1096.28	0.050	bdl	bdl	0.1870	295.5	87.5	0.192	bdl	1.24E+04	Trinity
BSA-4	1.95E+04	274.50	1280.07	0.017	bdl	bdl	0.1886	295.4	71.2	0.214	bdl	7.85E+03	Trinity
BSA-5	1.82E+05	682.35	1523.65	0.034	9.945	0.0283	0.1890	309.7	266.6	0.448	8.4	4.82E+03	Trinity
BSA-6	4.95E+04	154.44	359.80	0.041	9.890	0.0275	0.1890	306.1	320.4	0.429	13.0	1.51E+03	Trinity
BSA-7	1.23E+04	193.32	1135.14	0.029	bdl	bdl	0.1870	295.5	63.7	0.170	bdl	7.69E+03	Trinity
BSA-8	9.74E+03	229.41	1492.23	0.031	9.960	0.0291	0.1860	321.9	42.5	0.154	0.2	8.70E+03	Trinity
BSA-9	8.25E+04	660.60	1592.91	0.024	9.940	0.0284	0.1880	304.7	124.9	0.415	5.6	3.86E+03	Trinity
BSA-10	6.72E+04	414.28	1331.42	0.034	9.870	0.0279	0.1860	304.9	162.2	0.311	5.4	3.59E+03	Trinity
BSA-11	4.56E+04	404.01	1204.73	0.029	10.090	0.0288	0.1920	308.0	112.8	0.335	3.0	3.65E+03	Trinity
BSA-12	3.07E+04	407.49	1171.62	0.034	10.004	0.0287	0.1636	305.6	75.4	0.348	2.6	5.98E+03	Trinity
August 2013													
BSA-1-2	5.47E+04	11.13	185.44	0.028	9.923	0.0288	0.1966	333.3	4909.3	0.060	7.8	7.65E+02	Trinity
BSA-2-2	2.03E+04	34.21	297.82	0.028	9.965	0.0282	0.1871	307.3	592.3	0.115	5.8	4.46E+02	Trinity
BSA-3-2	1.84E+04	190.26	1082.91	0.040	9.945	0.0284	0.1890	295.5	96.9	0.176	bdl	1.05E+04	Trinity
BSA-5-2	1.04E+05	3.94	98.46	0.028	9.988	0.0288	0.2004	367.1	26324.0	0.040	14.7	1.46E+03	Trinity
BSA-6-2	3.16E+04	124.60	589.05	0.027	10.047	0.0287	0.1929	305.8	253.9	0.212	5.2	9.33E+02	Trinity
BSA-7-2	1.23E+04	174.57	1137.06	0.034	9.964	0.0280	0.1920	295.5	70.5	0.154	bdl	7.69E+03	Trinity
BSA-8-2	2.22E+05	390.29	338.79	0.028	9.890	0.0292	0.1927	327.1	569.2	1.152	20.8	8.08E+03	Trinity
BSA-10-2	1.68E+04	373.84	1634.80	0.027	9.944	0.0279	0.1900	304.2	45.0	0.229	1.2	1.95E+03	Trinity
BSA-11-2	2.18E+04	602.85	1476.68	0.021	10.030	0.0279	0.1870	301.6	36.1	0.408	2.4	4.12E+03	Trinity
BSA-12-2	2.61E+04	251.48	1024.18	0.026	9.790	0.0276	0.1899	302.1	103.8	0.246	3.9	4.92E+03	Trinity
BSA-13	2.07E+04	224.27	948.12	0.025	10.030	0.0287	0.1864	305.2	92.1	0.237	2.2	4.41E+03	Trinity
BSA-14	1.88E+04	669.89	1076.00	0.019	9.940	0.0293	0.1883	303.1	28.0	0.623	2.3	5.78E+03	Trinity
BSA-15	2.75E+04	255.05	1223.40	0.026	10.060	0.0291	0.1935	304.5	107.6	0.208	2.5	2.73E+03	Trinity
BSA-16	5.77E+04	356.69	1452.85	0.027	9.957	0.0282	0.1889	307.5	161.7	0.246	3.3	3.17E+03	Trinity
November 2013													
BSA-1-3	6.38E+04	13.09	181.76	0.03	9.870	0.0276	0.1960	335.6	4875.6	0.072	8.8	9.84E+02	Trinity
BSA-2-3	1.98E+04	31.10	285.35	0.03	9.940	0.0289	0.1920	311.9	637.9	0.109	4.2	2.87E+02	Trinity
BSA-3-3	2.03E+04	193.93	1154.37	0.04	9.740	0.0287	0.1890	295.4	104.6	0.168	bdl	8.33E+03	Trinity
BSA-6-3	2.64E+04	84.43	444.37	0.03	9.860	0.0278	0.1890	314.6	312.8	0.190	3.1	5.87E+02	Trinity
BSA-7-3	1.46E+04	183.41	1198.78	0.03	DNR	DNR	0.1870	295.3	79.8	0.153	DNR	8.51E+03	Trinity
BSA-8-3	2.41E+05	193.59	265.20	0.03	9.830	0.0294	0.1930	335.6	1243.1	0.730	22.6	4.88E+03	Trinity
BSA-10-3	1.37E+04	280.52	1484.25	0.02	9.870	0.0283	0.1890	307.9	48.9	0.189	0.7	1.08E+03	Trinity
BSA-11-3	2.38E+04	545.21	1359.63	0.03	9.932	0.0276	0.1870	306.7	43.7	0.401	1.6	3.21E+03	Trinity
BSA-12-3	2.39E+04	217.65	942.22	0.03	9.940	0.0290	0.1900	304.6	109.8	0.231	2.8	2.89E+03	Trinity
BSA-17	1.91E+04	248.64	1408.74	0.03	9.860	0.0299	0.1890	295.3	76.9	0.177	bdl	6.47E+03	Trinity
BSA-18	1.42E+04	267.35	1343.49	0.03	9.830	0.0286	0.1870	295.5	53.0	0.199	bdl	7.92E+03	Trinity
BSA-19	9.99E+03	243.77	1385.03	0.03	9.870	0.0283	0.1890	295.3	41.0	0.176	bdl	9.17E+03	Trinity
BSA-20	3.07E+04	314.75	1284.71	0.030	10.010	0.0279	0.1865	298.9	97.6	0.245	7.0	6.02E+03	Trinity
Background Avg.	3.18E+04	335.96	1275.75	0.03	9.936	0.0285	0.1876	302.3	89.4	0.265	3.2	5.83E+03	
Impacted Avg.	8.52E+04	98.37	294.10	0.03	9.919	0.0284	0.1922	321.7	3429.4	0.319	11.5	1.96E+03	

In combination with the consistent presence of tritium ($t_{1/2} = 12.3$ years) in all samples (1.4 to 12.8 tritium units (T.U.); Table 4.2), these data support the conclusion that groundwater in this study area reflects a mixture between relatively recently recharged, fresh meteoric water and an older salt- and hydrocarbon gas-rich groundwater sourced from an exogenous, gas- and brine-rich formation. Similar findings have been observed in groundwater overlying the Marcellus (Darrah et al., 2015b; Darrah et al., 2014; Harkness et al., 2017b; Kreuzer et al., 2018; Siegel et al., 2015; Warner et al., 2012) and other shales (Bordeleau et al., 2018b; Eymold et al., 2018; Moritz et al., 2015; Nicot et al., 2017a; Nicot et al., 2017b; Nicot et al., 2017c) and are consistent with prior interpretations from the current study area (Darrah et al., 2014; Nicot et al., 2013; Wen et al., 2016b).

The relationship between water isotopes (i.e., $\delta^2\text{H-H}_2\text{O}$, $\delta^{18}\text{O-H}_2\text{O}$) and salt contents further support the model for mixing between relatively young meteoric recharge and old, ^4He -rich groundwater. Water isotope values positively correlate with salinity. The most enriched $\delta^{18}\text{O-H}_2\text{O}$ and most ^4He -rich samples correspond to a value of $[\text{Cl}] = \sim 400$ mg/L (Figure 4.3E), while younger, more tritium-rich samples have the lowest salinity ($[\text{Cl}] = \sim 25$ mg/L), lowest $[\text{He}]$, and the most negative $\delta^{18}\text{O}$ and $\delta^2\text{H}$ values observed in water from the current study area.

Observed $[\text{N}_2]$ in groundwater samples are higher than the values expected for equilibrium with dissolved atmospheric (ASW) nitrogen (Figure 4.6; Table 4.3). Atmospheric gases dissolve into groundwater when meteoric water equilibrates with atmospheric gases prior to groundwater recharge into the subsurface according to Henry's Law (Weiss, 1970, 1971). As a result, natural groundwater samples are dominantly composed of nitrogen (92%) and argon (at a fixed ratio from the time of recharge, e.g., $\text{N}_2/\text{Ar} = \sim 38$) following the relatively rapid consumption of oxygen by

Table 4.6. Major and Hydrocarbon Gas Compositional and Stable Isotopic Data from Produced Gases. Concentrations are in ccSTP/cc.

Sample	[CH ₄]	[C ₂ H ₆]	[C ₃ H ₈]	[i-C ₄ H ₁₀]	[n-C ₄ H ₁₀]	[i-C ₅ H ₁₂]	[n-C ₅ H ₁₂]	[CO ₂]	[N ₂]	[O ₂]	[Ar] (x10 ⁻⁶)	$\frac{CH_4}{C_2H_6+i}$	$\frac{N_2}{Ar}$	$\frac{N_2}{CH_4}$	Prod. Form.	
Strawn-1	0.835	0.079	0.0024	DNR	DNR	DNR	DNR	0.003	0.056	<0.01	308	10.25	0.10	183	6.7E-02	Strawn
Strawn-2	0.845	0.069	0.0034	DNR	DNR	DNR	DNR	0.005	0.046	<0.01	998	11.67	0.09	46	5.5E-02	Strawn
Strawn-3	0.854	0.080	0.0212	DNR	DNR	DNR	DNR	0.003	0.033	<0.01	554	8.44	0.12	60	3.9E-02	Strawn
Strawn-4	0.844	0.091	0.0081	DNR	DNR	DNR	DNR	0.002	0.035	<0.01	259	8.52	0.12	135	4.2E-02	Strawn
Barnett-1	0.780	0.122	0.0459	0.0061	0.0131	0.0036	0.0043	0.009	0.009	<0.01	25	4.00	0.25	365	1.2E-02	Barnett
Barnett-2	0.716	0.154	0.0699	0.0092	0.0184	0.0038	0.0037	0.010	0.012	<0.01	26	2.77	0.36	464	1.7E-02	Barnett
Barnett-3	0.782	0.120	0.0456	0.0058	0.0130	0.0035	0.0041	0.010	0.011	<0.01	31	4.08	0.25	349	1.4E-02	Barnett
Barnett-4	0.709	0.159	0.0714	0.0097	0.0201	0.0046	0.0046	0.012	0.012	<0.01	24	2.64	0.38	504	1.7E-02	Barnett

Sample	$\frac{CO_2}{CH_4}$	$\frac{CH_4}{Ar}$	$\delta^{13}C-CH_4$ ‰	$\delta^{13}C-C_2H_6$ ‰	δ^2H-CH_4 ‰	$\delta^{13}C-CO_2$ ‰	$\delta^{15}N-N_2$ ‰	Prod. Form.
Strawn-1	3.72E-03	1.50E+06	-47.9	-37.9	-192.63	-2.31	-8.30	Strawn
Strawn-2	5.71E-03	4.60E+05	-47.6	-38.6	-187.51	-3.69	-11.90	Strawn
Strawn-3	3.56E-03	8.30E+05	-48.6	-37.0	-185.68	-5.72	-8.54	Strawn
Strawn-4	1.86E-03	1.80E+06	-47.6	-36.4	-193.13	-5.11	-9.06	Strawn
Barnett-1	1.09E-02	1.80E+07	-47.5	-35.4	-177.70	-9.72	-10.24	Barnett
Barnett-2	1.38E-02	1.60E+07	-45.4	-34.0	-183.76	-11.17	-14.35	Barnett
Barnett-3	1.25E-02	1.53E+07	-47.4	-35.5	-176.55	-8.61	-11.10	Barnett
Barnett-4	1.70E-02	1.82E+07	-45.6	-34.1	-181.64	-9.37	-11.40	Barnett

aerobic respiration (Weiss, 1970, 1971). While there can be minor differences in solubility levels of various atmospheric gases as a function of local temperature, salinity, and atmospheric pressure (i.e., altitude), the levels of atmospheric gases, including N₂ and Ar, are relatively uniform globally (Ballentine et al., 2002; Weiss, 1970, 1971). These atmospheric levels of N₂ can obfuscate the relative proportion of N₂ derived from ASW and natural gas (Darrah et al., 2013; Hunt et al., 2012).

In addition to the ubiquitous presence of large quantities of atmospheric N₂ in groundwater samples, thermogenic natural gases can show significant contributions of radiogenic ⁴⁰Ar*, where the * denotes the radiogenic component. Produced gases from oil and gas wells in this area yielded ⁴⁰Ar/³⁶Ar of up to 586, suggesting the potential for significant radiogenic contributions (Table 4.7). This level of ⁴⁰Ar* could influence the N₂/Ar by ~4 times if one tried to calculate the total atmospheric N₂ by using the N₂/Ar and assuming an atmospheric argon ratio of ⁴⁰Ar/³⁶Ar=295.5. Although the molecular abundance of non-hydrocarbon gases (e.g., N₂) can help define the natural baseline and/or help can differentiate between produced gases from the Strawn and Barnett (Kornacki and McCaffrey, 2011; Kornacki and McCaffrey, 2014), [N₂] is not a valid tracer in groundwater studies unless the data are corrected for all of the sources of nitrogen, including atmospheric nitrogen, excess air, air contamination, thermogenic source, biogenic sources, and/or fractionation by phase partitioning, and then characterized for the nitrogen isotopic ($\delta^{15}\text{N-N}_2$) composition.

Figures 4.6A and 4.7B-D show that small amounts of excess N₂ in baseline samples (after correction for radiogenic ⁴⁰Ar*), ranging from 2.1 to 17.1% excess N₂, display $\delta^{15}\text{N-N}_2$ values that range from -1.06‰ to 0.15‰ as compared to $\delta^{15}\text{N-N}_2 = 0$ for ASW or excess air. These values are consistent with the thermal metamorphism of organic matter ($\delta^{15}\text{N-N}_2 = <-4\text{‰}$) as the major source

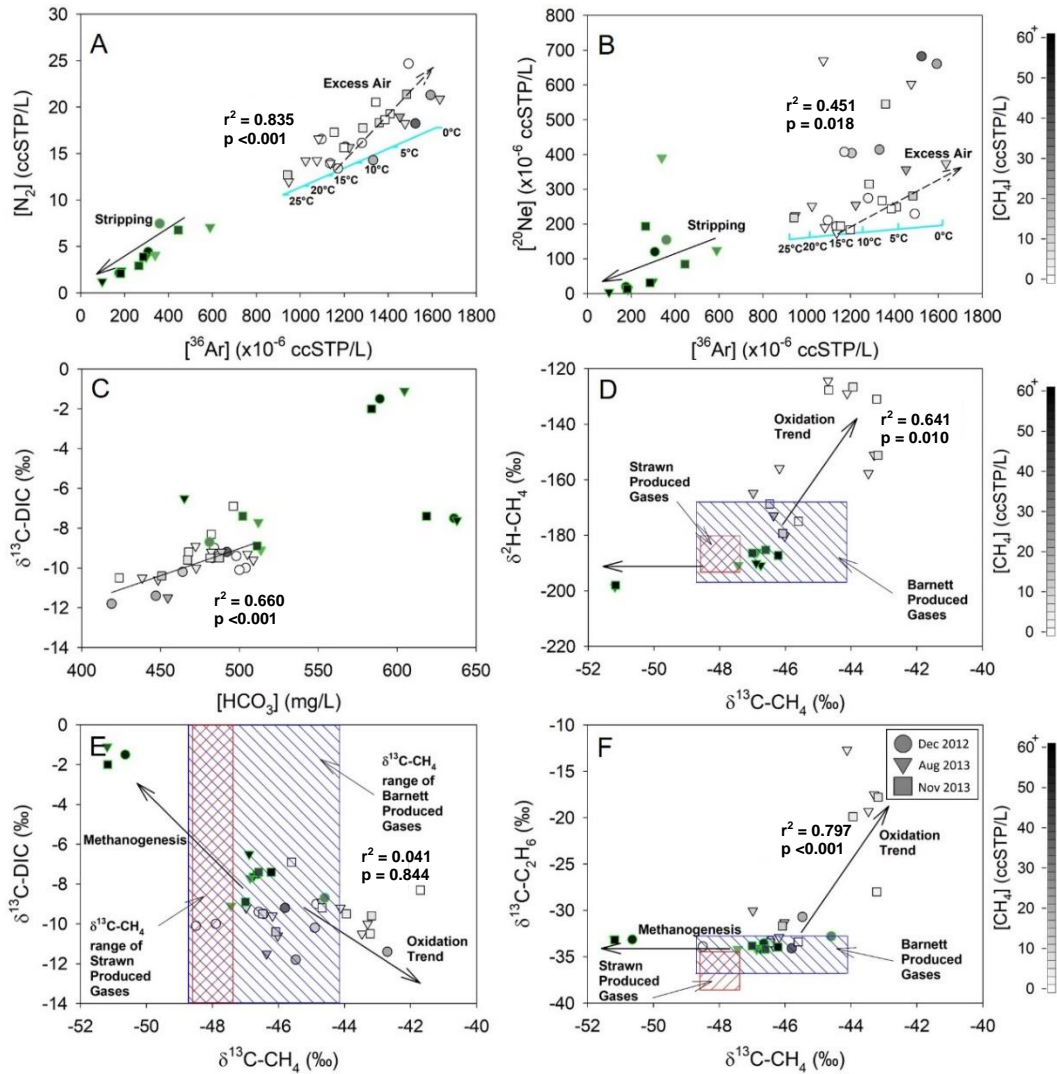


Figure 4.6: $[N_2]$ (A) and $[^{20}Ne]$ (B) vs. $[^{36}Ar]$, $\delta^{13}C-DIC$ vs. $[HCO_3^-]$ (C), and δ^2H-CH_4 (D), $\delta^{13}C-DIC$ (E), and $\delta^{13}C-C_2H_6$ (F) vs. $\delta^{13}C-CH_4$. Ranges for produced gases from the Strawn and Barnett include data from the current study and data assimilated from Darrah et al. (2014) and Nicot et al. (2017c). The background samples have normal ASW composition, but the five anomalous samples (green-rimmed circles), including the two that displayed pronounced changes between the initial and later sampling events, have significantly stripped ASW gas composition consistent with fugitive gas contamination. Because microbes tend to degrade higher-order aliphatic hydrocarbon compounds (i.e., C_{2+}) preferentially to CH_4 and also preferentially degrade the lighter isotopes of hydrocarbon compounds, natural gases that migrated into shallow aquifers over time should be degraded by methane oxidation, which is observed in the majority of background samples. By comparison, the five anomalous samples display increased [DIC] and minimal evidence for microbial oxidation consistent with the recent introduction of fugitive gas into the shallow aquifer.

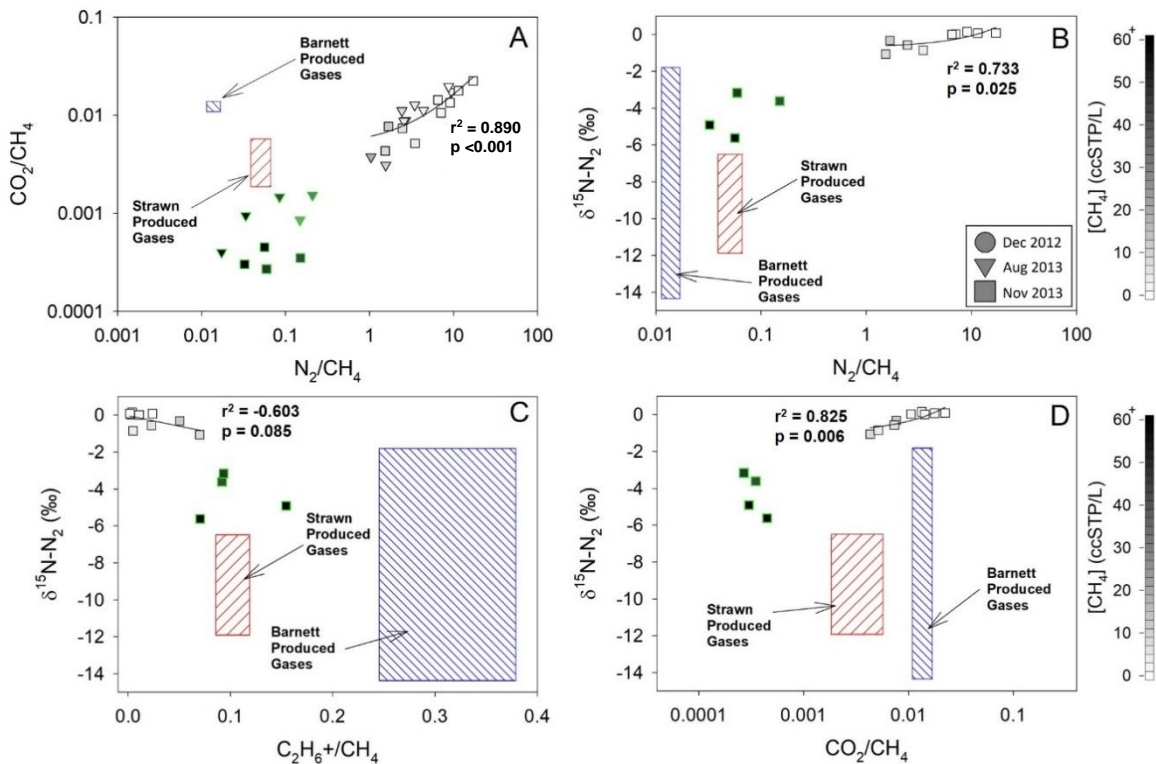


Figure 4.7: CO_2/CH_4 (A) and $\delta^{15}\text{N}-\text{N}_2$ (B) vs. N_2/CH_4 , $\delta^{15}\text{N}-\text{N}_2$ vs. $\text{C}_2\text{H}_6+\text{CH}_4$ (C), and $\delta^{15}\text{N}-\text{N}_2$ vs. CO_2/CH_4 (D). The ranges in production gas data include data from the current study and data assimilated from Larson et al. (2018). The molecular composition of hydrocarbons and non-hydrocarbons (CO_2/CH_4 , N_2/CH_4 , and $\text{C}_2\text{H}_6+\text{CH}_4$) and the isotopic composition of N_2 ($\delta^{15}\text{N}-\text{N}_2$) implicate fugitive gas contamination from a Strawn-produced natural gas as the most likely source of fugitive gas contamination consistent with previous reports (Darrah et al., 2014; Larson et al., 2018; Nicot et al., 2017c; Wen et al., 2016b; Wen et al., 2017). In this study area, these data are consistent with annulus conducted Strawn-like fugitive gas contamination from gas-producing horizons overlying the target Barnett Shale.

of excess (i.e., non-atmospheric) N₂ in the groundwater as opposed to sedimentary grains ($\delta^{15}\text{N-N}_2 = >2\%$) (Darrah et al., 2013; Kornacki and McCaffrey, 2011). A recent study by Larson et al. (2018) displayed a similar range for $\delta^{15}\text{N-N}_2$ and yielded similar conclusions. These $\delta^{15}\text{N-N}_2$ values and the presence of decreasing N₂/CH₄ ratios in the samples with the lowest $\delta^{15}\text{N-N}_2$ are consistent with the addition of a relatively small volume (<20%) of an exogenous hydrocarbon gas to shallow meteoric water (Figures 4.7B-D).

Table 4.7. Noble Gas Compositional and Isotopic Data from Produced Gases. Concentrations are in ccSTP/cc.

Sample	[⁴ He] (x10 ⁻⁶)	[²⁰ Ne] (x10 ⁻⁹)	[³⁶ Ar] (x10 ⁻⁹)	⁴ He/CH ₄ (x10 ⁻⁶)	³ He/ ⁴ He (R/R _A)	²⁰ Ne/ ²² Ne	²¹ Ne/ ²² Ne	³⁸ Ar/ ³⁶ Ar	⁴⁰ Ar/ ³⁶ Ar	²⁰ Ne/ ³⁶ Ar	⁴ He/ ²⁰ Ne	⁴ He/ ⁴⁰ Ar*	<u>Prod. Form.</u>
Strawn-1	1.28E+03	265	552	1.53E+03	0.0421	9.67	0.0304	0.1870	558.3	0.480	4.8E+03	8.8	Strawn
Strawn-2	3.36E+03	630	1813	3.97E+03	0.0402	9.73	0.0303	0.1880	550.9	0.350	5.3E+03	7.2	Strawn
Strawn-3	4.37E+03	168	1028	5.12E+03	0.0411	9.81	0.0361	0.1900	539.2	0.160	2.6E+04	17.5	Strawn
Strawn-4	1.91E+03	66	469	2.26E+03	0.0314	9.80	0.0299	0.1870	551.8	0.140	2.9E+04	15.9	Strawn
Barnett-1	7.14E+02	2.1	44	9.16E+02	0.0413	9.05	0.0671	0.1880	573.3	0.050	3.4E+05	59.0	Barnett
Barnett-2	7.25E+02	2.2	44	1.01E+03	0.0411	8.96	0.0649	0.1890	586.1	0.050	3.3E+05	56.2	Barnett
Barnett-3	6.53E+02	2.7	51	8.36E+02	0.0360	9.11	0.0624	0.1901	569.4	0.053	2.4E+02	46.5	Barnett
Barnett-4	8.13E+02	3.1	39	1.15E+03	0.0373	8.99	0.0637	0.1891	547.6	0.080	2.6E+02	82.8	Barnett

The correlation of hydrocarbon gases, exogenous [⁴He] and excess [N₂], stable isotopes of water ($\delta^2\text{H-H}_2\text{O}$ and $\delta^{18}\text{O-H}_2\text{O}$), and dissolved ions (e.g., Cl, Br, Sr) in the suite of baseline samples suggests that a relatively small volume of saline and hydrocarbon-rich groundwater migrated from a deeper source to the shallow aquifer on undetermined time scales and mixed with the local, modern (i.e., tritium active) meteoric groundwater. The strength of correlation between gas, salts, and isotopic proxies suggests coherent migration of these components and provides a suitable template for distinguishing between natural, gas-rich, saline water migration, and fugitive gas contamination.

4.4.3 Identifying Fugitive Gas Contamination

A subset of five drinking-water wells with elevated CH₄ levels (up to 71.48 ccSTP/L) are clearly distinct from the linear correlations between hydrocarbons, dissolved ions (e.g., Cl), water isotopes, and noble gases that are observed in the suite of baseline samples (Figures 4.5-7; bolded and italicized samples in Tables 4.1-3, 4.5). The noble gas data for each of these samples show significant stripping relative to ASW concentrations, indicative of a large volume of gas-phase migration in the subset of samples highlighted in green symbols (Figures 4.6A-B) (Darrah et al., 2014).

Darrah et al. (2014) reported that C₂H₆+/CH₄ versus $\delta^{13}\text{C-CH}_4$ and $^4\text{He}/^{40}\text{Ar}^*$ versus $^4\text{He}/^{20}\text{Ne}$ implicate natural gas release from the Strawn Group formations as the likely source for fugitive gas contamination in this subset of drinking-water wells. Consequently, Darrah et al. (2014) concluded that annulus-conducted Strawn gases, as opposed to Barnett gases, were likely transmitted from the relatively shallow, gas-charged Strawn formations to the shallow aquifer after the drilling of Barnett natural-gas wells provided a pathway for their release and transport. In separate studies, Wen et al. (2016b), Wen et al. (2017), and Larson et al. (2018) also concluded that fugitive gas was released from the Strawn formations, but implicate fugitive natural gas release related to the drilling of drinking-water wells that penetrate the Strawn formations. Here, I explore the capacity of additional gas-phase (compound-specific stable isotopes ($\delta^{13}\text{C-CH}_4$, $\delta^2\text{H-CH}_4$, and $\delta^{13}\text{C-C}_2\text{H}_6$) (Figure 4.6), non-hydrocarbon molecular gas composition (CO₂/CH₄, N₂/CH₄) and $\delta^{15}\text{N-N}_2$ (Figure 4.7)), and aqueous tracers ([SO₄], [DIC], and $\delta^{13}\text{C-DIC}$ (Figures 4.5-6, and 4.8)) to identify the presence of fugitive gas contamination.

Paired $\delta^{13}\text{C}-\text{CH}_4$, $\delta^2\text{H}-\text{CH}_4$, $\delta^{13}\text{C}-\text{C}_2\text{H}_6$, $\text{C}_2\text{H}_6+\text{CH}_4$ and $\delta^{13}\text{C}-\text{DIC}$ data provide important insights for the source and transport of natural gas into shallow aquifers in this study area (Figure 4.6). When natural gas migrates into shallow aquifers, bacteria can oxidize and degrade the hydrocarbons at relatively rapid metabolic rates depending on redox conditions and the presence of suitable microbial consortia. Microbial respiration and microbially-induced sulfate-paired oxidation tend to degrade higher order aliphatic hydrocarbon compounds (i.e., C_3H_8 , C_2H_6 , and other aliphatic hydrocarbons) preferentially to CH_4 and selectively degrade the lighter isotopes of hydrocarbon compounds when groundwater redox conditions (i.e., commonly described as the redox ladder) are favorable (Boreham and Edwards, 2008; Kessler et al., 2006; Kniermeyer et al., 2007; Kornacki and McCaffrey, 2011; Rowe and Muehlenbachs, 1999b).

Careful consideration of aqueous and gas geochemistry of groundwater reveals important geochemical differences between the drinking-water wells interpreted as being related to the stable baseline and those previously identified as displaying evidence for fugitive gas contamination (Darrah et al., 2014; Wen et al., 2016b). Baseline groundwater samples displayed strong linear correlation between SO_4 , Cl , and DIC (Figure 4.8). The strong positive correlation between SO_4 and Cl in baseline samples indicates a common source for both salts diluted by fresher sources of meteoric water within or during the transport of the relatively high salinity and gas-rich endmember into the shallow Trinity aquifer. The strong negative correlation between elevated DIC and Cl suggests that $[\text{DIC}]$ likely increase following the oxidation of organic carbon following mixing (dilution) with fresher water. This interpretation is supported by the strong negative correlation between SO_4 and DIC . Based on these data, sulfate reduction likely influences the hydrocarbon composition of the natural baseline samples as well.

Sulfate-paired oxidation preferentially degrades C_3H_8 , C_2H_6 , and other higher order aliphatic hydrocarbons, which causes the C_{2+}/C_1 to decrease and the $\delta^{13}C-CH_4$, δ^2H-CH_4 , $\delta^{13}C-C_2H_6$ in the residual hydrocarbon-phases to increase over time (Figure 4.6). The relatively slow seepage of hydrocarbons into shallow aquifers (i.e., at a rate slower than oxidation) would yield partially degraded aliphatic hydrocarbons (Kessler et al., 2006; Kornacki and McCaffrey, 2011; Rowe and Muehlenbachs, 1999b). By comparison, if oxidation rates exceed seepage rates, all hydrocarbon gases would be attenuated by microbial activity and converted to DIC, while SO_4 would eventually be exhausted. It is important to note that conservative tracers such as Cl and noble gases would remain as the only indicator of a previous episode of gas- and salt-rich fluid migration, while DIC and $\delta^{13}C-DIC$ can provide a (non-conservative) record of prior interactions. Conversely, if natural gas seepage rates exceed the rates of oxidation, hydrocarbon levels would remain high and both the molecular (C_{2+}/C_1) and isotopic ($\delta^{13}C-CH_4$, δ^2H-CH_4 , $\delta^{13}C-C_2H_6$) composition would be more consistent with their source.

Using this conceptual model, I investigated the extent to which microbes might have attenuated the hydrocarbons in shallow aquifers from this study. Plots of $\delta^{13}C-DIC$ versus [DIC], δ^2H-CH_4 versus $\delta^{13}C-CH_4$, $\delta^{13}C-DIC$ versus $\delta^{13}C-CH_4$, and $\delta^{13}C-C_2H_6$ versus $\delta^{13}C-CH_4$ (Figures 4.6C-F) show two distinct subsets of data, which correspond with homeowner reported changes in water quality. The baseline samples display moderate hydrocarbon oxidation paired with sulfate reduction that decreased [SO_4] and increased [DIC] (Figure 4.8C). These data are consistent with partial degradation of hydrocarbons by sulfate-paired oxidation. The observation of more highly degraded hydrocarbons is highlighted by progressively enriched δ^2H-CH_4 , $\delta^{13}C-CH_4$, and $\delta^{13}C-C_2H_6$ resulting from the preferential selection of the lighter isotopes of each hydrocarbon

component during microbial oxidation (Aharon et al., 1992; Knoller and Schubert, 2010) (Figure 4.6). Sulfate-paired oxidation likely occurred when waters mixed and encountered different redox conditions.

By comparison, the subset of samples with evidence of fugitive gas contamination do not display any quantifiable changes in the concentrations of Cl, Br, Na, Sr, or other conservative tracers (Figure 4.3). This subset of samples displays markedly higher concentrations of CH₄ (up to 71.48 ccSTP/L), C₂H₆ (up to 7.87 ccSTP/L), and C₃H₈ (up to 2.11 ccSTP/L) when compared to the values predicted by linear regression models of baseline samples. Two of the five samples influenced by fugitive gas contamination display elevated [DIC] and δ¹³C-DIC and decreased [SO₄], all of which are outside of the 95% confidence interval for linear regressions based on the best fits of the baseline. Two of the remaining three samples influenced by fugitive gas contamination displayed significant increases in hydrocarbon concentrations during the study period and small, but quantifiable increases in [DIC] and δ¹³C-DIC.

Samples with evidence of fugitive gas contamination display hydrocarbon and non-hydrocarbon molecular ratios (e.g., C₂H₆+/CH₄, N₂/CH₄, CO₂/CH₄) that are significantly different (Independent-Samples T Test p = <0.001, 0.001, and <0.001, respectively) from the majority of baseline samples. The molecular ratios reflect significant increases in the relative abundance of thermogenic hydrocarbons with respect to baseline samples supporting prior conclusions of fugitive hydrocarbon gas contamination in this subset of samples.

Once fugitive gas contamination has been identified, it is critical to determine the source and mechanism by which leakage occurred in order to evaluate potential risks to groundwater quality, develop strategies to mitigate leaks, and improve drilling and well completion techniques

(Darrah et al., 2014). Previous work in this area suggested that the molecular abundance of hydrocarbon (C_2H_6+/CH_4) and non-hydrocarbon gases (e.g., N_2/CO_2 or N_2/CH_4), compound-specific isotopes (e.g., $\delta^{13}C-C_2H_6$), and the isotopic compositions of non-hydrocarbon gases can help differentiate between fugitive gases derived from the Strawn and Barnett (Kornacki and McCaffrey, 2011). Non-hydrocarbon tracers are specifically important because it is difficult to differentiate between these sources using traditional hydrocarbon tracers (Figures 4.6-7) (Darrah et al., 2014; Kornacki and McCaffrey, 2011).

Each molecular tracer (e.g., C_2H_6+/CH_4 , N_2/CH_4 , CO_2/CH_4) displays values largely consistent with data from Strawn gases, and none of the parameters are uniquely consistent with Barnett gases. Thus, the simplest explanation is that fugitive gases were sourced from the Strawn (Figures 4.6D-F, 4.7). Nonetheless, post-genetic processes that occur in groundwater can alter molecular and isotopic ratios of natural gas and obfuscate their original source. These complications prohibit direct comparisons between the gas geochemistry in water and produced gases. For example, N_2 is the most abundant gas-phase component in recently recharged meteoric groundwater (~10-17 ccSTP/L), while the atmosphere constitutes a major source of potential contamination during sampling (~78%). For these reasons, a direct comparison between N_2 levels or ratios involving N_2 (e.g., N_2/CH_4) in groundwater and produced gas samples (Kornacki and McCaffrey, 2011) is tenuous unless the relative N_2 contributions from air-saturated water, excess air, and exogenous gases can be uniquely constrained. Similarly, because CO_2 is highly soluble (~28x more soluble in water than CH_4 at 10°C) and rapidly dissociates to DIC, the use of gas-phase $[CO_2]$ or ratios of CO_2 to other gases (e.g., CO_2/N_2 , CO_2/CH_4) in groundwater studies is problematic. As a result, the CO_2/CH_4 (and other ratios involving CO_2) collected from the gas-

phase must be considered as a minimum value. Thus, although it is tempting to use the ratios of N₂ and CO₂ (Figure 4.7) as an indicator of fugitive gas contamination from the Strawn Group formations, one must consider these limitations. For these reasons, while N₂ and CO₂ molecular tracers clearly have utility for identifying the presence of fugitive gas contamination, their application for determining the source of natural gas is quite restricted.

The isotopes of non-hydrocarbon gases, such as N₂ or CO₂ may provide additional insight and improve the utility of these tracers. In comparison to baseline samples, samples with evidence of fugitive gas contamination display significantly depleted $\delta^{15}\text{N-N}_2$ (-5.62 to -3.16‰). These more negative values likely represent mixing between ASW and an exogenous source of nitrogen derived from the degradation of organic matter. However, like the molecular composition of N₂, the $\delta^{15}\text{N-N}_2$ values do not uniquely implicate Strawn gases (nor do they identify a Barnett source). Instead, the observed $\delta^{15}\text{N-N}_2$ in groundwater samples is a function of the degree to which ASW gases have been stripped. Assuming an initial starting composition for [N₂] of 10-17 ccSTP/L and taking the average N₂/CH₄ for Strawn gases (0.051), the introduction of 51.4 ccSTP/L of CH₄ (the average CH₄ concentration in samples with other indicators of fugitive gas contamination) would only result in an increase of 2.6 ccSTP/L of N₂ or between 15.3 and 26.1% of the total N₂ in the groundwater sample. Those levels of non-atmospheric nitrogen contamination with Strawn gas would change the $\delta^{15}\text{N-N}_2$ in groundwater by a total of between -1.44 and -2.46‰. However, because stripping reduces the volume of initial ASW N₂, the residual mixture would contain a higher proportion of exogenous N₂ allowing deviations from atmospheric $\delta^{15}\text{N-N}_2$ to be quantified. Hence, like noble gases, $\delta^{15}\text{N-N}_2$ is a sensitive indicator for the occurrence of stripping and hence the presence of fugitive gas contamination (Darrah et al., 2014; Wen et al., 2016b). Nonetheless,

like the discussion of molecular tracers above, the role of $\delta^{15}\text{N-N}_2$ as a tracer for the source of natural gas is limited.

There are similar limitations to applying $\delta^{13}\text{C-CO}_2$. These limitations are discussed below but are largely related to the fact that the $\delta^{13}\text{C-CO}_2$ is buffered by dissolution into water and the labile nature of carbon during hydrocarbon oxidation, methanogenesis, and gas-water partitioning. Thus, while the abundance of N_2 or CO_2 and their isotopes can be valuable tracers for identifying the presence of fugitive gases, their utility as a method to fingerprint fugitive gas sources is actually quite limited, particularly in this setting.

4.4.4 Secondary Processes and Challenges with Identifying the Source of Fugitive Gas Contamination

While the inorganic geochemical dataset does not show evidence for the migration of formational brines (discussed further in 4.6), there are noticeable changes in $[\text{SO}_4]$ and $[\text{DIC}]$ for some of the impacted drinking-water wells. Importantly, these changes are the only observed differences in inorganic tracers between the baseline samples and the samples influenced by fugitive gas contamination.

The naturally-occurring hydrocarbon- and salt-rich endmember displays intermediate $[\text{DIC}]$ and relatively negative $\delta^{13}\text{C-DIC}$ ($\sim -12\text{‰}$). These $\delta^{13}\text{C-DIC}$ values are non-unique and consistent with soil organic matter and partial oxidation of hydrocarbon gases paired with sulfate reduction. The latter interpretation is supported by the presence of quantifiable levels of H_2S ($3\text{--}61 \times 10^{-6}$ ccSTP/L) in these samples. Importantly, this subset of samples inferred to be consistent with baseline does not display any deviations from the linear $\text{SO}_4\text{-Cl}$ trend (Figure 4.8A).

In contrast, several samples in the subset impacted by fugitive gas contamination display significant deviations from baseline samples for both $[\text{SO}_4]$ and $[\text{DIC}]$. The first two samples

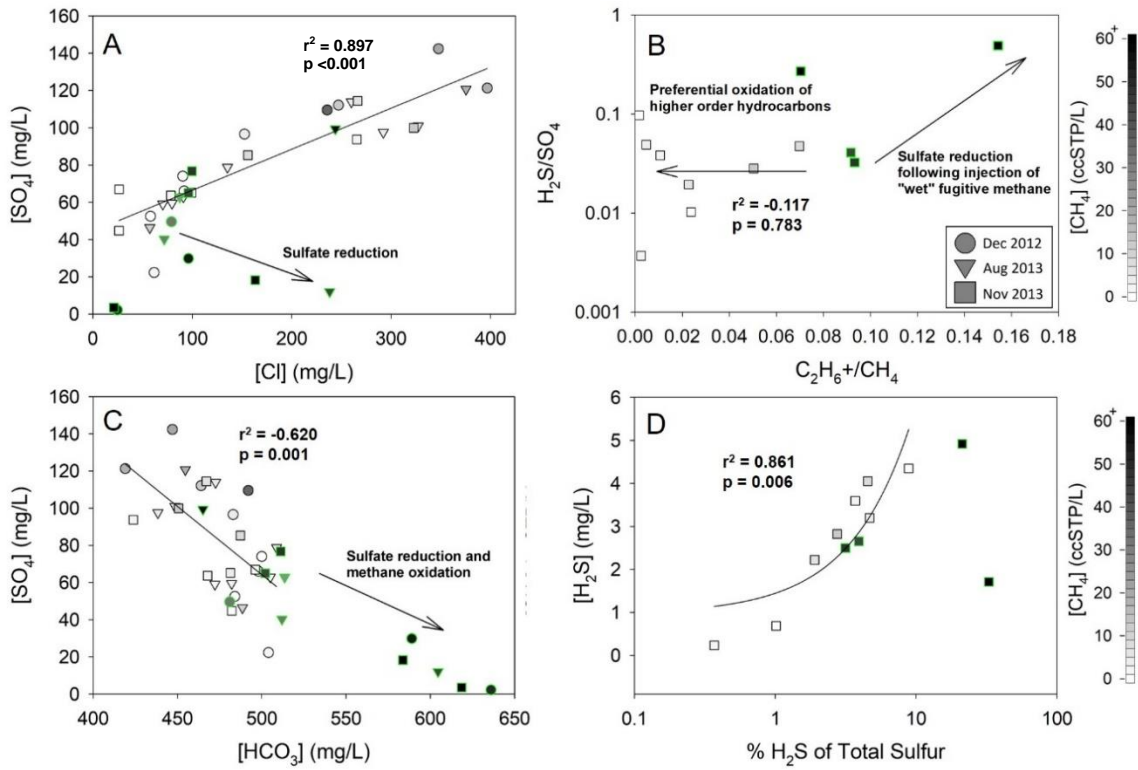


Figure 4.8: $[SO_4]$ vs. $[Cl]$ (A), H_2S/SO_4 vs. C_2H_6+/CH_4 (B), $[SO_4]$ vs. $[HCO_3]$ (C), and $[H_2S]$ vs. $H_2S\%$ of total $[S]$ (D). In background samples, SO_4 , HCO_3 , and Cl reflect a conservative 2-component mixing relationship independent of $[CH_4]$. In anomalous samples with evidence of fugitive gas contamination, there is a significant decrease in SO_4 and increase in HCO_3 and H_2S . These data are consistent with methane oxidation and sulfate reduction, which produces H_2S .

influenced by fugitive gas contamination show extensive depletion of SO_4 , while two of the remaining three samples (including two that experienced marked increases in CH_4 concentrations during the study) display trends of minor decreases in SO_4 concentrations during this study. Similarly, these samples displayed a marked enrichment of [DIC] and variable increases in $\delta^{13}\text{C}$ -DIC (Figure 4.5). Each of the three remaining samples displays higher [DIC] and $\delta^{13}\text{C}$ -DIC values that have experienced minor increases throughout time. Similar trends are observed when comparing the proportion of H_2S relative to SO_4 , which show nearly quantitative conversion of SO_4 to H_2S . These trends indicate that post-genetic sulfate-paired hydrocarbon oxidation following fugitive gas contamination degrades hydrocarbons and converts the sulfate pool to H_2S (Figure 4.8).

Bacterial sulfate reduction (BSR) converts SO_4 to H_2S and typically occurs in highly reducing conditions triggered from either mineralization of organic matter or bacterial CH_4 oxidation. BSR is known to occur in other methane-contaminated aquifers (Humez et al., 2016; Knoller and Schubert, 2010; Van Stempvoort et al., 2005; Van Stempvoort et al., 2007; Woda et al., 2018). In either scenario, the SO_4 reduction is typically associated with an increase of [DIC] and the occurrence of lighter $\delta^{13}\text{C}$ -DIC (Aharon et al., 1992; Van Stempvoort et al., 2005; Van Stempvoort et al., 2007). However, the occurrence of both elevated [DIC] and enriched $\delta^{13}\text{C}$ -DIC in samples with fugitive gas contamination (Figures 4.5D, 4.8C) initially appears inconsistent with this assertion.

I envision four plausible explanations that could account for the apparent mismatch between low SO_4 , elevated [DIC], and enriched $\delta^{13}\text{C}$ -DIC. These include: 1) the dissolution of enriched $\delta^{13}\text{C}$ -DIC from carbonate rocks present in the Trinity aquifer following H_2S generation;

2) preferential oxidation of higher aliphatic hydrocarbons; 3) an external source of CO₂ with a high δ¹³C; and 4) secondary methanogenesis.

Because there are no increases in [Ca] and [Sr] or changes in the Na/Cl or ⁸⁷Sr/⁸⁶Sr that should accompany base-exchanges reactions associated with the dissolution of carbonates (Figures 4.3-4), it is reasonable to rule out Scenario 1. The preferential oxidation of higher order hydrocarbons could account for the increase in [DIC], but would not produce sufficiently enriched δ¹³C-DIC. The δ¹³C of C₂₊ components in this study area have a range of δ¹³C-C_x between -34.3 and -28.1‰ (Hill et al., 2007; Rodriguez and Philp, 2010; Zumberge et al., 2012)) (Table 4.2), which cannot accommodate mass balance considerations of both [DIC] and δ¹³C-DIC. Further, no quantitative decrease in C₂₊/C₁ was observed in this subset of samples (Figures 4.6-8). The relative enrichment of DIC in the affected drinking-water wells (29 to 158 mg/L) corresponds to the addition of CO₂ (0.48 to 2.59 mmol CO₂/L of water), with two possible external sources for DIC in samples with evidence for fugitive gas contamination.

Here, I evaluate whether the Strawn-sourced gas is a viable explanation for all of the geochemical observations. Strawn gases contain up to 0.5% CO₂ by volume with a relatively enriched δ¹³C-CO₂ in this area (-2.31 to -5.72‰) (Table 4.6). Although Strawn [CO₂] are lower than those of the Barnett (0.9-1.2%), it is important to consider that these [CO₂] are actually ~12.5 times higher than the atmospheric values of CO₂. As a result, the [CO₂] in fugitive gas from the Strawn could lead to increases in [DIC] if released directly into the Trinity aquifer or in conditions of exceedingly high volumes of gas relative to water (i.e., V_{gas}/V_{water}).

Similarly, the elevated δ¹³C-CO₂ in Strawn-produced gases could also account for the observed increase in the δ¹³C-DIC. One potential conflict with this conclusion is that slow seepage

of Strawn gases into the Trinity aquifer is thought to account for baseline methane- and salt-rich fluids in the current study area (Darrah et al., 2014; Larson et al., 2018; Nicot et al., 2017a; Wen et al., 2017). The absence of a clear Strawn influence in baseline samples may instead reflect the highly soluble nature of CO₂ during fluid transport. The slow migration of Strawn gases would allow CO₂ from the Strawn to dissolve into and equilibrate with formation waters during fluid transport. By comparison, the transport of relatively large volumes of Strawn gases (i.e., extremely high $V_{\text{gas}}/V_{\text{water}}$) into the shallow aquifer would occur without sufficient opportunity for CO₂ to dissolve into formation waters and allow highly soluble CO₂ to reach the Trinity aquifer. As a result, it is plausible that the dissolution of CO₂ from Strawn-sourced fugitive gases (Scenario 3) could account for both trends of progressively enriched $\delta^{13}\text{C-DIC}$ and elevated [DIC] associated with sulfate reduction triggered by fugitive gas contamination.

Secondary methanogenesis (i.e., the conversion of previously oxidized hydrocarbons to CH₄ by microbial consortia) could also account for the observed enrichment in $\delta^{13}\text{C-DIC}$ (Scenario 4). The $\delta^{13}\text{C-DIC}$ of the DIC pool utilized to generate microbial CH₄ is dependent on the extent of hydrocarbon oxidation and the $\delta^{13}\text{C}$ of the oxidized compounds. Partial oxidation followed by secondary methanogenesis should be paired with a decrease in the DIC pool, increase in $\delta^{13}\text{C-DIC}$, and decrease in the $\delta^{13}\text{C-CH}_4$. Samples interpreted to have been influenced by fugitive gas contamination display more negative $\delta^{13}\text{C-CH}_4$ than the rest of the samples included in the current study, and in some cases $\delta^{13}\text{C-CH}_4$ is lower than the range of data observed for production gases from either the Barnett or Strawn produced gases. At least one of the samples (BSA-2) displays clear evidence for secondary methanogenesis with both the presence of more negative ($\delta^{13}\text{C-CH}_4$ ranges from -51.19 to -50.64‰ across the sampling times) and associated heavier $\delta^{13}\text{C-DIC}$ (-1.0

to -2.0‰ across the sampling times). However, one would anticipate that secondary methanogenesis would be associated with an overall decrease in [DIC]. Instead, the [DIC] for BSA-2 range from 583.8 to 604.6 mg/L, which is the second highest [DIC] in the current study. The degree of oxidation and associated [DIC] are difficult to constrain, which indicates that the observed [DIC] may reflect the partial loss of the original DIC pool, making it challenging to eliminate Scenario 4 based on the relative DIC levels. While the relationship between oxidation and secondary methanogenesis is markedly less clear for the remaining samples influenced by fugitive gas contamination, we note that each of these samples also displays relatively high [DIC], more positive $\delta^{13}\text{C-DIC}$, and lower $[\text{SO}_4]$ compared to baseline samples; these samples also displayed more negative $\delta^{13}\text{C-CH}_4$ (Figures 4.6-8). Although total H_2S concentrations were higher in some of the baseline samples, the highest $\text{H}_2\text{S}/\text{SO}_4$ were found in the subset of samples with evidence of fugitive gas contamination suggesting nearly quantitative conversion of sulfur to H_2S (Figure 4.8). Each of these observations is consistent with sulfate-paired oxidation followed by secondary methanogenesis (Scenario 4).

Although it is challenging to distinguish between Scenarios 3 or 4, a component of secondary methanogenesis is necessary to explain all of the data. A careful review of the $\delta^2\text{H-CH}_4$ versus $\delta^{13}\text{C-CH}_4$ displays a linear trend of more negative $\delta^{13}\text{C-CH}_4$ (ranging from -46.22 to -51.19‰) without any quantifiable changes in $\delta^{13}\text{C-C}_2\text{H}_6$ in the subset of samples with evidence for fugitive gas contamination (Figure 4.6F). If the DIC and $\delta^{13}\text{C-DIC}$ were related to the dissolution of migrated natural gas from the Strawn alone (Scenario 3), one would not anticipate a decrease in the $\delta^{13}\text{C-CH}_4$ composition. Mixing with a third endmember (e.g., primary microbial CH_4) could account for the linear trend observed in Figure 4.6F but cannot account for the

increases in DIC or decreases in SO_4 (which can be accounted for by sulfate-paired oxidation). However, while oxidation of Strawn-sourced gases can accommodate the observed changes in DIC and SO_4 , oxidation would influence *both* the $\delta^{13}\text{C}\text{-CH}_4$ and $\delta^{13}\text{C}\text{-C}_2\text{H}_6$, while influencing the $\delta^{13}\text{C}\text{-C}_2\text{H}_6$ to a greater extent. While contributions of Strawn-derived CO_2 (Scenario 3) cannot be ruled out, single-stage dissolution of CO_2 from Strawn-sourced gases alone cannot account for the mass balance of observed increases in [DIC]. In fact, assuming 100% of the CO_2 derived from a single pulse of fugitive Strawn-sourced gas dissolved into the Trinity aquifer, it would only account for an increase of [DIC] between 2.7 and 8.2 mg/L. These observations suggest Scenario 3 is only viable in a multiple stage process in which at least 12-37 volumes of Strawn-sourced gas migrated through the Trinity Aquifer and quantitatively dissolved the CO_2 (or more volumes with partial dissolution).

Based on all of these considerations, the most parsimonious explanation involves a multiple stage process. The first stage begins with the migration of fugitive Strawn-sourced gas (consistent with Scenario 3) to the Trinity aquifer. Next, the majority of Strawn-sourced CO_2 dissolves into groundwater of the Trinity Aquifer, which would increase the [DIC] and $\delta^{13}\text{C}\text{-DIC}$ and increase the CO_2 pool for methanogenic activity. In the third stage, sulfate-paired hydrocarbon oxidation increases the [DIC] and decreases the [SO_4]. If sulfate-paired aerobic oxidation was the terminal stage of the reaction the residual $\delta^{13}\text{C}\text{-CH}_4$ would be more positive than the original source; this trend is observed in baseline samples. However, if the microbial consortia utilize the newly developed, labile DIC pool to generate microbial CH_4 from the previously oxidized hydrocarbons, it will lead to an overall decrease in the $\delta^{13}\text{C}\text{-CH}_4$ without any changes in the $\delta^{13}\text{C}\text{-C}_2\text{H}_6$ and small increases in $\delta^{13}\text{C}\text{-DIC}$. As a result, a complete understanding of these multiple-stage processes

requires a fourth stage (secondary methanogenesis) to adequately explain the observed data. Similar reactions can influence the geochemistry of water and gas geochemical tracers in other fugitive gas studies, at least in instances where sulfate-paired aerobic oxidation is an intermediate step in the process of post-genetic hydrocarbon oxidation in shallow aquifers.

4.4.5 Comparison to Observations in Appalachian Basin

These observed changes in DIC and SO_4 are consistent with recent findings by Woda et al. (2018) who observed SO_4 reduction and the occurrence of H_2S formation in a normally-oxidizing groundwater system in Pennsylvania located near a producing natural gas well with known integrity issues, which they associated with sporadic gas release. Interestingly, they also observed metal reduction prior to the reduction of sulfate and the release of soluble Fe and Mn in their time series data. Although these trends were not seen in our dataset, there are important differences between the two study areas. The aquifers overlying the Marcellus in their region of study are normally oxidizing and have relatively low levels of SO_4 . As a result, increasingly reducing conditions must first pass through the metal reduction stage. This is observed first by the release of redox sensitive and potentially toxic trace elements into the groundwater in areas of anthropogenic gas release in PA (Woda et al., 2018). In our study area, the aquifer was naturally in a reduced state as indicated by the presence of active sulfate reduction, H_2S , and sulfate-paired hydrocarbon oxidation in baseline samples (Figure 4.8). Future studies in Parker County should monitor other redox sensitive and toxic trace metals (e.g., As) to determine if these secondary reactions impair water quality beyond safe drinking-water levels due to unnaturally reduced groundwater conditions.

Overall, these data confirm the presence of fugitive gas contamination in 5 of 20 drinking-water wells. Like Pennsylvania, our dataset identifies secondary changes in water quality related to the introduction of fugitive gases. However, those changes are dependent upon a given aquifer's position on the redox ladder and baseline geochemistry prior to the introduction of fugitive natural gas. In either case, the occurrence of fugitive gas contamination induces highly reducing conditions that leads to CH₄ oxidation and sulfate reduction in the Trinity aquifer. In combination, these processes favor the conversion of sulfate to H₂S. While these processes do not present emergent hazards like explosion, asphyxiation, or even metal contamination, they may produce a “geochemical hangover” in aquifers with naturally elevated SO₄ that can be converted to H₂S. Over time, this process may lead to chronic H₂S exposure and eventually lead to the release of oxyanion forming metals adsorbed onto aquifer solids.

4.4.6 Implications of Fugitive Gas Contamination

One of the public concerns related to shale gas drilling is the suggestion that fugitive gas contamination could precede the future migration of formational brines and/or hydraulic fracturing fluids containing radionuclides and other toxic compounds (Darrah et al., 2014; Llewellyn et al., 2015; Vengosh et al., 2014). Although multiple lines of geochemical evidence suggest the presence of fugitive gas contamination in five drinking-water wells, these data show that there is no evidence for the arrival of hydraulic fracturing fluids and/or formation water. These conclusions are based on the lack of any changes in the linear relationships between the majority of inorganic constituents (e.g., Ca, Na, Cl, Br, Sr, $\delta^{11}\text{B}$, $^{87}\text{Sr}/^{86}\text{Sr}$), including the drinking-water wells with evidence of fugitive gas contamination (Darrah et al., 2014). In fact, with the exception of SO₄, HCO₃, and their isotopes, the regression of inorganic data for samples with evidence of fugitive gas

contamination (including those that changed over time) is indistinguishable from a regression of the baseline samples. These results suggest a single continuous population that is unaltered by the presence of fugitive gas contamination for most inorganic components and is consistent with the lack of any addition of an exogenous brine component during the time period of this study. These results preclude the current migration of formational brines (and likely hydraulic fracturing fluids) from the deep subsurface to shallow aquifers in this study area, at least through the time interval of this investigation.

4.5. Conclusions

Previous studies implicated Strawn Group produced gases as the likely source of fugitive gas contamination in a subset of shallow groundwater drinking-water wells in Parker County, Texas based on a combination of hydrocarbon molecular and stable isotopic compositions, dissolved ion geochemistry, and noble gas geochemistry. Here, the ability to identify fugitive gas, the source formation of contamination, and secondary environmental impacts have been tested using a more comprehensive suite of geochemical parameters including stable isotopes of water, $\delta^{11}\text{B}$, $^{87}\text{Sr}/^{86}\text{Sr}$, $\delta^{13}\text{C}$ and $\delta^2\text{H}$ of CH_4 and C_2H_6 , $\delta^{13}\text{C}$ -DIC, and $\delta^{15}\text{N}$ - N_2 , $[\text{H}_2\text{S}]$, and ratios of major gases, in addition to the previously used geochemical techniques. These data confirm the presence of fugitive gas in a subset of samples that is clearly distinct from baseline mixing between a high salinity, high SO_4 endmember and recently recharged meteoric water. The data presented here also suggest stable isotopes such as nitrogen $\delta^{15}\text{N}$ - N_2 and major gas ratios such as N_2/CH_4 , CO_2/CH_4 may be used to identify fugitive gas contamination but are only useful for identifying the sources if all components of N_2 (e.g., excess air) or reactions involving CO_2 (e.g., carbonate dissolution) can be constrained, which is not the case in the current study area. A combination of geochemical

data suggest that secondary reactions includes sulfate-paired hydrocarbon oxidation, secondary methanogenesis, and the formation of H₂S.

Chapter 5. Concluding Remarks

In order to properly evaluate the presence of thermogenic natural gas in scenarios of naturally-occurring migration and fugitive gas contamination, the work presented in this document has highlighted both the importance of integrating a diverse suite of geochemical techniques as well as the full consideration of processes that may affect hydrocarbons once present in shallow groundwater. In particular, the work presented here suggests inert noble gases are a critical geochemical tool for distinguishing between *in situ* processes of post-genetic modification of hydrocarbons such as oxidation and secondary methanogenesis or alteration following transport or mixing. For the first time, the process of secondary methanogenesis following the aerobic microbial oxidation of thermogenic hydrocarbons has been quantifiably modeled and applied to previously published groundwater data and the new data presented herein. Secondary methanogenesis may explain commonly observed hydrocarbon geochemical signatures that were previously presumed to result from extreme hydrocarbon molecular and stable isotopic fractionation as a result of solubility partitioning during migration and mixing with microbial gas.

Future work in the field of hydrocarbon contamination of shallow groundwater should focus on the potential secondary effects resulting from microbial degradation of natural gas. Recent work in the Appalachian Basin observed the redox-controlled release of metals such as iron as a result of intermittent pulses of fugitive gas that was subsequently oxidized by microbes. Evidence of changing redox states were also observed in the work presented here from Parker County, Texas. The sudden change from oxidizing to reducing conditions may release other, more

toxic metals (e.g., arsenic) and this should be monitored in areas suggested to be contaminated by fugitive gas.

References

- Adams, M.M., Hoarfrost, A.L., Bose, A., Joye, S.B. and Girguis, P.R. (2013) Anaerobic oxidation of short-chain alkanes in hydrothermal sediments: potential influences on sulfur cycling and microbial diversity. *Frontiers in microbiology* 4110.
- Aeschbach-Hertig, W., El-Gamal, H., Wieser, M. and Palcsu, L. (2008) Modeling excess air and degassing in groundwater by equilibrium partitioning with a gas phase. *Water Resources Research* 44(W08449).
- Aeschbach-Hertig, W., Peeters, F., Beyerle, U. and Kipfer, R. (1999) Interpretation of dissolved atmospheric noble gases in natural waters. *Water Resources Research* 35(9), 2779-2792.
- Aharon, P., Graber, E.R. and Roberts, H.H. (1992) Dissolved carbon and delta-C-13 anomalies in the water column caused by hydrocarbon seeps on the northwestern Gulf of Mexico slope. *Geo-Marine Letters* 12(1), 33-40.
- Anderson, J.S., Romanak, K.D., Yang, C., Lu, J., Hovorka, S.D. and Young, M.H. (2017) Gas source attribution techniques for assessing leakage at geologic CO₂ storage sites: Evaluating a CO₂ and CH₄ soil gas anomaly at the Cranfield CO₂-EOR site. *Chemical Geology* 45493-104.
- Baldassare, F.J., McCaffrey, M.A. and Harper, J.A. (2014) A geochemical context for stray gas investigations in the northern Appalachian Basin: Implications of analyses of natural gases from Neogene-through Devonian-age strata. *AAPG Bulletin* 98(2), 341-372.
- Ballentine, C.J., Burgess, R. and Marty, B. (2002) Tracing fluid origin, transport and interaction in the crust, in: Porcelli, D., Ballentine, C.J., Wieler, R. (Eds.), *Noble Gases in Geochemistry and Cosmochemistry*, 539-614.
- Ballentine, C.J. and Burnard, P.G. (2002) Production, release and transport of noble gases in the continental crust, in: Porcelli, D., Ballentine, C.J., Wieler, R. (Eds.), *Noble Gases in Geochemistry and Cosmochemistry*, 481-538.
- Ballentine, C.J., Mazurek, M. and Gautschi, A. (1994) Thermal constraints on crustal rare-gas release and migration-Evidence from Alpine fluid inclusions. *Geochimica et Cosmochimica Acta* 58(20), 4333-4348.
- Barry, P., Lawson, M., Meurer, W.P., Cheng, A. and Ballentine, C. (2018) Noble gases in deepwater oils of the US Gulf of Mexico. *Geochemistry, Geophysics, Geosystems* 19(11), 4218-4235.
- Battani, A., Sarda, P. and Prinzhofer, A. (2000) Basin scale natural gas source, migration and trapping traced by noble gases and major elements: the Pakistan Indus basin. *Earth and Planetary Science Letters* 181(1-2), 229-249.
- Bennett, B. and Dudas, M.J. (2003) Release of arsenic and molybdenum by reductive dissolution of iron oxides in a soil with enriched levels of native arsenic. *Journal of Environmental Engineering and Science* 2(4), 265-272.

- Bernard, B.B. (1978) Light hydrocarbons in marine sediments. Texas A and M University, College Station, TX.
- Bernard, B.B., Brooks, J.M. and Sackett, W.M. (1976) Natural gas seepage in the Gulf of Mexico. *Earth and Planetary Science Letters* 31(1), 48-54.
- Bordeleau, G., Rivard, C., Lavoie, D., Lefebvre, R., Ahad, J.M., Xu, X. and Mort, A. (2018a) A multi-isotope approach to determine the origin of methane and higher alkanes in groundwater of the St. Lawrence Platform, Saint-Édouard area, eastern Canada. *Environmental Geosciences* 25(3), 75-100.
- Bordeleau, G., Rivard, C., Lavoie, D., Lefebvre, R., Malet, X. and Ladevèze, P. (2018b) Geochemistry of groundwater in the Saint-Édouard area, Quebec, Canada, and its influence on the distribution of methane in shallow aquifers. *Applied geochemistry* 8992-108.
- Boreham, C.J. and Edwards, D.S. (2008) Abundance and carbon isotopic composition of neopentane in Australian natural gases. *Organic Geochemistry* 39(5), 550-566.
- Boreham, C.J., Golding, S.D. and Glikson, M. (2001) Reply to Comment of Smith and Pallasser on "Factors controlling the origin of gas in Australian Bowen Basin coals". *Organic Geochemistry* 32(1), 207-210.
- Bosch, A. and Mazar, E. (1988) Natural gas association with water and oil as depicted by atmospheric noble gases: case studies from the southeastern Mediterranean Coastal Plain. *Earth and Planetary Science Letters* 87(3), 338-346.
- Bowker, K.A. (2007) Barnett shale gas production, Fort Worth Basin: Issues and discussion. *AAPG Bulletin* 91(4), 523-533.
- Brantley, S.L., Yoxheimer, D., Arjmand, S., Grieve, P., Vidic, R., Pollak, J., Llewellyn, G.T., Abad, J. and Simon, C. (2014) Water resource impacts during unconventional shale gas development: The Pennsylvania experience. *International Journal of Coal Geology* 126140-156.
- Burruss, R.C. and Laughrey, C.D. (2010) Carbon and hydrogen isotopic reversals in deep basin gas: Evidence for limits to the stability of hydrocarbons. *Organic Geochemistry* 41(12), 1285-1296.
- Carothers, W.W. and Kharaka, Y.K. (1980) Stable carbon isotopes of HCO₃⁻ in oil-field waters—implications for the origin of CO₂. *Geochimica et Cosmochimica Acta* 44(2), 323-332.
- Castonguay, S., Lavoie, D., Dietrich, J. and Laliberté, J.-Y. (2010) Structure and petroleum plays of the St. Lawrence Platform and Appalachians in southern Quebec: insights from interpretation of MRNQ seismic reflection data. *Bulletin of Canadian Petroleum Geology* 58(3), 219-234.
- Chatellier, J.-Y., Flek, P., Molgat, M., Anderson, I., Ferworn, K., Larsen, N.L. and Ko, S. (2013) Overpressure in shale gas: When geochemistry and reservoir engineering data meet and agree. *AAPG Memoirs* 103: Critical Assessment of Shale Resource Plays 45-69.
- Clark, T.H. and Globensky, Y. (1973) Portneuf et parties de St-Raymond et de Lyster: comtés de Portneuf et de Lotbinière. Ministère des richesses naturelles, Direction générale des mines, Rapport Géologique.
- Comeau, F.-A., Kirkwood, D., Malo, M., Asselin, E. and Bertrand, R. (2004) Taconian mélanges in the parautochthonous zone of the Québec Appalachians revisited: Implications for foreland basin and thrust belt evolution. *Canadian Journal of Earth Sciences* 41(12), 1473-1490.

- Cuoco, E., Tedesco, D., Poreda, R.J., Williams, J.C., De Francesco, S., Balagizi, C. and Darrah, T.H. (2013) Impact of volcanic plume emissions on rain water chemistry during the January 2010 Nyamuragira eruptive event: Implications for essential potable water resources. *Journal of Hazardous Materials* 244570-581.
- Darrah, T.H. (2018) Time to settle the fracking controversy. *Groundwater* 56(2), 161-162.
- Darrah, T.H., Jackson, R.B., Vengosh, A., Warner, N.R. and Poreda, R.J. (2015a) Noble Gases: A New Technique for Fugitive Gas Investigation in Groundwater. *Groundwater* 53(1), 23-28.
- Darrah, T.H., Jackson, R.B., Vengosh, A., Warner, N.R., Whyte, C.J., Walsh, T.B., Kondash, A.J. and Poreda, R.J. (2015b) The evolution of Devonian hydrocarbon gases in shallow aquifers of the northern Appalachian Basin: Insights from integrating noble gas and hydrocarbon geochemistry. *Geochimica et Cosmochimica Acta* 170, 321-355.
- Darrah, T.H. and Poreda, R.J. (2012) Evaluating the accretion of meteoritic debris and interplanetary dust particles in the GPC-3 sediment core using noble gas and mineralogical tracers. *Geochimica et Cosmochimica Acta* 84, 329-352.
- Darrah, T.H., Prutsman-Pfeiffer, J.J., Poreda, R.J., Campbell, M.E., Hauschka, P.V. and Hannigan, R.E. (2009) Incorporation of excess gadolinium into human bone from medical contrast agents. *Metallomics* 1(6), 479-488.
- Darrah, T.H., Tedesco, D., Tassi, F., Vaselli, O., Cuoco, E. and Poreda, R.J. (2013) Gas chemistry of the Dallol region of the Danakil Depression in the Afar region of the northern-most East African Rift. *Chemical Geology* 339, 16-29.
- Darrah, T.H., Vengosh, A., Jackson, R.B., Warner, N.R. and Poreda, R.J. (2014) Noble gases identify the mechanisms of fugitive gas contamination in drinking-water wells overlying the Marcellus and Barnett Shales. *Proceedings of the National Academy of Sciences of the United States of America* 111(39), 14076-14081.
- Dessort, D., Poirier, Y., Sermondadaz, G. and Levaché, D. (2003) Stable isotope geochemistry of gas associated to oil biodegradation, 21st IMOOG, Krakow, Poland.
- Dowling, C.B., Poreda, R.J., Basu, A.R., Peters, S.L. and Aggarwal, P.K. (2002) Geochemical study of arsenic release mechanisms in the Bengal Basin groundwater. *Water Resources Research* 38(9).
- Drollette, B.D., Hoelzer, K., Warner, N.R., Darrah, T.H., Karatum, O., O'Connor, M.P., Nelson, R.K., Fernandez, L.A., Reddy, C.M., Vengosh, A., Jackson, R.B., Elsner, M. and Plata, D.L. (2015) Elevated levels of diesel range organic compounds in groundwater near Marcellus gas operations are derived from surface activities. *Proceedings of the National Academy of Sciences of the United States of America* 112(43), 13184-13189.
- Duchaine, Y., Tourigny, Y., Beaudoin, G. and Dupuis, C. (2012) Potentiel en gaz naturel dans le Groupe d'Utica, Québec, in: Laval, U. (Ed.), Québec City, Québec, Canada.
- Dusseault, M. and Jackson, R. (2014) Seepage pathway assessment for natural gas to shallow groundwater during well stimulation, in production, and after abandonment. *Environmental Geosciences* 21(3), 107-126.
- Eltschlager, K.K., Hawkins, J.W., Ehler, W.C., Baldassare, F. and Dep, P. (2001) Technical measures for the investigation and mitigation of fugitive methane hazards in areas of coal mining, in: Enforcement, U.D.o.t.I.O.o.S.M.R.a. (Ed.), Pittsburgh, PA.
- Etiopé, G., Feyzullayev, A., Milkov, A.V., Waseda, A., Mizobe, K. and Sun, C.H. (2009) Evidence of subsurface anaerobic biodegradation of hydrocarbons and potential secondary

- methanogenesis in terrestrial mud volcanoes. *Marine and Petroleum Geology* 26(9), 1692-1703.
- Eymold, W.K., Swana, K., Moore, M.T., Whyte, C.J., Harkness, J.S., Talma, S., Murray, R., Moortgat, J.B., Miller, J., Vengosh, A. and Darrah, T.H. (2018) Hydrocarbon-Rich Groundwater above Shale-Gas Formations: A Karoo Basin Case Study. *Groundwater* 56(2), 204-224.
- Faber, E. and Stahl, W. (1984) Geochemical surface exploration for hydrocarbons in North Sea. *AAPG Bulletin* 68(3), 363-386.
- Flippin, J.W. (1982) The stratigraphy, structure, and economic aspects of the Paleozoic strata in Erath county, north central Texas, in: Martin, C.A.E. (Ed.), *Petroleum geology of the Fort Worth Basin and Bend arch area*. Dallas Geological Society, 129-155.
- Fontenot, B.E., Hunt, L.R., Hildenbrand, Z.L., Carlton, D.D., Jr., Oka, H., Walton, J.L., Hopkins, D., Osorio, A., Bjorndal, B., Hu, Q.H. and Schug, K.A. (2013) An Evaluation of Water Quality in Private Drinking Water Wells Near Natural Gas Extraction Sites in the Barnett Shale Formation. *Environmental Science & Technology* 47(17), 10032-10040.
- Fuex, A. (1980) Experimental evidence against an appreciable isotopic fractionation of methane during migration. *Physics and Chemistry of the Earth* 12725-732.
- Gilfillan, S.M., Ballentine, C.J., Holland, G., Blagburn, D., Sherwood Lollar, B., Stevens, S., Schoell, M. and Cassidy, M. (2008) The noble gas geochemistry of natural CO₂ gas reservoirs from the Colorado Plateau and Rocky Mountain provinces, USA. *Geochimica et Cosmochimica Acta* 72(4), 1174-1198.
- Gilfillan, S.M.V., Sherwood Lollar, B., Holland, G., Blagburn, D., Stevens, S., Schoell, M., Cassidy, M., Ding, Z.J., Zhou, Z., Lacrampe-Couloume, G. and Ballentine, C.J. (2009) Solubility trapping in formation water as dominant CO₂ sink in natural gas fields. *Nature* 458(7238), 614-618.
- Globensky, Y. (1987) *Géologie des Basses-Terres du Saint-Laurent*. Ministère de l'Énergie et des Ressources du Québec, Québec, Québec.
- Globensky, Y. (1993) *Lexique stratigraphique canadien: région des Appalaches, des Basses-Terres du Saint-Laurent et des îles de la Madeleine*. Ministère de l'énergie et des ressources, Québec, Québec, 327.
- Harkness, J.S., Darrah, T.H., Moore, M.T., Whyte, C.J., Mathewson, P.D., Cook, T. and Vengosh, A. (2017a) Naturally occurring versus anthropogenic sources of elevated molybdenum in groundwater: Evidence for Geogenic contamination from Southeast Wisconsin, United States. *Environmental Science & Technology* 51(21), 12190-12199.
- Harkness, J.S., Darrah, T.H., Warner, N.R., Whyte, C.J., Moore, M.T., Millot, R., Kloppmann, W., Jackson, R.B. and Vengosh, A. (2017b) The geochemistry of naturally occurring methane and saline groundwater in an area of unconventional shale gas development. *Geochimica et Cosmochimica Acta* 208, 302-334.
- Harkness, J.S., Dwyer, G.S., Warner, N.R., Parker, K.M., Mitch, W.A. and Vengosh, A. (2015) Iodide, Bromide, and Ammonium in Hydraulic Fracturing and Oil and Gas Wastewaters: Environmental Implications. *Environmental Science & Technology* 49(3), 1955-1963.
- Harkness, J.S., Swana, K., Eymold, W.K., Miller, J., Murray, R., Talma, S., Whyte, C.J., Moore, M.T., Maletic, E.L., Vengosh, A. and Darrah, T.H. (2018) Pre-drill Groundwater Geochemistry in the Karoo Basin, South Africa. *Groundwater* 56(2), 187-203.

- Heilweil, V.M., Grieve, P.L., Hynek, S.A., Brantley, S.L., Solomon, D.K. and Risser, D.W. (2015) Stream measurements locate thermogenic methane fluxes in groundwater discharge in an area of shale-gas development. *Environmental Science & Technology* 49(7), 4057-4065.
- Henry, J.D. (1982) Stratigraphy of the Barnett shale (Mississippian) and associated reefs in the northern Fort Worth Basin, in: Martin, C.A.E. (Ed.), *Petroleum geology of the Fort Worth Basin and Bend arch area*. Dallas Geological Society, 157-178.
- Herkommer, M.A. and Denke, G.W. (1982) Stratigraphy and hydrocarbons, Parker County, Texas. *Dallas Geological Society*.
- Hildenbrand, Z.L., Carlton, D.D., Jr., Fontenot, B.E., Meik, J.M., Walton, J.L., Taylor, J.T., Thacker, J.B., Korlie, S., Shelor, C.P., Henderson, D., Kadjo, A.F., Roelke, C.E., Hudak, P.F., Burton, T., Rifai, H.S. and Schug, K.A. (2015) A Comprehensive Analysis of Groundwater Quality in The Barnett Shale Region. *Environmental Science & Technology* 49(13), 8254-8262.
- Hill, R.J., Jarvie, D.M., Zumberge, J., Henry, M. and Pollastro, R.M. (2007) Oil and gas geochemistry and petroleum systems of the Fort Worth Basin. *AAPG Bulletin* 91(4), 445-473.
- Holocher, J., Peeters, F., Aeschbach-Hertig, W., Kinzelbach, W. and Kipfer, R. (2003) Kinetic model of gas bubble dissolution in groundwater and its implications for the dissolved gas composition. *Environmental Science & Technology* 37(7), 1337-1343.
- Humez, P., Mayer, B., Ing, J., Nightingale, M., Becker, V., Kingston, A., Akbilgic, O. and Taylor, S. (2016) Occurrence and origin of methane in groundwater in Alberta (Canada): gas geochemical and isotopic approaches. *Science of the Total Environment* 5411253-1268.
- Hunt, A.G., Darrah, T.H. and Poreda, R.J. (2012) Determining the source and genetic fingerprint of natural gases using noble gas geochemistry: A northern Appalachian Basin case study. *AAPG Bulletin* 96(10), 1785-1811.
- Isotech (2011) Collection of groundwater samples from domestic and municipal water wells for dissolved gas analysis, in: Laboratories, e.I. (Ed.), Champaign, IL.
- Jackson, R.B., Vengosh, A., Carey, J.W., Davies, R.J., Darrah, T.H., O'Sullivan, F. and Petron, G. (2014) The environmental costs and benefits of fracking. *Annual Review of Environment and Resources* 39.
- Jackson, R.B., Vengosh, A., Darrah, T.H., Warner, N.R., Down, A., Poreda, R.J., Osborn, S.G., Zhao, K.G. and Karr, J.D. (2013) Increased stray gas abundance in a subset of drinking water wells near Marcellus shale gas extraction. *Proceedings of the National Academy of Sciences of the United States of America* 110(28), 11250-11255.
- Jarvie, D.M., Claxton, B.L., Henk, F. and Breyer, J.T. (2001) Oil and shale gas from the Barnett Shale, Ft Worth Basin, Texas, AAPG Annual Meeting Program, A100.
- Jarvie, D.M., Hill, R., Pollastro, R., Wavrek, D., Claxton, B. and Tobey, M. (2003) Evaluation of unconventional natural gas prospects: The Barnett Shale fractured shale gas model, Proceedings of European Association of International Organic Geochemists Meeting, Krakow, Poland, 60-70.
- Jenden, P.D., Drazan, D.J. and Kaplan, I.R. (1993) Mixing of thermogenic natural gases in northern Appalachian Basin *AAPG Bulletin* 77(6), 980-998.
- Kang, M., Christian, S., Celia, M.A., Mauzerall, D.L., Bill, M., Miller, A.R., Chen, Y., Conrad, M.E., Darrah, T.H. and Jackson, R.B. (2016) Identification and characterization of high

- methane-emitting abandoned oil and gas wells. *Proceedings of the National Academy of Sciences of the United States of America* 113(48), 13636-13641.
- Kerans, C. (1988) Karst-controlled reservoir heterogeneity in Ellenburger Group carbonates of west Texas. *AAPG Bulletin* 72(10), 1160-1183.
- Kerr, R.A. (2010) Natural Gas From Shale Bursts Onto the Scene. *Science* 328(5986), 1624-1626.
- Kessler, J.D., Reeburgh, W.S. and Tyler, S.C. (2006) Controls on methane concentration and stable isotope ($\delta^2\text{H-CH}_4$ and $\delta^{13}\text{C-CH}_4$) distributions in the water columns of the Black Sea and Cariaco Basin. *Global Biogeochemical Cycles* 20(4), 366-375.
- Kharaka, Y.K. and Specht, D.J. (1988) The solubility of noble gases in crude oil at 25–100 C. *Applied Geochemistry* 3(2), 137-144.
- Kinnaman, F.S., Valentine, D.L. and Tyler, S.C. (2007) Carbon and hydrogen isotope fractionation associated with the aerobic microbial oxidation of methane, ethane, propane and butane. *Geochimica et Cosmochimica Acta* 71(2), 271-283.
- Kipfer, R., Aeschbach-Hertig, W., Peeters, F. and Stute, M. (2002) Noble gases in lakes and ground waters, in: Porcelli, D., Ballentine, C.J., Wieler, R. (Eds.), *Noble Gases in Geochemistry and Cosmochemistry*, 615-700.
- Kirschbaum, M.A., Schenk, C.J., Cook, T.A., Ryder, R.T., Charpentier, R.R., Klett, T.R., Gaswirth, S.B., Tennyson, M.E. and Whidden, K.J. (2012) Assessment of undiscovered oil and gas resources of the Ordovician Utica Shale of the Appalachian Province. USGS Fact Sheet 2012-3116.
- Kniemeyer, O., Musat, F., Sievert, S.M., Knittel, K., Wilkes, H., Blumenberg, M., Michaelis, W., Classen, A., Bolm, C. and Joye, S.B. (2007) Anaerobic oxidation of short-chain hydrocarbons by marine sulphate-reducing bacteria. *Nature* 449(7164), 898-901.
- Knoller, K. and Schubert, M. (2010) Interaction of dissolved and sedimentary sulfur compounds in contaminated aquifers. *Chemical Geology* 276(3-4), 284-293.
- Kornacki, A. and McCaffrey, M. (2011) Applying Geochemical Fingerprinting Technology to Determine the Source of Natural Gas Samples Obtained from Water Wells in Parker County and Hood County. *Weatherford Laboratories, Houston*.
- Kornacki, A.S. and McCaffrey, M. (2014) Monitoring the Active migration and biodegradation of natural gas in the Trinity group aquifer at the Silverado development in Southern Parker County, Texas, AAPG Annual Convention and Exhibition Search and Discover Article, 6-9.
- Kreuzer, R.L., Darrah, T.H., Grove, B.S., Moore, M.T., Warner, N.R., Eymold, W.K., Whyte, C.J., Mitra, G., Jackson, R.B. and Vengosh, A. (2018) Structural and hydrogeological controls on hydrocarbon and brine migration into drinking water aquifers in southern New York. *Groundwater* 56(2), 225-244.
- Ladevèze, P. (2017) Aquifères superficiels et ressources profondes: le rôle des failles et des réseaux de fractures. INRS-ETE.
- Ladevèze, P., Rivard, C., Lavoie, D., Séjourné, S., Lefebvre, R. and Bordeleau, G. (2019) Fault and natural fracture control on upward fluid migration: insights from a shale gas play in the St. Lawrence Platform, Canada. *Hydrogeology Journal* 27(1), 121-143.
- Ladevèze, P., Rivard, C., Lefebvre, R., Lavoie, D., Parent, M., Malet, X., Bordeleau, G. and Gosselin, J. (2016) Travaux de caractérisation hydrogéologique dans la plateforme sédimentaire du Saint-Laurent, région de Saint-Édouard-de-Lotbinière, Québec. *Dossier Public* 8036112.

- Larson, T.E., Nicot, J.P., Mickler, P., Castro, M.C., Darvari, R., Wen, T. and Hall, C.M. (2018) Monitoring stray natural gas in groundwater with dissolved nitrogen. An example from Parker County, Texas. *Water Resources Research* 54(9), 6024-6041.
- Lavoie, D. (2008) Appalachian foreland basin of Canada. *Sedimentary Basins of the World* 565-103.
- Lavoie, D., Pinet, N., Bordeleau, G., Ardakani, O.H., Ladevèze, P., Duchesne, M.J., Rivard, C., Mort, A., Brake, V. and Sanei, H. (2016) The Upper Ordovician black shales of southern Quebec (Canada) and their significance for naturally occurring hydrocarbons in shallow groundwater. *International Journal of Coal Geology* 158, 44-64.
- Lavoie, D., Rivard, C., Lefebvre, R., Séjourné, S., Thériault, R., Duchesne, M.J., Ahad, J.M., Wang, B., Benoît, N. and Lamontagne, C. (2014) The Utica Shale and gas play in southern Quebec: geological and hydrogeological syntheses and methodological approaches to groundwater risk evaluation. *International Journal of Coal Geology* 126, 77-91.
- Llewellyn, G.T., Dorman, F., Westland, J.L., Yoxtheimer, D., Grieve, P., Sowers, T., Humston-Fulmer, E. and Brantley, S.L. (2015) Evaluating a groundwater supply contamination incident due to Marcellus Shale gas development. *Proceedings of the National Academy of Sciences of the United States of America* Early Edition.
- Lorant, F., Prinzhofer, A., Behar, F. and Huc, A.Y. (1998) Carbon isotopic and molecular constraints on the formation and the expulsion of thermogenic hydrocarbon gases. *Chemical Geology* 147(3-4), 249-264.
- Martini, A.M., Walter, L.M., Ku, T.C., Budai, J.M., McIntosh, J.C. and Schoell, M. (2003) Microbial production and modification of gases in sedimentary basins: A geochemical case study from a Devonian shale gas play, Michigan basin. *AAPG Bulletin* 87(8), 1355-1375.
- Martini, A.M., Walter, L.M. and McIntosh, J.C. (2008) Identification of microbial and thermogenic gas components from Upper Devonian black shale cores, Illinois and Michigan basins. *AAPG Bulletin* 92(3), 327-339.
- Mastalerz, V., De Lange, G.J. and Dählmann, A. (2009) Differential aerobic and anaerobic oxidation of hydrocarbon gases discharged at mud volcanoes in the Nile deep-sea fan. *Geochimica et Cosmochimica Acta* 73(13), 3849-3863.
- Milkov, A.V. and Dzou, L. (2007) Geochemical evidence of secondary microbial methane from very slight biodegradation of undersaturated oils in a deep hot reservoir. *Geology* 35(5), 455-458.
- Milkov, A.V. and Etiope, G. (2018) Revised genetic diagrams for natural gases based on a global dataset of >20,000 samples. *Organic Geochemistry* 125109-120.
- Molofsky, L.J., Connor, J.A., Wylie, A.S., Wagner, T. and Farhat, S.K. (2013) Evaluation of Methane Sources in Groundwater in Northeastern Pennsylvania. *Groundwater* 51(3), 333-349.
- Montegrossi, G., Tassi, F., Vaselli, O., Buccianti, A. and Garofalo, K. (2001) Sulfur species in volcanic gases. *Analytical Chemistry* 73(15), 3709-3715.
- Montgomery, S.L., Jarvie, D.M., Bowker, K.A. and Pollastro, R.M. (2005) Mississippian Barnett Shale, Fort Worth basin, north-central Texas: Gas-shale play with multi-trillion cubic foot potential. *AAPG Bulletin* 89(2), 155-175.
- Moore, M.T., Vinson, D.S., Whyte, C.J., Eymold, W.K., Walsh, T.B. and Darrah, T.H. (2018) Differentiating between biogenic and thermogenic sources of natural gas and hydrocarbon

- geochemistry. *Geological Society, London* From source to seep: Geochemical applications in hydrocarbon systems (Special publications), 468-505.
- Moritz, A., Helie, J.F., Pinti, D.L., Larocque, M., Barnetche, D., Retailleau, S., Lefebvre, R. and Gelinas, Y. (2015) Methane Baseline Concentrations and Sources in Shallow Aquifers from the Shale Gas-Prone Region of the St. Lawrence Lowlands (Quebec, Canada). *Environmental Science & Technology* 49(7), 4765-4771.
- Nicot, J.-P., Huang, Y., Wolaver, B.D. and Costley, R.A. (2013) Flow and salinity patterns in the low-transmissivity Upper Paleozoic aquifers of North-Central Texas. *Gulf Coast Association of Geological Societies Journal* 253-67.
- Nicot, J.P., Larson, T., Darvari, R., Mickler, P., Sloten, M., Aldridge, J., Uhlman, K. and Costley, R. (2017a) Controls on methane occurrences in shallow aquifers overlying the Haynesville Shale gas field, East Texas. *Groundwater* 55(4), 443-454.
- Nicot, J.P., Larson, T., Darvari, R., Mickler, P., Uhlman, K. and Costley, R. (2017b) Controls on methane occurrences in aquifers overlying the Eagle Ford Shale play, South Texas. *Groundwater* 55(4), 455-468.
- Nicot, J.P., Mickler, P., Larson, T., Castro, M.C., Darvari, R., Uhlman, K. and Costley, R. (2017c) Methane occurrences in aquifers overlying the Barnett shale play with a focus on Parker County, Texas. *Groundwater* 55(4), 469-481.
- Norville, G. and Muehlenbachs, K. (2018) Insights from stable isotope geochemistry surveillance in the unconventional Horn River Basin play, Unconventional Resources Technology Conference, Houston, Texas, 3986-4003.
- Osborn, S.G., McIntosh, J.C., Hanor, J.S. and Biddulph, D. (2012) Iodine-129, Sr-87/Sr-86, and trace elemental geochemistry of northern Appalachian Basin brines: evidence for basinal-scale fluid migration and clay mineral diagenesis. *American Journal of Science* 312(3), 263-287.
- Osborn, S.G., Vengosh, A., Warner, N.R. and Jackson, R.B. (2011) Methane contamination of drinking water accompanying gas-well drilling and hydraulic fracturing. *Proceedings of the National Academy of Sciences* 108(20), 8172-8176.
- Oxburgh, E.R., Onions, R.K. and Hill, R.I. (1986) Helium isotopes in sedimentary basins. *Nature* 324(6098), 632-635.
- Pallasser, R. (2000) Recognising biodegradation in gas/oil accumulations through the $\delta^{13}\text{C}$ compositions of gas components. *Organic Geochemistry* 31(12), 1363-1373.
- Pape, T., Bahr, A., Rethemeyer, J., Kessler, J.D., Sahling, H., Hinrichs, K.U., Klapp, S.A., Reeburgh, W.S. and Bohrmann, G. (2010) Molecular and isotopic partitioning of low-molecular-weight hydrocarbons during migration and gas hydrate precipitation in deposits of a high-flux seepage site. *Chemical Geology* 269(3-4), 350-363.
- Pernaton, E., Prinzhofer, A. and Schneider, F. (1996) Reconsideration of methane isotope signature as a criterion for the genesis of natural gas - Influence of migration on isotopic signatures. *Revue De L Institut Francais Du Petrole* 51(5), 635-651.
- Pinti, D.L., Béland-Otis, C., Tremblay, A., Castro, M.C., Hall, C.M., Marcil, J.-S., Lavoie, J.-Y. and Lapointe, R. (2011) Fossil brines preserved in the St-Lawrence Lowlands, Québec, Canada as revealed by their chemistry and noble gas isotopes. *Geochimica et Cosmochimica Acta* 75(15), 4228-4243.

- Pinti, D.L. and Marty, B. (1995) Noble gases in crude oils from the Paris Basin, France: Implications for the origin of fluids and constraints on oil-water-gas interactions. *Geochimica et Cosmochimica Acta* 59(16), 3389-3404.
- Pollastro, R.M., Hill, R.J., Jarvie, D.M. and Henry, M.E. (2003) Assessing undiscovered resources of the Barnett-Paleozoic total petroleum system, Bend Arch-Fort Worth Basin province, Texas, AAPG Southwest Section Convention, Fort Worth, Texas.
- Pollastro, R.M., Jarvie, D.M., Hill, R.J. and Adams, C.W. (2007) Geologic framework of the Mississippian Barnett Shale, Barnett-Paleozoic total petroleum system, bend arch-Fort Worth Basin, Texas. *AAPG Bulletin* 91(4), 405-436.
- Prinzhofer, A. and Pernaton, E. (1997) Isotopically light methane in natural gas: bacterial imprint or diffusive fractionation? *Chemical Geology* 142(3-4), 193-200.
- Prinzhofer, A.A. and Huc, A.Y. (1995) Genetic and post-genetic molecular and isotopic fractionations in natural gases. *Chemical Geology* 126(3-4), 281-290.
- Rivard, C., Bordeleau, G., Lavoie, D., Lefebvre, R. and Malet, X. (2018a) Can groundwater sampling techniques used in monitoring wells influence methane concentrations and isotopes? *Environmental Monitoring and Assessment* 190(4), 191.
- Rivard, C., Bordeleau, G., Lavoie, D., Lefebvre, R. and Malet, X. (2018b) Temporal variations of methane concentration and isotopic composition in groundwater of the St. Lawrence Lowlands, eastern Canada. *Hydrogeology Journal* 26(2), 533-551.
- Rodriguez, N.D. and Philp, R.P. (2010) Geochemical characterization of gases from the Mississippian Barnett Shale, Fort Worth Basin, Texas. *AAPG Bulletin* 94(11), 1641-1656.
- Rowe, D. and Muehlenbachs, A. (1999a) Low-temperature thermal generation of hydrocarbon gases in shallow shales. *Nature* 398(6722), 61-63.
- Rowe, D. and Muehlenbachs, K. (1999b) Isotopic fingerprints of shallow gases in the Western Canadian Sedimentary Basin: Tools for remediation of leaking heavy oil wells. *Organic Geochemistry* 30, 861-871.
- Salad Hersi, O. (2012) Biostratigraphic constraints on chronostratigraphic intraformational relationships within the Lower–Middle Ordovician Beekmantown Group, Laurentian margin: eastern Ontario and southwestern Quebec, Canada. In: Derby, J.R., Fritz, R.D., Longacre, S.A., Morgan, W.A., Sternbach, C.A. (Eds.), *The Great American Carbonate Bank: The Geology and Economic Resources of the Cambrian–Ordovician Sauk Megasequence of Laurentia AAPG Memoirs* 98, 559-574.
- Schlegel, M.E., McIntosh, J.C., Bates, B.L., Kirk, M.F. and Martini, A.M. (2011) Comparison of fluid geochemistry and microbiology of multiple organic-rich reservoirs in the Illinois Basin, USA: Evidence for controls on methanogenesis and microbial transport. *Geochimica et Cosmochimica Acta* 75(7), 1903-1919.
- Schoell, M. (1980) The hydrogen and carbon isotopic composition of methane from natural gases of various origins. *Geochimica et Cosmochimica Acta* 44(5), 649-661.
- Schoell, M. (1983) Genetic characterization of natural gases. *AAPG Bulletin* 67(12), 2225-2238.
- Schout, G., Hartog, N., Hassanizadeh, S.M. and Griffioen, J. (2018) Impact of an historic underground gas well blowout on the current methane chemistry in a shallow groundwater system. *Proceedings of the National Academy of Sciences of the United States of America* 115(2), 296-301.

- Scott, A.R., Kaiser, W. and Ayers Jr, W.B. (1994) Thermogenic and secondary biogenic gases, San Juan basin, Colorado and New Mexico--implications for coalbed gas producibility. *AAPG Bulletin* 78(8), 1186-1209.
- Séjourné, S., Lefebvre, R., Malet, X. and Lavoie, D. (2013) Synthèse géologique et hydrogéologique du Shale d'Utica et des unités sus-jacentes (Lorraine, Queenston et dépôts meubles), Basses-Terres du Saint-Laurent, Québec, in: Canada, C.g.d. (Ed.), 165.
- Siegel, D.I., Azzolina, N.A., Smith, B.J., Perry, A.E. and Bothun, R.L. (2015) Methane concentrations in water wells unrelated to proximity to existing oil and gas wells in northeastern Pennsylvania. *Environmental Science & Technology* 49(7), 4106-4112.
- Siegel, D.I., Lesniak, K.A., Stute, M. and Frape, S. (2004) Isotopic geochemistry of the Saratoga springs: Implications for the origin of solutes and source of carbon dioxide. *Geology* 32(3), 257-260.
- Smith, S. and Kennedy, B. (1983) The solubility of noble gases in water and in NaCl brine. *Geochimica et Cosmochimica Acta* 47(3), 503-515.
- Solomon, D.K., Hunt, A. and Poreda, R.J. (1996) Source of radiogenic helium 4 in shallow aquifers: Implications for dating young groundwater. *Water Resources Research* 32(6), 1805-1813.
- Solomon, D.K., Poreda, R.J., Cook, P.G. and Hunt, A. (1995) Site characterization using $3\text{H}/3\text{He}$ groundwater ages, Cape Cod, MA. *Groundwater* 33(6), 988-996.
- Solomon, D.K., Poreda, R.J., Schiff, S.L. and Cherry, J.A. (1992) Tritium and He 3 as groundwater age tracers in the Borden aquifer. *Water Resources Research* 28(3), 741-755.
- St-Julien, P., Slivitsky, A. and Feininger, T. (1983) A deep structural profile across the Appalachians of southern Quebec. *Geological Society of America Memoirs* 158, 103-111.
- Sweeney, R. and Taylor, P. (1999) Biogenic methane derived from biodegradation of petroleum under environmental conditions and in oil & gas reservoirs, in: Schoell, M. (Ed.), Proceedings AAPG Hedberg Research Conference on Natural Gas Formation and Occurrence, Tulsa, Oklahoma, 6-10.
- Texas, R.C.o. (2019a) Public GIS Viewer.
- Texas, R.C.o. (2019b) Texas Barnett Shale Total Natural Gas Production 2000 through July 2019.
- Tilley, B. and Muehlenbachs, K. (2013) Isotope reversals and universal stages and trends of gas maturation in sealed, self-contained petroleum systems. *Chemical Geology* 339, 194-204.
- Torgersen, T., Drenkard, S., Farley, K., Schlosser, P. and Shapiro, A. (1994) Mantle helium in groundwater of the Mirror Lake Basin, New Hampshire, USA, in: Matsuda, J. (Ed.), *Noble Gas Geochemistry and Cosmochemistry*, 279-292.
- Torgersen, T. and Kennedy, B. (1999) Air-Xe enrichments in Elk Hills oil field gases: role of water in migration and storage. *Earth and Planetary Science Letters* 167(3-4), 239-253.
- Turner, G.L. (1957) Paleozoic stratigraphy of the Fort Worth Basin, in: Societies, A.F.W.G. (Ed.), 1957 Joint Field Trip Guidebook, 57-77.
- USGS (2011) National Field Manual for the collection of water-quality data, US Geological Survey, Washington, DC.
- Valentine, D.L., Kessler, J.D., Redmond, M.C., Mendes, S.D., Heintz, M.B., Farwell, C., Hu, L., Kinnaman, F.S., Yvon-Lewis, S., Du, M.R., Chan, E.W., Tigreros, F.G. and Villanueva, C.J. (2010) Propane Respiration Jump-Starts Microbial Response to a Deep Oil Spill. *Science* 330(6001), 208-211.

- Van Stempvoort, D., Maathuis, H., Jaworski, E., Mayer, B. and Rich, K. (2005) Oxidation of fugitive methane in ground water linked to bacterial sulfate reduction. *Groundwater* 43(2), 187-199.
- Van Stempvoort, D.R., Armstrong, J. and Mayer, B. (2007) Microbial reduction of sulfate injected to gas condensate plumes in cold groundwater. *Journal of Contaminant Hydrology* 92(3-4), 184-207.
- Vautour, G., Pinti, D.L., Méjean, P., Saby, M., Meyzonnat, G., Larocque, M., Castro, M.C., Hall, C.M., Boucher, C. and Roulleau, E. (2015) $3\text{H}/3\text{He}$, 14C and $(\text{U}-\text{Th})/\text{He}$ groundwater ages in the St. Lawrence Lowlands, Quebec, Eastern Canada. *Chemical Geology* 413, 94-106.
- Vengosh, A., Jackson, R.B., Warner, N., Darrah, T.H., Kondash, A., Gibbs, A. and Gibbs, B. (2014) A critical review of the risks to water resources from unconventional shale gas development and hydraulic fracturing in the United States. *Environmental Science & Technology* 48(15), 8334-8348.
- Vengosh, A., Kloppmann, W., Marei, A., Livshitz, Y., Gutierrez, A., Banna, M., Guerrot, C., Pankratov, I. and Raanan, H. (2005) Sources of salinity and boron in the Gaza strip: Natural contaminant flow in the southern Mediterranean coastal aquifer. *Water Resources Research* 41(1).
- Vinson, D.S., Blair, N.E., Martini, A.M., Larter, S.R., Orem, W.H. and McIntosh, J.C. (2017) Microbial methane from in situ biodegradation of coal and shale: a review and reevaluation of hydrogen and carbon isotope signatures. *Chemical Geology* 453, 128-145.
- Walper, J.L. (1982) Plate tectonic evolution of the Fort Worth Basin, in: Martin, C.A.E. (Ed.), *Petroleum geology of the Fort Worth Basin and Bend Arch area*. Dallas Geological Society, 237-251.
- Warner, N.R., Darrah, T.H., Jackson, R.B., Millot, R., Kloppmann, W. and Vengosh, A. (2014) New Tracers Identify Hydraulic Fracturing Fluids and Accidental Releases from Oil and Gas Operations. *Environmental Science & Technology* 48(21), 12552-12560.
- Warner, N.R., Jackson, R.B., Darrah, T.H., Osborn, S.G., Down, A., Zhao, K.G., White, A. and Vengosh, A. (2012) Geochemical evidence for possible natural migration of Marcellus Formation brine to shallow aquifers in Pennsylvania. *Proceedings of the National Academy of Sciences of the United States of America* 109(30), 11961-11966.
- Weaver, T., Frappe, S. and Cherry, J. (1995) Recent cross-formational fluid flow and mixing in the shallow Michigan Basin. *Geological Society of America Bulletin* 107(6), 697-707.
- Weiss, R.F. (1970) Solubility of nitrogen, oxygen, and argon in water and seawater. *Deep-Sea Research* 17(4), 721-725.
- Weiss, R.F. (1971) Solubility of helium and neon in water and seawater. *Journal of Chemical and Engineering Data* 16(2), 235-241.
- Weiss, R.F. and Kyser, T.K. (1978) Solubility of krypton in water and sea water. *Journal of Chemical and Engineering Data* 23(1), 69-72.
- Wen, T., Castro, M.C., Ellis, B.R., Hall, C.M. and Lohmann, K.C. (2015) Assessing compositional variability and migration of natural gas in the Antrim Shale in the Michigan Basin using noble gas geochemistry. *Chemical Geology* 417356-370.
- Wen, T., Castro, M.C., Hall, C.M., Pinti, D.L. and Lohmann, K.C. (2016a) Constraining groundwater flow in the glacial drift and saginaw aquifers in the Michigan Basin through helium concentrations and isotopic ratios. *Geofluids* 16(1), 3-25.

- Wen, T., Castro, M.C., Nicot, J.-P., Hall, C.M., Larson, T., Mickler, P. and Darvari, R. (2016b) Methane Sources and Migration Mechanisms in Shallow Groundwaters in Parker and Hood Counties, Texas: A Heavy Noble Gas Analysis. *Environmental Science & Technology* 50(21), 12012-12021.
- Wen, T., Castro, M.C., Nicot, J.-P., Hall, C.M., Pinti, D.L., Mickler, P., Darvari, R. and Larson, T. (2017) Characterizing the noble gas isotopic composition of the Barnett Shale and Strawn Group and constraining the source of stray gas in the Trinity Aquifer, north-central Texas. *Environmental Science & Technology* 51(11), 6533-6541.
- Wen, T., Niu, X., Gonzales, M., Zheng, G., Li, Z. and Brantley, S.L. (2018) Big groundwater data sets reveal possible rare contamination amid otherwise improved water quality for some analytes in a region of Marcellus Shale development. *Environmental science & technology* 52(12), 7149-7159.
- Wen, T., Woda, J., Marcon, V., Niu, X., Li, Z. and Brantley, S.L. (2019) Exploring How to Use Groundwater Chemistry to Identify Migration of Methane near Shale Gas Wells in the Appalachian Basin. *Environmental Science & Technology* 53(15), 9317-9327.
- Whiticar, M., Faber, E. and Schoell, M. (1985) Hydrogen and Carbon Isotopes of C1 to C5 Alkanes in Natural Gases: Abstract. *AAPG Bulletin* 69(2), 316-316.
- Whiticar, M.J. (1990) A geochemical perspective of natural gas and atmospheric methane. *Organic Geochemistry* 16(1-3), 531-547.
- Whiticar, M.J. (1994) Correlation of Natural Gases with Their Sources: Chapter 16: Part IV. Identification and Characterization. *AAPG Memoir 60: The petroleum system--from source to trap*, 261-283.
- Whiticar, M.J. (1999) Carbon and hydrogen isotope systematics of bacterial formation and oxidation of methane. *Chemical Geology* 161(1-3), 291-314.
- Whiticar, M.J., Faber, E. and Schoell, M. (1986) Biogenic methane formation in marine and fresh-water environments- CO₂ reduction vs. acetate fermentation isotope evidence. *Geochimica et Cosmochimica Acta* 50(5), 693-709.
- Woda, J., Wen, T., Oakley, D., Yoxtheimer, D., Engelder, T., Castro, M.C. and Brantley, S.L. (2018) Detecting and explaining why aquifers occasionally become degraded near hydraulically fractured shale gas wells. *Proceedings of the National Academy of Sciences of the United States of America* 115(49), 12349-12358.
- Wong, C.I., Kromann, J.S., Hunt, B.B., Smith, B.A. and Banner, J.L. (2014) Investigating Groundwater Flow Between Edwards and Trinity Aquifers in Central Texas. *Groundwater* 52(4), 624-639.
- Zhou, Z., Ballentine, C.J., Schoell, M. and Stevens, S.H. (2012) Identifying and quantifying natural CO₂ sequestration processes over geological timescales: The Jackson Dome CO₂ Deposit, USA. *Geochimica et Cosmochimica Acta* 86, 257-275.
- Zumberge, J., Ferworn, K. and Brown, S. (2012) Isotopic reversal ('rollover') in shale gases produced from the Mississippian Barnett and Fayetteville formations. *Marine and Petroleum Geology* 31(1), 43-52.